

University of Nottingham
UK | CHINA | MALAYSIA

Institute of Sustainable Energy Technology

Department of Architecture and Built Environment

Faculty of Engineering

Investigation of Sustainable Energy Technologies and Energy Performance Prediction for Deep Energy Retrofit in Single-family Houses

Thesis by

Ke Qu, BEng

Thesis submitted to the University of Nottingham

For the Degree of Doctor of Philosophy

February 2022

Abstract

According to the EU Commission projection (2016/547/EU), the current average renovation rate is far below the expected rate of 3% to achieve carbon neutrality in building sectors by 2050. This is due to the fact that, during the building retrofit optimisation process, the decision-making criteria and objectives are generally optimised separately, and homeowners' motivations are often ignored or not carefully defined in most research especially. In Europe, 68% of residential building stocks are single-family houses in European countries with roughly 54% constructed before the 1970s with poor energy efficiency. However, few studies address the issue of 'Rapid and accurate energy-economic performance prediction of deep energy retrofit in single-family houses' over the past decades. Recently, this issue has been discussed in limited research via the Black- or White-box based building energy models to predict post-retrofit energy-economic performance. Applying the Black-box models, low accuracy occurs due to inadequate data, neglect of coupling effects in deep energy retrofit combinations and lack of complex heat transfer phenomena in single-family houses. Conversely, the White-box models with time-consuming and numerous dynamic simulations are found to be cumbersome.

This PhD research aimed at investigating a rapid and accurate Energy-Flow based Ensemble Calibration (EF-EC) model for energy prediction of deep energy retrofit in single-family houses using the high-efficient sustainable retrofit technologies, which will be integrated with homeowners' engagement in a novel Motivation-Objective-Criteria (MOC) based retrofit approach to optimize the final retrofit decisions.

In this research, innovative envelop retrofit technologies include façade insulation, glazing insulation and efficient daylighting pipe technologies, which can be used to reduce the thermal energy and electricity load for both heating and cooling requirements. Innovative energy system retrofit technologies includes 1) liquid desiccant-based air cooler and dehumidifier, and 2) solar assisted heat pump. Numerical models have been established for each technology with validation by measurement in either laboratory or field test, with results data to clearly identify and calibrate the performance under real conditions. The EF-EC model is applied in a case study building representing a single-family house constructed in the 1960s in northern Italy with poor insulation and high energy consumption under the typical Mediterranean climatical context. Furthermore, 17 retrofit measures are proposed by the RezBuild Project Consortium, and classified into passive, active and renewable categories, with a domain of 20,735 comprehensive energy retrofit combinations generated. Retrofit motivations are categorised into three typical types: 1) Self-living, 2) Rental or sale, and 3) Investment, under five objectives: Energy Reduction Rate (ERR), Initial Investment (II), Discounted Payback Period (DPP), Bills Reduction Rate (BRR) and Carbon Reduction Rate (CRR). A UK semi-detached house is applied as the reference building to investigate the impact of homeowners' engagement on the decision-making of various retrofit measures.

Compared with the IES VE simulation results, the maximum discrepancy of the EF-EC model is 6% with an absolute discrepancy of 2.9 kWh/m2, where the energy reduction rate is in the range of 76% - 89%. Therefore, the calculation discrepancy has been improved by 63% - 75%. This research using the EF-EC

model could save up to 90% of calculation time, with 0.72s computing time on a single combination. According to the cost-optimal results neglecting homeowners' motivation, it is evident that the mismatch of optimal retrofit combinations occurs between the minimum Initial Investment (II) and Discounted Payback Periods (DPP), with optimal ERR of 72%-79% and 82%-93%, respectively. The sensitivity analysis results are conducted, indicating that the optimal retrofit measures and baseline energy consumption input are in good agreement, with a 10% discrepancy. Thus, the proposed inclusive Motivation-Objective-Criteria approach can incorporate homeowners' engagement in the building retrofitting design process, serving as a decision-making supporting tool to accelerate building retrofit with maximised user acceptance and market penetration.

Keywords:

Sustainable energy technologies; Energy performance; Deep energy retrofit; Single-family houses; Building retrofit; Decision-making optimisation

List of publications

International Journal Papers

1. Qu K, Chen X, Ekambaram A, Cui Y, Gan G, Økland A, Riffat S. A novel holistic EPC related retrofit approach for residential apartment building renovation in Norway. *Sustainable Cities and Society*, 54(2020): P. 101975. DOI: https://doi.org/10.1016/j.scs.2019.101975.

2. Chen X, Qu K, Calautit J, Ekambaram A, Lu W, Fox C, Gan G, Riffat S. Multi-criteria assessment approach for a residential building retrofit in Norway. *Energy and Buildings*, 215(2020): P. 109668. DOI: https://doi.org/10.1016/j.enbuild.2019.109668.

3. Jarimi, H., Qu, K., Zhang, S., Lv, Q., Liao, J., Chen, B., Lv, H., Cheng, C., Li, J., Su, Y., Dong, S. and Riffat, S., 2020. Performance Analysis of a Hybrid Thin Film Photovoltaic (PV) Vacuum Glazing. *Future Cities and Environment*, 6(1), p.2. DOI: http://doi.org/10.5334/fce.73.

4. Qu, K., Chen, X., Wang, Y., Calautit, J., Riffat, S. & Cui, X. 2021. Comprehensive energy, economic and thermal comfort assessments for the passive energy retrofit of historical buildings - A case study of a late nineteenth-century Victorian house renovation in the UK. Energy, 220, 119646. DOI: https://doi.org/10.1016/j.energy.2020.119646.

5. Wang, Y., Qu, K., Chen, X., Gan, G. & Riffat, S. 2022a. An innovative retrofit Motivation-Objective-Criteria (MOC) approach integrating homeowners' engagement to unlocking low-energy retrofit in residential buildings. Energy and Buildings, 111834. DOI: https://doi.org/10.1016/j.enbuild.2022.111834.

6. Wang, Y., Qu, K., Chen, X., Zhang, X. & Riffat, S. 2022b. Holistic electrification vs deep energy retrofits for optimal decarbonisation pathways of UK dwellings: A case study of the 1940s' British post-war masonry house. Energy, 241, 122935. DOI: https://doi.org/10.1016/j.energy.2021.122935.

7. Barreto, G., Qu, K., Wang, Y., Iten, M. & Riffat, S. 2022. An Innovative Window Heat Recovery (WHR) System with Heat Pipe Technology: Analytical, CFD, Experimental Analysis and Building Retrofit Performance. Energy Report, DOI: http://dx.doi.org/10.2139/ssrn.3960587.

International Conference Papers

1. Qu K, Riffat S. Human-based inclusive approach for residential building retrofit: review and strategies. 7th International Conference on Sustainable Places (SP 2019), June 2019, Cagliari, Italy.

2. Qu K, Chen X, Riffat S. An overview of holistic approach to achieve net zero energy residential building retrofit. 17th International Conference on Sustainable Energy Technologies (SET 2018), Wuhan, China.

3. Qu K, Chen X, Riffat S. An innovative hollow fibre based dehumidification–cooling system for residential building retrofits: Experiments and case study. 18th International Conference on Sustainable Energy Technologies (SET 2019), Kuala Lumpur, Malaysia.

4. Qu K, Wang Y, Dodo A, Chen X, Pedro A, Riffat S. A data-driven based validation and calibration approach to building energy simulation model for accurate pre-retrofit design predictions. Proceedings of Ecos 2021 - The 34 rth International Conference On Efficiency, Cost, Optimization, Simulation and

Environmental Impact of Energy Systems June 27-July 2, 2021, Taormina, Italy

5. Qu K, Wang Y, Chen X, Dodo A, Zheng T, Cimini V, Riffat S. An inclusive decision-making approach for selection of comprehensive energy-retrofit combinations in a typical Italian 1960s' multi-family house. Proceedings of Ecos 2021 - The 34 rth International Conference On Efficiency, Cost, Optimization, Simulation and Environmental Impact of Energy Systems June 27-July 2, 2021, Taormina, Italy

Acknowledgement

I would like to express sincere gratitude to my supervisors Professor Saffa Riffat, Dr Guohui Gan and Dr Siddig A Omer who encouraged me to push the boundaries in every step of my research. I am proud of being your student, and grateful for the tremendous support and guidance you provided me with.

Special thanks to Dr Xiangjie Chen, Dr Hasila Jarimi, and Dr Ziwei Chen who generously shared their experience, knowledge and help me both technically and academically. Furthermore, this research would not have been possible without the technical support from the support of the technicians of the laboratory: Tony Gospel, Dave Oliver, Andrew Mathew and Jonny Moss for their professional and enthusiastic help and support with my experimental work. I am also grateful to my dear colleagues, especially Ms Tianhong Zhen, Ms Jiarui Sun, Dr Hongyu Bai, Miss Yixin Wang and Mr Mingen Han for discussing problems I encountered with me during my research. I also would like to thank Zeny Amante Roberts for her sincere help. Most importantly, I would like to thank my cherished bosom friend Mr Yuhao Wang, for the stimulating discussions, for the sleepless nights we were working together before deadlines, for the days of mutual encouragement and support, and for all the fun we have had in the past and my life in general. Some of us get dipped in flat, some in satin, some in gloss.... But every once in a while you find someone who's iridescent, and when you do, nothing will ever compare. The ancients said: life is a bosom friend.

I have utmost respect and appreciation from my family: my parents (Mr Qingbin Qu and Ms Xianfeng Hu) and grandparents (Ms Zongxiu Zhang and Ms Shenglan Liu) for supporting me financially and spiritually throughout the whole journey. Thank you for the tremendous trust, support and encouragement you

have provided me with throughout my life.

I would also like to acknowledge the support and contributions from European Commission Horizon 2020 project RezBuild (project contract number: 768623), and European Commission Horizon 2020 project SureFit (project contract number: 894511), as well as project partners participations.

Table of Contents

ABSTRACT ..... **I**

LIST OF PUBLICATIONS ..... **IV**

ACKNOWLEDGEMENT ..... **VII**

TABLE OF CONTENTS ..... **IX**

NOMENCLATURE ..... **XIII**

LIST OF FIGURES ..... **XVII**

LIST OF TABLES ..... **XX**

1. INTRODUCTION **21**

1.1 RESEARCH BACKGROUND 21
1.2 STATEMENT OF THE PROBLEMS 23
1.3 AIMS AND OBJECTIVES 26
1.4 NOVELTY OF THE RESEARCH 27
1.4.1 Performance determination of advanced retrofit technologies 27
1.4.2 Rapid and accurate prediction of deep energy retrofit performance in single-family houses 28
1.4.3 Homeowners' retrofit motivations, objectives, and criteria could be considered in the decision-making process 28
1.5 SCOPE OF THE RESEARCH 29
1.6 RESEARCH METHODOLOGY 30
1.6.1 Background investigation and literature review 30
1.6.2 Modelling and experimental analysis of retrofit technologies and performance modification 30
1.6.3 Model establishing, validation, and uncertainty analysis 30
1.6.4 Inclusive Motivation-Objective-Criteria (MOC) approach integrating homeowners' engagement 31
1.7 THESIS STRUCTURE 32

2. LITERATURE REVIEW **35**

2.1 INTRODUCTION 35
2.2 RESIDENTIAL BUILDING RETROFIT BACKGROUND 36
2.2.1 Building retrofit status in EU and UK 37
2.2.2 Deep energy retrofit in single-family houses 39
2.3 BUILDING RETROFIT TECHNOLOGIES 43
2.3.1 Passive retrofit technologies 43
2.3.1.1 Vacuum insulation panels 45
2.3.1.2 Aerogel insulation panels 48
2.3.1.3 Vacuum glazing windows 50
2.3.2 Building energy system retrofit technologies 52
2.3.2.1 Solar boosted heat pump 52
2.3.2.2 Ground source heat pump 54
2.3.2.3 Air source heat pump 55
2.3.2.4 Hybrid photovoltaic and thermal PV/T technology 56
2.3.2.5 Desiccant solution cooling and dehumidification technologies 57
2.4 WHITE- AND BLACK- BOX BASED BUILDING ENERGY PREDICTION MODEL 59
2.4.1 Data-driven (or Black-box model) based Building Performance Simulation for building retrofit analysis 59
2.4.2 Physics-based (or White-box model) Building Performance Simulation for building

retrofit analysis *62*
2.4.3 Existing research gap and the novelty proposed in this research *65*
2.5 WILLINGNESS-TO-PAY AND EPC LABELLING FOR RESIDENTIAL BUILDING RETROFIT 66
2.6 MULTI-OBJECTIVE OPTIMISATION ALGORITHMS 70
2.7 RETROFIT MOTIVATIONS AND HOMEOWNERS' ENGAGEMENT 79
2.8 CONCLUSION 87

3. ON-SITE TEST OF INNOVATIVE ENVELOPE RETROFIT TECHNOLOGIES FOR ENERGY DEMAND REDUCTION 90

3.1 INTRODUCTION 90
3.2 FIELD TEST RIG SET UP ON SITE 92
3.2.1 Test rig for façade insulation materials *92*
3.2.2 Test rig for glazing insulation *96*
3.3 SILICA BASED VACUUM INSULATION PANELS 98
3.4 STARCH-AEROGEL INSULATION PANELS 101
3.5 VACUUM GLAZING 104
3.6 THIN FILM PV VACUUM GLAZING (PV-VG) 106
3.6.1 Design concept *106*
3.6.2 Result and discussion – Electricity conversion efficiency *109*
3.6.3 Results and discussion – U-value *113*
3.7 DAYLIGHTING PIPES 115
3.8 CONCLUSION 118

4. INNOVATIVE SYSTEM FOR HEATING, COOLING AND DEHUMIDIFICATION 121

4.1 INTRODUCTION 121
4.2 HOLLW FIBRE-BASED LIQUID DESICCANT COOLING AND DEHUMIDIFICATION UNIT 121
4.2.1 Concept *121*
4.2.2 Numerical modelling *124*
4.2.2.1 Heat and mass transfer 125
4.2.2 Test rig setup *133*
4.2.3 Assessment criteria *136*
4.2.3.1 Air side effectiveness (εsen, εlat) 136
4.2.4 Results and discussion *138*
4.2.4.1 Experimental validation 138
4.2.4.2 Parametric analysis 142
4.3 SOLAR-ASSISTED HEAT PUMP INTEGRATED WITH THERMAL STORAGE AND PV PANELS (SAHP-TS-PV) 150
4.3.1 Concept *150*
4.3.2 Test rig setup *157*
4.3.3 COP correlation *160*
4.4 SUMMARY 162

5. AN INNOVATIVE ENERGY-FLOW BASED ENSEMBLE CALIBRATION (EF-EC) MODEL FOR RETROFIT BUILDING ENERGY-ECONOMIC PERFORMANCE PREDICTION 164

5.1 INTRODUCTION 164
5.2 POST-RETROFIT ENERGY MODEL 166
5.2.1 Input-output energy flow framework *169*
5.2.2 Post-retrofit demand outputs *173*
5.2.3 Coupling matrices for input-output energy flow *177*
5.2.4 Post-retrofit energy inputs *179*
5.3 CASE STUDY 182
5.3.1 Baseline building energy simulation (Pre-retrofit energy inputs) *187*
5.3.2 Comprehensive retrofit combinations *189*
5.4 MODEL VALIDATION AND UNCERTAINTY ANALYSIS 193

5.4.1 MODEL VALIDATION 195
5.4.2 UNCERTAINTY AND SENSITIVITY ANALYSIS 196
5.4.2.1 Uncertainty analysis 197
5.4.2.2 Results comparisons and calibration via sensitivity analysis 200
5.5 CONCLUSION 203

6. AN INNOVATIVE MOTIVATION-OBJECTIVE-CRITERIA (MOC) RETROFIT OPTIMISATION APPROACH INTEGRATING HOMEOWNERS' ENGAGEMENT 206

6.1 INTRODUCTION 206
6.2 METHODS 206
6.2.1 Multi-objective assessment approach 209
6.2.2 Retrofit motivations, objectives and weights 212
6.2.3 Calculation method 216
6.3 CASE STUDY 221
6.4 RESULTS AND DISCUSSIONS 227
6.4.1 Cost-optimal results neglecting homeowners' motivation 228
6.4.2 Multi-criteria optimisation results and discussion 231
6.4.3 Sensitivity analysis with respect to input data 236
6.5 CONCLUSIONS 238

7. CONCLUSIONS AND FUTURE WORKS 242

7.1 DISCUSSION AND CONCLUSIONS 242
7.1.1 Modelling and experimental results of innovative retrofit technologies 242
7.1.2 EF-EC energy prediction model 242
7.1.3 MOC retrofit optimisation approach 243
7.2 RECOMMENDATIONS AND FUTURE WORK 244
7.2.1 Algorithm improvement, interaction and visualisation 244
7.2.2 multi-scale retrofit strategy 245
7.2.3 Fast retrofit strategy and operation analysis 245
7.2.4 Cost-effective dwelling electrification retrofit 247

REFERENCE 248

APPENDIX 5-1 BUILDING SITE, SURROUNDINGS AND CLIMATE CONDITIONS 267

APPENDIX 5-2 BUILDING FABRIC, AIRTIGHTNESS, THERMAL BRIDGING AND ENERGY SYSTEMS 272

APPENDIX 5-3 THE DETAILS ENERGY PERFORMANCES OF INDIVIDUAL TECHNOLOGY 279

APPENDIX 5-4 ALL INPUT PARAMETERS OF THE PRE- AND POST-RETROFIT MODEL 284

APPENDIX 5-5 DETAILED RETROFIT MEASURES IN REAL BUILDING 287

APPENDIX 5-6 DETAILS OF 30 RETROFIT COMBINATIONS AND CALCULATION RESULTS 288

APPENDIX 6-1 ENERGY PERFORMANCE CERTIFICATION (EPC) CALCULATION METHOD 293

APPENDIX 6-2 MULTI-OBJECTIVE WEIGHTING SCORES FOR VARIOUS HOMEOWNERS' SURVEY WITH THREE RETROFIT MOTIVATIONS 295

APPENDIX 6-3 RESIDENTIAL BUILDING TYPOLOGY 297

APPENDIX 6-4 RETROFIT MEASURES AND TECHNICAL SPECIFICATIONS 300

APPENDIX 6-5 CRITERIA, OPTIMAL COMBINATIONS AND ASSESSMENT VALUES WITHOUT CONSIDERING MOTIVATIONS 302

APPENDIX 6-6 CRITERIA, OPTIMAL COMBINATIONS AND ASSESSMENT VALUES FOR THREE

MOTIVATION TYPES 304

NOMENCLATURE

Symbol	Term	Unit
C_{inv}	Initial investment	€
C_{ec}	Specific equivalent carbon saving cost	€/kgCO_2
D	Post-retrofit energy demand	kWh
d_{pc}	Pre-cooling degree	
E_r	Final energy consumption reduction	kWh
E_r^*	Specific energy reduction	kWh/m^2
EC_r	Equivalent carbon emission reduction	kgCO_2
EC_r^*	Specific equivalent carbon emission	kgCO_2/m^2
f	Baseline energy demand-supply conversion factor	%
i	The serial number of combinations	
K-value	Thermal Conductivity	W/mK
l	Baseline energy demand	kWh
Lux	Lighting luminance	lux/m^2
MRR	Moisture Remove Rate	g/s
n	The serial nuber of alternative measures	
p	Possibility	
Q_C	Cooling Capacity	W
R-value	Thermal Resistance	m^2K/W
RH	Relative Humidity	%
s	Solar radiation	W/m^2
T	Temperature	℃

T_c	Specific cost payback periods	€/kWh
T_e	Specific energy payback periods	years/kWh
T_{ec}	Specific equivalent carbon payback periods	years/(kgCO_2/m^2)
X	Solution concentration	%

Greek letters

ε_{sen}	Sensible effectiveness	
ε_{lat}	Latent effectiveness	
ω_{eq}	Equilibrium humidity ratio	
ω	Demand calibration factor	%
μ	Energy demand-supply calibration factors	%
σ	Energy consumption	kWh
η_e	Energy reduction rate	%
η_e	Energy reduction rate	%
φ_{bills}	Post-retrofit annual energy bills	€

Subscripts and Superscripts

a	air
amb	Ambient
sol	Solution
e	Electricity
in	Inlet
mem	Membrane
out	Outlet

re	Renewable energy
R_r	Real discount rate
R	Interest rate
R_i	Inflation rate

Abbreviations

Abbreviation	Term
ASHP	Air Source Heat Pump
CNC	Cellulosic Nanocrystal Technology
COP	Coefficient of Performance
CHP	Combined Heat and Power
COMB	Combination
DOM	Decision-making Optimisation Model
DOE-2	Building Energy Use and Cost Analysis Software
DPP	Discounted payback periods
DHW	Domestic Hot Water
EPBD	Energy Performance Building Directive
EPC	Energy Performance Certification
EER	Energy Efficient Rate
EPS	Expanded polystyrene
ERP	Energy Reduction Package
GHG	Greenhouse Gas
GSHP	Ground Source Heat Pump
GWP	Global Warming Potential

HVAC	Heating Ventilation and Air Conditioner
IESVE	Integrated Environmental Solution Virtual Environment
KCOOH	Potassium Formate
MPF	Multi-objective Performance Factor
NPV	Net Present Value
NTU	Number of Heat Transfer Unit
PV	Photovoltaic
PVDF	Polyvinylidene Fluoride
PIR	Polyisocyanurate Insulation
PNC	Parameter Nonlinear Calibration
SPF	System Performance Factor
SC	Solar Collector
TRNSYS	Transient System Simulation Tool
TFA	Total floor area
VIP	Vacuum Insulation Panels
VG	Vacuum Glazing
WSHP	Water Source Heat Pump

List of Figures

Figure 1-1 *Thesis structure and chapter relations* 34
Figure 2-1 *EU residential building GHG emission and reduction rate from 2008 to 2017 (Data source: (Eurostat, 2016))* 38
Figure 2-2 *Equivalent primary renovation rate in 14 EU countries by the end of 2016 (Data source:)* 39
Figure 2-3 Single-family house percentage in total EU building stocks (Data Sources from (Haffner, September 2010)) 40
Figure 2-4 Classification of insulation materials according to materials (Papadopoulos, 2005, Aditya et al., 2017) 44
Figure 2-5 *Cross section of VIPs (Schiavoni et al., 2016)* 46
Figure 2-6 Comparative thermal conductivity measurements of VIP panels with degradation of vacuum pressure (Tetlow et al., 2017) 47
Figure 2-7 Window configuration with nano-silica aerogel 49
Figure 2-8 Relation between thickness and rendering cost 50
Figure 2-9 The example of direct (a) and indirect (b) SB-HPWH configurations 54
Figure 2-10 Retrofit cost/area of different levels in EU residential buildings . 67
Figure 2-11 Major retrofit investment in eight EU countries 67
Figure 2-12 Distribution of EPC building stock by label A-E (Data source: (Tadeu et al., 2015)) 70
Figure 2-13 Schematic cost optimal pathway 75
Figure 2-14 Simplified lumped-parameter building model (3R2C) (Andrade-Cabrera et al., 2019) 76
Figure 2-15 Lumped-parameter building model topology for detached house archetype (Andrade-Cabrera et al., 2019) 77
Figure 2-16 Lumped-parameter building model topology for mid-floor apartment archetype (Andrade-Cabrera et al., 2019) 77
Figure 3-1 E. ON house south-east façade experiment site 94
Figure 3-2 U-value test with existing wall construction 94
Figure 3-3 U-value of the existing wall of the E. ON house façade 95
Figure 3-4 U-value test with interior wall insulation with silica based vacuum insulation panels 100
Figure 3-5 U-value of silica based vacuum insulation panels (72 continuous nights) 100
Figure 3-6 Thermal comfort with silica based vacuum insulation panels (72 continuous nights) 101
Figure 3-7 U-value test with interior wall insulation with starch-based aerogel insulation panels 103
Figure 3-8 U-value of interior wall with starch-based aerogel insulation panels (72 continuous nights) 103
Figure 3-9 Thermal comfort with starch-based aerogel based vacuum insulation panels (72 continuous nights) 104

Figure 3-10 External and internal view of vacuum glazing 106
Figure 3-11 U-value of vacuum glazing (72 continuous nights) 106
Figure 3-12 Physical structure of PV VG-4L (a) (b) 108
Figure 3-13 The PV-VG prototype 109
Figure 3-14 Testing performance of PV VG-4L 111
Figure 3-15 PV electricity conversion efficiency with solar radiation 113
Figure 3-16 U-value of PV VG-4L in different time periods (a) (b) (c) 115
Figure 3-17 Outlook view of David House 116
Figure 3-18 Position of daylighting pipes in David House 116
Figure 3-19 Lighting performance with lighting pipes 118
Figure 3-20 Efficiency of daylighting pipe performance 118
Figure 4-1 Polymer hollow fibre liquid desiccant air dehumidification and cooling cycle. 122
Figure 4-2 Diagram of a domestic installation of Liquid desiccant dehumidification and cooling system. 123
Figure 4-3 Polymer hollow fibre dehumidifier and cooling system. 124
Figure 4-4: Flow chart of the solution method. 131
Figure 4-5 The test rig of the novel cross flow hollow fibre integrated evaporative cooling module (A) and the connections with the environmental chamber (B) 134
Figure 4-6 The 3-D model image of the hollow fibre module core design 134
Figure 4-7 Core structure of single unit for both evaporative cooling and desiccant dehumidification 136
Figure 4-8 Effect of inlet air temperature on outlet air humidity and solution temperature 142
Figure 4-9 Effect of inlet air relative humidity on outlet air humidity and solution concentration 143
Figure 4-10 Effect of air mass flow rate on outlet air temperature/humidity and solution concentration 144
Figure 4-11 Effect of solution mass flow rate on outlet air temperature/humidity and solution concentration 146
Figure 4-12 Effect of solution inlet temperature on outlet air temperature/humidity and solution concentration 147
Figure 4-13 Effect of solution concentration and inlet air temperature on outlet relative humidity. 147
Figure 4-14 Hybrid system COP with variables of inlet air temperature and relative humidity 149
Figure 4-15 Solar assisted heat pump system integrated in residential building. 150
Figure 4-16: Schematic diagram of solar assisted heap pump. 152
Figure 4-17: (a) Pressure - Enthalpy (P-h) and (b) Temperature – Entropy (T-s) diagrams of the therml cyle. 153
Figure 4-18 Test rig of the SAHP 158

Figure 4-19 Hot water storage tank 158
Figure 4-20 Solar radiation simulator and light regulator 160
Figure 4-21 Working sample of the thermodynamic panels 160
Figure 4-22 The relation between heating COP and plate surface temperature *Tp* 161
Figure 5-1 Concept of the EF-EC model 165
Figure 5-2 Breakdown and calculation process of EF-EC model 168
Figure 5-3 Sketch of the hybrid thermal and electrical energy flows in a single building scenario 169
Figure 5-4 Southern and Northern facade views for the case study building. 183
Figure 5-5 Study section and the part for retrofit intervention (the left half of the building) 183
Figure 5-6 Baseline model in IES VE 185
Figure 5-7 Floor plans for the case study building 186
Figure 5-8 Demand output loads by types 189
Figure 5-9 Schematic illustration for the selected individual retrofit measures 193
Figure 5-10 Uncertainty variation rates (UVRs) for the selected 30 retrofit combinations 198
Figure 5-11 Final energy inputs discrepancies compared with the IES VE simulation 201
Figure 6-1 Flowchart of the research structure 208
Figure 6-2 Case study building models (a) established in IES in combination with its adjacent building (left half is the research object) (b) 3D geometric wireframe view (c) On-site image 224
Figure 6-3 30-years average ambient weather conditions (a-solar radiation, b-temperature, c-wind velocity) 226
Figure 6-4 Initial Investment (II) under full-scale energy reduction rate (ERR) 230
Figure 6-5 Discounted payback periods (DPP) under full-scale energy reduction rate (ERR) 230
Figure 6-6 The relation between II and MPF under M1 type 232
Figure 6-7 The relation between the ERR and MPF under M2 type 234
Figure 6-8 The relation between DPP and MPF under M3 type 235
Figure 6-9 Optimal technologies from M1 to M3 236
Figure 6-10 Optimal technologies from M1 to M3 with 20% and 30% of baseline energy consumption as the input data 238
Figure 7-1 Retrofit example of a residential house with fast retrofit technologies 246
Figure 7-2 Post-retrofit renderings demonstration 246
Figure 7-3 Cycle of 'off-site manufacture & on-site assembly' retrofit implementation 247

List of Tables

Table 2-1 Multi-objective optimisation cases and optimisation scale..... 71
Table 2-2 Summary of the previous studies on building retrofit multi-objective optimisation based on different retrofit motivations and objectives 83
Table 3-1 Specific technical data of experiment equipment 93
Table 3-2 Measured parameters and uncertainties 97
Table 3-3 Lighting test equipment..... 116
Table 3-4 Actual thermal and economic performance of silica-based VIP.... 119
Table 4-1 List of parameters used in the simulations. 132
Table 4-2 Comparison between measurements and numerical for $ma = 57$ m^3/h..... 138
Table 4-3 Comparison between measurements and numerical for $ma = 114$ m^3/h..... 139
Table 4-4 Comparison between measurements and numerical for $ma = 171$ m^3/h..... 141
Table 4-5 Thermal COP for different inlet temperature and relative humidity 148
Table 4-6 Electrical COP for different inlet temperature and relative humidity. 148
Table 4-7: System geometric and thermal parameters and relevant thermodynamic properties (Leonforte et al., 2022) of the R134a refrigerant. 156
Table 4-8 Measurement devices and their accuracy..... 157
Table 5-1 Main parameters for the cost-optimal analysis of the proposed research 186
Table 5-2 Baseline monthly building energy consumptions based on the simulation results..... 187
Table 5-3 Summary of the selected energy retrofit measures 189
Table 5-4 Computing time on a single combination 194
Table 5-5 Model validation among real building energy consumption, IES VE simulation and EF-EC model..... 196
Table 5-6 Average calculation and absolute discrepancies using the Black-box model in deep energy retrofit prediction of single-family houses..... 202
Table 6-1 Weight assumption of five motivations 213
Table 6-2 Economic indicators and energy prices..... 221
Table 6-3 The baseline energy performance and validation..... 227
Table 6-4 The relations between EPC and ERR for the reference building... 233

1. Introduction

1.1 Research background

Under the Paris Agreement (Nations;, 2015), The European Commission has set up a clear target to reduce at least 40% of the greenhouse gas by 2030 and achieve carbon neutrality by 2050. Improving energy efficiency is one of the most crucial strategies to achieve this target. According to the International Energy Agency (Khatib, 2012), energy efficiency should be recognised as the 'first fuel', offering a win-win-win in lower emissions, lower energy bills and improved energy security.

Energy consumption in domestic buildings accounts for about 30% of Britain's total energy budget and 20% of UK greenhouse gas emissions (Change, 2015). A significant improvement in energy efficiency and the reduction of carbon emissions is urgently needed for Europe and the UK to decarbonise the building sector, limit its dependence on primary energy sources and reduce household energy bills. Building retrofit represents one of the most energy-efficient and affordable pathways to meet the common climate goals.

According to the English Housing Survey (Ministry of Housing, 2019), more than half (57%) of the UK's homes were built before 1965, making the building stock in the UK less energy efficient with high carbon emissions compared with other European countries (Lowe and Chiu, 2020). To meet the UK's climate change targets, the building sector will need to improve nearly every home in Britain with energy efficiency measures at a rate of more than 1.5 homes every minute between now and 2050 (2019). The selection of proper building retrofit

interventions is critically important to ensuring a cost-effective transition to a carbon-neutral and resilient society in the near future.

The increasingly severe energy crisis and the demand for improving building indoor environmental quality and comfort levels have triggered great incentives for accelerating the development of energy-efficient and innovative building technologies in the built environment sector.

Buildings are long-term assets that can have a life span of more than 50 years, and 75-90% of those standing today are expected to remain in use in 2050 (Commission). However, in Europe, building renovations are carried out at low demolition rates (0.1% per year) and low renovation rates (1.2% per year). Most of the existing buildings in Europe are not energy efficient (Ma et al., 2012, Webb, 2017, Rabani et al., 2017). According to Broin et al. (Project, 2013 January, Ó Broin et al., 2013), buildings in Europe consume about 40% of the total European energy usage and contribute to almost 36% of greenhouse gases. In order to comply with the Kyoto Protocol goals and help to decarbonize the European economy, the Energy Performance of Building Directive (EPBD) was established in 2002 (Commission, 2002) and updated in 2010 , setting strict targets for the building sector with the estimated 40% greenhouse gases reduction by 2030. To achieve such an energy target, the EU needs to boost the number of deep renovations and speed up the existing stock's renovation rate to above 2% annually . Within this context, many retrofit renovations have been made to existing buildings to reduce energy consumption (Tadeu et al., 2015), improve indoor thermal comfort and air quality (Psomas et al., 2016) and move towards Low or Zero Energy Buildings (Kylili and Fokaides, 2015, Desideri et

al., 2013). Comprehensive reviews on building retrofit have been presented by Ma et al. (Ma et al., 2012) and Mazzarela (Mazzarella, 2015).

According to ZEBRO2020 data (ZEBRA, 2015), the equivalent major renovation rate in 14 EU countries (Spain, Poland, Belgium, Romania, Italy, Sweden, Netherland, Lithuania, Czech Republic, Germany, Austria, France, Slovakia, Norway) by the end of 2016, has an average annual renovation rate of 1.10%, with the range varied from 0.08% (in Spain) to 2.40% (in Norway). In order to achieve European Union's policy goals, the rate of retrofitting has to increase from its current levels of 0.08% – 2.40% to at least 3% of the housing stock per year (Sandberg et al., 2016, Wilson et al., 2018).

1.2 Statement of the problems

Building retrofit has long been considered not only as the most effective approach to improve building energy efficiency, eliminate dependency on primary energy (natural gas, electricity) and reduce the associated carbon footprint but also as an evolving vehicle to continuously improve occupants' living standards (in the form of improved indoor comfort level, air quality and reduced noise level). These benefits, however, are not well articulated by policymakers and in building sectors and therefore are often not well received by the key stakeholders (i.e. homeowners, landlords, investors, SMEs). The obstacles to building retrofit are also multi-dimensional and vary primarily according to the building typologies, energy usage by different occupants, and climatic conditions.

Moreover, it is apparent that several limitations exist in multi-objective

optimisation regarding the motivations for building retrofit, which can be summarised in the following perspectives:

1) Lack of in-depth and comprehensive understanding of the homeowners' motivations to undertake building retrofit. Most research focused on retrofitting to improve building energy efficiency and energy-cost optimum solely for self-living purposes. However, little attempt has been made to investigate other retrofit motivations such as retrofit for sale, rental, and investment.
2) Lack of inclusive decision-making models considering comprehensive retrofit objectives with homeowners' engagement. Energy savings is the primary goal of the research works. However, other objectives (such as energy bill reduction, financial investment to improve home values in the building market, and the requirements under EPC regulations) are addressed in the practical retrofit projects, which affect the retrofit strategies and final decision-making process dramatically.

In recent years, researchers have identified two methods to perform post-retrofit Building Performance Simulation (BPS): data-driven (or Black-box model (Deb and Schlueter, 2021)) based method and physics-based (or White-box model (Hamdaoui et al., 2021)) based BPS method. Substantial research efforts (Li et al., 2021) have been made in the literature by applying both methods to perform BPS to predict the impact of various Energy Retrofit Measures (ERMs) on the economic, environmental, and social benefits of building renovations.

The limitations for the applications of both White- and Black-box models under the deep retrofit context can be categorised into four areas:

1) Inadequate data requirement – Numerous training are required to generate the Black-box model for the pre-retrofit design of each building, especially in dwellings, due to the lack of consideration thorough building specifics (fabric construction, floor plans), external factors (local weather conditions, shadings) and occupants' behaviours (energy usage, occupancy schedule, energy sources and retrofit preferences), which will significantly affect the hidden connections in the Black-box models;
2) Neglect of coupling effects in deep energy retrofit combinations – Low accuracy of energy performance prediction occurred in deep energy retrofit combinations using the Black-box model due to neglect of the coupling effects in versatile retrofit measures, resulting in system mismatch issues;
3) Lack of complex heat transfer phenomena in single-family houses – Differ from office and apartment buildings, single-family houses have diverse geometry and distinctive occupancy behaviours. Low accuracy presents in building energy prediction of single-family houses using the Black-box model, attributed to the lack of complex heat transfer phenomena between the heating terminals and indoor comfort requirements;
4) Time-consuming – The White-box models that attempt to simulate energy transfer processes to a higher accuracy level dynamically are considerably more computationally expensive. Quasi-steady state models can be used to reduce computational times but often at the expense of accuracy. A trade-off between simulation accuracy and

complexity in the computational process needs to be carefully addressed.

Therefore, the above-mentioned two types of BPS models cannot fully address the crucial research challenges in optimising deep energy retrofit combinations rapidly and accurately for single-family houses.

1.3 Aims and objectives

Based on research background and current challenges, this PhD research aims at investigating a rapid and accurate Energy-Flow based Ensemble Calibration model for energy prediction of deep energy retrofit in single-family houses using the high-efficient sustainable retrofit technologies, which will be integrated with homeowners' engagement in a novel Motivation-Objective-Criteria (MOC) based retrofit approach to optimize the final retrofit decisions.

In comparison to the building retrofit cost-effective prediction and assessment model in previous research, this PhD study will explore the use of a novel Energy-Flow based Ensemble Calibration (EF-EC) model to tackle this issue for rapid and accurate energy-reduction calculation with comprehensive energy retrofit combinations for deep energy retrofit in single-family houses. Besides, an innovative Motivation-Objective-Criteria (MOC) approach will be applied for the decision-making optimisation of retrofit measures considering homeowners' engagement and their retrofit motivations.

In achieving the aims, a number of specific objectives have been set out as detailed below:

1) Evaluating current residential building energy performance, retrofit rates,

retrofit technologies, energy prediction models and optimisation methods;

2) Modelling and experimental analysing the high-efficient retrofit technologies;

3) Establishing an innovative Energy-Flow based Ensemble Calibration (EF-EC) model to rapidly and accurately predict the post-retrofit energy performance for deep energy retrofit in single-family houses;

4) Establishing an innovative retrofit Motivation-Objective-Criteria (MOC) approach integrating homeowners' engagement for retrofit decision-making optimisation.

1.4 Novelty of the Research

1.4.1 Performance determination of advanced retrofit technologies

The thermal and electrical performance of advanced retrofit technologies are analysed and verified using modelling and experimental analysis. The energy performance of envelope insulation technologies such as vacuum insulation panels, aerogel insulation panels, vacuum glazing panels and PV vacuum glazing panels and efficient daylighting pipes are not included in the standard database in most building simulation software. Moreover, the energy performance of innovative heating, cooling and dehumidification systems is not fixed values, depending on the environmental parameters such as solar radiation, ambient air temperature, relative humidity, and wind velocity. According to the investigation in this research, the correlated energy performance calculation formulation is established.

1.4.2 Rapid and accurate prediction of deep energy retrofit performance in single-family houses

this research proposes a novel Energy-Flow based Ensemble Calibration (EF-EC) model by integrating the complex heat transfer models of the White-box approach, the layered node-connection framework of the Black-box approach, and the baseline energy performance simulated in the BPS software. This model can be employed to examine and predict the energy performance for all possible retrofit combination interventions from dual perspectives (energy and cost-optimal), with reduced computation time and effort. Deeply rooted in the White-box approach, the energy transfer model is decoupled into transient thermal and electrical energy flows rather than dynamic building simulation software. Besides, the flow principles are established in each layer between nodes connection from energy inputs to demand outputs in the framework of the Black-box approach, thereby avoiding cumbersome computational efforts in building energy simulation software.

In this way, instead of establishing and running countless potential retrofit combinations in IES VE dynamic simulation, which are extremely time-consuming, a rapid and transient numerical calculation could be achieved.

1.4.3 Homeowners' retrofit motivations, objectives, and criteria could be considered in the decision-making process

In general, the decision-making criteria and objectives are optimised separately in the literature (Seddiki et al., 2016, Khadra et al., 2020, Montana et al., 2020), and homeowners' motivations are ignored or not carefully defined in these

research works. In order to tackle this and promote bottom-up building renovation which will be motivated by the homeowners, this study establishes an innovative Motivation-Objective-Criteria (MOC) approach integrated with homeowners' engagement to support the decision-making process for selecting building retrofit measures, according to different homeowners' retrofit motivations, objectives and criteria. Adopting the MOC approach at the pre-retrofit design and decision-making process of building renovation will enable the key stakeholders (users, employers, and suppliers) with access to transparent and well-quantified energy, economic, environmental, and social benefits, thereby immensely stimulating the future Renovation Wave (Commission) driven by the end-users.

1.5 Scope of the research

In this study, the decision-making optimisation model of comprehensive energy-retrofit combinations is investigated, focusing on the residential building retrofit to help homeowners to make decisions on various retrofit technology combinations, which considering the priority/requirement of the homeowners to different motivation aspects from energy reduction rate, carbon reduction rate, initial investment, discounted payback periods, and post-retrofit annual energy bills. Several case studies are conducted to test the performance of the decision-making optimisation model in different climates, building types, construction years, which could also give instructions to specific types to most of the building conditions in the EU and UK.

1.6 Research methodology

In this thesis, the methodology is mainly based on the following stages:

1.6.1 Background investigation and literature review

The residential building retrofit status in the EU/UK and the main challenges and motivations for residential building retrofit have been studied and compared. In the literature review, the state-of-the-art of innovative high-performance retrofit technologies from the energy demand side and energy supply side has been investigated to understand the development and the energy reduction potential. Besides, previous research on building energy prediction models and multi-objective optimisation algorithms have been reviewed to analyse the advantages and drawbacks of existing modelling design concepts, which could help to design and develop the foundation of the potential calculation model.

1.6.2 Modelling and experimental analysis of retrofit technologies and performance modification

The experimental test is conducted on real building sites to validate and modify the modelling performance with the potential environmental impact factors, such as ambient wind velocity, solar radiations, ambient temperatures, ambient relative humidity, etc. With the performance modification in real conditions, the modified performance coefficients/functions will be used in further energy calculation modelling work.

1.6.3 Model establishing, validation, and uncertainty analysis

A novel Energy-Flow based Ensemble Calibration (EF-EC) model is established. This model consists of three layers 1) input neurons, 2) complex heat and electrical transfer models, and 3) output neurons. By replacing the layer

of hidden neurons with complex heat and electrical transfer models in conventional Black-box models, the coupling effects in deep energy retrofit combinations and complex heat transfer phenomena are thoroughly considered in this issue. Besides, the computational efforts are substantially reduced with only a few simulations of baseline heat and electrical demands and heat and electrical coefficients of individual retrofit measures conducted by building performance simulation software. A semi-detached 1960s Italian single-family house is selected as a case study to validate this model by comparing the calculation results with real energy consumption of baseline and post-retrofit scenarios.

1.6.4 Inclusive Motivation-Objective-Criteria (MOC) approach integrating homeowners' engagement

An inclusive Motivation-Objective-Criteria (MOC) approach is established, aiming to bring forward optimised decision-making for building renovation, accommodating different homeowners' retrofit motivations, objectives and criteria. Retrofit motivations are categorised into three typical types: 1) Self-living, 2) Rental or sale, and 3) Investment, under five objectives: Energy Reduction Rate (ERR), Initial Investment (II), Discounted Payback Period (DPP), Bills Reduction Rate (BRR) and Carbon Reduction Rate (CRR). A novel Multi-motivation Performance Factor (MPF) concept is proposed to assess the holistic post-retrofit building performance with comprehensive retrofit combinations. The weighted sum method (WSM) is adopted to evaluate the comprehensive energy-retrofit combinations for analysing and discussing the impacts of different motivations weights on selecting retrofit technologies and combinations. A UK semi-detached house is applied as the reference building to

investigate the impact of homeowners' engagement on the decision-making of various retrofit measures.

1.7 Thesis structure

The thesis includes seven chapters with relations illustrated in Figure 1-1.

The work details are summarized below:

Chapter 1: The research background are provided with a statement of the current problems in recent research, and then the aims and objectives, novelty, scope and methods of the thesis are introduced.

Chapter 2: The literature review is summarized in six stages, including 1) residential building retrofit status, especially the deep energy retrofit problems in single-family houses; 2) advanced building retrofit technologies; 3) Existing white- and black- box based building energy performance prediction models; 4) willingness-to-pay and EPC labelling for residential buildings; 5) multi-objective optimisation algorithms; 6) literature review on homeowners' engagement.

Chapter 3: Innovative envelope retrofit materials for energy demand reduction are tested on a field scale to figure out the key performance indicators, with test objects of façade insulation, glazing insulation, and efficient daylighting devices. Besides, according to the change of environmental impact factors, the performance coefficients and functions will be modified with those main variants, which can be applied in the modelling work in Chapters 5-6.

Chapter 4: Innovative systems for heating, cooling and dehumidification are

investigated with modelling and experimental test to figure out the key performance indicators, including 1) desiccant cooling and dehumidification; 2) Solar assisted heat pump. Besides, according to the change of environmental impact factors, the performance coefficients and functions will be modified with those main variants, which can be applied in the modelling work in Chapters 5-6.

Chapter 5: An innovative concept proposed with a novel Energy-Flow based Ensemble Calibration (EF-EC) model to predict the deep energy retrofit energy-economic performance rapidly and accurately in single-family houses. Besides, a semi-detached 1960s Italian single-family house is selected as a case study to validate this model by comparing the calculation results with real energy consumption of baseline and post-retrofit scenario

Chapter 6: This chapter establishes an innovative retrofit Motivation-Objective-Criteria (MOC) approach to support the decision-making process for selecting building retrofit measures, which adapts to different homeowners' retrofit motivations, objectives and criteria. A British semi-detached single-family house is applied as the reference building to demonstrate the proposed MOC decision-making approach to select comprehensive energy-retrofit combinations with and without the homeowners' engagement.

Chapter 7: This chapter presents conclusions and discussions of the retrofit technologies, EF-EC energy prediction model and MOC retrofit optimisation approach. This section will also give further work and suggestions by introducing some future research directions and some issues identified in the research.

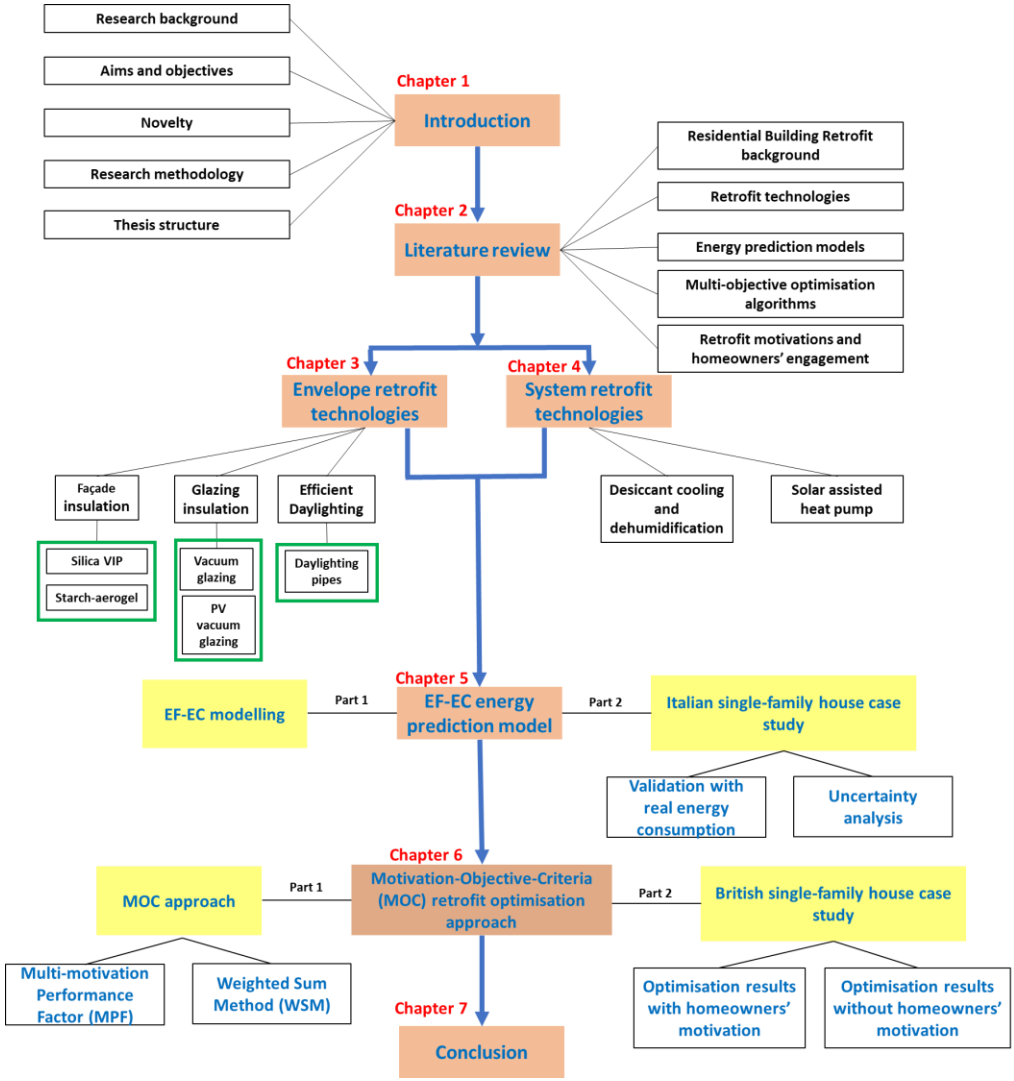


Figure 1-1 *Thesis structure and chapter relations*

2. Literature review

2.1 Introduction

The Europe Commission is calling for a climate and carbon-neutral society in 2050 with strategies by the end of November 2018. The strategies show policies and actions to achieve the short-term (2030), mid-term (2040) and long-term (2050) requirements, considering both the overall aims of the European Union and the variation of each country (European Commission, 2007b). Besides, the EU leaders also set three European 2020 targets by the end of 2007, and enacted in 2009, which requires 1) 20% reduction of greenhouse gas emission compared with 1990 level; 2) 20% share of renewable energy in the final energy consumption; 3) 20% improvement in energy-efficient (European Commission, 2007a). Eurostat has collected the data of energy and carbon emissions in each specific section from 1990. According to the record (Eurostat, 2016), the greenhouse gas emission level in 1990 was approximately 5720 Mton $CO_{2,eq}$, which is calculated as a total quantity of EU 28 countries. Following the long-term 2050 roadmap of the European Parliament and the European Council, the Commission is aimed at reducing greenhouse gas emissions by 80-95% compared to 1990, and keeping the global temperature increase to below 2°C and pursue efforts to keep it to 1.5°C , which is in line with the Paris Agreement (EUROPEAN COMMISSION, 2011). Therefore, according to the requirements of the 2050 roadmap to a climate-neutral EU target, the Energy Performance of Buildings and Directive (EPBD) proposed clear guidance with policies, indicators, and investment decisions to support the achievement of the short-term (2030), mid-term (2040) and long-term (2050) targets, by decarbonise the

building stock, which is approximately 36% of all equivalent CO_2 emissions (Eureopean Commission, 2018) by the end of 2050 in EU countries.

Residential buildings have a significant impact on the overall EU carbon emissions. Various intervention strategies have been investigated to promote energy-efficient and cost-effective research to reduce carbon emissions in residential buildings. However, efficient retrofit technologies and optimized decision-making mechanisms have not been fully understood in existing studies. Therefore, this chapter will conduct a literature review on the retrofit status, existing advanced retrofit technologies, multi-criteria assessment methods and optimisation methods for decision-making of the residential building retrofit combinations.

2.2 Residential building retrofit background

Retrofit is the introduction of new materials, products and technologies into an existing building to reduce the energy needed to occupy that building. However, renovation or refurbishment often indicates repair or aesthetically enhancing a building without aiming to reduce its energy use (Baeli, Oct 2013).

In this context, the term ‘net-zero carbon’ has started to enter the mainstream. Businesses, government and civil society are all grappling with what net-zero carbon will mean for them and how it can be achieved in practice (UK-GBC, 2019). In late 2018, An IPCC special report on the impacts of global warming of 1.5 ℃ above pre-industrial levels and related global greenhouse gas emission pathways, in the context of strengthening the global response to the threat of climate change, sustainable development, and efforts to eradicate poverty (Intergovernmental Panel on Climate Change, 2018). The World Green Building Council is catalysing the construction and property industry to lead the transition

to a net-zero carbon built environment through its Advancing Net Zero campaign, which the UK Green Building Council (UKGBC) has embraced and adopted for a UK context (UK-GBC, 2019). In the UK, the operation of buildings accounts for around 30 per cent of emissions, mainly from heating, cooling and electricity use (Thalfeldt et al., 2018).

2.2.1 Building retrofit status in EU and UK

According to the commission's assessment indicator, an average of 3% stock retrofit rate (EUR-Lex, 2019) is a minimum requirement to achieve the overall energy-efficient target. Therefore, existing buildings must have a significant deep retrofit with high-efficient alternative measures, and meanwhile, address the indoor environmental conditions, which helps to transform the existing properties into nearly zero-energy buildings in 2050. However, the increasing living standards need final energy consumption, which needs high energy efficient interventions to exist buildings to decouple the increasing primary energy consumptions with the growth of indoor comfort levels.

As the Energy Performance of buildings and Directive analysed, 36% of equivalent carbon emission is responsible by building stock. Therefore, it is critical to reducing the carbon emission in the building section (EUR-Lex, 2018). Figure 2-1 indicates the EU residential building greenhouse gas emission and its reduction rate from 2008 to 2017, collected after the 2020 climate strategy made by the European Union. As shown in the figure, carbon emissions reduced 11.4% to 875 Mton $CO_{2,eq}$ in 2014 compared by 2008, which accounts for 19.8% of the overall EU carbon emission. However, with the growth of the EU economy, the carbon emission of the residential building stock increased from 875 (2014) to 933 (2017) Mton $CO_{2,eq}$, which indicates the building energy efficiency

improvement do not meet the requirement of the reduction of the carbon emissions. Besides, at the end of the year 2017, only 5.6% of the GHG emission reduction in the residential building section and accounts for 20.6% of the overall GHG emission in the EU, which is far from the 20% energy efficiency target in the 2020 climate plan. Therefore, it is crucial to understand the residential building stock and its retrofit market.

The building stock can be categorized into two parts, including residential and non-residential sections, by the function of the property use. The non-residential section includes public buildings, office buildings, industrial buildings, commercial buildings, educational buildings, health buildings, which have different features from ownership, age of people, occupancy, time of use, specific requirements for temperature and humidity. However, the residential buildings are different from the non-residential buildings with the retrofit funding supplied by the owner, which makes them different in the retrofit process.

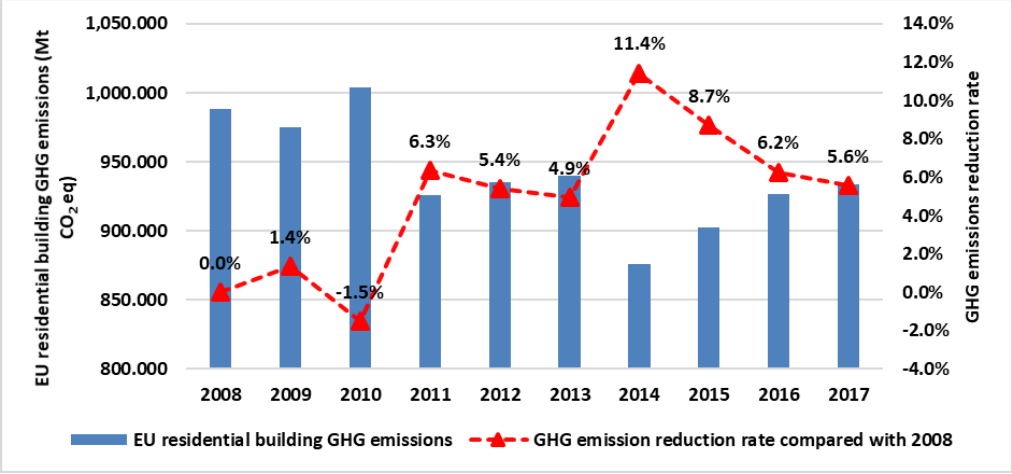


Figure 2-1 *EU residential building GHG emission and reduction rate from 2008 to 2017 (Data source: (Eurostat, 2016))*

Figure 2-2 indicates the equivalent primary renovation rate in 14 EU countries (Spain, Poland, Belgium, Romania, Italy, Sweden, Netherland, Lithuania, Czech

Republic, Germany, Austria, France, Slovakia, Norway) by the end of 2016, and the renovation rate is also described in the left map with blue colour from light to dark, which represents the renovation rate from low to high. As shown in the figure, EU-14 has an average annual renovation rate of 1.10%, varying from 0.08% (in Spain) to 2.40% (in Norway). However, even the highest renovation rate in Norway do not meet the required EU target of 3% annually. Therefore, it is significant to have a deep understanding of the barriers that changeling the residential building renovation rate,

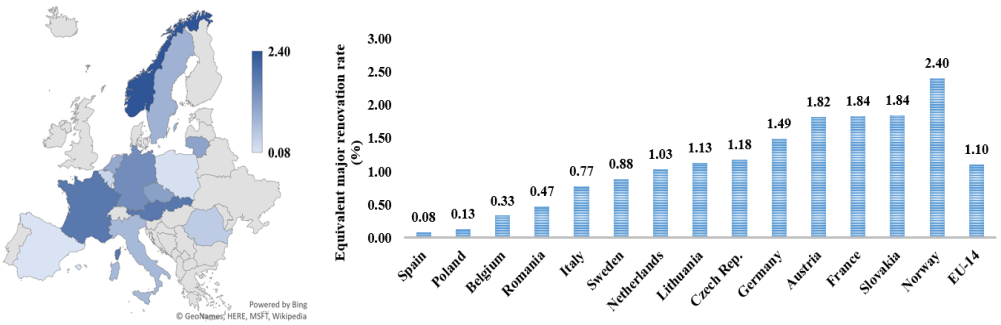


Figure 2-2 *Equivalent primary renovation rate in 14 EU countries by the end of 2016 (Data source:)*

2.2.2 Deep energy retrofit in single-family houses

From Economidou's research (Economidou et al., 2011), a share of 75% of useful floor space in the European building stock is residential buildings. According to the Building Performance Institute Europe (BPIE) study (iBRoad, June 2020), the residential building stock can be classified into single-family houses (68%), multi-family houses (24%) and apartment blocks (8%). A single-family house is referred to as a house designed for one family to occupy where it is meant to be occupied as one dwelling unit (Fontan, Feb 6, 2021) with approximately 54% (iBRoad, June 2020) of such building stock constructed before the 1970s whose energy efficiency are poor with high consumption.

Mayer et al. (Mayer et al., 2022) revealed that little attention has been paid to retrofit strategies for single-family houses in previous studies which have been addressed in recent years. As indicated in Figure 2-3, most European countries have a high percentage of single-family housing stock. And it is done by the property owners to implement retrofit decisions, which are often very complicated involving the considerations of the initial cost, energy savings and payback period.

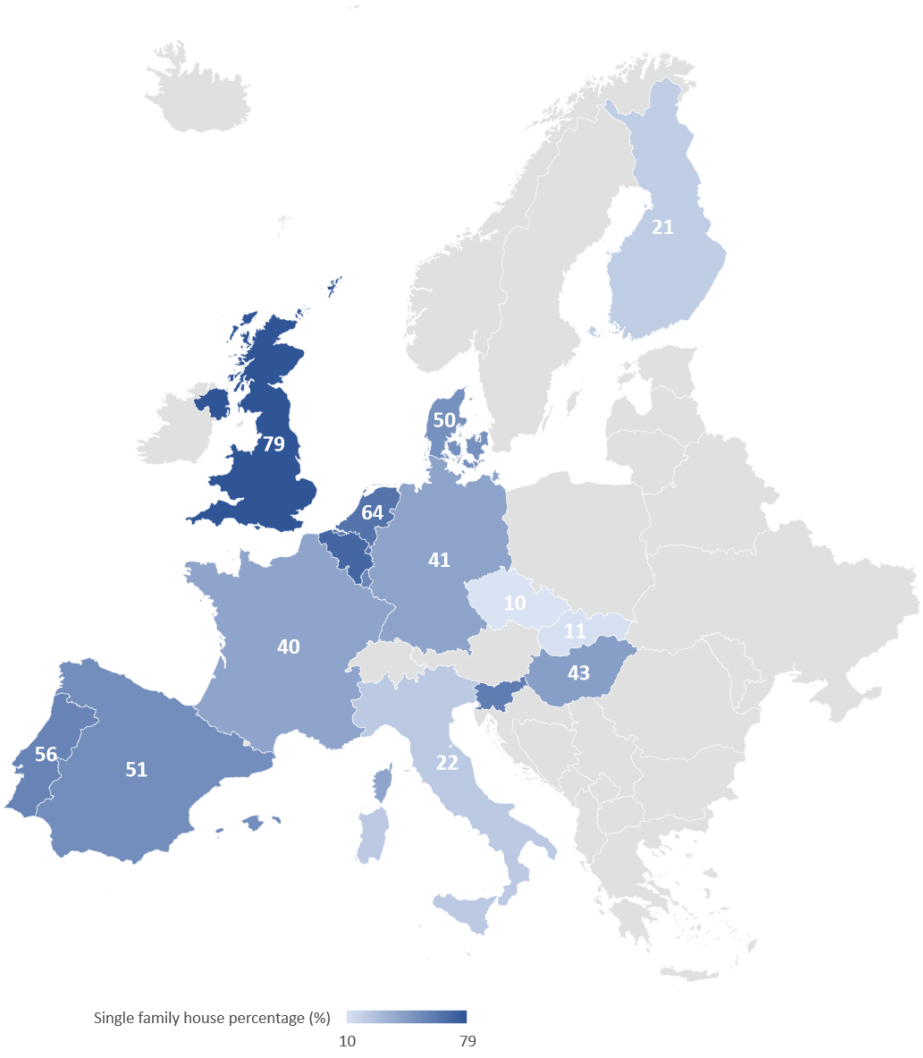


Figure 2-3 Single-family house percentage in total EU building stocks (Data Sources from (Haffner, September 2010))

Currently, the majority of the building retrofit projects in the EU are aiming at improving the building thermal performance, under the current Renovation Wave promoted by the European Commission (SIMSON, 18/03/2021) as part of its strategic energy plans to improve the energy efficiency of the existing building stocks (Ma et al., 2012). In the UK, for example, this renovation wave has seen a steep decline in renovation rates since 2013 due to a decrease in the "low-hanging fruits" (i.e., building stocks with poor thermal performance) and lack of funding for deep renovation (Business, 2017). The Energy Performance of Buildings Directive (EPBD) (Hulme) promoted the subsequent “deep energy retrofit” incorporating active and renewable retrofit measures, which is quite challenging to realise, with low financial incentives and user awareness.

The International Energy Agency (IEA)-EBC Annex 61 team (Zhivov and Lohse, 2021) has proposed the following definition of Deep Energy Retrofit (DER): DER is a major building renovation project in which site energy use intensity (including plug loads) has been reduced by at least 50% from the pre-renovation baseline, leading to the improvement of indoor environmental quality and comfort. Meanwhile, the Energy Department from the European Parliament (Commision, 2016) stated that the average initial investment cost for an energy reduction of 60%-90% during the renovation stage is 330 €/m^2. In 2018, the recast EPBD ((EU), 30 May 2018) integrated several stringent guidance and a series of measurable milestones between 2030 and 2040, intending to accelerate the agenda of DER in European building stocks. As indicated by IEA Annex 56 (Agency), the achievement of near-zero primary energy consumption as a result of DER would often require significantly high initial investment costs, which are primarily unacceptable for homeowners and investors. This could be manifested

by the study of (Zhivov and Lohse, 2021), which showed that the energy-saving potential could only reach averagely around 66.4% for the selected twenty-six DER building projects implemented in the world. Besides, one DER project of a detached dwelling in Greece conducted by Fabrizio et al. (Ascione et al., 2019) indicated that the initial investment cost in the renovation stage is 406 €/m^2, which is 23 % higher than most of the building renovation projects conducted in Europe. The case study of a low-rise multi-family apartment in Sweden manifested by Ambrose et al. (Dodoo et al., 2017) indicated that the retrofit investment cost is 68 % higher than the EU standard. In Kai's research (Streicher et al., 2020), the initial investment cost of a detached dwelling in Switzerland is 64 % higher than the standard with 540 €/m^2. Likewise, two high-rise apartments in Estonia (Kuusk et al., 2014) and Denmark (Morelli et al., 2012) have been studied with a similar inflation trend of 8% and 11% with 357 €/m^2 and 366 €/m^2, respectively. Therefore, the challenge remains in identifying the cost-efficient equilibrium between a decarbonised energy supply and reducing the final energy consumption in building stocks, which creates a massive bottleneck for the uptake of DER in the building sector. Moreover, the recognition of DER by the end-users and their willingness to adopt DER is not well stimulated and incentivised.

Therefore, the deep energy retrofit in single-family houses should be carefully addressed to improve the building energy efficiency. In recent years, researchers have identified two methods to perform post-retrofit Building Performance Simulation (BPS): data-driven (or Black-box model (Deb and Schlueter, 2021)) based method and physics-based (or White-box model (Hamdaoui et al., 2021)) based BPS method. Substantial research efforts (Li et al., 2021) have been made

in the literature by applying both methods to perform BPS to predict the impact of various Energy Retrofit Measures (ERMs) on the economic, environmental, and social benefits of building renovations.

2.3 Building retrofit technologies

Building energy demand reduction retrofit in the cold climates is very important, which requires excellent attention before starting energy supply retrofitting steps to reduce the capacity/sizing of energy supply systems and increase economic performance. Demand retrofit is mainly focused on reducing the energy load in the aspects of heating, cooling, and electricity for lighting and other electronic appliances. Envelope insulation and airtightness/ventilation improvement play a significant role in reducing the heating and cooling load. Electricity load is mainly focused on increasing the daylighting usage and energy efficiency of electronic appliances. This section will illustrate the research status and analyse the pros and cons of existing demand retrofit technologies.

2.3.1 Passive retrofit technologies

Space heating and cooling energy account for up to 60% of overall energy consumption (Pérez-Lombard et al., 2011) in traditional residential building stocks in cold and temperate climates. To reduce the heating/cooling demand requires efforts of 1) improvement of the envelope insulation including walls and glazing; 2) increase of the airtightness and reduce the natural ventilation; 3) installation of heat recovery system to mechanical ventilation devices; 4) installation of the control system for temperature, humidity and CO_2.

Envelope insulation can be categorized into four types according to the materials and compositions, which are mainly organic, inorganic, combined-material and new technology material, as structurally shown in Figure 2-4.

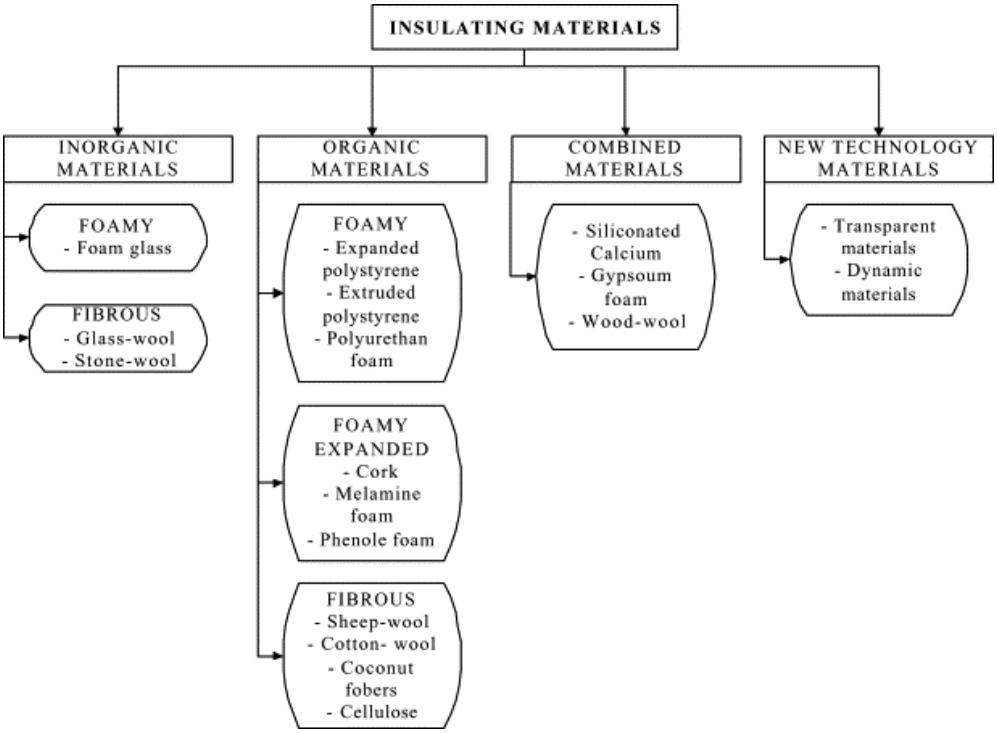


Figure 2-4 Classification of insulation materials according to materials (Papadopoulos, 2005, Aditya et al., 2017)

From the perspective of insulation materials, to achieve a U-value of 0.1 $w/m^2 \cdot k$ for passive/low-carbon house retrofit ((BPIE), October 2011), most of the insulation materials of external wall installation has a maximum thickness regulation to avoid occupation of the street spaces and street/external wall view due to regulations of the local committee. Moreover, due to the regulations and conservations to the external wall, most internal wall insulation is applied using high-performance insulation materials. However, insulation thickness is again caused problems of internal space reduction due to insulation work. The commercial insulation materials may not satisfy the increasingly improved

retrofit requirement, which requires research and development of advanced retrofit materials with 1) low thickness, 2) low-payback periods, and 3) high insulation performance.

To cope with the problems of using conventional demand retrofit technology on external wall insulation, recent researchers have designed and developed several innovative insulation materials to reduce the building demand by application on the building envelope. Apart from building facade retrofit, existing window glazing upgrading (Ariosto et al., 2019) and airtightness improvement are also essential methods to enhance the building thermal performance. The innovative advanced technologies focused on four main types, vacuum insulation panels, aerogel insulation panels, vacuum insulation glazing and PCM insulation panels.

2.3.1.1 Vacuum insulation panels

Nowadays, with physical size reduction from micro-structure to nanostructure, more research focuses on the aerogels and silicon-based vacuum insulated panels (VIP) technologies due to their low thermal conductivity with approximately 0.005-0.015 $w/m \cdot k$ benefits from the Knudsen diffusion phenomenon (Chen et al., 2015b). VIPs are constituted by a core material installed with getters, desiccants and opacifiers and covered by a multilayer envelope (as shown in Figure 2-5). Furthermore, usually, the most common core material is fumed silica, and also polyurethane, expanded polystyrene, silica aerogels, expanded perlite and their mixtures, and also glass fibre can be used.

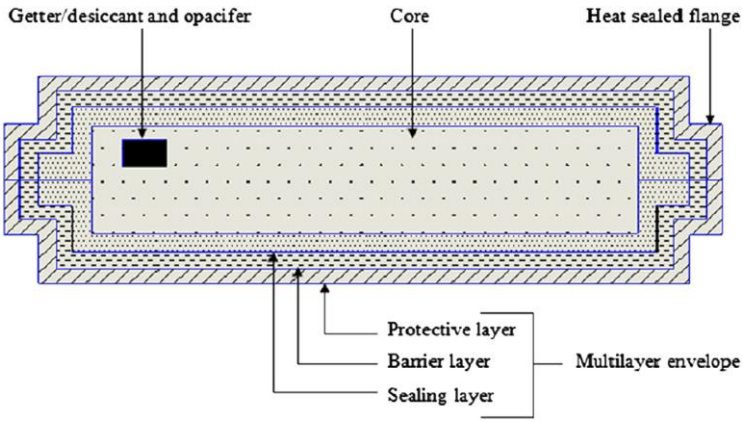


Figure 2-5 *Cross section of VIPs (Schiavoni et al., 2016)*

The most commonly used material of VIP panels is fumed silica with thermal conductivity of 0.0037-0.0041 $w/m \cdot k$ when the inside pressure is at 10 Pa and core density between 140 and 180kg/m^3 (Schiavoni et al., 2016). However, there are three main challenges for the VIP technology, including 1)expensive cost due to its high energy consumption in silica purification process; 2) low sustainable properties because of ageing and degradation, and also it is not biodegraded and not able to be recycled; 3) the water vapour may be condensed at the surface of VIP panels, which increases the risk of the wall damage. Therefore, a further investigation focuses on substituting with a similar physical structure, also called the cellulosic nanocrystal (CNC) technologies. The CNC based VIP panels have a slightly higher thermal conductivity of 0.0117-0.0135 $w/m \cdot k$ when the inside pressure is at 10 Pa and core density between 127 and 170kg/m^3 (Schiavoni et al., 2016). However, it is limited to typical manufacturing using acid-catalysed hydrolysis, which high-efficiency separation technologies need to be improved. The ageing and degradation problems are especially significant for VIP panels and must be paid enough attention to when applying these materials in building insulation. For multi-layer

envelops, VIPs have finite air tightness leading to degradation in pressure on aging, with a typical annual 1 mbar loss. If the pressure inside the panels is attained the atmospheric pressure with 1 bar at the end of its functional life, the thermal conductivity of fumed silica based VIP is $0.02 w/m \cdot k$, approximately half that of alternatives, which is showed in *Figure 2-6*. It is clear that the thermal conductivity of glass fiber-based panel is around $0.039 w/m \cdot k$, and CNC based panel is around $0.036\ w/m \cdot k$, PU form based panel is around $0.032\ w/m \cdot k$ when the inside pressure reaches 1 bar. Especially after using the VIP insulations for ten years, the silica-based Panel is still around $0.005\ w/m \cdot k$. However, the glass fibre based panel reaches $0.020\ w/m \cdot k$, and the CNC based panel reaches $24\ w/m \cdot k$, and the PU form-based Panel reaches $0.027\ w/m \cdot k$.

Bjørn Petter Jelle (Baetens et al., 2010) did a survey that the cost of mineral wool insulation will be around $20€/m^2$ per 35cm thick layer. However, if the market considers the same insulation performance, the equivalent VIP systems need $200€/m^2$ per 6cm thick layer (Jelle, 2011).

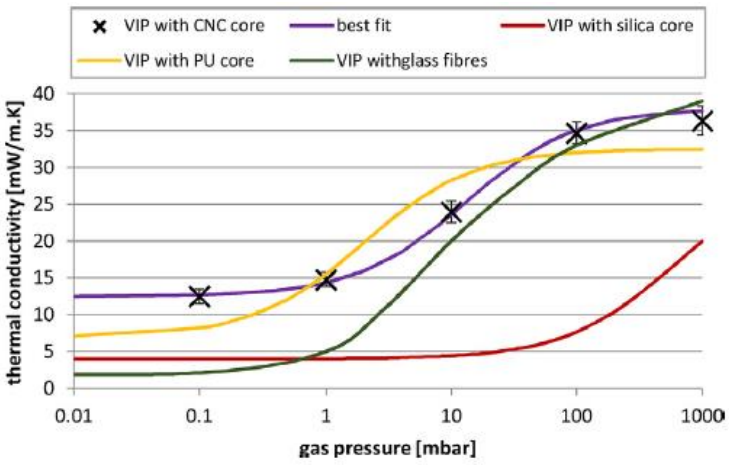


Figure 2-6 Comparative thermal conductivity measurements of VIP panels with degradation of vacuum pressure (Tetlow et al., 2017)

2.3.1.2 Aerogel insulation panels

Aerogels are produced by extracting the liquid component from silica gels without collapse of the solid matrix in the gel (Wikipedia, 2011). Based on the Knudsen effect, thermal conductivity becomes very low. Due to its high prosperity, the mechanical strength of aerogels is respectively low. It is available in high performance required application, however, it cost much. Current research is aimed at two main categories:

- Reduce the cost to manufacture aerogel
- Windows and skylight using due to its nature of translucency

Recent years have seen significant advances in the development of innovative materials and products such as aerogel-based aggregate coatings (Ghazi Wakili et al., 2014) and Vacuum insulation panels (Alam et al., 2017), due to their superior thermal performance and less space occupancy, which is extremely valuable for the applications as thermal insulation in building renovation. Biswas et al. (Biswas et al., 2019) evaluated numerically and experimentally the energy-saving potential of applying Vacuum insulation panels (VIP) onto the exterior wall for a single-story building in a cold climate. The heat flow variations for both pre-retrofit and post-retrofit scenarios were compared, with heat energy saving around 46%. To mitigate thermal bridges, five different aerogel-based thermal coatings were produced by Fantucci et al. (Fantucci et al., 2019), and their thermal conductivities were measured experimentally in the laboratory. The optimal product was chosen and applied to the external wall of an existing building in Turin, Italy. The results indicated that around 1.6 ℃ of internal temperature increase could be observed after the renovation. Aitana Sáez de

Guinoa investigated the a nano-technological aerogel-based panel for building insulation. As a result, due to its low thermal conductivity (0.015 W/mK), only 10 mm aerogel based insulation panel is needed to achieve the same level of insulation of 25 mm thickness of standard Expanded Polystyrene Panel. Muhammad Abdul Mujeebu and et al. investigated the Energy performance and economic viability of nano-aerogel glazing and vacuum insulation panels in multi-story office building. The results indicate that nano-aerogel glazing windows could save 14% energy compared to double glazing windows. The window configuration with nano-silica aerogel is shown in Figure 2-7.

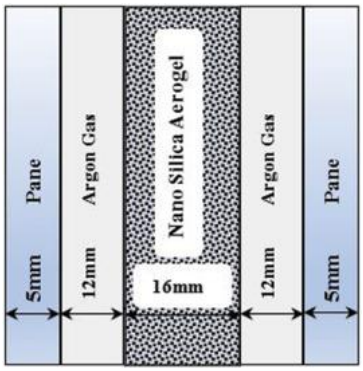


Figure 2-7 Window configuration with nano-silica aerogel

Mohamad Ibrahim and et al. investigated Building envelopes with aerogel-based insulating renderings from both experimental and numerical study. Results show that the optimum rendering thickness is 1.7–4.4 cm, and the payback period is in the range of 1.4–2.7 years, depending on the climate. The relation between thickness and rendering cost is illustrated in Figure 2-8.

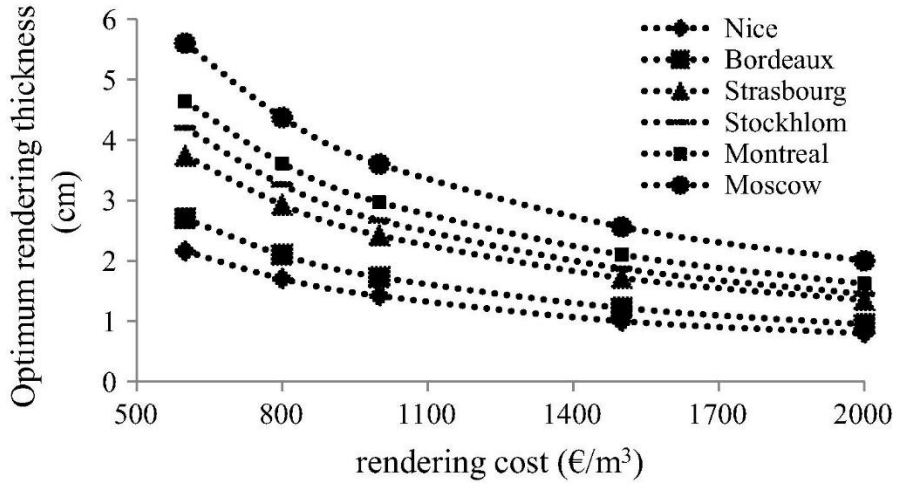


Figure 2-8 Relation between thickness and rendering cost

2.3.1.3 Vacuum glazing windows

In recent years, researchers have shown interest in the study of vacuum glazing technology. Innovative designs were developed and researched. Among them are; Bao et al. (2014), who has introduced a novel hybrid vacuum/triple glazing system in which a vacuum glazing unit is enclosed by two glass panels to form a triple glazing unit system. To eliminate additional loads due to pressure differences that can cause unwanted breakage, they designed an equalized air pressure arrangement on both sides of the vacuum glazing unit. Fang et al. (2015) have performed a simulation model using a finite volume model on the thermal performance of triple vacuum glazing (TVG) sealed using indium alloy and 4 mm thick glass panes. In their validated computer simulation work, the emissivity values of the glass sheets were varied from 0.18 to 0.03. The simulated centre U-values are reduced from 0.41 $Wm^{-2}K^{-1}$ to 0.22 $Wm^{-2}K^{-1}$ for a 0.4 m by 0.4 m size triple vacuum glazing. Memon (2017) introduced a triple vacuum glazing using Cerasolzer CS186 alloy as the edge sealant. From the 3D finite element model, the centre of glass U-value of 0.33 $Wm^{-2}K^{-1}$ is found

achievable. Memon and Eames (2017) investigated the building heating performance when retrofitted with the composite edge sealed triple vacuum glazing.

An annual space-heating energy savings of 14.58% and 15.31% are expected to be achieved. Meanwhile, if single glazing windows are replaced with the designed triple vacuum glazing, a heat loss reduction of 12.92% and 2.69% is achievable. Research on vacuum glazing technology has also led to integrating the technology with other advanced glazing technology. Fang et al. (2010) have introduced an integration between electrochromic (EC) with vacuum glazing (VG) technology. The EC component was arranged facing the outdoor environment. For an incident solar radiation of 300 W m^{-2}, simulations show that the EC layer is opaque, and the inside temperature of the glass pane is higher than the indoor temperature.

Meanwhile, for solar radiation of 1000 W m^{-2}, the outdoor glass pane temperature exceeds the indoor glass pane temperature, of which, as a consequence, heat is transferred from outdoors to indoors. Ghosh et al. (2017) integrated a suspended particle device (SPD) with vacuum glazing. In their study, a strong correlation between the measures of the clearness of the atmosphere or clearness index was evaluated for south-facing vertical glazing. For a clearness index below 0.5, the SPD-vacuum glazing transmission was 17% and 1.1% for transparent and opaque states. A group of researchers from China (Zhang et al., 2017) proposed integrating a thin-film PV glazing with a vacuum glazing. The glazing prototype was designed and manufactured so that a lamination layer was sandwiched between the thin film PV glazing unit and a vacuum glazing unit, and both are independently manufactured. According to

the researchers, although semi-transparent photovoltaic windows can generate electricity in situ, they also significantly increase the cooling load of buildings due to the waste heat as a by-product. The experiment has been conducted, and the results have indicated that the prototype can generate electricity and help reduce the cooling load and improve indoor thermal comfort. Recently, researchers Ghosh et al. (2018) investigated a combined semi-transparent multi-crystalline PV vacuum glazing. In their research, both thermal and electrical performance has been investigated. They have found that the combination of multi-crystalline PV cells with vacuum glazing provides a low overall heat transfer coefficient, reduces solar heat gain, generates clean electricity and allows comfortable daylight.

2.3.2 Building energy system retrofit technologies

2.3.2.1 Solar boosted heat pump

Solar PV panels can convert solar energy to electricity output at an efficiency of approximately 15% (Elnozahy et al., 2015). The balance of solar energy is lost to the environment as heat. Thus, we can use the waste solar thermal heat and the electricity from the PV panels to boost the work of Heat pump systems. Especially during cold ambient periods, the solar thermal collector can collect the low-grade heat from the incident solar energy and serve as an evaporator to boost the temperature of the working fluid in the evaporator. In this way, the heat pump cycle can transfer heat from a low-grade solar collector to thermal storage in the form of high temperatures. Sankey diagrams can calculate the energy performance of the PV/thermal boosted Domestic water heating. In the calculation, the COP of the direct solar boosted heat pump is up to 4.2, and the system efficiency is up to 3.64 (Harrison, 2017). According to the recent

literature, there are mainly two approaches that emerged in the commercial market:

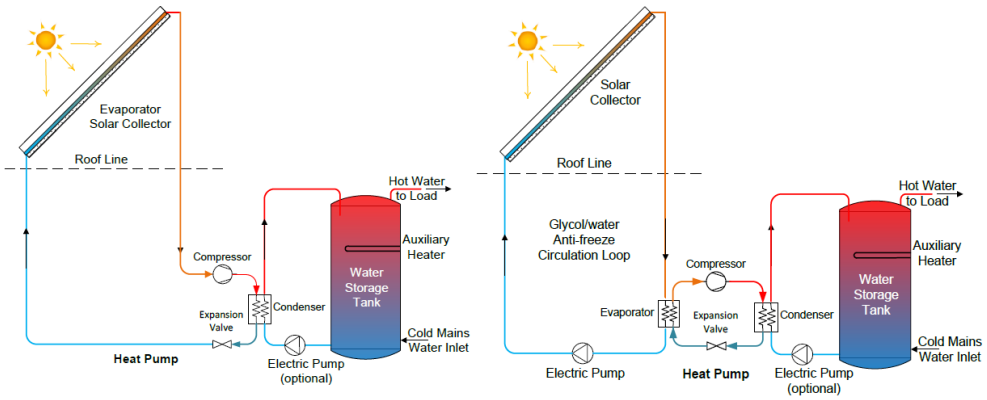
1) Direct expansion SB-HPWH system

In the direct-expansion approach, refrigerant is circulated directly through the solar collectors (O'Dell et al., 1984, Y.W. Li, December 2007, Ito et al., 1999, Ito et al., 2005, Kuang and Wang, 2006, Chow et al., 2010). Furthermore, the absorber of the solar collector becomes evaporator directly. However, the two main risks are the leakage of traditional refrigerants and high installation costs.

2) Indirect SB-HPWH system

In the SB-HPWH system, the working principle is similar to direct ones, and the solar collector is in a closed loop with a heat exchanger to the evaporator of a heat pump. This is primarily used in much colder areas where the antifreeze heat transfer fluid cannot be directly contacted with the domestic water storage cycle (Webb, 2017, Franco et al., 2015, Cristofari et al., 2015). Although the installation is simplified, additional components include the electric heat pump and the heat exchanger.

The example of direct (a) and indirect (b) SB-HPWH configurations are shown in Figure 2-9 (Harrison, 2017).



(a) (b)

Figure 2-9 The example of direct (a) and indirect (b) SB-HPWH configurations

2.3.2.2 Ground source heat pump

A ground source heat pump system usually consists of three main components: a ground heat exchanger, a heat pump, and a heat distribution system. An open-loop system with groundwater as a heat source is most widely used. However, there are some disadvantages, such as limited water availability, fouling, and pipe correction. Also, environmental issues covering the use of groundwater are increasingly severe. These limitations have made the research focus transferred to a closed-loop ground source heat pump. These buried closed-loop pipes consisted of circulated refrigerants direct expansion or water/antifreeze solution indirectly connected with another heat exchanger.

The overall efficiency for GSHP is inherently higher than the air source heat pump due to the relatively stable ground temperatures, which is higher than the mean air temperature in winter and lower in summer. The heat pump output temperature is ranged from 50-55℃, and no more than 65℃ (Caskey and Groll, 2018). Commercially used products usually perform with COP=4 in space heating and COP=2.75 in domestic water heating (Wu et al., 2018). Also, the

lifespan of GSHP is expected to be 20-25 years, and the ground coil will last for 50 years. As the literature indicated, with ground coil depth less than 2m, the ground temperature will follow the air temperature and show marked seasonal variations. With ground coil depth below 10m, the ground temperature will maintain a stable temperature, which is approximately the same as the mean annual air temperature (Luo et al., 2016). Depending on the geology and soil conditions of the UK, the ground temperature is stable at around 10-14℃ (Energy saving trust, 2007).

One of the main challenges is the cost of such GSHP systems. They are taking the example of SLINKY systems. The capital costs for horizontally installed ground source to water heat pump systems will cost around 600-1150$£/kW$, and 850-1500$£/kW$ for vertical installed systems (Luo et al., 2016).

2.3.2.3 Air source heat pump

The commonly used air-water or air-air source heat pump has been widely used in the building retrofit process due to its relatively low investment, easy installation, and compact space requirement. However, it will reduce much energy efficiency when the medium temperature gets low, and further, the temperature difference will also be reduced, which will, in turn, reduce the thermal efficiency, especially in the cold climate areas. In the literature (Caskey and Groll, 2018, O'Dell et al., 1984, Schibuola et al., 2018, Thilakarathne and Treur, 2016), using compact air-source heat pump water heater systems can achieve 70% of energy saving compared with commercial electric-resistance water heating. Moreover, the COP of the heat pump can achieve 2.9, with a system efficiency of 2.67. However, due to low air temperature in the cold

surrounding environment, the application is limited in cold climates market.

2.3.2.4 Hybrid photovoltaic and thermal PV/T technology

Photovoltaic has been widely used recently in different applications with an electricity efficiency in markets ranging from 12%-19% (Wikipedia, 2018) for inorganic PV panels and 3%-15% (Yu, 2014) of organic photovoltaic panels. Company SUNPOWER can produce a type of solar cell with high efficiency, up to 21.5% (Sunpower, October 2015).

Three main problems challenge the development of PV panels:

1) Relatively high initial investment and low electricity output.
2) Dust and other particles that accumulate on the surface of the panels will reduce the electricity efficiency
3) Overheating of the PV panels will result in electricity degradation. The efficiency of a solar cell declines by about 0.25%-0.5% for every 1 degree Celsius increase in temperature (Nižetić et al., 2016).

Many investigations have been made to explore the solutions to both dust accumulations and cooling technologies. Besides all other technologies, there is a possibility of improving the overall performance of PV panels by integrating the PV and thermal collector, also called the PV/T technologies. According to the results, there is an improvement of 16.3% of the overall increase in electricity output (Nižetić et al., 2016). The water-based PV/technology-enhanced solar electrical and thermal efficiency by 9.1% and 42%, respectively (Zhang et al., 2013). In another study, a simple passive automatic cooling and cleaning system using a thin film of water is developed for a standalone PV system (Elnozahy et

al., 2015). This study figures out a 29% increase in electric fields, together with a 45.5% and 39% reduction in temperatures of the front and rear faces of the module, respectively. Current PV/Thermal costs are approximately 3-5 times that of standard PV modules. However, it is expected that these prices will drop as volume and competition increase in the marketplace (Harrison, 2017).

2.3.2.5 Desiccant solution cooling and dehumidification technologies

Air conditioning system is recognized as an indispensable method of improving human beings' thermal comfort and living conditions since early twentieth century. With the growing concerns about the greenhouse gas emissions, the aggravating primary energy shortage and increasing energy demand, the energy consumption of buildings is at a critical stake, which accounts for 40% of energy demand in Europe (LRg., 2006). According to (Parliament, 2010), in Europe, 6% of office, commercial and industry buildings are air-conditioned, with a total volume of 20 million cubic meters. In hot and humid climatic conditions, air conditioning system accounts for more than 50% of the total building energy consumption (Pérez-Lombard et al., 2008) (Lior, 2012). The current widely used vapour compression system plays dominant role in the market. However, vapour compression system has the disadvantages of intensive energy consumption and low performance in hot and humid climate. Moreover, the possible leakage of high GWP refrigerants will lead to the depletion of Ozone Layer, which further contributes to the global warming and other associated environmental and social changes. Hence, the novel energy efficient and environment-friendly cooling systems develop to be the research topics for scientific researches. In the past few decades, evaporative cooling system arouses great attentions among the

researchers due to the fact that it is more environment-friendly with the water used as working fluids, simple in structure configuration, and less consumption in primary energy. Direct evaporative cooling system works under the following principle: the incoming hot and humid air gets direct contact with the circulating water, causing the evaporation of the water and the air temperature will be reduced accordingly. Consequently, the evaporated water, in the form of vapour will be absorbed by the air, which leads to the humidity increase of the outlet air. As the key element in desiccant cooling system, desiccant is a material that has a significant capacity of holding water. With the advantages of light weight, corrosion resistant and no liquid droplet carryover (Chen et al., 2016b) (Chen et al., 2016a), hollow fibres have been considered as alternatives to porous media or metallic materials for the manufacturing of dehumidifier. However, the works conducted by these researchers (Zhang et al., 2016) (Zhang and Zhang, 2014) (Huang et al., 2016) (Zhang et al., 2012) (Huang et al., 2012) were mainly focussed on the theoretical modelling such as using free surface model (Zhang et al., 2012), with LiCl or CaCl2 as the liquid desiccant. The application of aqueous potassium formate (KCOOH) solution as the liquid desiccant in polymer hollow fibre integrated liquid desiccant cooling system has never been analysed by researchers (Zhang et al., 2012) (Huang et al., 2012). This research presents a novel two-stage dehumidification and cooling system, which is based on the integration of a pre-cooled liquid desiccant dehumidification process and a pre-cooled water-cooling process. The system performance is tested with the laboratory test and served as the input information to simulation model. And a residential building retrofit case study in Italy is implemented by applying the innovative retrofit technology to demonstrate the retrofit performance with the

novel two-stage dehumidification and cooling system.

2.4 White- and Black- box based building energy prediction model

2.4.1 Data-driven (or Black-box model) based Building Performance Simulation for building retrofit analysis

The black-box models, which are fully dependent on the measured data, have an obvious increasing application trend in the domain of building energy modelling. The main advantage of this model lies in the fact that it could be directly trained with measured data and not involve any previous building heat transfer phenomena (Hrovatin and Zorić, 2018). Furthermore, it is allowable that the black-box models employ complicated system dynamics without engaging with system intricacies and could be re-trained and amended with new data (Guo et al., 2018). The most investigated machine learning approaches in performing BPS are Artificial Neural Network (ANN) (Wong et al., 2010), Support Vector Machine (SVM) (Qiong et al., 2010), and ensemble models (Papadopoulos et al., 2017).

To accurately predict the future building performance by incorporating weather data and building operation parameters, Smarra et al. (Smarra et al., 2018) investigated the potential of combing the Model Predictive Control (Sturzenegger et al., 2016) with a machine learning approach using random forests algorithm. This algorithm was applied to simulate the energy usage situation of an apartment building, with an average error of 3% compared to the BPS performed in EnergyPlus. Tharmpoulidis et. al (Thrampoulidis et al., 2021) proposed an ANN-based machine learning algorithm to approximate optimal building retrofit solutions by identifying hidden node combinations for key

features of the building layers and retrofit solutions, with the aim to generate outputs in terms of energy performance, carbon emissions and costs. The adoption of such model for building retrofit at a larger or building cluster scale will require substantial computation costs involving numerous training efforts. However, such proposed model is bespoke trained based on specific building fabric and local weather conditions, as well as occupants' behaviours (Qu et al., 2021), which are not always easily accessible. Therefore, these input datasets can be significantly diversified for buildings with different typologies and climatic conditions.

Shen et al. (Shen et al., 2019) proposed a Pareto front based Multi-Objective Genetic Algorithm (MOGA) in a campus apartment block with 20 passive retrofit measures selected. The results showed an average error of 2.5% compared with the simulation results from EnergyPlus. Asadi et al. (Asadi et al., 2014) proposed an optimisation model using a genetic algorithm and ANN approach to quantitatively assess technology choices in a building block retrofit project with passive and renewable retrofit actions. Compared with the TRNSYS analysis, an average error of 1.4% occurred within 95 cases. Deb et. al (Deb et al., 2021) proposed a Recurrent Neural Networks (RNNs) algorithm for cost-optimal building retrofit on a single-family dwelling, where the retrofit measures are selected using feature significance approaches. Previous studies concentrated on assessing only passive retrofit combinations or integrating simple renewables, which barely takes into account the deep energy retrofit by combining passive, active and renewable measures. Yao et al. (Yao et al., 2021) pointed out that the coupling effects of different retrofit measures have a significant impact on building energy performance, especially in both heating and cooling required

areas. For most of the ANN approaches, passive retrofit measures are likely to be retained with a fixed value where incoming and outcoming connections are removed from the neural networks when the measure is not selected. Neglecting the coupling effects, insulation measures will result in the reduction of heating demands in winter and the increase of cooling demands in summer. In addition, the selected cooling devices may not meet the increased cooling demands, resulting in system mismatch issues. Therefore, it is essential to consider the coupling effects in deep energy retrofit combinations to avoid system mismatch issues.

Based on the initial simulation results from EnergyPlus as the input data, Ascione et al. (Ascione et al., 2017a) adopted an ANN approach to generate two sets of algorithms for BPS existing building stocks and renovated building stocks in the southern part of Italy. The BPS results from the ANN algorithms showed an average error of 2.73% in reference building compared to the results generated by the physic model in EnergyPlus. By applying such ANN approach in the renovated office and apartment building stocks, outcomes showed an average error of 1.5% indicating a reliable prediction of energy performance and retrofit scenarios for such building types. Conversely, a maximum of 22.27% error occurred in the renovated single-family houses which feature detached, semi-detached and terraced houses (Ascione et al., 2017a). Differ from office and apartment buildings, the geometric diversities and distinctive occupancy behaviours result in the complex heat transfer phenomena between the heating terminals and the indoor comfort requirements. Therefore, it is of vital importance to seek an incorporated solution considering complex heat transfer phenomena in rapid and accurate decision-making for single-family house

retrofit.

Previous studies have shown that the Black-box model has low accuracy to make rapid decisions for deep energy retrofit in single-family houses due to inadequate data requirements, neglect of coupling effects in deep energy retrofit combinations and lack of complex heat transfer phenomena in single-family houses.

2.4.2 Physics-based (or White-box model) Building Performance Simulation for building retrofit analysis

Deeply rooted in the fundamental heat and energy transfer principles, physics-based BPS has been proved to be a powerful tool to support the investigations of strategic retrofit solutions, focussing on the combinations of a wide range of energy-retrofit measures. White-box models can be classified into two categories, established either upon dynamic simulation software (such as EnergyPlus (Crawley et al., 2001), TRNSYS , ESP-r (Wang et al., 2016), and IES VE) or via multi-zone dynamic thermal simulation models (i.e., lumped parameter models with the reduced order (Goyal and Barooah, 2012)). Embedded with a range of key parameters based on multiple green building regulations and rating systems, the former has been popular among design engineers and architects, with the ability to analyse and visually present dynamic performances focusing on solar, lighting, energy, costs, etc. With the accessibility to a robust weather database provided by world meteorological organisations, these BPS programmes can dynamically present a comprehensive annually energy consumption profile under changing locations and climatic conditions. The latter is normally based on transient energy and mass balance equations in the form of lumped thermal resistances/capacitors with reduced

order (Gustafsson, 1998). With the advantages of simplicity and less computational efforts, this lump parameter model has been applied to simulate the dynamic temperature (Ji et al., 2016) and humidity profiles which serve as the crucial inputs for optimising the heating/cooling demands (Tang and Wang, 2019) of the Heating, Ventilation and Air Condition (HVAC) systems for the multi-zone buildings (i.e., commercial buildings, apartment building blocks).

Recently, a range of energy retrofit measures, including several passive retrofit measures(i.e., building envelope thermal insulations (Qu et al., 2021), airtightness (Qu et al., 2020) and glazing (Wang et al., 2015b)), active retrofit measures (i.e., the upgrading of building service systems (Araújo et al., 2016), the integrations of smart sensors/technologies and renewables), as well as different occupancy behaviour and energy usage profiles (Ben and Steemers, 2014), have been individually and jointly evaluated by researchers recently. A dynamic model using Simulink to analyse the thermal performance of a single building was proposed by Gouda et al. (Gouda et al., 2000), focusing on manipulating the window and shading design to maximise the available winter solar radiation with minimum impact on increasing the summer indoor temperature. McKinley and Alleyne (McKinley, 2008) conducted the physics-based BPS via EnergyPlus simulation to determine a range of time-dependent and time-independent variables, considering solar radiation as the input thermal load. Dynamic simulation models were established by Murray et al. (Murray et al., 2012) to compare the pre and post-retrofit energy consumptions of a historical building in Ireland. The results indicated that 55.6% of energy reduction could be achieved via selected deep retrofit measures. In addition, Murphy et al. (Murphy et al., 2021) investigated white and grey box modelling

and calibrating techniques and compared models to empirical data on modelling a retrofit Net Zero Energy Building (NZEB) with natural ventilation. Results showed that the White-box model produced slightly more accurate results with the root mean square error 1.5% higher than the Grey-box model and displayed better generalisation abilities when calibrated and validated using identical data. Zacekova et al. (Žáčeková et al., 2014) and Sturzenegger et al. (Sturzenegger et al., 2016) concluded that the biggest obstacle to implementing physical model-based BPS in building retrofit processes is the substantial simulation efforts and the iterations required to establish and modify the dynamic simulations based on different combinations packages of potential energy-efficient measures. This is particularly true when dealing with apartment building blocks (Tonellato et al., 2021), commercial buildings (García Kerdan et al., 2016) and even large building clusters (Walker et al., 2020). Therefore, the white-box models enable it to perform robust and versatile BPS, evaluate energy savings and economic feasibility at a preliminary retrofit design stage, and identify a range of strategic retrofit combinations.

However, the white-box models that are widely used for detailed retrofit analysis in single-family houses, yet are found to be burdensome and often require hard-to-obtain information since it is subject to building-physics principles and requires exhaustive input data (Guo et al., 2018). Moreover, due to model complexity, heterogeneity and high computational efforts involved in the simulation process, it is almost impossible to perform all the possible retrofit combinations based on the available energy retrofit measures at the preliminary design stage for building retrofit.

2.4.3 Existing research gap and the novelty proposed in this research

The limitations for the applications of both White- and Black-box models under the deep retrofit context can be categorised into four areas:

1) Inadequate data requirement – Numerous trainings are required to generate the Black-box model for the pre-retrofit design of each building, especially in dwellings, due to the lack of consideration thorough building specifics (fabric construction, floor plans), external factors (local weather conditions, shadings) and occupants' behaviours (energy usage, occupancy schedule, energy sources and retrofit preferences), which will significantly affect the hidden connections in the Black-box models;

2) Neglect of coupling effects in deep energy retrofit combinations – Low accuracy of energy performance prediction occurred in deep energy retrofit combinations using the Black-box model due to neglect of the coupling effects in versatile retrofit measures, resulting in system mismatch issues;

3) Lack of complex heat transfer phenomena in single-family houses – Differ from office and apartment buildings, single-family houses have diverse geometry and distinctive occupancy behaviours. Low accuracy presents in building energy prediction of single-family houses using the Black-box model, attributed to the lack of complex heat transfer phenomena between the heating terminals and indoor comfort requirements;

4) Time-consuming – The White-box models that attempt to simulate energy transfer processes to a higher accuracy level dynamically are considerably more computationally expensive. Quasi-steady state models can be used to reduce computational times but often at the expense of accuracy. A trade-off between

simulation accuracy and complexity in the computational process needs to be carefully addressed.

Therefore, the above-mentioned two types of BPS models cannot fully address the crucial research challenges in optimising deep energy retrofit combinations rapidly and accurately for single-family houses.

2.5 Willingness-to-pay and EPC labelling for residential building retrofit

Figure 2-10 describes Retrofit cost/area of different levels in residential buildings, including 18 EU countries. The average retrofit cost of EU 18 countries is 162 €/m^2, with an average dwelling retrofit size of 116.7 m^2, which results in the average retrofit investment for each dwelling of 18933 €, as shown in Figure 2-11. The retrofit level can be divided into three levels: light retrofit, medium retrofit, and deep retrofit. As required by the EPBD, most of the buildings in the EU need a deep retrofit by the end of 2050 to achieve a carbon-neutral society. Combining Figure 2-10 and Figure 2-11, we could find the deep retrofit cost of 226 €/m^2 is much higher than the light and medium retrofit with 83 and 122 €/m^2, respectively, which results in an average of 26381 € for deep retrofit in EU countries. In the view of the deep retrofit section, German dwellings need the most expensive investment for approximately 42188 € for individual deep retrofit. Italy, Lithuania, and Sweden need 31178, 29420, and 28113 € for the investment of deep retrofit, which is slightly higher than the average cost of the data collected in eight EU countries. Therefore, such retrofit investment is a considerable expense for single families (especially for low-income groups) without the government's insufficient funding, which decreases the willingness of the residential house owners to pay for the retrofit related works.

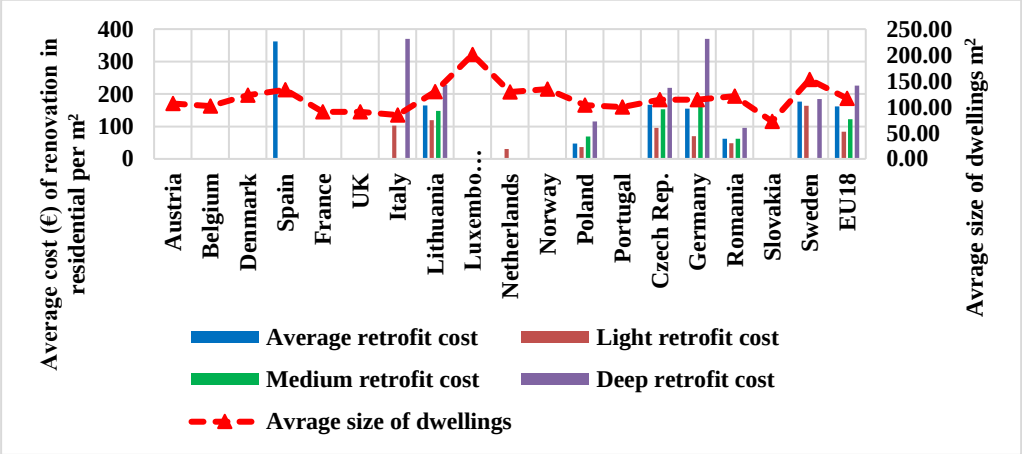
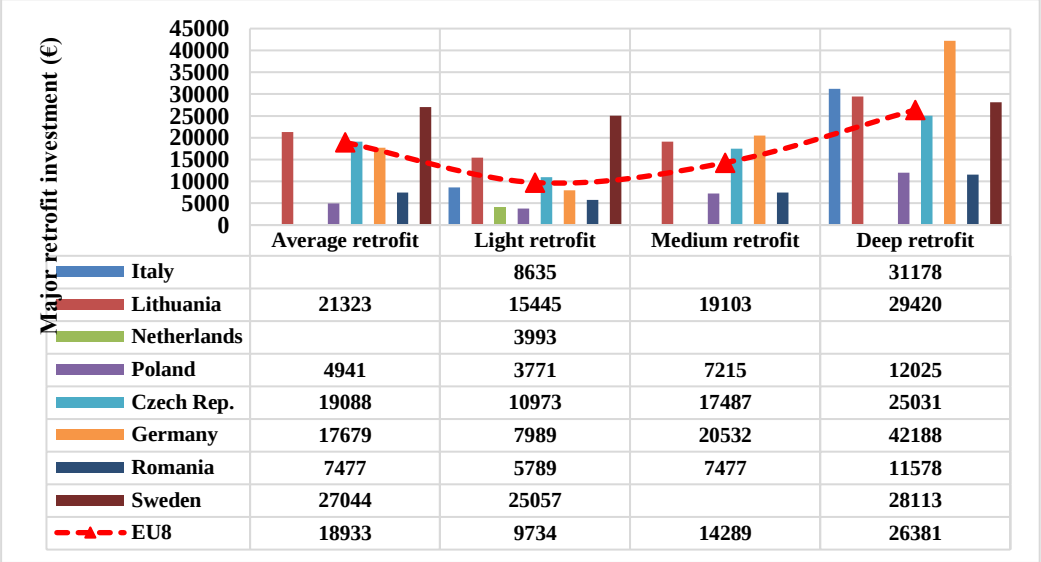


Figure 2-10 Retrofit cost/area of different levels in EU residential buildings



	Average retrofit	Light retrofit	Medium retrofit	Deep retrofit
Italy		8635		31178
Lithuania	21323	15445	19103	29420
Netherlands		3993		
Poland	4941	3771	7215	12025
Czech Rep.	19088	10973	17487	25031
Germany	17679	7989	20532	42188
Romania	7477	5789	7477	11578
Sweden	27044	25057		28113
EU8	18933	9734	14289	26381

Figure 2-11 Major retrofit investment in eight EU countries

According to the discussion of the above four barriers of building retrofit, including properties' features, house owners' preference, installation time and willingness to pay, it is significant to have a deep understanding of the motivations for house owners to retrofit measures for their properties. The six main motivations for residential building retrofit are summarised as follows, which is usually interacted with each other:

1) Improve the comfortable indoor level

2) Energy saving
3) Reducing energy bills cost
4) Improve the value of the properties as a financial investment
5) Government legal regulations for the minimum EPC grades to sell or rent
6) Influence of peers and the next generation.

Niamh et al. (Murtagh et al., 2019) investigated the occupants' motivation with a study of a large-scale survey (n=1007) in southern England, which is exposed to increasing temperatures and frequent heatwaves as global warming effects. It figures out that the existing building environment can mitigate with the health risk of overheating. Two-thirds of the sample had experienced overheating on at least a few occasions across all housing types, which enhances people's motivation to make energy-efficient retrofits to improve their indoor comfort level. Bon-Gang et al. (Hwang et al., 2017) investigated the residents' perceptions of green retrofit in a mature residential estate in Singapore with a questionnaire survey to 90 residents who had just completed a pilot green retrofit program. The survey results show that 86% of residents are satisfied with the retrofit program and more than 50% of residents were supportive of having their individual properties retrofitted with the willingness to bear the retrofit investment. Besides, reducing low energy bills cost is the top motivation that drives residents to retrofit the properties. Robert et al. (Baumhof et al., 2018) surveyed 218 German owner-occupiers of single and two-family houses about the critical motivations for energy-related refurbishment.

The European Directives 2002/91/EC (2002) EPBD and the EPBD 2 (recast) 2010/31/UE have been introduced into the European Legislation with two main requirements for each building, either new or retrofit:

1) the minimum energy performance requirements must be met to promote energy-efficient new buildings the EPBD 2 envisages Nearly Zero Energy Buildings (NZEB) - and energy retrofit, also with the promotion of renewable energy sources;
2) The Real Estate sector must have the Energy Performance Certificate (EPC), which provides, even in the case of new construction, all the information on energy labelling and the building's energy consumption.

Most European countries have widely adopted the EPC concept as a policy-based commercial method to push the increase of the retrofit market. It is noticed that EPC is determined as an assessment standard to evaluate the building energy performance after the retrofit work. Besides, many countries are applying the EPC related laws to improve the energy retrofit rates of the residential buildings, as shown in Figure 2-12. UK government has set a minimum EPC grade E for letting or renting the residential and commercial properties, which will affect 18% of commercial properties in England and Wales with house ratings of "F" or "G" (Davidson). As for the Norwegian regulations, the minimum requirement for EPC is grade C to allow residential buildings to be let or rented (Skaran). Landlords in Germany and Italy have been banned from granting a tenancy to a new or existing tenant if the property has an EPC rating of band F or G (Jones). The critical EPC standards in Sweden also set a restriction of a minimum EPC rate of E grade for rental property, which will be raised to D or C grade in 2020 (Law). Therefore, EPC as a policy regulation is also an important motivation to push the process of a residential building retrofit. Figure 2-12 describes the distribution of EPC building stock by label A to E in 10 EU countries by the end of 2015, with a total of 11.982 million EPC registered residential building stock.

In the EU10 countries, EPC label groups into A, B, C, D, E grades, with percentage distribution of 4.33%, 20.13%, 23.39%, 19.41%, and 32.74%, respectively, which results in at least 52.15% (Label D, E) of the existed residential buildings need further retrofit. Among the 10 countries, UK has the largest number of EPC registered residential buildings with 5.964 million homes. And the Italy and Norway has the large number of inefficient residential buildings with EPC label D and E, which accounts for 84.48% and 84.75% of the EPC registered residential building stock, respectively.

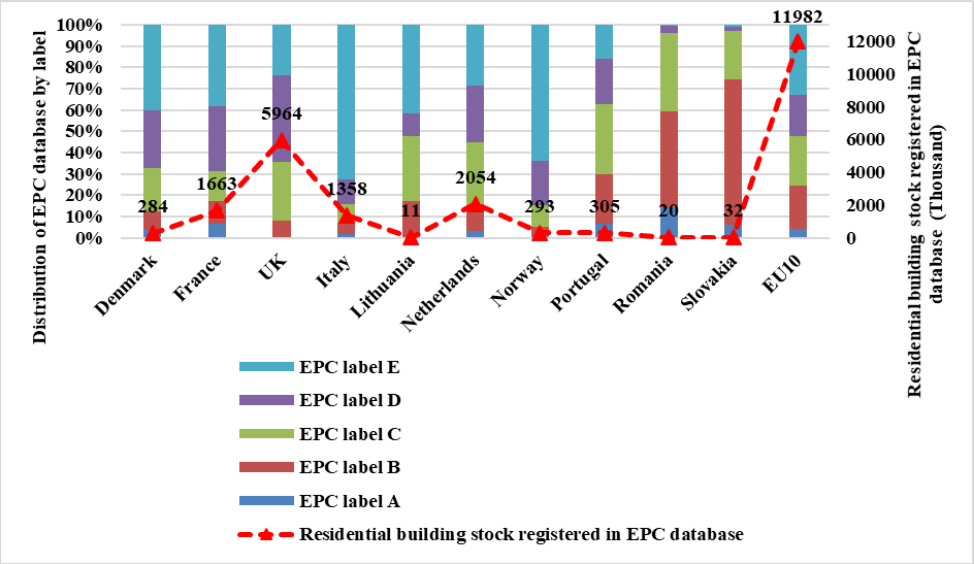


Figure 2-12 Distribution of EPC building stock by label A-E (Data source: (Tadeu et al., 2015))

2.6 Multi-objective optimisation algorithms

Residential buildings have a significant impact on the overall EU carbon emissions. To reduce carbon emissions in residential buildings, various intervention strategies have been investigated to promote residential building energy efficient and cost-effective research. When choosing the renovation solution, literature refers to as choosing out of a list of renovation solutions applied one by one (Wanga, et al., (Wang et al., 2015a)); The measures are either

added to the previous one or they are grouped in different packages in order to increase the energy saving potential (Lohse, et al., (Lohse et al., 2016)). Jankovic (Jankovic, 2019) investigated the 1940s' Birmingham dwelling retrofit with final energy reduction, initial investment and payback time in a local optimization scale. The payback time is approximately 16 to 38 years, with energy reduction range of 42% to 56%, and initial investment of £10k-85k. Chen et al. (Chen et al., 2019a) investigated the cost-effectiveness retrofit combinations in a 1980s' Oslo apartment block, with 14% to 83% of primary energy reduction. Besides, the relative initial investment is increasing from 189€/m2 to 351€/m^2 with lowest payback time of 4 years. Delmastro et al. (Delmastro et al., 2016), Ashrafian et al. (Ashrafian et al., 2016), Ortiz et al. (Ortiz et al., 2016) and Dodoo et al. (Dodoo et al., 2017) investigated the global optimization results in a certain energy retrofit scale. Most of the discussed retrofit optimisation cases are summarized in Table 2-1. However, most of the payback time is not calculated in these papers. Therefore, it is difficult to evaluate the optimum results among payback time, energy reduction, and initial investment.

Table 2-1 Multi-objective optimisation cases and optimisation scale

Reference No	Construction year	Site location	Assessment indicator	Payback periods	Final energy consumption	Initial investment	Optimisation Scale
Jankovic (Jankovic, 2019)	1940s-1950s	Birmingham, UK	ROI	16-38 years	42%-56% reduction	£10k-85k	Local

Chen et al. (Chen et al., 2019a)	1980s	Oslo, Norway	EEES	4-142 years	14%-83% reduction	189-351 €/m^2	Local
Ashrafian et al. (Ashrafian et al., 2016)	1980s-1990s	Istanbul, Turkey	N/A	5-50years	75-125 kWh/m^2year	99-135 €/m^2	Global
Delmastro et al. (Delmastro et al., 2016)	Before 1960s	Torino, Italy	socio-economic factors	N/A	45-75 kWh/m^2	156-232 €/m^2	Global
Salata et al. (Salata et al., 2017)	Before 1970s	Rome, Italy	Annual economic return	15-30 years	11-51 kWh/m^2	109160-192700 €	Local
Jermyn et al. (Jermyn and Richman, 2016)	Before 1940s	Toronto, Canada	$EnerPHit_{EQUIV}$	N/A	64%-89% reduction	$30,000–$80,000	Local
Ortiz et al. (Ortiz et al., 2016)	1990s	Catalonia	EPC label	N/A	22%-59% reduction	355-535 €/m^2	Global
Thomsen et al.	1960s	Denmark	N/A	N/A	35% reduction	1302 €/m2	Local

(Thomsen et al., 2015)							
Serrano-Jimenez et al. (Serrano-Jimenez et al., 2017)	1960s	Seville, Spain	Cost-Optimal ratio	15-30 years	50%-90% reduction	735-7369 €	Local
Pinto et al. (Francisco Pinto and Carrilho da Graça, 2018)	1970s	Groningen, Netherland	Life-cycle cost	14-15 years	74-85 kWh/m^2	6200-8000€	Local
Dodoo et al. (Dodoo et al., 2017)	1970s	Lindvägen, Sweden	NPV	N/A	32-51% heat reduction ;19%-35% electricity reduction	72.4-174.7€/m^2	Global

Zhang et al (Zheng et al., 2019b) applied a screening methodology to analyse the possible energy and economic performance of building retrofit with multiple energy retrofit measures package. In the strategy implementation, energy saving

potentials of each individual measures are calculated with analytical calculation model, and as well as life-cycle cost. However, the analytical calculation model only quantified the energy–savings of single technique and calculated the final energy saving potential in a linear sum of each retrofit measures, without considering the interactive effects to energy saving potential by combining the retrofit measures. Although the research discussed the risk variables including investment, energy saving and energy prices, and considered these uncertain parameters, the solution is to adjust the calculation formula with fluctuation coefficients and relative risk assessment, according to the randomly probability distribution by Monte Carlo simulation, which is highly dependent on selecting the appropriate probability distribution function. Therefore, it is difficult to apply this methodology in residential buildings retrofit, as the probability distribution is highly influenced by occupants' behaviours. And, the coupling between multiple energy retrofit measures is still not solved. What's more, in the decision-making process, only 19 plans of retrofit combinations are considered with totally 19 available numbers of retrofit measures, which can not be directly used as the assessment criteria, due to lack of comparable combination samples.

Alves et al (Alves et al., 2018) identified and analysed the energy-saving potential of an existing building stock category, with a local sensitivity analysis applied to prioritize the retrofit measures and a sequential search method employed to evaluates efficient measures combinations, in order to understanding the existing building stock for further energy policies. Besides, local sensitivity analysis is achieved by calculating the influence coefficient, which is dependent on the simulation tool: EnergyPlus. And the final cost-effective option is chosen as the optimal point for the iteration. The schematic

cost optimal pathway is cited, as shown in Figure 2-13, with abbreviation of ERP represents for energy retrofit packages. However, this approach can not be used to make decisions to real residential building retrofit, due to the time consuming with the increasing iteration numbers, which is dependent on the of comparable combination samples. Therefore, only local optimal retrofit combinations can be found, which may not satisfy the house owners as lack of holistic comparison.

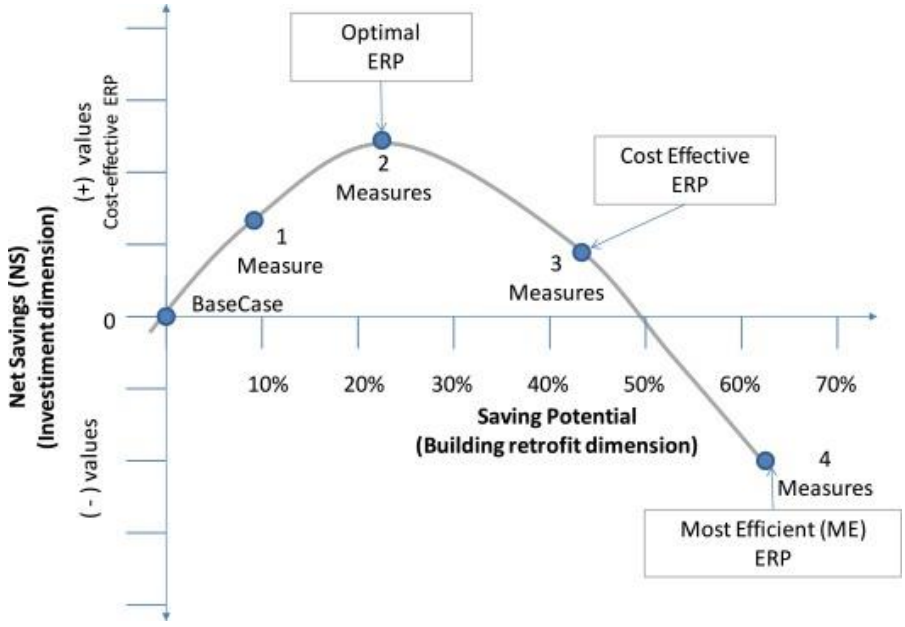


Figure 2-13 Schematic cost optimal pathway

Andrade-Cabrera et al (Andrade-Cabrera et al., 2020) using the Ensemble calibration models to make decisions for cost-optimal residential envelope retrofit, which is an automated model calibration methodology with lumped parameter building energy models. The ensemble calibration model is used to predict the potential building energy demand with retrofit design, which is based on the integration mechanism (Andrade-Cabrera et al., 2017, Andrade-Cabrera et al., 2019, Berthou et al., 2014) of baseline building demand (heating, cooling, and electricity demand). And, it is significant that the coupling effects between

multiple energy retrofit measures can be retained due to the integration mechanism of the ensemble calibration model. Therefore, the ensemble calibration can maintain the baseline building thermo-physical meaning and structure, and better capture the transient results of dynamic energy demand reduction due to flexible retrofit measures, which allows for a rapid and accurate estimation of building demand calculation. Andrade-Cabrera et al (Andrade-Cabrera et al., 2019) also introduced three lumped-parameter building models to test the application of Ensemble Calibration in different building sceneries, including a simplified lumped-parameter building model (3R2C) with three thermal resistances and two thermal capacity (as shown in Figure 2-14), a detached house archetype (9R6C) with nine thermal resistances and six thermal capacity (as shown in Figure 2-15), and a mid-floor apartment archetype (10R7C) with ten thermal resistances and seven thermal capacity (as shown in Figure 2-16). Results find the calculated building demand using ensemble calibration model matches well with different building type and varied weather conditions.

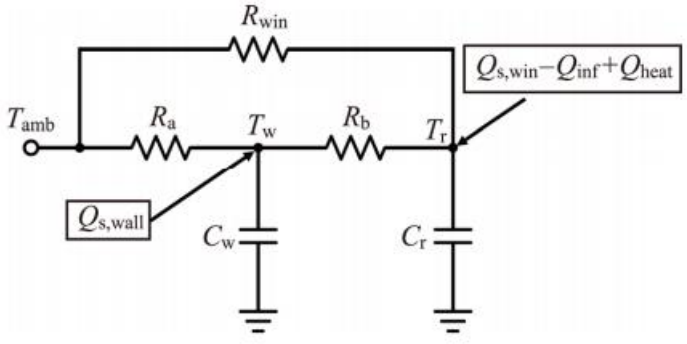


Figure 2-14 Simplified lumped-parameter building model (3R2C) (Andrade-Cabrera et al., 2019)

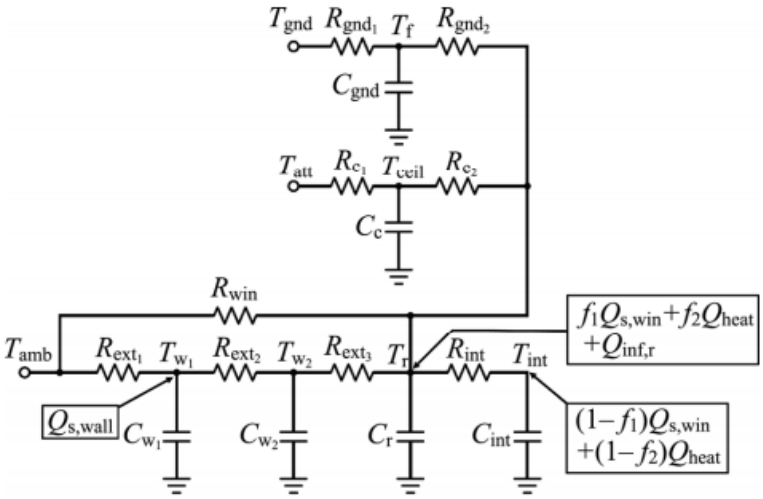


Figure 2-15 Lumped-parameter building model topology for detached house archetype (Andrade-Cabrera et al., 2019)

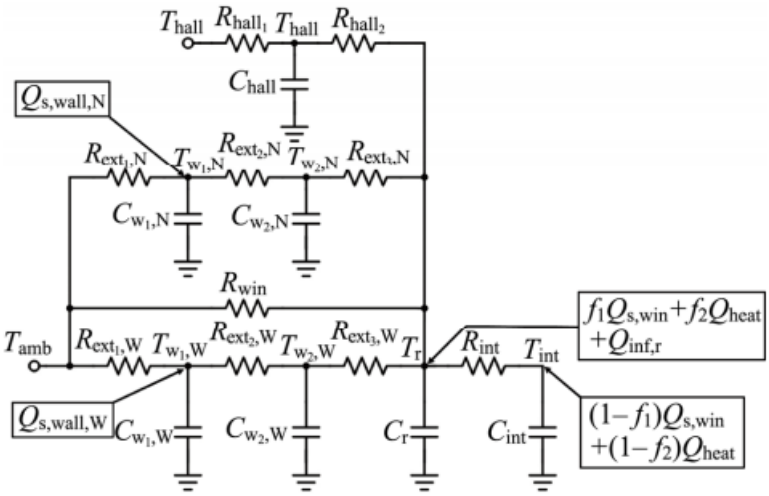


Figure 2-16 Lumped-parameter building model topology for mid-floor apartment archetype (Andrade-Cabrera et al., 2019)

This research is a continuity of previous research (Chen et al., 2019a) funded by European Commission Horizon 2020 project "RezBuild" (Salvadó et al., 2019). The previous research has been focused on applying multi-criteria assessment approach on a residential building block renovation in Norway. Eleven passive, active and renewable energy measures were defined and selectively integrated

into a total of 18 combination packages. The energy, costs and environment impacts from these combination packages were evaluated by the following parameters: primary energy consumption, payback period, global cost and carbon emission reduction. The results showed that these parameters in their current form could not be used the crucial indicators to inform retrofit decision-making. For instance, better energy consumption does not necessarily link to shorter payback period, especially for innovative retrofit measures for which the technology maturity and readiness often determine the product market price. Therefore, it is noticed that there would exist one combination package which yield relatively low payback period with high primary energy consumption, in comparison with another combination package whose payback period is longer but with better energy saving potential. It is therefore very crucial to define a single indicator which could evaluate the impact of retrofit combinations at the nexus of energy saving potential, payback period and global costs.

Most of the researchers are focused on developing an accurate and multi-objective model or algorithms to make a global optimized decision for retrofit design. Shen et al. (Shen et al., 2019) proposed a multi-objective optimization and lifecycle cost-analysis method to resolve the optimization problem in a fast manner with recourse to non-dominate sorting differential evolution algorithm, with applying hourly dynamic modelling tool SimBldPy and agglomerative hierarchical clustering technique. Yong He et al. (He et al., 2019) presented an intelligent optimization method with integration of particle swarm optimization and genetic algorithm to investigate the retrofit strategy under financial budget restraint. Tiberiu et al. (Catalina et al., 2013) demonstrate a multiple regression model for fast prediction of the heating energy demand, and validated with the

measured data from 17 blocks of flats. Wu et al. (Wu et al., 2016) proposed a concept for large scale building energy retrofit with time-building-technology (TBT) framework, which need optimization approaches, such as genetic algorithm, differential evolution and neighbourhood field optimization. However, due to the several variable parameters input by the retrofit designers, the number of dimensions increased to around 7-11. Given that each design parameter has three alternatives, Seven parameters and three alternatives have already lead to $3^7 = 2{,}187$ combinations. If all 11 parameters will be accounted to get a global optimization, there would be at least $3^{11} = 177{,}147$ combinations. With such a large number of combinations, the exploration of the solutions results are difficult to achieve, neither the calculation time and solution space. Therefore, a contradiction arises: How to make a balance between acquiring the optimized combination solutions and achieving a rapid pre-retrofit strategy design. Besides, most published researches have concentrated on integrating individual renovation measures into the existing buildings with linear superposition of each element measures without considering the internal relations of them. Thus, there is limited research into the interaction between individual renovation measures and their associated impact on the final energy consumption reduction and carbon emissions.

2.7 Retrofit motivations and homeowners' engagement

Several studies (Martek et al., 2019, Baumhof et al., 2018, Matosović and Tomšić, 2018, Mills and Rosenfeld, 1996) have been carried out to evaluate the barriers that prevent the stakeholders from making firm decisions in implementing building retrofit and the impacts of homeowners' engagements on the final retrofit choices. Barriers of the uptake for residential building retrofit

could be summarised in the following aspects:

1) Unsatisfied energy reduction rate performance (Qu et al., 2021, Chen et al., 2020, Synnefa et al., 2017, Serrano-Jiménez et al., 2020);

2) Exceeded equivalent carbon emission reduction rate (Pokhrel et al., 2021, Opher et al., 2021, Udovichenko et al., 2021) ;

3) Insufficient investment fund (Shaikh et al., 2017, Rosso et al., 2020, Hu et al., 2021, Ascione et al., 2020, Prabatha et al., 2020);

4) Unacceptable payback periods (Christersson et al., 2015, Cascio et al., 2017);

5) Unexpected annual energy bills for homeowners (Elsharkawy and Rutherford, 2018, Li et al., 2019, Birkha Mohd Ali et al., 2021, Elsharkawy and Rutherford, 2015, Charles et al., 2019, Al-Saadi et al., 2017).

Moreover, Martek et al. (Martek et al., 2019) reveal that most residential end-users do not purchase green home technologies, and without their 'buy-in', building energy sustainable retrofit transition will fail across Australia. Their findings concluded that effective financial incentives should be in place, with direct links in residential real estate markets, in order to promote low carbon building retrofit. Baumhof et al. (Baumhof et al., 2018) proposed a Motivation-Opportunity-Ability (MOA) approach to investigate various factors influencing the homeowners' energy-related retrofit decision-making process, taking a single and two-family house in Germany as a case study. The authors summarised five positive elements in support of the retrofit decision-making process: energy bill savings, supporting social surroundings, owners' willingness to take out a loan, and intention to improve a building's structural condition. Matosović et al.

(Matosović and Tomšić, 2018) evaluated the homeowners' retrofit choices considering different income classes based on a Croatian case study. The results indicated that homeowners in all income classes had a similar level of willingness-to-pay for similar energy efficiency measures (which could lead to the reductions of the energy bills), with the main differences being their capacity to invest for the future. Mills et al. (Mills and Rosenfeld, 1996) concluded that it would often be the non-energy benefits (e.g. enhanced thermal comfort, increased lighting technologies, and improved indoor air quality) that motivate retrofit decisions to adopt energy-efficient technologies. Saint-Gobain(Robin Brylewski, September 2016) investigated 3,000 homeowners and renters to list the most important features that they would want in their ideal home, and it is interesting that the top three responses related to security, running costs and the absence of damp or condensation.

Therefore, it would be of great importance to apply a novel approach and establish a comprehensive linkage between the stakeholders' motivations/willingness towards various energy-efficient measures and their actual economic, energy-saving, and social benefits when adopting building retrofits. The established linkage should also be displayed in a user-friendly and accessible manner to increase the awareness of the associated benefits among key stakeholders and decision-makers, thereby greatly motivating and maximising the market uptake of low carbon building retrofit towards 2050. Moreover, it is suggested for policymakers to consider the household status and annual income into the future energy efficiency policies.

Due to the definition difference of building retrofit rates across countries and do not correspond to the same energy savings level, the data are hardly comparable.

Because of the lack of an official European definition, Research stated that EU-14 has an average annual renovation rate of 1.10%, with the range varied from 0.08% (in Spain) to 2.40% (in Norway). Therefore, existing buildings must have a significant deep retrofit with high-efficient alternative measures, and meanwhile, address the issues of indoor environmental conditions, which helps to transform the existing properties into nearly zero-energy buildings. However, the increasing living standards need final energy consumption, which needs high energy efficient interventions to existed buildings to decoupling the increasing primary energy consumptions with the growth of indoor comfort levels. Although a threefold increase in building retrofit rate is required to reach the 2030 targets and carbon neutrality by 2050, according to their simulation results, the current stock's natural retrofit requirements are also required.

Thus, according to the previous analysis, it is significant to understand homeowners' motivations to take the retrofit measures for their properties and how the design technologies are adapted to the householder. Hence, regarding the motivations of residential buildings, retrofitting can be categorised into three sectors, including 1) retrofit to self-living, which will mainly consider the energy bill savings, initial investment; 2) retrofit to rent or sale, which is focused on the initial investment and the post-retrofit EPC level (decided by the energy-saving potential); 3) retrofit as an investment, taking account of the payback periods and initial investments. Therefore, five main retrofit objectives for residential building retrofit are summarised as following, which is usually interacted with each other:

1) Improve the indoor comfortable level (Murtagh, 2019, Michał Piasecki and Grze´skowiak, 19 November 2020, Haddad et al., 2020, Zuhaib et al., 2018,

Habibi, 2017, Hirst et al., 1985) ;

2) Energy-saving (Xin et al., 2018, Zheng et al., 2019a, Mikulić et al., 2016, Berardi and Manca, 2017, Catrini et al., 2020, Chen et al., 2015a, Tang et al., 2020, Shen et al., 2021, Sugár et al., 2020, Elsharkawy and Rutherford, 2018, Somasundaram et al., 2020) ;

3) Reducing energy bills cost (Ibn-Mohammed et al., 2014, Robertson et al., 2015, Vilches et al., 2017, Zhang and Augenbroe, 2018, Preciado-Pérez and Fotios, 2017) ;

4) Improve the value of the properties as a financial investment (Cho et al., 2020b, Cho et al., 2020a, McArthur and Jofeh, 2016, Tuominen et al., 2012) ;

5)Government legal regulations for the minimum EPC (Energy Performance Certification) grades to sale or rent (Fan and Xia, 2018, Gangolells et al., 2020, Li et al., 2019, Khayatian et al., 2017, Droutsa et al., 2016, Fleckinger et al., 2019, Tronchin and Fabbri, 2012);

Table 2-2 Summary of the previous studies on building retrofit multi-objective optimisation based on different retrofit motivations and objectives

Ref.	Country/City	Optimal method	Retrofit motivations	Retrofit objectives					Optimised results
				Comfort	Energy	Bill	Investment	EPC	
(Pisello and Asdrubali, 2014)	Perugia, Italy	Cost-effective optimal	Profitable investments	√	√	√			1) Energy bills reduce to £45.76 /year (priority in OB2); 2) Energy bills reduce to £28.16 /year (priority in OB1).
(Bar	Abu Dhabi,	Energy Plus-	Self-living	√	√				Energy savings of

bosa and Azar, 2018)	UAE	MATLAB coupling matrix							24.4% can be achieved without any effect on the comfort and well-being of building occupants
(Shao et al., 2014)	Aachen, Germany	NSGA-II algorithm and Pareto-front optimum	Self-living	√	√			√	The optimised energy reduction rate is 80.3% with an initial investment of £161 €/m^2 under requirements of low carbon emissions and low investment costs
(Papadopoulos and Azar, 2016)	Abu Dhabi, UAE	multiple linear regression surrogate model	Self-living	√	√				Providing occupants with control over their building systems can mitigate uncertainty in human actions on the built environment's performance.
(Azar et al., 2016)	Abu Dhabi, UAE	MATLAB-Energy Plus coupling engine	Self-living	√	√				Energy savings of 19% are observed without compromising thermal comfort levels.
(Miu and Hawkes, 2020	London, UK	N/A	Rental		√	√	√	√	Seven retrofit behaviour typologies are concluded based on widely

)									available socio-demographic and business data.
(Fan and Xia, 2018)	Hubei, China	Linear regression	Rental		√	√		√	The optimisation model considered retrofitting a building's walls, windows, and roof and installing a rooftop PV system to achieve better energy performance.
(Qu et al., 2020)	Oslo, Norway	Energy Limiting Difference (ELD) - EPC optimisation method	Rental		√			√	Retrofit combination level 'Extensive Retrofit' indicates the potential energy-saving range of 51%–83%, with all the COMBs satisfying the EPC grade B and most of the COMBs reaching EPC grade A.
(Jafari and Valentin, 2017)	Albuquerque, New Mexico	Linear regression	Self-living		√	√	√		The results of the model show that the budget of £9,680 for energy retrofitting of the case study can minimise the total LCC of the building for the homeowner
(Ben	Bucharest,	House of	Self-living	√				√	The better the

zar et al., 2020)	Romanian	Quality (HoQ) model	and rental						stakeholder's satisfaction, the more efficient the retrofit process and the EPC improvement.
(Brown et al., 2014)	Salford, UK	Survey, questionnaires and empirical research	Rental, sale and investment		√	√		√	The findings are relevant for the social housing sector and effectively deliver programmes such as the Green Deal and the Energy Company Obligation within the UK.
(Aravena et al., 2016)	Dublin, Ireland	Three-stage decision-making process	Self-living	√	√			√	The optimisation model considered retrofitting a building's walls, windows, and roof and installing a rooftop PV system to achieve better energy performance. Requirement on the EPC rating is taken as one of the objectives to ensure policy compliance, and a tax incentive program is considered in the model to

									maximise economic offset to the long payback period of the envelope retrofit.

Table 2-2 summarises previous research outcomes on building retrofit multi-objective optimisation results according to the defined retrofit motivations and objectives. It could be found that several limitations existed in multi-objective optimisation regarding the motivations on building retrofit, which could be categorised as following perspectives:

1) Lack of in-depth and comprehensive understanding of the motivations to building retrofit from the perspective of the homeowners. Most researches focused on retrofit to improve building energy efficiency and energy-cost optimum solely for the self-living purpose. However, hardly any research has investigated other retrofit motivations for sale, rental, and investment.
2) Lack of inclusive decision-making models considering comprehensive retrofit objectives (as summarised from OB1 to OB5) with homeowners' engagements. However, other objectives (such as energy bill reduction, financial investment to improve home values in the building market, and legal regulations EPC requirements) are addressed in the practical retrofit projects, which affect the retrofit strategies and final decision-making process dramatically.

2.8 Conclusion

This Chapter summarized the literature review based on the previous researches

on the residential building retrofit case study and high-performance retrofit technologies. In the description of the background, section 2.2 introduces the building retrofit status in EU and UK, from the perspectives of carbon emission amount and reduction rate in residential building section. From the perspective of carbon emissions, residential building accounts for 20.6% and 14.6% of the overall carbon emissions in EU and UK by the end of 2017. According to the EU commission's assessment indicator, an average of 3% stock retrofit rate annually is a minimum requirement to achieve the overall energy efficient target. However, the average stock retrofit rate is 1.10% in 14 main EU countries. Furthermore, main challenges and motivations for residential building retrofit are discussed in detail.

Section 2.3 discussed the high-performance building retrofit measures, which are categorized by passive retrofit technologies the system retrofit technologies.

The limitations for the applications of both White- and Black-box models under the deep retrofit context can be categorised into four areas:

1) Inadequate data requirement

2) Neglect of coupling effects in deep energy retrofit combinations

3) Lack of complex heat transfer phenomena in single-family houses

4) Time-consuming

Therefore, the above-mentioned two types of BPS models cannot fully address the crucial research challenges in optimising deep energy retrofit combinations rapidly and accurately for single-family houses.

Finally, multi-objective optimisation algorithms are introduced with previous

literatures, such as direct numerical simulation method, Monte Carlo simulation method, EnergyPlus based software simulation, Ensemble Calibration method, screening method, dynamic modelling tool. Besides, the optimisation scale is discussed with local and global size.

Moreover, it is apparent that several limitations exist in multi-objective optimisation regarding the motivations for building retrofit, which can be summarised in the following perspectives:

1) Lack of in-depth and comprehensive understanding of the homeowners' motivations to undertake building retrofit..

2) Lack of inclusive decision-making models considering comprehensive retrofit objectives with homeowners' engagement.

In general, the decision-making criteria and objectives are optimised separately in the literature [60-62], and homeowners' motivations are ignored or not carefully defined in these research works.

3. On-site test of innovative envelope retrofit technologies for energy demand reduction

3.1 Introduction

Compared with new buildings, traditional and historical building renovation is even more challenging, as the selection and application of the building retrofit measures need to be extremely careful, in order to maintain the building's unique architectural appreance and integratiy(Godwin, 2011). According to Whitmanet et al. (Whitman, 2016), buildings constructed before 1919 in the UK, could be considered as historical buildings, exhibiting special architectural features and cultural/historical values. In the UK, the reign of Queen Victoria (1837-1901) has witnessed successive housing booms, resulting in the construction of millions of Victorian houses which now represents the key characteristics of many towns and cities in Britain (Marshall, 1986).The character of the old/historical buildings should be respected and preserved as much as possible, and a proper balance between energy efficiecny improvement and historcial building conservation needs to be striken when applying building renovation (Godwin, 2011).

The reviewed studies in Chapter 2 have attempted to tackle the traditional/histrocial building energy renovations from different angles. It is still quite challenging to define and apply an array of appropiriate building retrofit measures for historical building renovations, in order to maintain the building's integratiy and in the meanwhile achieve higher level indoor thermal comfort. For these traditional/historical building renovations, proper building retrofit measures should be selected, which are not just energy efficient and affordable.

But more importantly, the renovation measures should impose the least impact on the external architectural characters of the buildings, and also provide considerable improvement on the indoor thermal comfort and living conditions. Any retrofit interventions which will affect or damange the materials, proportions, and craftsmanship of the historic buildings should be strictly avoided. Moreover, from the homeowners' perspective, their decisions on building renovations are not only related to potential energy saving and associated cost benefit. More often, they will be motivated to undertake building renovation if it proves to provide increased thermal comfort and indoor living conditions. Under this context, a range of Passive retrofit measures are defined (Chen et al., 2019a) in the research, with special focus on improving the existing building envelope thermal performance by means of additional thermal mass to the interior wall, window upgrading and airtightness improvements, etc.

Therefore, this chapter describes innovative fabric insulation technologies, including interior façade insulation, glazing insulation and efficient daylighting pipes. Innovative interior façade insulation materials have two types of silica-based vacuum insulation panels and starch-aerogel insulation panels, which are more space-saving than traditional insulation materials with Polyisocyanurate insulation (PIR) and mineral wool insulation. Innovative glazing insulation is vacuum glazing and thin film PV vacuum glazing (PV-VG), which has well performance compared with traditional types of single, double and triple glazing. Moreover, efficient daylighting technology is included with daylighting pipes. These innovative retrofit technologies are tested in the creative energy homes in University of Nottingham, with house name of E.ON house and David house, to

investigate and validate the real performance of application on site, which could help to adjust the performance data according to the on-site testing results.

3.2 Field test rig set up on site

3.2.1 Test rig for façade insulation materials

Façade interior insulation is installed and tested on the south-east wall of E.ON house at University of Nottingham, United Kingdom with latitude of 52.9438ºN, and longitude of -1.1934ºW, as shown in Figure 3-1. There are four thermocouples used to monitor the external and internal air temperature which are 30mm distance from the wall surface with two thermocouples in each side, as recommended by BRE U-value test standard (Milsom, 2016). And another two thermocouples used to measure the ambient temperature and internal air temperature 100mm away from the wall surface with one thermocouple in each side. Besides, one heat flux sensor is installed on the interior wall surface to measure the heat flux through the wall. A 1 kW convective heater was used as the heat source for indoors. It worth emphasising that the heat flux monitoring of the insulated wall has been conducted under two conditions: during the day (with solar heat radiation) and during the night (without solar heat radiation). During the day, the reading measured by the heat flux sensor for the thermal transmittance is given by the value of the heat gain, which is derived from the difference between the internal heater and external solar radiation. During the night, the value of the heat gain is derived from only the internal heater. Therefore, the focus of experiment during the night is the thermal transmittance or the U-value, which is used in further sections of this Chapter to indicate the U-value performance of the insulation materials.

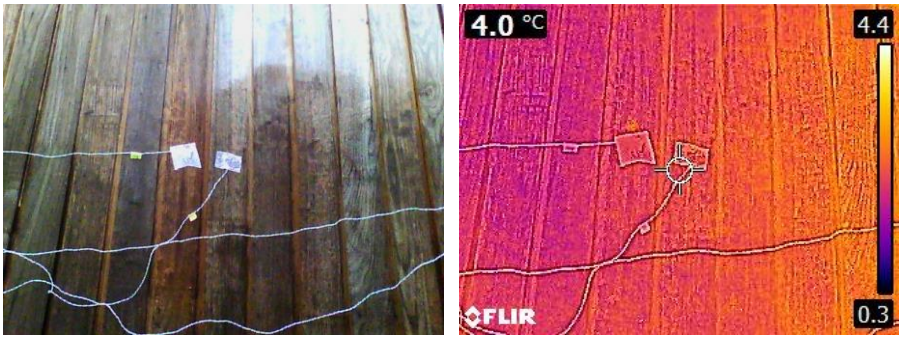
The external and internal test rig installations are shown in Figure 3-2 with thermograph images. The specific technical data of experiment equipment is listed as shown in Table 3-1.

Table 3-1 Specific technical data of experiment equipment

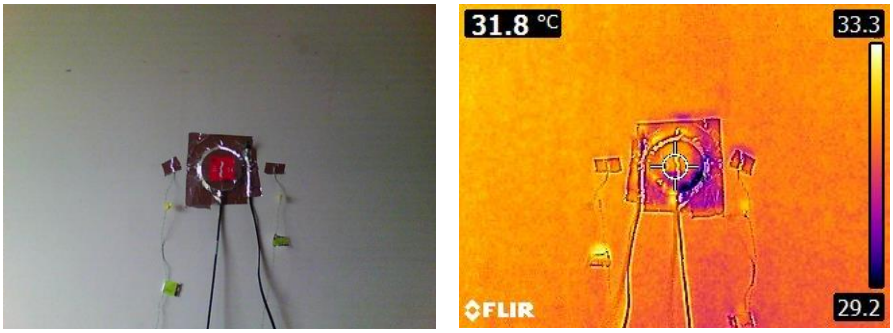
Experiment equipment	Series name	Test range	Resolution	Accuracy
Thermocouples	RS PRO Type-"K" 2m length	-75℃ to +260℃	0.1	±0.75%
Data logger	Datataker DT80 Series 2	±30 mVdc	0.25 μV	±0.35%
Heat flux sensor	Hukesflux Thermal Sensors HFP01	-2000 to +2000 W/m²	0.1 W/m²	± 3%
Thermal imaging camera	FLIR E4	-20℃ +250℃	0.1℃	± 2%



Figure 3-1 E. ON house south-east façade experiment site



(1) External wall view with thermograph



(1) Internal wall view with thermograph

Figure 3-2 U-value test with existing wall construction

The experiment is carried out in a consequent 72 hour from 19th November 2019 to 22th November 2019, with data analysed only in night time, as shown in Figure 3-3. According to the experiment test, the average U-value of the E. ON house façade is calculated with the heat flux divided by the temperature difference

between external and internal air temperature. Therefore, the post-processed U-value data is of the existing wall surface is approximately 0.23W/m^2.K (tested in 2019), which is slightly higher than the theoretical U-value of thermal structure of the design with U-value of 0.18W/m^2.K (façade constructed in 2007). Therefore, the U-value increased by 28% within 12 years' degradation compared with the construction renovation year in 2007. The thermal resistance of original wall is calculated by 1 divided by the U-value of original thermal wall, which gets the value of 4.35 m^{2}K/W, as can be used as the constant value in the calculation process of performance with installation of insulation panels.

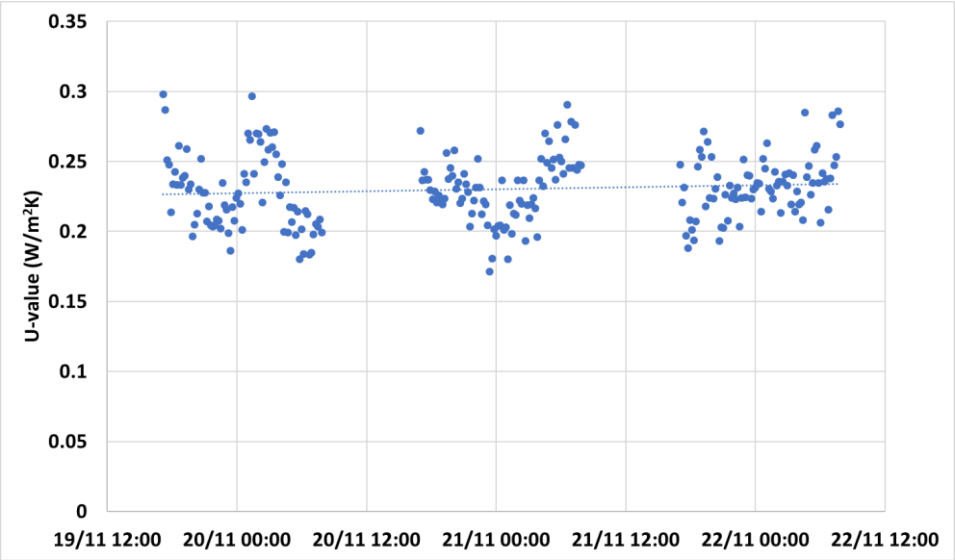


Figure 3-3 U-value of the existing wall of the E. ON house façade

The calculation process of the thermal conductivity coefficient (λ_{ins}) is calculated with thickness of the insulation panels (h_{ins}) divided by the thermal resistance of the insulation panels (R_{ins}), as shown in Eq. (3-1). The thermal resistance of insulation panels (R_{ins}) is calculated by the difference between the total thermal resistance (R_{tot}) and original wall thermal resistance (R_{ow}) and the surface thermal resistance $R_{surface}$, as shown in Eq. (3-2). The original wall

thermal resistance (R_{ow}) is constant and calculated before the installation of all other insulation technologies. Total thermal resistance (R_{tot}) is the sum of thermal resistances including original wall thermal resistance and insulation thermal resistance as shown in Eq. (3-3), which is calculated by the ratio between 1) the internal and external air temperature difference and 2) heat flux through the wall.

$$\lambda_{ins} = \frac{h_{ins}}{R_{ins}} \quad \text{Eq. (3-1)}$$

$$R_{ins} = R_{tot} - R_{ow} - R_{surface} \quad \text{Eq. (3-2)}$$

$$R_{tot} = \frac{\Delta T_{air}}{\emptyset_{wall}} = \frac{T_{a,i} - T_{a,o}}{\emptyset_{wall}} \quad \text{Eq. (3-3)}$$

3.2.2 Test rig for glazing insulation

The performance of the vacuum glaing and PV-VG under real sky conditions still needs to be investigated. To carry out the testing, the prototypes were installed at E. ON research house at the University of Nottingham, United Kingdom with latitude of 52.9438° N, and longitude of 1.1934° W. It is worth emphasising that the outdoor monitoring of the glazing insulation has been conducted under two conditions; during the day and during the night (at zero solar radiation). The thermal and electrical characteristics of the vacuum glazing and PV-VG under real conditions were monitored using the sensors as summarised in Table 3-2. During the day, the reading given by the heat flux sensor for the thermal transmittance is not reliable due to the input of solar radiation to the heat flux sensor and also due to the absorbed solar radiation by the PV layer. Therefore, during the day, the only parameters that are being considered are the electrical power generation by the PV-VG. The typical

monitoring period is between 9:30 a.m. to 6:00 p.m. in a typical day of May and June. Meanwhile, the focus of the experiment during the night is the thermal transmittance measurement or U-value. A 1kW radiator was used as the heat source for indoors.

Table 3-2 Measured parameters and uncertainties

Experiment equipment	Series name	Test range	Resolution	Accuracy
Thermocouples	RS PRO Type-"K" 2m length	-75℃ to +260℃	0.1	±0.75%
Data logger	Datataker DT80 Series 2	±30 mVdc	0.25 μV	±0.35%
Heat flux sensor	Hukesflux Thermal Sensors HFP01	-2000 to +2000 W/m²	0.1 W/m²	± 3%
Pyranometer	Kipp & Zonen CM22 Pyranometer	0-4000 W/m²	The instrument has an analog output, therefore the resolution is infinite	5W/m^2

Data Acquisition	RO4 with Keysight 34972A	100mV to 300V, 10mA to 1A	0.003mV, 0.005mA	Electric current (I) (±1.5 μA) Voltage (V) (± 190 μV)

3.3 Silica based vacuum insulation panels

The basic concept of vacuum insulation panels technology is to evacuate the core material to reach low enough pressure values to obtain Knudsten number (Lorenzati et al., 2017) $K_n \geq 1$, which means the ratio of the mean free path of the gas molecule is higher than the characteristic size of the porous media. And accordingly, the thermal conductivity of gas can be neglected with reduction of the overall U-value in a large amount, which resulting the total thermal conductivity mainly depends on the solid conductivity and infra-red radiation in the porous. Besides, the actual thermal performance of the vacuum insulation panels could be different from the laboratory tested performance, with two main phenomenon influencing the performance: 1) the thermal bridge of the edge sealing of the vacuum insulation panels will improve the overall U-value; 2) the aging effects. Therefore, the actual thermal performance will be discussed with on-site measuring data.

The silica based vacuum insulation panels with thickness of 40mm and surface area of 0.316m^2 (0.40m×0.79m) is installed on part of the experiment wall,

which is compared with original wall part without insulation panels. One heat flux sensor is installed on the surface of the interior insulation panel, with another one installed on the original wall part, which has 200mm distance away from the edge of the insulation panels.

To investigate the performance with installation of silica based vacuum insulation Panel (VIP) on the interior wall, 3 successive days (72hours) are carried out from 22th November 2019 to 25th November 2019. The installed samples are shown in Figure 3-4, as well as the thermograph imaging, which indicates the temperature of the panel central point is approximately 33.5℃.

As shown in Figure 3-5, the average U-value with the silica based VIP is reduced from 0.23 W/m^2.K (original wall) to 0.08 W/m^2.K, with fluctuation range floated between 0.06 W/m^2.K and 0.11 W/m^2.K. And according to the calculation equation Eq. (1) to Eq. (3) described in section 3.2.1, the thermal conductivity of the central panel of the silica based vacuum insulation panels is calculated as 0.005 W/mk is slightly higher than the theory value of 0.004 W/mk. And the K-value is varied from 0.003 to 0.008 W/mk with the effects of the thermal bridges. Besides, the internal air temperature with 100mm distance (average 34.44℃) is 1.18℃ higher than that with 30mm distance (average33.26℃), And the external ambient temperature with 100mm distance (average 7.85℃) is 0.68℃ lower than that with 30mm distance away from the insulation panel surface (average 8.53℃).

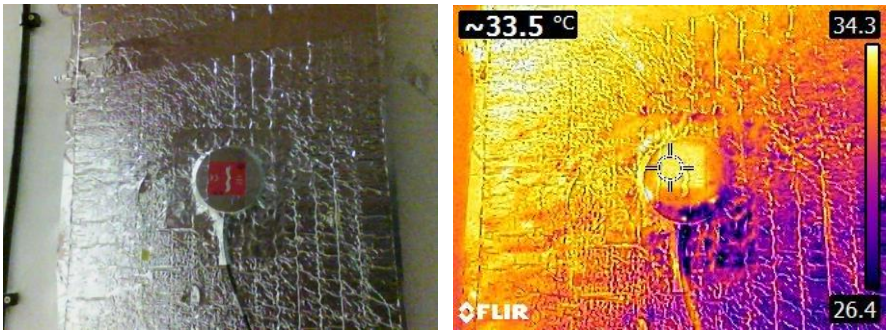


Figure 3-4 U-value test with interior wall insulation with silica based vacuum insulation panels

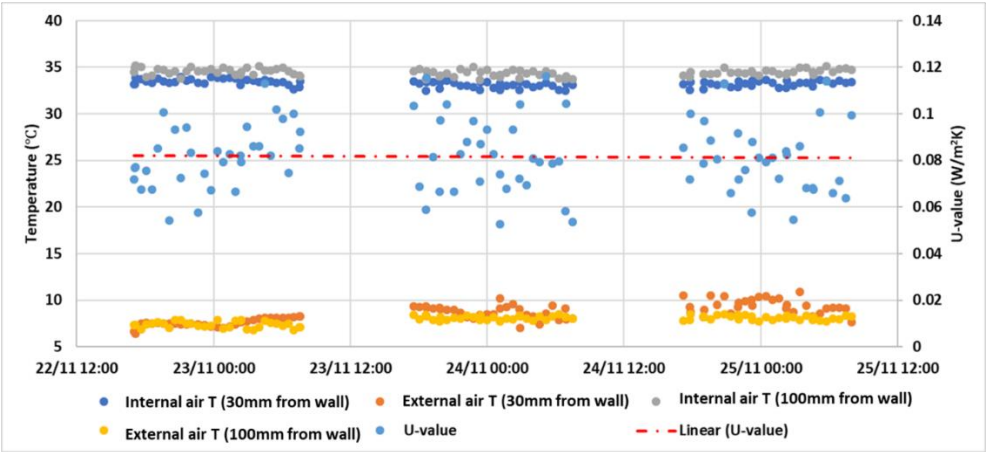


Figure 3-5 U-value of silica based vacuum insulation panels (72 continuous nights)

Figure 3-6 indicates the thermal comfort improvement with silica based vacuum insulation panels under the external ambient temperature of approximately 8℃. It is found that the internal and external air temperature (30mm distance away from the wall surface) difference with insulation panel is approximately 24.73 ℃, which is 3.29℃ improved compared with the air temperature difference of approximately 21.44℃ without the insulation panels. Therefore, the internal insulated air temperature increased by 2.96℃ compared with the original wall without insulation materials.

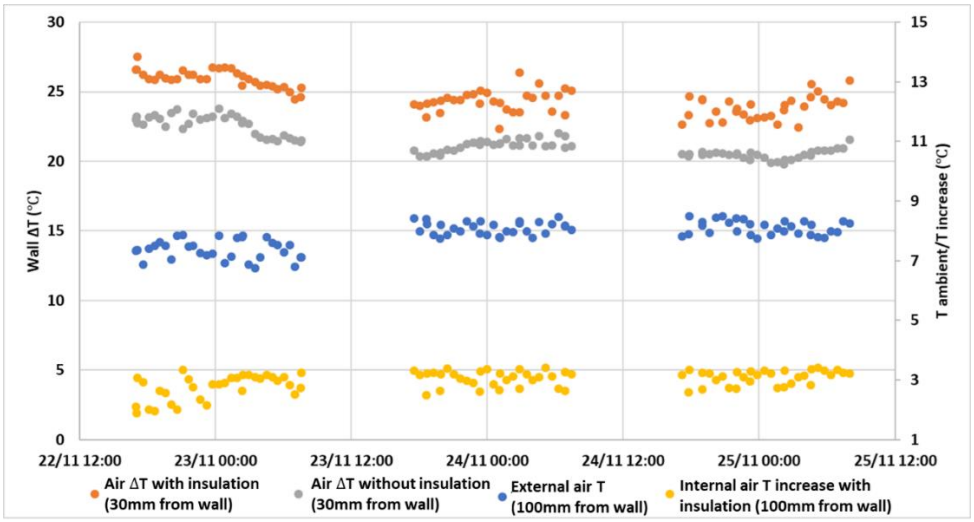


Figure 3-6 Thermal comfort with silica based vacuum insulation panels (72 continuous nights)

3.4 Starch-aerogel insulation panels

In the past decade, a large research effort worldwide has been devoted to developing polysaccharide-based aerogels. This has been stimulated by the fact that the raw materials of conventional aerogels with environmentally friendly requirement. Therefore, development of polysaccharide-based aerogels has attracted extensive interest from researchers. The polysaccharide-based aerogels are formulated from natural ingredients, with excellent eco-friendly biodegradable feature and hence maximizing the polysaccharide ingredients in aerogels has become a tendency (Wang et al., 2019b). Starch is one of the most abundant natural cellulose, widely existing in nature world, which could be used for convenient preparation of starch-based aerogel insulation materials. In this section, starch-aerogel may become a key ingredient in novel insulation materials due to their unique properties, including biocompatibility, sustainability, low toxicity and renewability (Wang et al., 2019b).

The starch-based aerogel insulation panels with thickness of 45mm and surface

of 0.123m^2 (0.35m×0.35m) is installed on part of the experiment wall, which is compared with original wall part without insulation panels. One heat flux sensor is installed on the surface of the interior insulation panel, with another one installed on the original wall part, which has 200mm distance away from the edge of the insulation panels.

To investigate the performance with installation of starch-based aerogel insulation Panel on the interior wall, 3 successive days (72hours) are carried out from 2th December 2019 to 5th December 2019. The installed samples are shown in *Figure 3-7*, as well as the thermograph imaging, which indicates the air temperature with 30mm distance from the panel central point is approximately 35.3℃.

As shown in *Figure 3-8*, the average U-value with the starch-based aerogel insulation panel is reduced from 0.23 W/m^2.K (original wall) to 0.16 W/m^2.K, with fluctuation range floated between 0.13 W/m^2.K and 0.20 W/m^2.K. And according to the calculation equation Eq. (1) to Eq. (3) described in section 3.2.1, the thermal conductivity of the starch-based aerogel insulation panels is calculated as 0.024 W/mk is slightly higher than the theory value of 0.023 W/mk. However, the K-value is varied from 0.013 to 0.069 W/mk.

Besides, the internal air temperature with 100mm distance from the panel (average 30.97℃) is 1.92℃ higher than that with 30mm distance (average 29.05℃). And the external ambient temperature with 100mm distance from the panel (average 3.03℃) is 0.18℃ lower than that with 30mm distance (average 2.86℃).



Figure 3-7 U-value test with interior wall insulation with starch-based aerogel insulation panels

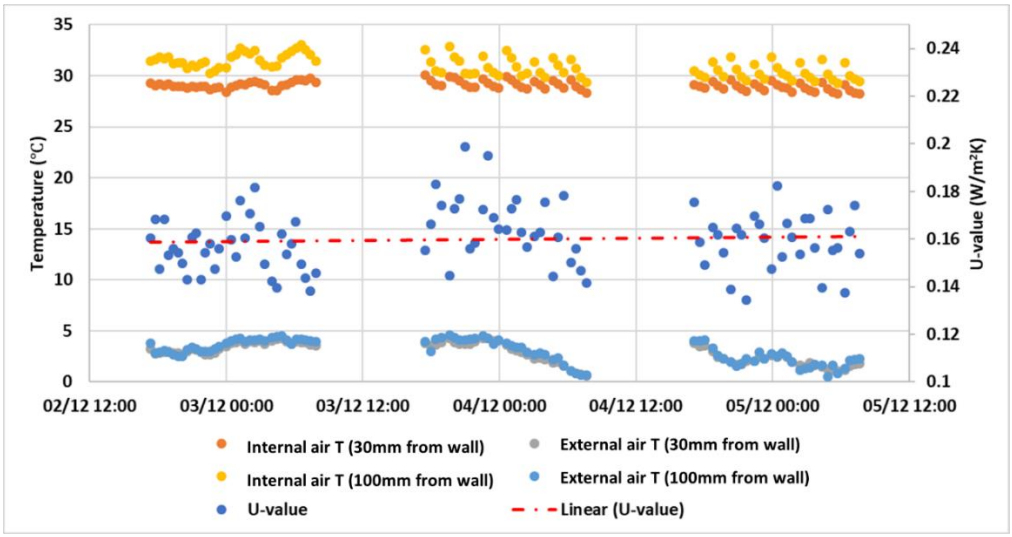


Figure 3-8 U-value of interior wall with starch-based aerogel insulation panels (72 continuous nights)

Figure 3-9 indicates the thermal comfort improvement with starch-based aerogel insulation panels under the external ambient temperature (100mm distance) of approximately 3.0 ℃. It is found that the internal and external 30mm air temperature difference with insulation panel is approximately 26.19 ℃, which is 4.56 ℃ improved compared with the 30mm air temperature difference of approximately 21.63℃ without the insulation panels. Therefore, the internal insulated air temperature (30mm wall diantance) increased by 1.19℃ compared

with the original one without insulation materials.

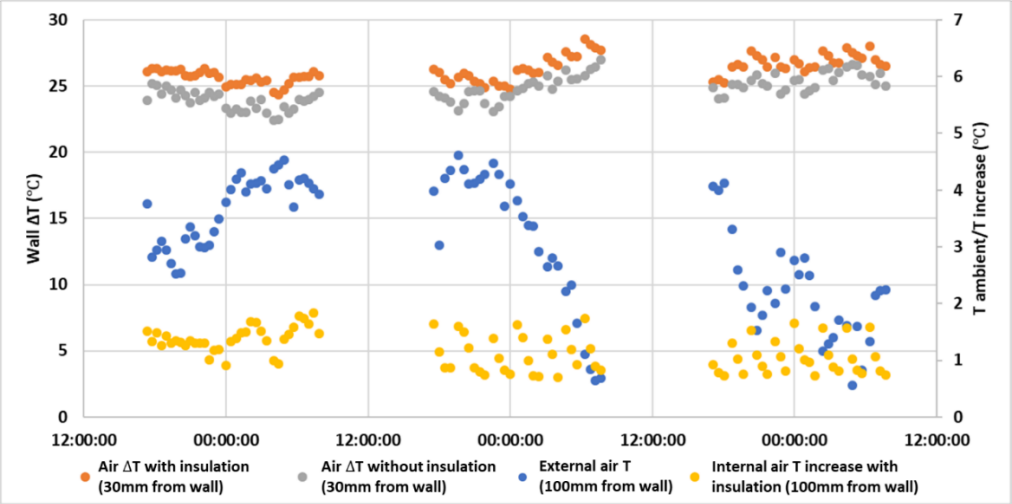


Figure 3-9 Thermal comfort with starch-based aerogel based vacuum insulation panels (72 continuous nights)

3.5 Vacuum glazing

Glazing facades and windows visually connect the building interiors to the outdoor environment to promote resident relaxation and keep a comfortable daylight (Ghosh and Norton, 2018). Vacuum glazing (VG) represent an alternative to traditional insulation glazing due to its high thermal performance within a smaller thickness of insulation. The VG consists of two panes of glass separated by an evacuated gap at very low pressure less than 0.1 Pa (Katsura et al., 2020). These two glass panes were supported with a very tiny pillars normally made of stainless steel and hermetically sealed (Memon et al., 2019).

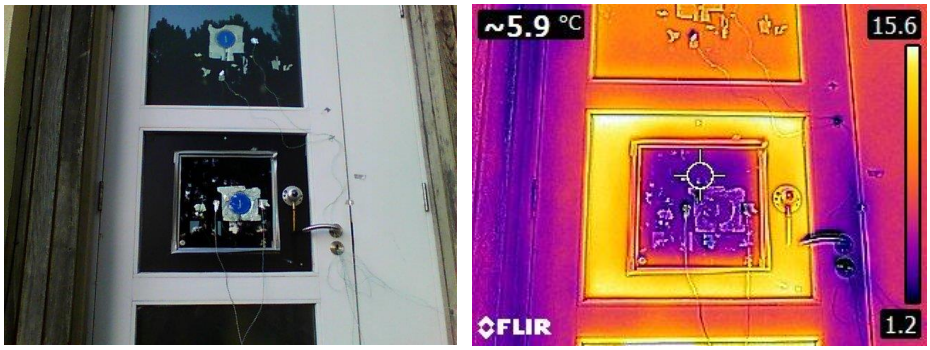
The previous single glazing panel with thickness of 1.5mm and surface of 0.12 m^2 (0.40m×0.30m) is replaced by vacuum glazing panels with thickness of 7mm. One heat flux sensor is installed on the surface of the interior vacuum glazing panel. Besides, two thermocouples are installed with 30mm distance

away from the panel surface. Another two thermocouples are installed with 100mm distance away from the panel surface.

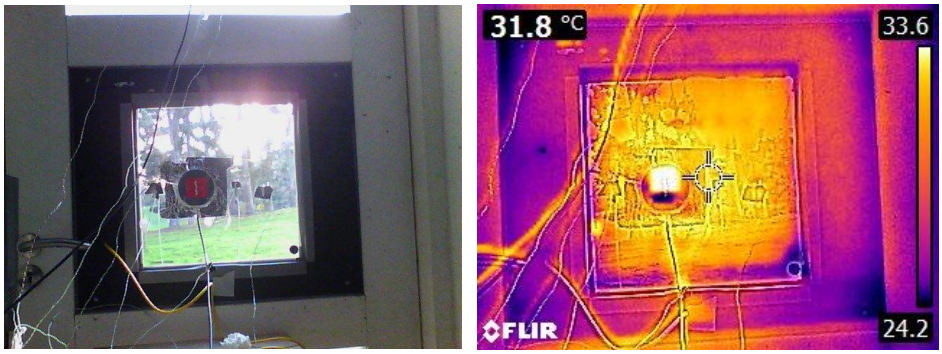
To investigate the performance with installation of vacuum glazing insulation Panel, 3 successive days (96hours) are carried out from 21th May 2019 to 24th May 2019. *Figure 3-10* (1) shows the external view of the vacuum glazing, as well as the thermograph imaging, indicating the external air temperature (30mm distance of the panel central point) of approximately 5.9℃. The internal view of the vacuum glazing panel is shown in *Figure 3-10* (2), with internal air temperature (30mm distance of the panel central point) of 31.8℃.

As shown in *Figure 3-11*, the average U-value with the vacuum glazing insulation panel is reduced from 3.5 W/m^2.K (single glazing) to 0.80 W/m^2.K, with fluctuation range floated between 0.70 W/m^2.K and 0.90 W/m^2.K.

Besides, the internal air temperature (100mm distance of the panel central point) (average 28.36℃) is 5.69℃ higher than the external air temperature (100mm distance of the panel central point) (average 22.67℃), And the external ambient temperature with 100mm distance (average 13.28℃) is 0.83℃ lower than the that with 30mm distance (average 12.45℃).



(1) External view of vacuum glazing with thermograph



(2) Internal view of vacuum glazing with thermograph

Figure 3-10 External and internal view of vacuum glazing

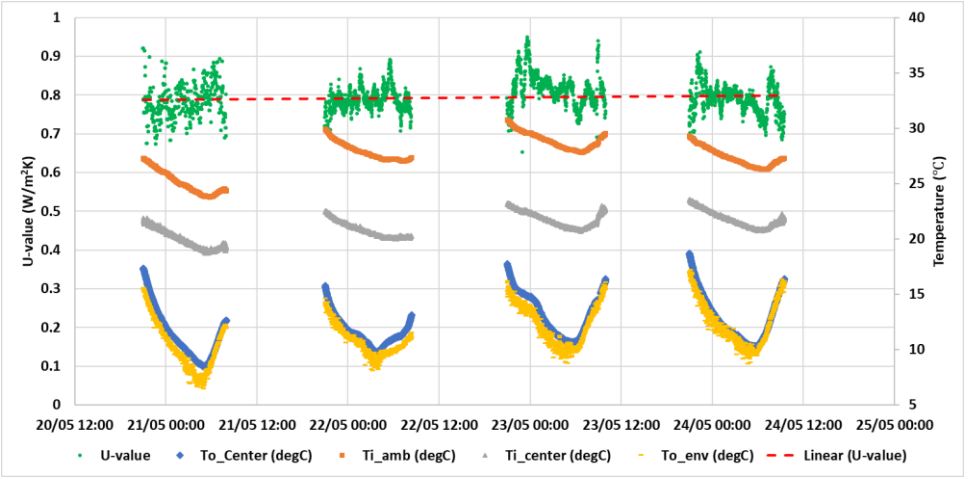


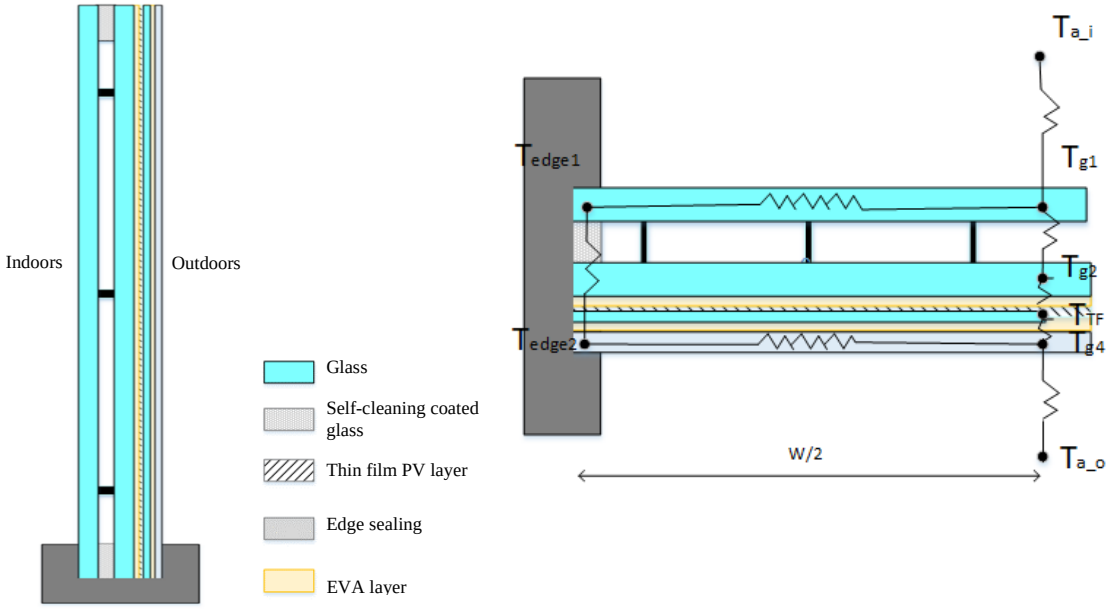
Figure 3-11 U-value of vacuum glazing (72 continuous nights)

3.6 Thin film PV vacuum glazing (PV-VG)

3.6.1 Design concept

The design of PV-VG is illustrated in *Figure 3-12* (a). PV-VG involves an integration between a thin film PV glazing with a double vacuum glazing (both manufactured independently) and an additional layer of self-cleaning coated glass with total 4 layers of glass units which gives the total thickness of 14 mm. The layers were combined via Ethylene Vinyl Acetate (EVA) film using an autoclave facility set at its optimum temperature and pressure.

The thermal resistance network for the PV-VG is shown in *Figure 3-12* (b). Both the width and the length of the PV-VG have the same length and denoted as *W*. The heat transfer was analysed based on the following temperature nodes which are; the average glass temperature facing indoors denoted by $Tg_{1,}$ the average internal glass temperature denoted by $Tg_{2,}$ the average temperature of the thin film PV glazing denoted by T_{TF} and the average temperature of the self-cleaning coated glass denoted by $Tg_{4.}$ The lateral heat transfer ends at the point right at the edge sealing and the temperature was denoted as $T_{edge1.}$ Due to high thermal conductivity of the edge sealing, it acts as a short circuit for the heat transfer at the edges of the glazing. Meanwhile, due to high thermal conductivity between *g2* and *g4*, the lateral heat conduction in the glass slab *g2* and thin film PV glazing (*TF)* are assumed negligible. The temperature of the position in *g4*, of which the edge heat transfer takes place is denoted as $T_{edge2.}$ For the uninsulated edges, there will be heat transferred from the internal ambient to the area around the edges.



a) Schematics of PV VG-4L *b) the thermal resistance network*

Figure 3-12 Physical structure of PV VG-4L (a) (b)

The thermal resistance network implies that, at certain level of solar radiation and ambient temperature, the internal surface temperature is in general lower than the external surface temperature. This can be explained as follows. When the PV panel absorbed solar radiation, a fraction of the absorbed solar radiation will be converted into electricity meanwhile a fraction will be wasted in the form of heat. In the summer, this can be considered as an advantage since the installation of PV glazing would normally cause additional heating during summer of which in return, increase the cooling load of the building.

According to calculation in literature (Hasila Jarimi 2020), MATLAB is used to carry out the iteration process with Newton-Raphson iteration technique to estimate the heat transfer coefficients of the variables with average of 0.57W/m^2.K. A PV-VG prototype using an amorphous silicon (α-Si) solar cell as shown in *Figure 3-13* was manufactured.



Figure 3-13 The PV-VG prototype

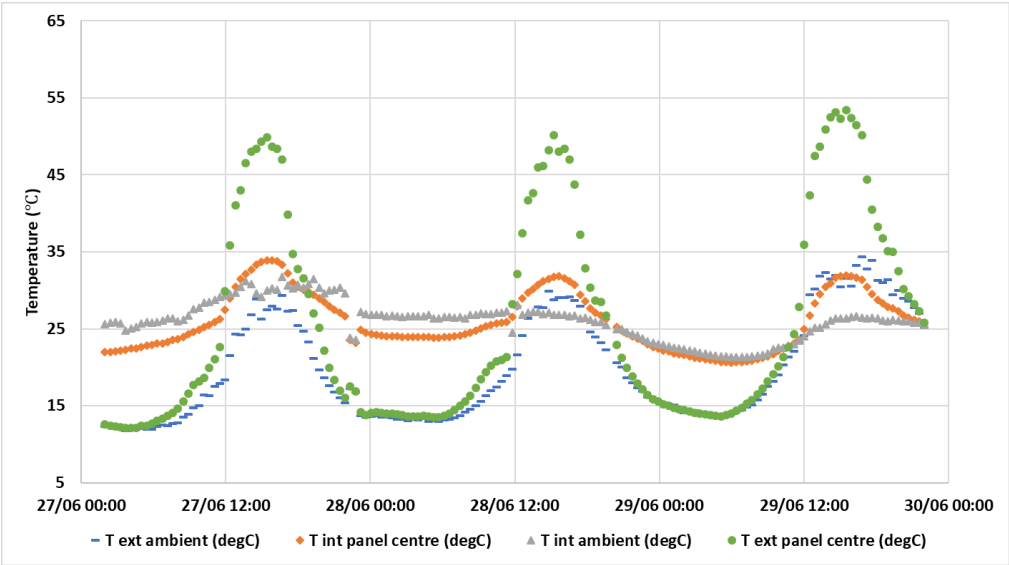
3.6.2 Result and discussion – Electricity conversion efficiency

Figure 3-14 (a) and (b) show the solar radiation, electricity conversion efficiency, surface temperatures of the PV-VG of both internal and external, ambient temperature of both internal and external, during the day and night. It should be noted that for the data taken on the 27th to 30th of June 2019, the internal heat source was switched off during the day meanwhile, the average heating temperature was set at 30 ˚C during the night (i.e. from 8 p.m. to 4 a.m. the next day). On the day of testing, the sky was in a clear sky condition and hence clear pattern of solar radiation curve with the time of the day was obtained. Three sets of experiments during the day were conducted to evaluate the performance of the PV electricity conversion efficiency on the 27^{h} to 30st of June 2019. Besides, three sets of experiments during the nights were conducted to evaluate the performance of the thermal transmittance coefficient (U-value).

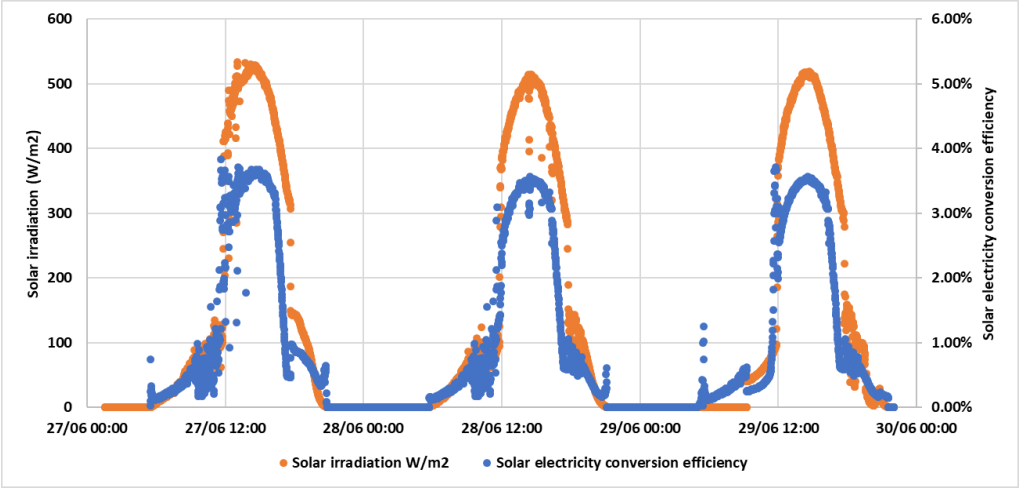
During the aforementioned period, the average intensity of the incident solar radiation dropped for a step change from 500 W/m² to 0 W/m2 and the temperature profiles clearly follows an exponential decay lagging behind the

step change. It is worth noting that, in both graphs, at low to zero solar radiation, the indoor panel surface centre temperature of the PV VG-4L is in general higher than its external panel central surface temperature. However, as the incident solar radiation increases, the external panel surface temperature increases, and finally higher than that of internal panel surface when solar radiation higher than 300W/m^2. The trend of the graph is explained as follows; when the PV component of the PV VG-4L absorbed the incident solar radiation, a fraction was converted into electrical energy meanwhile the rest was wasted in the form of heat. However, the vacuum layer behind the PV component of the PV VG-4L act as the insulation layer or barrier to the wasted heat from being transferred indoors. As a result, the external surface temperature of the PV VG-4L became higher compared to its internal surface temperature. In the summer, this will be an advantage in comparison to the typical installation of BIPV in double glazed configuration. For the data analysis, the temperatures, solar radiation and heat flux were recorded for every 1 s meanwhile, the electrical parameters were recorded for every 10 s.

In terms of efficient building sector, there is a great potential for building-integrated PV technologies (BIPV) to offer potential energy savings of a building by generating solar energy resources captured via the building materials itself. According to the electricity efficiency described in *Figure 3-14*(b), the maximum solar electricity efficiency occurred with 3.7% when solar radiation reaches approximately 520W/m^2.



(a) Ambient and panel temperature with testing of PV VG-4L



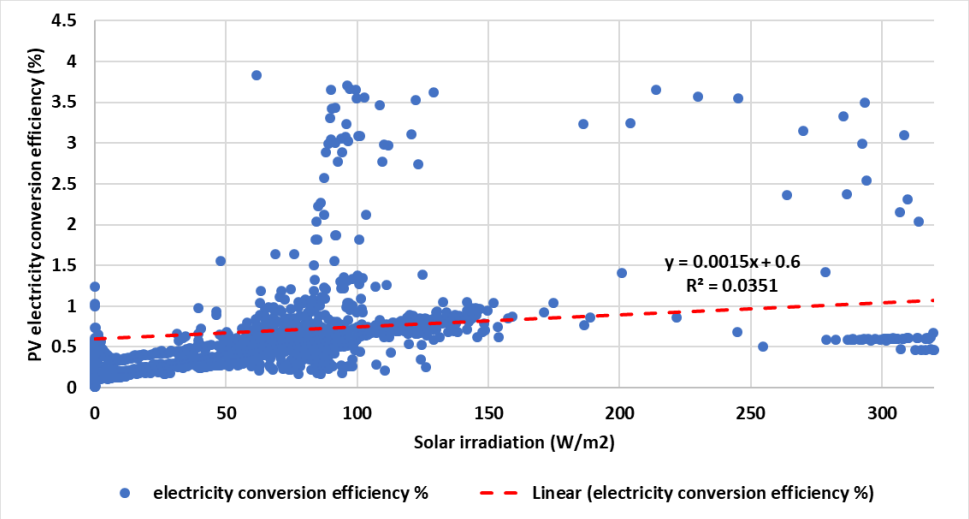
(b) Solar and electricity conversion efficiency with testing of PV VG-4L

Figure 3-14 Testing performance of PV VG-4L

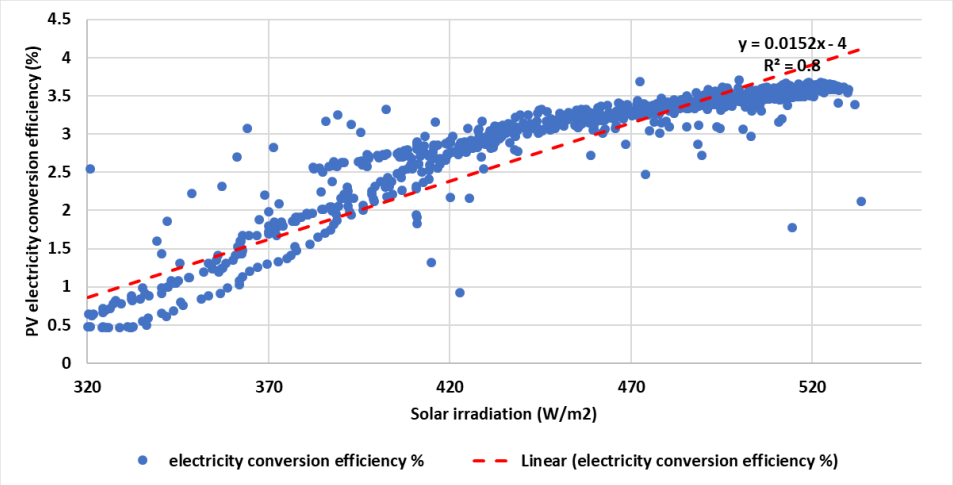
In order to clearly demonstrate the solar electricity conversion efficiency trend with the increasing of the solar radiation, the relationship between the solar radiation and the electricity conversion efficiency is concluded in *Figure 3-15*(a) and *Figure 3-15*(b), which can furtherly used in the future modelling with building retrofit project. Besides, it is noted that the impact of temperature

change to the PV electricity conversion efficiency is not considered. In *Figure 3-15*(a), the average PV electricity conversion efficiency increased from 0 to 1.08% with increasing rate of 0.15% under solar radiation lower than 320W/m^2. However, the average PV electricity conversion efficiency increased from 1.05% to 3.90% with increasing rate of 1.52% under solar radiation varied from 320W/m^2 to 550W/m^2. Therefore, it is figured out that the PV electricity conversion efficiency increasing rate is changed from 0.15% to 1.52% with solar radiation varied between 0-320W/m^2 and 320-550W/m^2, respectively. The function of solar PV electricity conversion efficiency (f(s)) with solar radiation (s) is illustrated as Eq. (3-4).

$$f(s) = \begin{cases} 0.15\% \times s + 0.6, & 0 < s < 320 \\ 1.52\% \times s - 4.0, & 320 \leq s < 550 \end{cases} \quad \text{Eq. (3-4)}$$



(a) PV electricity conversion efficiency with solar radiation below 300W/m^2

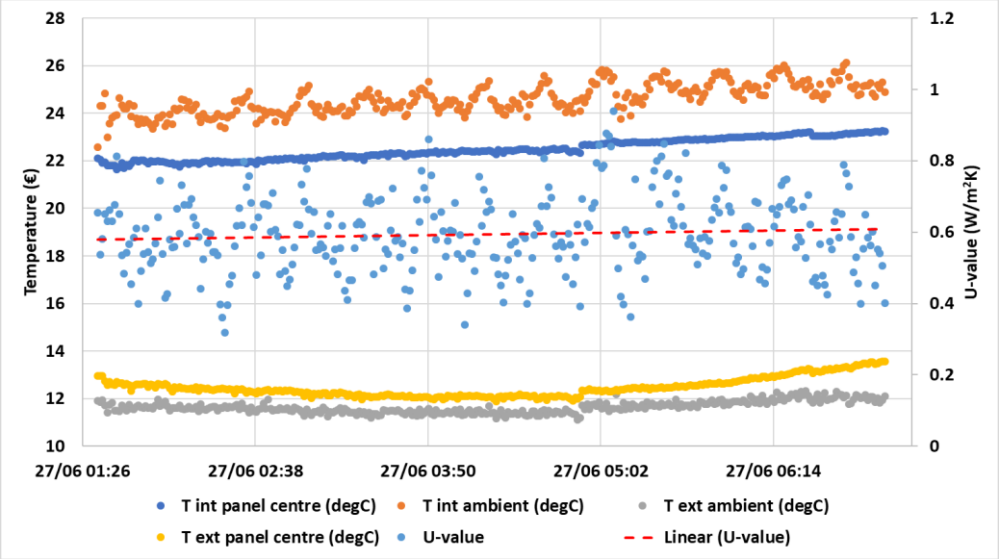


(b) PV electricity conversion efficiency with solar radiation above 300W/m^2

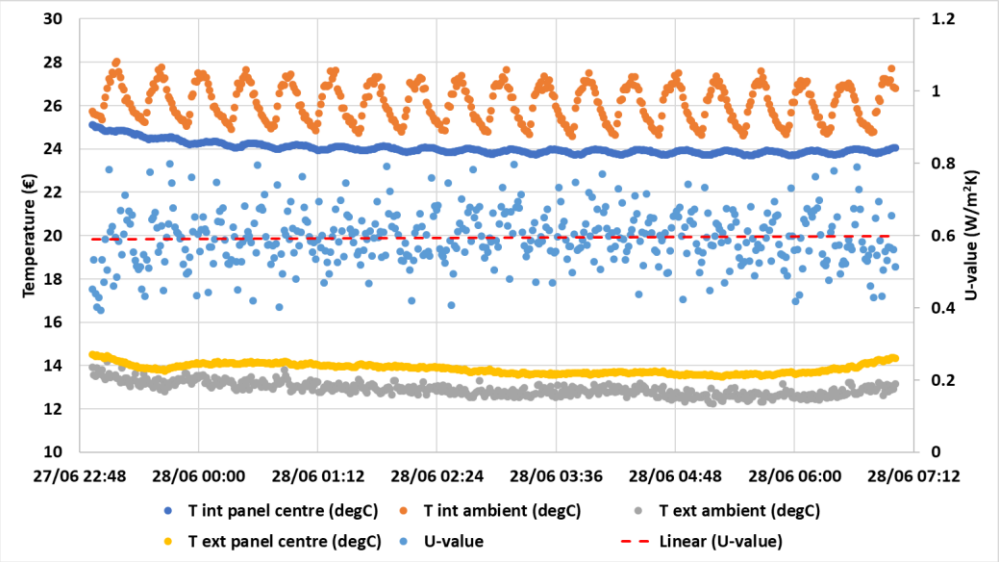
Figure 3-15 PV electricity conversion efficiency with solar radiation

3.6.3 Results and discussion – U-value

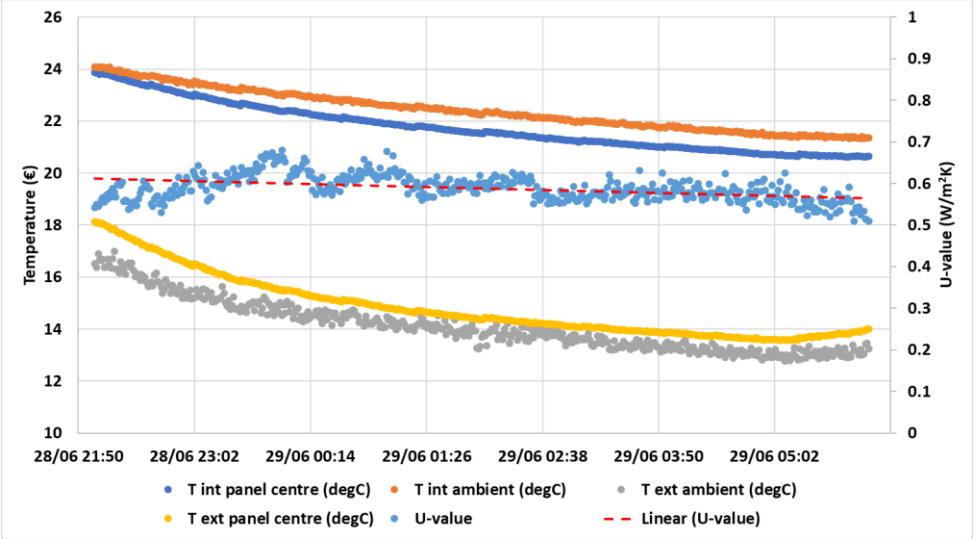
Figure 3-16(a) (b) and (c) indicates the measured U-value with air temperature of both internal and external side. The measurement is carried out in three successive days from 27th to 30th June in 2019. Besides, there are approximately 10℃ difference between the internal and external ambient air temperature. According to the heat flux and air temperature difference of internal and external sides, the U-value is calculated with an average of 0.60 W/m^2.K, which has error difference of 5.3% compared with U-value of 0.57 W/m^2.K in theory.



(a) U-value test of PV-VG in 27th June 2019



(b) U-value test of PV-VG in 28th June 2019



(c) U-value test of PV-VG in 29th June 2019

Figure 3-16 U-value of PV VG-4L in different time periods (a) (b) (c)

3.7 Daylighting pipes

Lighting pipes are installed in the toilets of the David house, which is located in the community of creative energy homes, University of Nottingham, Nottingham, United Kingdom. The outlook view of David house is shown in *Figure 3-17*, with plan geometry in *Figure 3-18*. The position of lighting pipes is indicated in *Figure 3-18*. Light meters are installed in both internal and external to test the performance of lighting luminance and the lighting transmittance efficiency with the test equipment as shown in Table 3-3.



Figure 3-17 Outlook view of David House

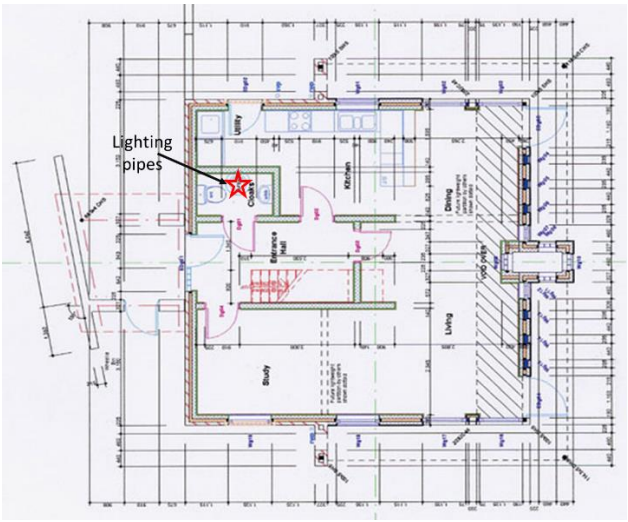


Figure 3-18 Position of daylighting pipes in David House

Table 3-3 Lighting test equipment

Experiment equipment	Series name	Application scale	Test range	Resolution	Accuracy
Light meter	RS PRO IM203 Light	Lighting luminanace	-75℃ to +260℃	0.1	±3%

	Meter				

Figure 3-19 indicates the lighting performance with daylighting pipes, which is tested in 48 hours from 10th July 2019 to 12th July 2019. The test results indicate that the maximum inside lighting luminance is 332 lux/m^2 with average lighting luminance of 160 Lux in daytime. The maximum lighting transmittance efficiency is occurred in 5.77% with average of 1.3%, as shown in *Figure 3-20*. The outdoor lighting level is approximately 10000 lux/m^2 on a clear day. In the place closest to the windows, the light level may be reduced to approximately 1000 lux/m^2. According to the standard "EN 12464 Light and lighting - Lighting of workplaces -Indoor working spaces (November 2002)", the minimum illuminance is 50 lux/m^2 for walls and 30 lux/m^2 for ceilings. The lighting level is more common in the range of 500 - 1000 lux/m^2 depending on activity. Additional lighting luminance is often necessary to compensate low levels. The calculated efficiency demonstrates the daily lighting luminance could achieve approximately 1300lux/m^2 within a sunny day without clouds (in the base of 10000lux/m^2), which can achieve the minimum lighting luminance of 250lux/m^2 for easy office work, 150lux/m^2 for home and 50lux/m^2 for toilets. The lighting intensity higher than 50lux (requirement for toilets) began from 7:10AM and finished at 19:50AM.

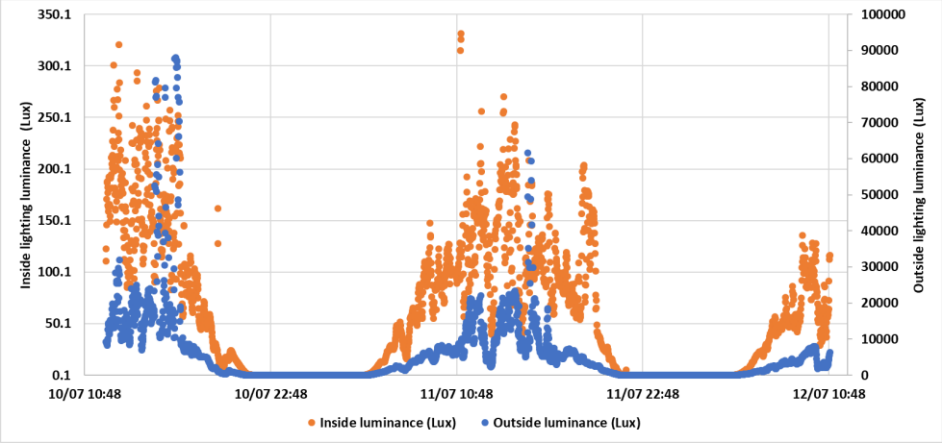


Figure 3-19 Lighting performance with lighting pipes

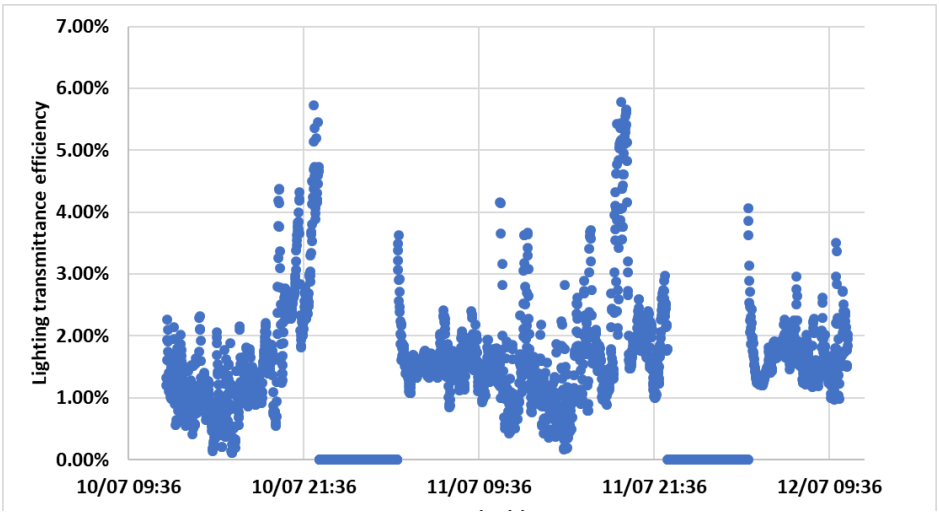


Figure 3-20 Efficiency of daylighting pipe performance

3.8 Conclusion

This chapter concludes the innovative envelop retrofit technologies in aspects of façade insulation, glazing insulation and efficient daylighting pipe technologies, which can be used to reduce the thermal energy and electricity load for both heating and cooling requirements. Façade insulation materials include two types of silica-based VIP panels, and starch-aerogel insulation panel, which are tested on-site with comparisonof original wall. Advanced glazing insulation technologies are refereed to vacuum insulation panels and PV vacuum glazing

panels (PV-VG), which is compared with the original single glazing window. And finally, efficient lighting device of daylighting pipes are used to reduce the lighting electricity consumption, and improve the indoor lighting comfort. The main research findings for these technologies are summarized in Table 3-4, which will be used in case study modelling in Chapter 6.

Table 3-4 Actual thermal and economic performance of silica-based VIP

	Theory performance	On-site installation performance (average value)	Performance variation scale	Other technical data
Silica-based vacuum insulation panels	K-value=0.004 W/mk	K-value varied between 0.005 to 0.008 W/mK	K-value= 0.003-0.008 W/mk	Density ρ =288 kg/m^3; Specific heat C_h =800J/kg.K
Starch-aerogel insulation panels	K-value=0.023 W/mk	K-value=0.024 W/mk	K-value= 0.013-0.069 W/mk	Density ρ = 1500 kg/m^3; Specific heat C_h = 2260J/kg.K

Vacuum glazing	U-value=0.80 $W/m^2.K$	U-value=0.80 $W/m^2.K$	U-value=0.70-0.9 $W/m^2.K$	N/A
Thin film PV vacuum glazing (PV-VG)	U-value=0.57 $W/m^2.K$; solar electricity efficiency=3.7%	U-value=0.60 $W/m^2.K$; solar electricity efficiency is varied according to the solar radiation intensity	U-value=0.40-0.8 $W/m^2.K$; solar electricity efficiency is varied from 0.15% to 3.9%	
Daylighting pipes	N/A	Average indirect lighting transmittance efficiency=1.30%	Direct lighting transmittance efficiency=5.77 %	N/A

4. Innovative system for heating, cooling and dehumidification

4.1 Introduction

Chapter 3 have fully described the advanced demand retrofit technologies to reduce the building thermal heating/cooling and electricity load. To further improve the building energy efficiency, it is significant to apply advanced supply retrofit technologies to improve the energy supply efficiency. Therefore, this chapter will introduce three innovative retrofit technologies including potassium-formate-water cascade air cooling dehumidifier, solar assisted heat pump, and thin film PV 4-layer vacuum glazing. The advanced technologies can efficiently meet the requirement of 1) space cooling and dehumidification load in hot and humid climate; 2) space heating load and domestic hot water generation; 3) renewable electricity demand. However, the three innovative technologies proposed and researched in recent years without technical standard and enough technical data in market. Therefore, this chapter will give calibration guidance of system performance based on the variation of environment, which may highly affect the overall energy performance, such as pre-cooling degree of the solution, solar radiation, ambient wind velocity, etc. And the calibrated results of the three technologies will be used in Chapter 5 and chapter 6 for calculation of the building energy consumption in retrofit design process.

4.2 Hollw fibre-based Liquid desiccant cooling and dehumidification unit

4.2.1 Concept

The purpose of the polymer hollow fibre liquid desiccant system is to dehumidify and cool the supplied to building fresh air. The return air (from inside to outside of the building) is used directly in the process of regeneration of the desiccant solution. In Figure 4-1is presented the details of the components

of the complete system.

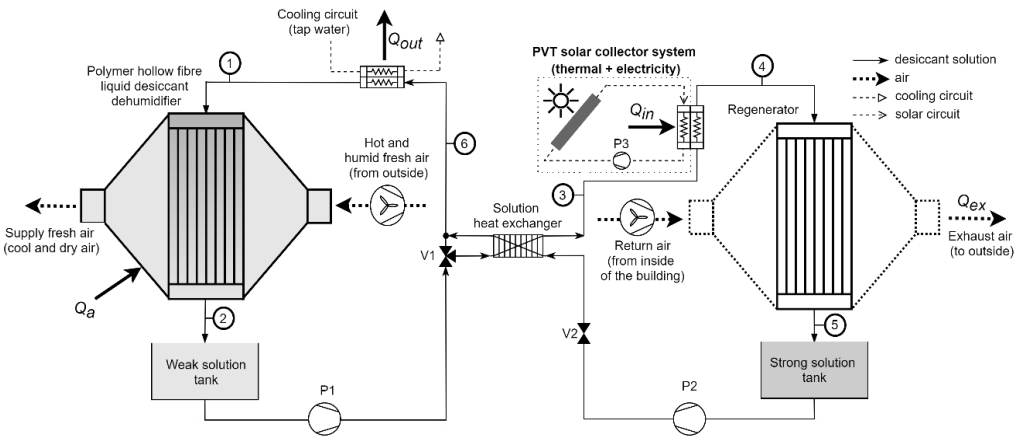


Figure 4-1 Polymer hollow fibre liquid desiccant air dehumidification and cooling cycle.

This system consists in two main circuits, which are a cold circuit (on the left of the solution heat exchanger) and hot circuit (on the right of the solution heat exchanger). The cold circuit is where air is dehumidified and cooled, and the hot circuit is the cycle for regeneration of the solution desiccant (remove the excess of water/increase solution concentration). The thermal energy from the PVT solar collector is used to heat the solution and the electricity can be used for the fans and pumps. The complete cycle is divided in six parts, which are:

- Between 1 and 2: Air is dehumidified and cooled, and consequently the concentration of the liquid desiccant solution decreases and the its temperature increase.
- Between 2 and 3: The weak solution is pre-heated by the strong solution…
- Between 3 and 4: The solution is heated up to around 60°C by the PVT solar collector.

- Between 4 and 5: Return air is used to remove the excess of water in the solution in the regenerator. In this process the solution became a strong solution and cooled by the return air.
- Between 5 and 6: The strong solution is pre-cooled by the weak solution.
- Between 6 and 1: The strong solution is cooled by tap water, and the cycle is repeated.

The solution can also be transferred directly from point 2 to 6 if the concentration is higher than an established value. This control is done by valve V1.

Regarding integration of desiccant system to the building, Figure 4-2 presents the configuration. The system is a compact unit, which include all the circuit and separately we have the two-solution tanks. This configuration has the advantage that it is near the PVT solar collector system, which avoid extra hydraulic circuit for the solar system.

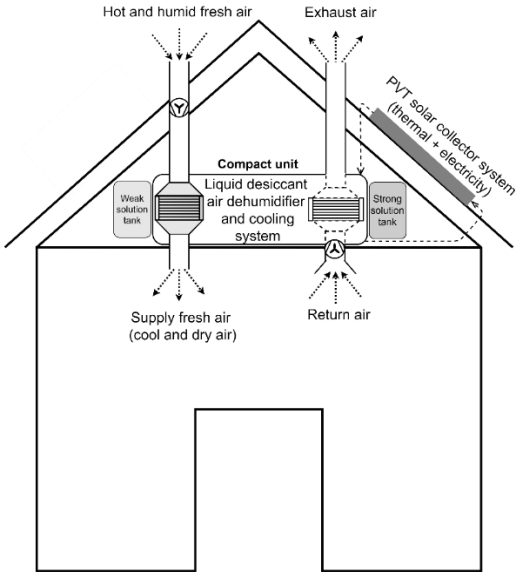


Figure 4-2 Diagram of a domestic installation of Liquid desiccant dehumidification and cooling system.

4.2.2 Numerical modelling

The numerical model is divided in two models. The first is related to the core of desiccant system, where the numerical model is based in an equivalent two-dimensional geometry. For the regeneration cycle of the desiccant solution, the conservation equation of the complete cycle is solved.

The system is made of a cylinder packed with polymer hollow fibre tubes as shown in Figure 4-3.

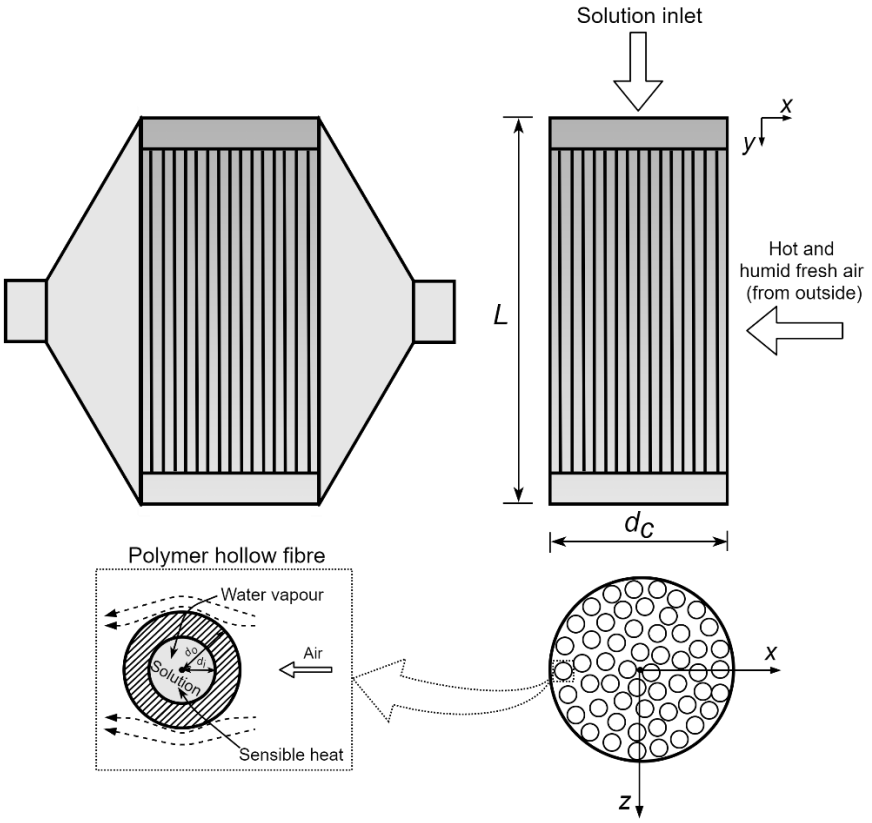


Figure 4-3 Polymer hollow fibre dehumidifier and cooling system.

Due to the complexity of modelling this system, the following simplifications are used:

- Air flow only in x direction and liquid desiccant in y direction
- The condensation of water vapour only occurs in the solution

- The physical properties of air and solution are considered constant
- Equivalent two-dimension geometry is used
- The fibres are uniformly distributed inside the cylinder (uniform packing)
- The system is adiabatic (no heat is lost to surrounding)

4.2.2.1 Heat and mass transfer

- Air side:

Energy conservation equation:

$$\frac{\dot{m}_a}{n_{eq} d_h} c_{p,a} \left(\frac{\partial T_a}{\partial x}\right) = h_{ov}(T_s - T_a) \qquad \text{Eq. (4-1)}$$

where $\dot{m}_a$, $c_{p,a}$ and T_a are the air mass flow rate, specific heat capacity and temperature, respectively, h_{ov} is the overall heat transfer coefficient between air and solution, T_s is the solution temperature, d_h is the equivalent hydraulic diameter of air channel and n_{eq} is the equivalent number of fibres, defined as:

$$n_{eq} = \frac{n_f \pi d_o}{d_c} \qquad \text{Eq. (4-2)}$$

in which n_f is the total number of fibres, d_o is the outside diameter of the fibres and d_c is the dehumidifier diameter. Regarding overall heat transfer coefficient, it depends of the heat conduction in the material of the fibre and the convection in air and desiccant solution sides. For heat transfer coefficient in air side (h_a), the following correlation for the Nusselt number (Nu_a) is used (James Welty, 2006):

$$\mathrm{Nu}_a = \frac{h_a d_h}{\lambda_a} = 1.13 C_1 \mathrm{Re}_a^m \mathrm{Pr}_a^{1/3} \qquad \text{Eq. (4-3)}$$

where λ_a is the thermal conductivity of air, C_1 and m were adjusted to fit the experiments presented in Section 3.1 which support of reference values (James Welty, 2006), Pr_a is air Prandtl number and Re_a is the air Reynold number defined as:

$$\mathrm{Re}_a = \frac{d_h u_{a,max}}{\nu_a} \qquad \text{Eq. (4-4)}$$

in which ν_a is the kinematic viscosity of air and $u_{a,max}$ is the air maximum velocity of air passing through the channels defined as:

$$u_{a,max} = \frac{u_{a,in} d_h}{d_h - d_o} \qquad \text{Eq. (4-5)}$$

where $u_{a,in}$ is the air inlet velocity. The equivalent hydraulic diameter d_h is defined as:

$$d_h = \frac{(1-\phi) d_c^2}{n_f d_o + d_c} \qquad \text{Eq. (4-6)}$$

in which ϕ is the packing fraction defined as:

$$\phi = \frac{n_f \pi d_o^2}{\pi d_c^2} \qquad \text{Eq. (4-7)}$$

The inlet velocity of air is defined as:

$$u_{a,in} = \frac{\dot{m}_a}{\rho_a A_{a,in}} \qquad \text{Eq. (4-8)}$$

where $\dot{m}_a$ and ρ_a are the air mass flow rate and density, respectively, and $A_{a,in}$ is the inlet cross-section void space of air, defined as:

$$A_{a,in} = \frac{\pi d_c L}{4}(1-\phi) \qquad \text{Eq. (4-9)}$$

in which L is the height of the dehumidifier.

Mass conservation equation:

$$\frac{\dot{m}_a}{n_{eq} d_h}\left(\frac{\partial \omega_a}{\partial x}\right) = k_{ov}(\omega_s - \omega_a) \qquad \text{Eq. (4-10)}$$

where ω_a and ω_s are the air and solution humidity ratio, respectively, and k_{ov} is the overall coefficient of mass transfer, which depends on the mass transfer coefficient of air side k_a. For air side, the following correlation for the Sherwood number (Sh_a) is used (Zhang, 2011):

$$\mathrm{Sh}_a = \frac{k_a d_h}{\psi_a} = (14.06\phi^4 - 29.21\phi^3 + 22.59\phi^2 - 7.71\phi + 1.03)\mathrm{Re}_a^{0.33}\mathrm{Sc}_a^{0.33}\tau_k \qquad \text{Eq. (4-11)}$$

in which ψ_a is the water vapor diffusivity in air, and Sc_a is the Schmidt number defined as:

$$\mathrm{Sc}_a = \frac{\mu_a}{\rho_a \psi_a} \qquad \text{Eq. (4-12)}$$

and τ_k is the fractal dimension of the fibre packing defined as (Ebrahimpour and Maerefat, 2011):

$$\tau_k = 0.882\tau_p - 0.535 \qquad \text{Eq. (4-13)}$$

where τ_p varies between 1 (irregular packing) and 2 (regular packing).

- *Solution side:*

Energy conservation equation:

$$\frac{\dot{m}_s}{n_{eq} d_i} c_{p,s} \left(\frac{\partial T_s}{\partial y}\right) = h_{ov}(T_a - T_s) + h_{cw} k_{ov} \rho_a (\omega_a - \omega_s) \qquad \text{Eq. (4-14)}$$

where $\dot{m}_s$, $c_{p,s}$ and T_s are the solution mass flow rate, specific heat capacity and temperature, respectively, d_i is the internal diameter of the fibres and h_{cw} is the heat of condensation of water. For heat transfer coefficient in solution side (h_s), the following correlation for Nusselt number (Nu_s) (Chen et al., 2019b) (Zhang et al., 2000) was used:

$$\mathrm{Nu}_s = \frac{h_s d_i}{\lambda_s} = 3.658 + \frac{0.085 \left[\frac{\mathrm{Re}_s \mathrm{Pr}_s d_i}{L}\right]}{1 + 0.047 \left[\frac{\mathrm{Re}_s \mathrm{Pr}_s d_i}{L}\right]^{0.67}} \qquad \text{Eq. (4-15)}$$

where λ_s and Pr_s are the thermal conductivity and Prandtl number of the liquid desiccant solution. The Reynolds number of the solution in a single fibre is calculated as:

$$\mathrm{Re}_s = \frac{4\dot{m}_s}{n_f \mu_s \pi d_i} \qquad \text{Eq. (4-16)}$$

where μ_s is the solution dynamic viscosity.

Mass conservation equation:

$$\frac{\dot{m}_s}{n_{eq} d_i} \left(\frac{\partial X_s}{\partial y}\right) = k_{ov} \rho_a (\omega_s - \omega_a) \qquad \text{Eq. (4-17)}$$

where X_s is the solution concentration. The mass transfer coefficient in the solution side k_s is related to the Sherwood number (Sh_s) using (Chen et al., 2019b):

$$\mathrm{Sh}_s = \frac{k_s d_i}{\psi_s} = 1.62\left(\frac{d_i^2 u_{s,in}^2}{L\psi_s}\right)^{\frac{1}{3}} \quad \text{Eq. (4-18)}$$

where $u_{s,in} = 4\dot{m}_s/\left(n_f \pi d_i^2\right)$ is the inlet velocity of solution in a single fibre and ψ_s is the water vapor diffusivity in solution. The solution humidity ratio ω_s is calculated as (Chen et al., 2019b):

$$\omega_s = 0.622\frac{P_s}{P_{atm} - P_s} \quad \text{Eq. (4-19)}$$

in which P_{atm} is the atmospheric pressure (kPa) and P_s is the solution vapour pressure (kPa) (Elmer, 2017)calculated as(Elmer, 2017):

$$P_s = X_s exp^{\gamma} exp^{P_{H_2O}} \quad \text{Eq. (4-20)}$$

where P_{H_2O} is the water vapour pressure (kPa) (Elmer, 2017)in the desiccant solution calculated as:

$$P_{H_2O} = 73.649 - \left(\frac{7258.2}{T_s}\right) - 7.3037\ln(T_s) + 4.1653 \times 10^{-6} T_s^2 \quad \text{Eq. (4-21)}$$

and γ is the activity coefficient of water and is calculated as (Elmer, 2017):

$$\gamma = A\,(1 - Z)^2\left(1 + 4.19Z\left(Z - \frac{2}{3}\right)\right) \quad \text{Eq. (4-22)}$$

where

$$A = -2.08 - \left(\frac{1336}{T_s}\right) \quad \text{Eq. (4-23)}$$

in which T_s has the unit of Kelvin. The parameter Z is calculated using(Elmer, 2017):

$$Z = \frac{AX_m}{AX_m + B(1 - X_m)} \qquad \text{Eq. (4-24)}$$

where

$$B = -3.42 - \left(\frac{1039}{T_s}\right) \qquad \text{Eq. (4-25)}$$

and

$$X_m = \frac{1}{1 + \left(\frac{18.015X_s}{84.11(1 - X_s)}\right)} \qquad \text{Eq. (4-26)}$$

The relative (RH_a) and specific humidity (ω_a) of air are related as (Murray, 1966):

$$\omega_a = \frac{0.622RH_a p_{sat}}{P_{atm} - 0.378RH_a p_{sat}} \qquad \text{Eq. (4-27)}$$

where p_{sat} is defined as (Murray, 1966):

$$p_{sat} = 610.78 \exp\left(\frac{17.27(T_a - 273.16)}{T_a - 35.86}\right) \qquad \text{Eq. (4-28)}$$

and T_a has unit of Kelvin.

Overall heat and mass transfer coefficients:

The overall heat and mass transfer coefficients are calculate using, respectively:

$$h_{ov} = \left(\frac{1}{h_s}\left(\frac{d_o}{d_i}\right) + \frac{d_o - d_i}{\lambda_f}\left(\frac{2d_o}{d_o + d_i}\right) + \frac{1}{h_a}\right)^{-1} \qquad \text{Eq. (4-29)}$$

$$k_{ov} = \left(\frac{1}{k_s}\left(\frac{d_o}{d_i}\right) + \frac{d_o - d_i}{\psi_f}\left(\frac{2d_o}{d_o + d_i}\right) + \frac{1}{k_a}\right)^{-1} \qquad \text{Eq. (4-30)}$$

where λ_f and ψ_f are the mass thermal conductive and mass diffusivity of the hollow fibre, respectively. The equations are solved in GNU Octave language according to the flowchart presented in Figure 4-4.

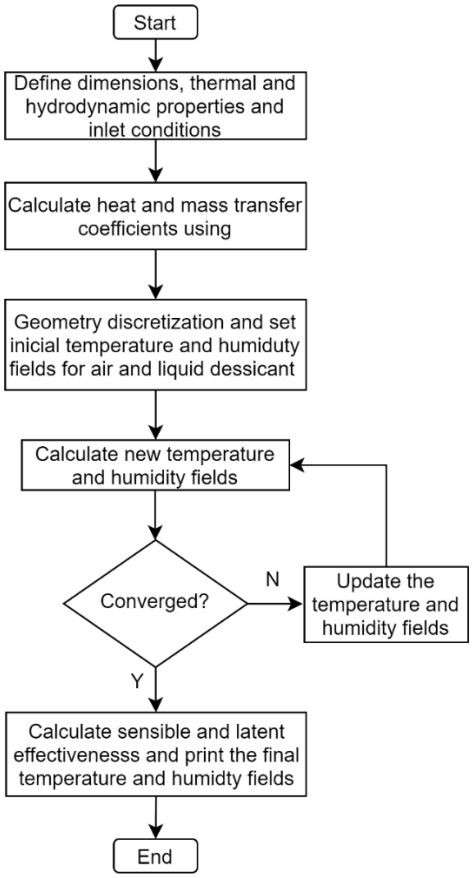


Figure 4-4: Flow chart of the solution method.

Table 4-1 presentes the parameters of the reference configuration, in which L and d_c are the height and dimeter of the dehumidifier, respectively, n_f is the number of hollow fibers, d_o and d_i are the outside and inside diameter of the hollow fibers, ψ_a, ψ_s and ψ_f the vapor water diffusivity in air, solution and

hollow fibre, respectively. The λ_f and λ_s are the thermal conductivity of hollow fibre and solution respectively, $c_{p,s}$, μ_s and ρ_s are the specific heat capacity, dynamic viscosity and density of solution, respectively, h_{cw} is the heat of condensation of water, P_{atm} is the atmospheric pressure and τ_p stand for uniform distribution of the packing of fibres.

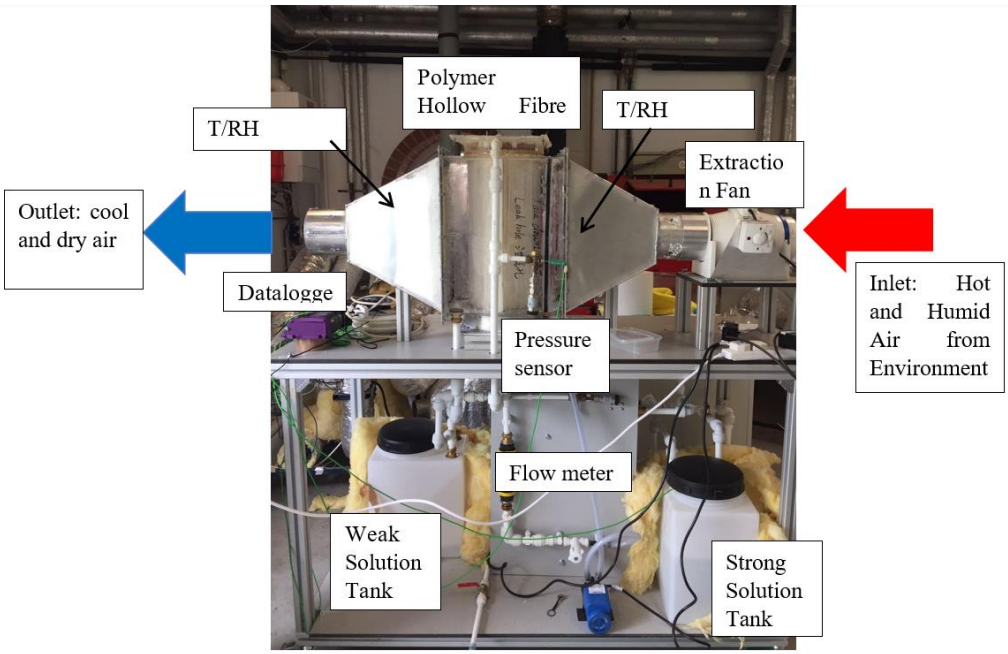
Table 4-1 List of parameters used in the simulations.

Parameter	Value
L (cm)	60
d_c (cm)	20
n_f	5000
d_o (mm)	1.6
d_i (mm)	1.4
ψ_a (m^2 s^{-1})	0.1
ψ_s (m^2 s^{-1})	3e-3
ψ_f (m^2 s^{-1})	1.1e-4
λ_f (W m^{-1} K^{-1})	0.17
λ_s (W m^{-1} K^{-1})	0.444
$c_{p,s}$ (J kg^{-1} K^{-1})	3100
μ_s (Pa s)	5.1e-3
ρ_s (kg m^{-3})	1445
h_{cw} (kJ kg^{-1})	2501
P_{atm} (Pa)	101 325
τ_p	2

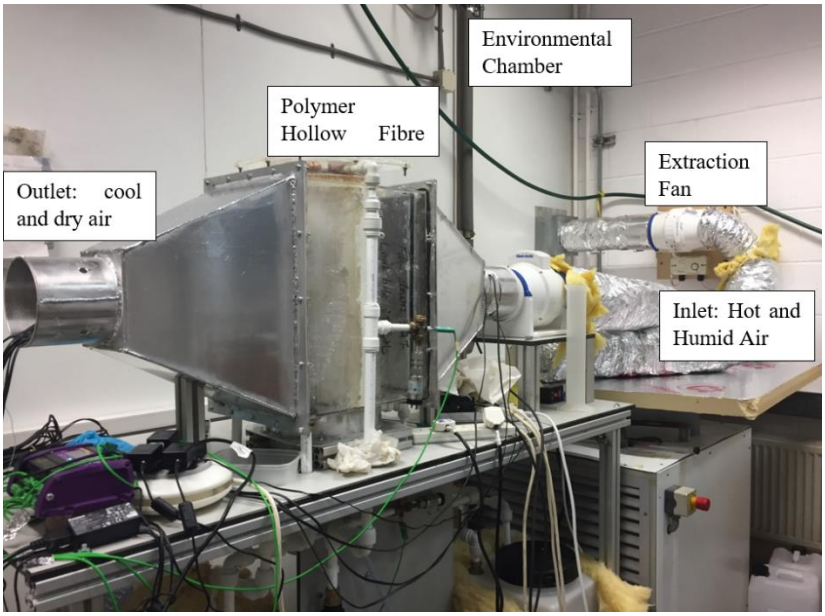
For air, the thermal and hydrodynamic properties are considered constant at 20°C.

4.2.2 Test rig setup

The performance tests for the design concept is separated into two different units, including an air dehumidification unit with liquid desiccant solutions of potassium formate (KCOOH), and a water evaporative cooling unit. The two different functional units have the same physical structure as shown in Figure 4-5, with difference of liquid fluent. The hollow fiber module core is designed with 3D structure modelled in Figure 4-6.



(A) The test rig of the novel cross flow hollow fibre



(B) connections with the environmental chamber

Figure 4-5 The test rig of the novel cross flow hollow fibre integrated evaporative cooling module (A) and the connections with the environmental chamber (B)

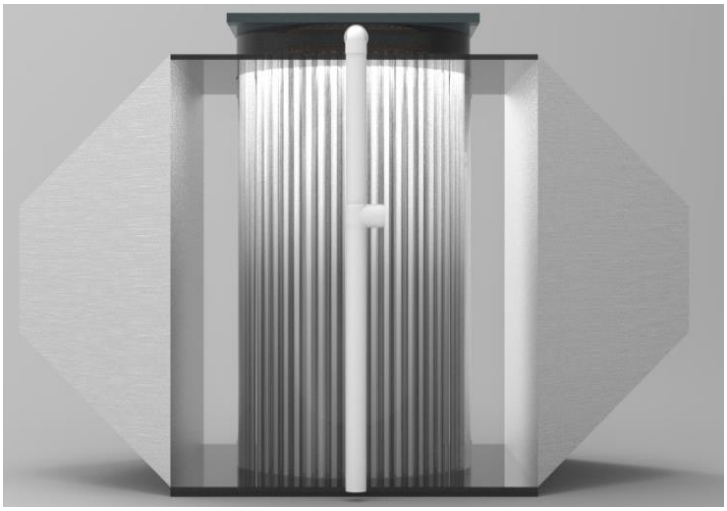


Figure 4-6 The 3-D model image of the hollow fibre module core design

At the beginning of each test, the environmental chamber was set to the required temperature and humidity level. As soon as the temperature and humidity

reached the desired values, the solution/water circulation pump and the fan in the air stream direction will be switched on. The air velocity is measured at five different positions along the cross sections of the outlet aluminium tunnel, using the air velocity probes connected to a recorder (Testo 454). In order to minimize the experimental testing errors, four humidity and temperature sensors (EK-H4, Sensirion, UK) were located at the inlet (point 1 in Figure 4-7) and outlet (point 2 in Figure 4-7) of the air stream respectively, to measure the inlet and outlet conditions of the air stream. Additional K type thermocouples were used to measure the temperature of the desiccant solution entering and leaving the hollow fibre module. The aluminium air tunnel was connected with a variable frequency drive centrifugal fan, which was linked directly with the environmental chamber. A centrifugal pump was employed to circulate solution/water from the solution/water tank to the top of the hollow fiber module. 8 nozzles were allocated at the top of the module with the aim to make sure the cross section of the hollow fiber module could be wetted entirely.

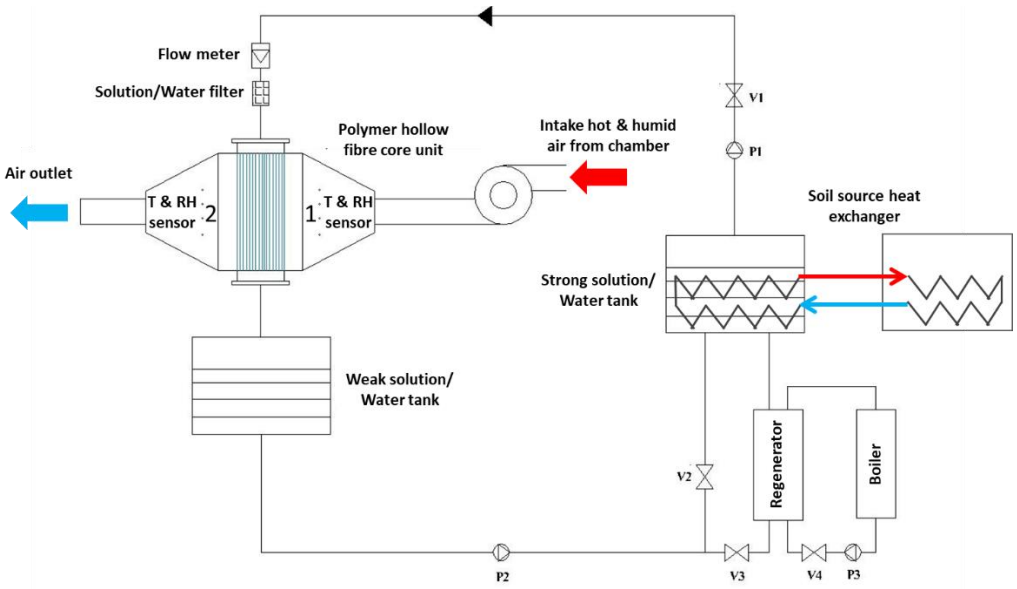


Figure 4-7 Core structure of single unit for both evaporative cooling and desiccant dehumidification

For each test, the temperature and humidity values were recorded every 20 seconds until the time when the system reached steady states as indicated by the humidity and temperature sensor readings. The accuracy of the measuring instruments used was: ±0.2% for temperature, ±0.5% for pressure, ±2% for air velocity, and ±2% for relative humidity.

4.2.3 Assessment criteria

4.2.3.1 Air side effectiveness (ε_{sen}, ε_{lat})

Air side effectiveness has been widely applied to evaluate the performance of dehumidification and cooling process. The performance of the system is found through calculation of the sensible effectiveness (ε_{sen}) and latent effectiveness (ε_{lat}).

The air side sensible heat effectiveness (ε_{sen}) is an important parameter to evaluate the heat transfer performance between the intake air and the inside solution fluid. This is defined as the ratio between the actual temperature change of the air passing through the hollow fibres ($T_{a,in} - T_{a,out}$), and the maximum possible temperature difference in the hollow fibre units ($T_{a,in} - T_{sol,in}$):

$$\varepsilon_{sen} = \frac{T_{a,in} - T_{a,out}}{T_{a,in} - T_{sol,in}} \quad \text{Eq. (4-31)}$$

Where, $T_{a,in}$ and $T_{a,out}$ represents the inlet and outlet air dry-bulb temperature. $T_{sol,in}$ represents for the temperature of inlet solutions.

The air side latent heat effectiveness (ε_{lat}) is significant to evaluate the mass

transfer performance or moisture remove effectiveness of the air. Because of the water vapour pressure difference, the hot air with high humidity will transport the water into the inside of the hollow fibres. In the process, the water vapour can pass through the micro porous on the surface of the hollow fibres, and the water changes from vapour to liquid. This is defined as the ratio between the actual ($\omega_{a,in} - \omega_{a,out}$) and maximum possible difference of the specific humidity ($\omega_{a,in} - \omega_{eq}$):

$$\varepsilon_{lat} = \frac{\omega_{a,in} - \omega_{a,out}}{\omega_{a,in} - \omega_{eq}} \quad \text{Eq. (4-32)}$$

Where, $\omega_{a,in}$ and $\omega_{a,out}$ is the relative humidity of inlet air and outlet air. ω_{eq} is the equilibrium humidity ratio of air at the inlet condition of the desiccant solution, of which the vapour pressure is a function of concentration and temperature of the solution (Chen et al., 2018), which is calculated as Eq. (4-33):

$$\omega_{eq} = 0.622 \frac{P_{sol}(X_{sol}, T_{sol})}{P_{atm} - P_{sol}(X_{sol}, T_{sol})} \quad \text{Eq. (4-33)}$$

Where, P_{atm} is the atmospheric pressure; P_{sol} is the vapour pressure of desiccant solution at the specific concentration X_{sol} and temperature T_{sol}. The desiccant solution concentration X_{sol} can be determined by the solution temperature and density as shown in Equation (2). P_{sol} can be calculated with the empirical correlation derived by Cisternas and Lam (Cisternas and Lam, 1991), as shown below:

$$\text{Log}P_{sol} = \text{K I} \left[A - \frac{B}{T - E_s}\right] + \left[C - \frac{D}{T - E_s}\right] \quad \text{Eq. (4-34)}$$

Where P_{sol} is the solution equilibrium vapour pressure (kPa); I is the molar concentration (mol/kg); K is an electrolyte parameter relating to solute

(KCOOH); A, B, C, D and E_s are parameters regarding to solvent (water).

Regarding the performance of the regenerative cycle, it can be obtained through calculation of thermal COP_{th} and electrical COP_{elec}, defined, respectively, as:

$$COP_{th} = \frac{Q_a}{Q_{in}} \quad \text{Eq. (4-35)}$$

$$COP_{elec} = \frac{Q_a}{W_p + W_f} \quad \text{Eq. (4-36)}$$

where Q_a is the cooling capacity (sensible and latent), Q_{in} is the input of thermal energy to cycle (from the solar thermal collector) and W_p and W_f are the total electric power consumed in the pumps and fans, respectively.

4.2.4 Results and discussion

4.2.4.1 Experimental validation

For validation, the model is adjusted to the same experimental condition and the measurements and numerical results are compared. The measured and modelled air outlet temperature and relative humidity were compared for three different inlet air mass flow rates, which are: $\dot{m}_a = 57$ m^3/h, 114 m^3/h and 171 m^3/h. The solution mass flow rate was fixed to 2 litters per minute with a concentration of 40%. Table 4-2 to Table 4-4 present the comparison between experimental and numerical for different inlet temperature of solution $T_{s,in}$ and different inlet temperature $T_{a,in}$ and relative humidity of $RH_{a,in}$ air.

Table 4-2 Comparison between measurements and numerical for $\dot{m}_a = 57$ m^3/h.

Inlet conditions			Experimental			Numerical			Error (%)		
$T_{s,in}$	$T_{a,in}$	$RH_{a,in}$	$T_{s,out}$	$\bar{T}_{a,out}$	$\overline{RH}_{a,ou}$	$T_{s,out}$	$\bar{T}_{a,out}$	$\overline{RH}_{a,out}$	$\bar{T}_{s,out}$	$\bar{T}_{a,o}$	$\overline{RH}_{a,out}$

(°C)	(°C)	(%)	(°C)	(°C)	(%)	(°C)	(°C)	(%)			
23.2	29.8	72.8	25.0	27.9	72.3	25.6	27.6	67.5	2.5	1.2	6.6
21.3	29.4	73.0	23.3	26.0	70.7	24.2	26.7	66.4	3.9	2.5	6.1
17.4	29.3	73.6	20.0	25.3	67.3	21.5	25.2	64.2	7.4	0.3	4.5
17.6	29.3	72.3	22.4	25.0	63.6	21.5	25.3	63.8	3.9	1.1	0.3
14.2	29.4	74.1	19.5	25.0	66.5	19.2	24.2	62.9	1.3	3.4	5.5
16.9	29.4	72.1	22.3	25.3	63.8	21.0	25.1	63.3	5.6	0.7	0.9
15.0	29.4	72.3	21.4	24.5	62.0	19.7	24.4	62.4	8.0	0.4	0.7
12.7	29.4	74.8	19.5	24.4	64.2	18.2	23.6	62.6	6.8	3.3	2.5
9.2	29.4	74.9	16.5	23.7	59.9	15.5	22.4	61.7	6.0	5.8	3.0
13.6	29.3	73.2	22.0	23.9	65.0	18.7	23.9	62.2	15.1	0.2	4.2

Table 4-3 Comparison between measurements and numerical for $\dot{m}_a = 114$ m^3/h.

Inlet conditions			Experimental			Numerical			Error (%)		
$T_{s,in}$ (°C)	$T_{a,in}$ (°C)	$RH_{a,in}$ (%)	$T_{s,out}$ (°C)	$\bar{T}_{a,out}$ (°C)	$\overline{RH}_{a,ou}$ (%)	$T_{s,out}$ (°C)	$\bar{T}_{a,out}$ (°C)	$\overline{RH}_{a,ou}$ (%)	$\bar{T}_{s,out}$	$\bar{T}_{a,ou}$	$\overline{RH}_{a,out}$

20.9	29.8	72.5	23.3	27.4	71.5	24.9	27.9	68.7	7.0	1.8	3.9
23.8	29.4	72.5	27.6	27.9	70.1	26.4	28.2	70.0	4.5	1.0	0.2
18.9	29.3	71.1	23.4	27.9	66.3	23.3	27.0	67.2	0.4	3.1	1.4
14.6	29.2	72.7	20.4	27.2	69.7	20.7	26.0	67.3	1.6	4.5	3.5
15.0	29.3	71.9	20.9	27.5	69.3	21.0	26.1	66.8	0.2	5.1	3.6
19.6	29.5	71.5	26.1	27.5	68.6	23.9	27.3	67.7	8.5	0.6	1.4
20.3	29.4	71.0	26.8	27.2	69.7	24.2	27.4	67.6	9.7	0.7	3.0
19.4	29.4	70.9	26.0	27.5	68.7	23.6	27.2	67.3	9.1	1.1	2.1
14.0	29.2	72.3	20.7	26.9	68.8	20.3	25.8	66.9	2.0	4.0	2.7
13.0	29.1	74.0	19.9	26.9	69.6	19.8	25.5	67.9	0.7	5.2	2.5
17.5	29.4	70.7	24.4	26.7	67.2	22.5	26.8	66.6	7.9	0.4	0.9
19.4	29.5	71.2	26.3	27.1	68.9	23.7	27.3	67.4	9.8	0.7	2.1
9.3	29.4	71.3	16.8	26.2	66.8	17.1	24.8	65.9	1.8	5.0	1.3
18.5	29.5	71.9	26.4	27.3	69.2	23.3	27.1	67.6	11.9	0.7	2.3
13.0	29.4	73.0	21.0	25.5	66.1	19.8	25.7	67.2	5.6	0.9	1.8

14.4	29.2	71.6	22.6	25.9	67.1	20.5	25.9	66.5	9.4	0.0	0.9
15.2	29.2	71.7	23.7	26.6	70.0	21.0	26.1	66.7	11.4	2.0	4.6

Table 4-4 Comparison between measurements and numerical for $\dot{m}_a = 171$ m^3/h.

Inlet conditions			Experimental			Numerical			Error (%)		
$T_{s,in}$ (°C)	$T_{a,in}$ (°C)	$RH_{a,in}$ (%)	$T_{s,out}$ (°C)	$\bar{T}_{a,out}$ (°C)	$\overline{RH}_{a,ou}$ (%)	$T_{s,out}$ (°C)	$\bar{T}_{a,out}$ (°C)	$\overline{RH}_{a,ou}$ (%)	$\bar{T}_{s,out}$	$\bar{T}_{a,out}$	$\overline{RH}_{a,out}$
22.8	30.2	71.7	26.2	28.8	71.2	26.5	29.0	69.8	1.1	0.8	2.0
17.3	29.9	69.2	22.5	27.4	71.5	23.0	27.8	66.9	2.3	1.5	6.4
16.9	30.1	72.2	22.8	27.9	70.7	23.3	27.9	69.1	2.1	0.2	2.3
17.7	31.0	71.4	23.7	28.0	71.3	24.2	28.8	68.5	2.1	2.9	3.8
16.5	30.2	71.4	23.3	27.7	68.9	23.0	27.9	68.4	1.3	0.9	0.6
14.7	29.9	70.0	21.6	26.9	71.2	21.6	27.3	67.2	0.1	1.5	5.6
13.5	29.9	70.2	21.4	27.0	70.8	20.9	27.1	67.3	2.4	0.6	4.8
11.2	30.3	70.6	19.3	27.1	69.3	19.7	27.1	67.6	2.3	0.2	2.4
12.9	31.	69.9	21.3	26.8	69.7	21.2	27.9	67.1	0.7	4.1	3.8

	0										
12.1	30.0	70.4	21.7	27.0	69.8	20.1	27.0	67.5	7.4	0.2	3.4

4.2.4.2 Parametric analysis

Effect of inlet air temperature:

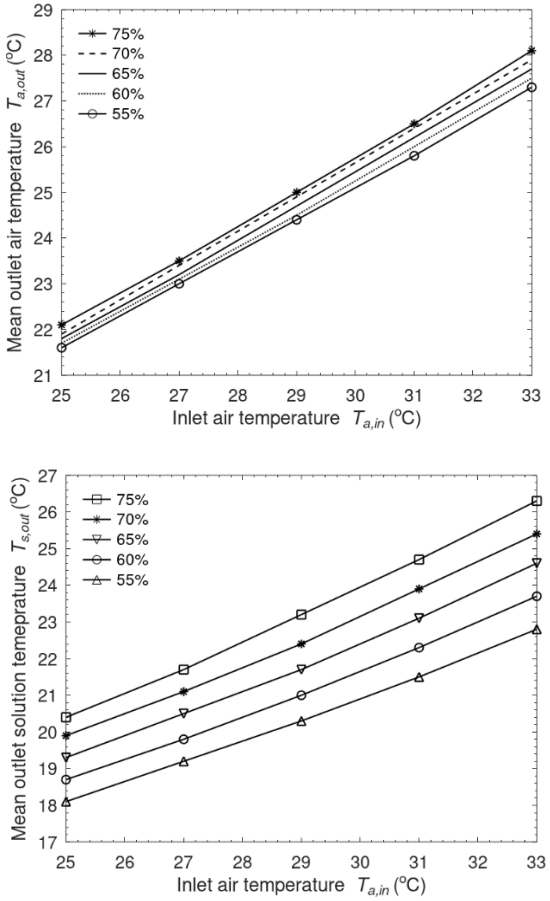


Figure 4-8 Effect of inlet air temperature on outlet air humidity and solution temperature

It is figured out from Figure 4-8 that both air and solution mean outlet temperatures increase with the increment of the inlet air temperature under different humidity ranging from 55% to 75%. However, the growth rate is relatively rapid for solution mean outlet temperature with the increasing

humidity than that of airside. For the air mean outlet temperature at five different humidities, the minimum and maximum temperature differences are 0.5℃ and 0.8℃, respectively. For the solution mean outlet temperature at five different humidity, the minimum and maximum temperature differences are 1.7℃ and 3.5℃, respectively.

Effect of inlet air relative humidity:

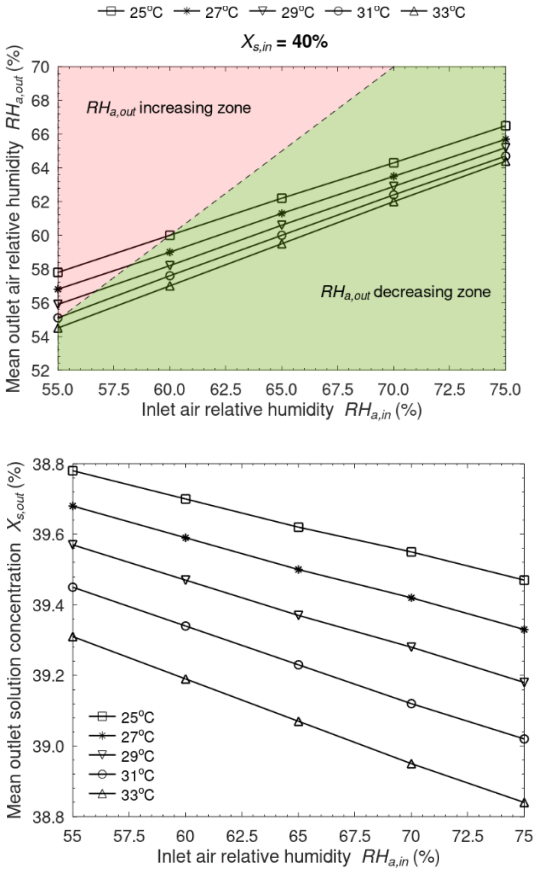


Figure 4-9 Effect of inlet air relative humidity on outlet air humidity and solution concentration

As depicted in Figure 4-9, two distinctive zones of mean air outlet relative humidity (increasing and decreasing zones) are determined within which $RH_{a,in}$ equals $RH_{a,out}$ at 60% of inlet air humidity level. In the increasing zone, the inlet

air humidity is less than that of the outlet humidity, and vice versa in the decreasing zone (i.e., $RH_{a,in}$ = 55%, $RH_{a,out}$ =58%). Moreover, the inlet air relative humidity is proportional to its outlet humidity with the air temperature rise. Nonetheless, the relationship between inlet air relative humidity and mean outlet solution concentration shows dissimilarities where the mean outlet solution concentration air inlet humidity declines with the inlet humidity rise, with minimum and maximum concentration differences of 0.47% and 0.63%, respectively.

Effect of air mass flow rate:

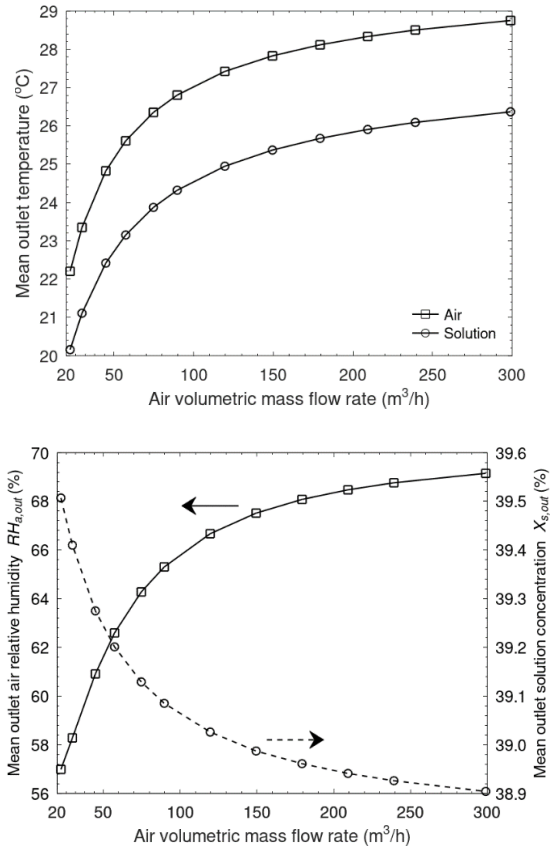
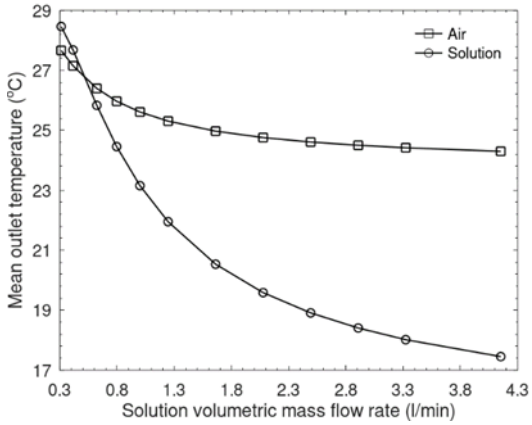


Figure 4-10 Effect of air mass flow rate on outlet air temperature/humidity and solution concentration

It is discovered from Figure 4-10 that both air and solution mean outlet

temperatures escalate with the increasing air mass flow rate at 40% concentration indicating a higher cooling capacity, where the minimum and maximum temperature differences between air and solution are 2.05 ℃ and 2.38 ℃, respectively. Specifically, the outlet temperature increases speedily with a relatively smaller air mass flow rate, whereas increasing steadily with a larger value. Unlike the variation trend of outlet temperature, the solution outlet humidity decreases with the increasing air mass flow rate causing a comparable concentration decline, while outlet humidity at the airside ascends with the air mass flow rate, which is an unacceptable and unreasonable scenario. Therefore, an optimised air mass flow rate has been found as 57m^3/h to cope with the issue.

Effect of solution mass flow rate:



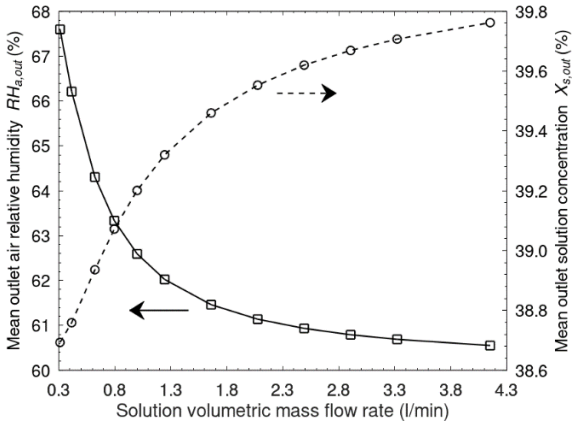
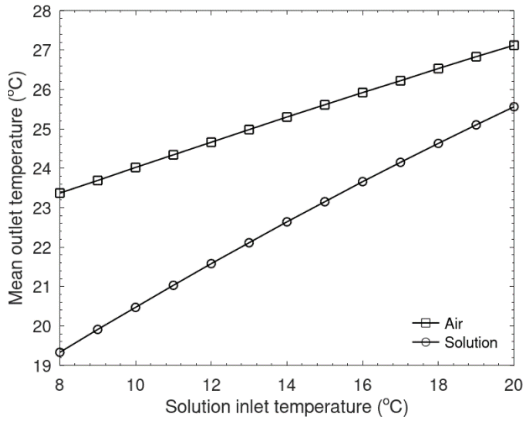


Figure 4-11 Effect of solution mass flow rate on outlet air temperature/humidity and solution concentration

It is discovered from Figure 4-11 that both air and solution mean outlet temperatures decline with increasing solution mass flow rate at 40% concentration, where the minimum and maximum temperature differences between air and solution are 0.53℃ and 6.85℃, respectively. Likewise, the air outlet humidity decreases with the increasing solution mass flow rate causing the concentration reduction. In addition, the optimised solution mass flow is 1 l/min.

Effect of solution inlet temperature:



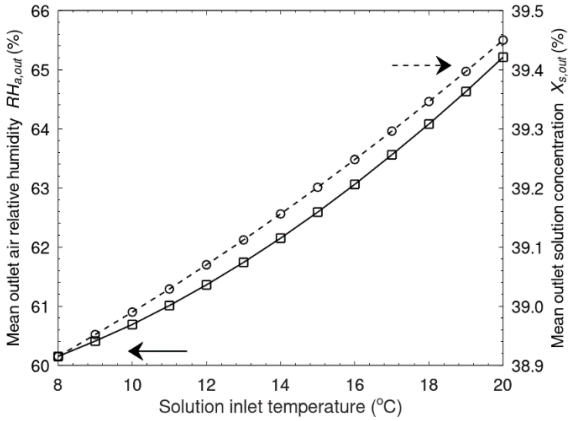


Figure 4-12 Effect of solution inlet temperature on outlet air temperature/humidity and solution concentration

It is figured out from Figure 4-12 that both air and solution mean outlet temperatures increase with the surge of solution inlet temperature with the minimum and maximum temperature differences of 1.57 ℃ and 4.04 ℃, respectively. Similarly, the relationship between solution inlet temperature and outlet air humidity shows the same variation trend as the former parameter. Both air and solution side outlet air humidity rise with the increasing solution inlet temperature.

Effect of solution concentration:

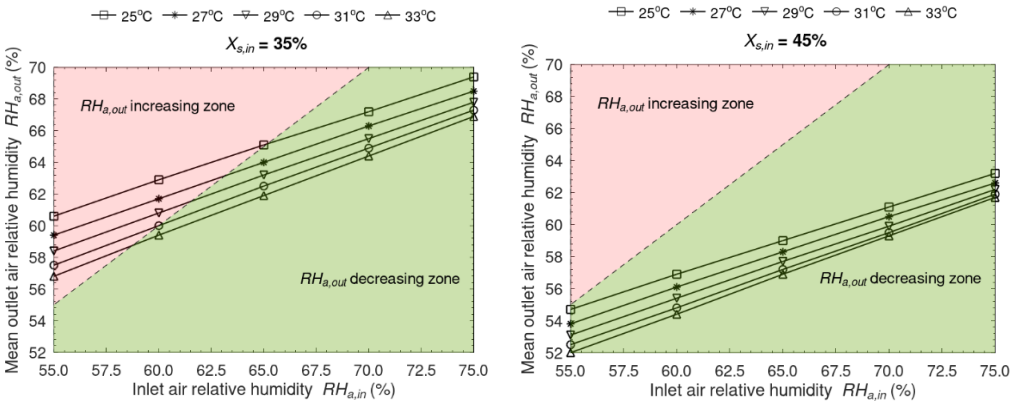


Figure 4-13 Effect of solution concentration and inlet air temperature on outlet relative humidity.

As the abovementioned descriptions in Figure 4-9, the increasing and decreasing zones are ascertained. Figure 4-13 illustrates the relations between the air inlet and outlet mean relative humidity under different solution concentration circumstances (35% and 45%). Albeit the increasing trends are identical to that of 40% concentration, the optimised solution concentration is chosen as 40% since the decreasing zone expands with the increasing concentration, which leads to higher expenses and more system complexities.

Thermal COP and Electrical COP:

The thermal COP and Electrical COP with different inlet temperature and relative humidity are calculated with results in Table 4-5 and Table 4-6, respectivelly.

Table 4-5 Thermal COP for different inlet temperature and relative humidity

	$RH_{a,in}$ (%)					
$T_{a,in}$	55	60	65	70	75	
25	0.09	0.11	0.12	0.14	0.16	
27	0.12	0.14	0.16	0.18	0.20	
29	0.16	0.18	0.20	0.22	0.24	COP_{th}
31	0.19	0.22	0.24	0.26	0.29	
33	0.23	0.26	0.29	0.31	0.34	

Table 4-6 Electrical COP for different inlet temperature and relative humidity.

	$RH_{a,in}$ (%)

$T_{a,in}$	55	60	65	70	75	
25	1.57	1.83	2.10	2.36	2.62	
27	2.07	2.37	2.66	2.96	3.25	
29	2.61	2.94	3.27	3.60	3.92	COP_{elec}
31	3.19	3.56	3.92	4.28	4.64	
33	3.81	4.21	4.61	5.01	5.41	

Moreover, the hybrid system COP formulation is correlated as the relation with both inlet air temperature and relative humidity as shown in Eq. (4-37) and Figure 4-14.

$$COP = (0.0034 \times T_{a,in} - 0.0331) \times RH_{a,in} + (0.0929 \times T_{a,in} - 3.6587) \quad \text{Eq. (4-37)}$$

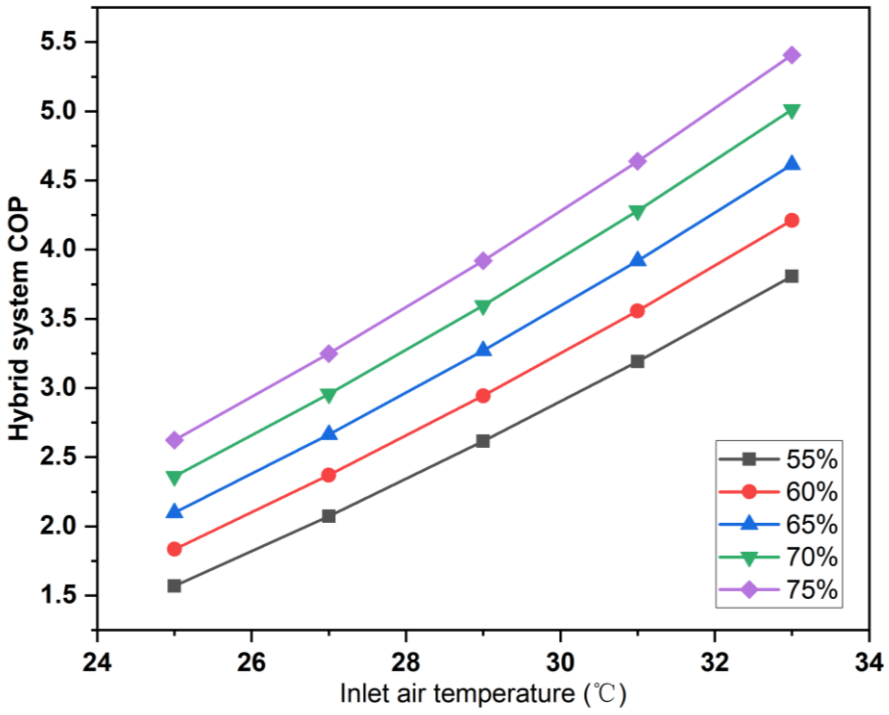


Figure 4-14 Hybrid system COP with variables of inlet air temperature and relative humidity

4.3 Solar-assisted heat pump integrated with thermal storage and PV panels (SAHP-TS-PV)

4.3.1 Concept

The concept of solar assisted heat pump (SAHP) is the same as a traditional heat pump. The main difference is the using of a thermodynamic solar panel (solar collector) as evaporator, which permits extraction of heat from environment and the absorbed solar radiation in the solar panel. Figure 4-15 presents a typical configuration of a direct expansion solar assisted heat pump in residential building.

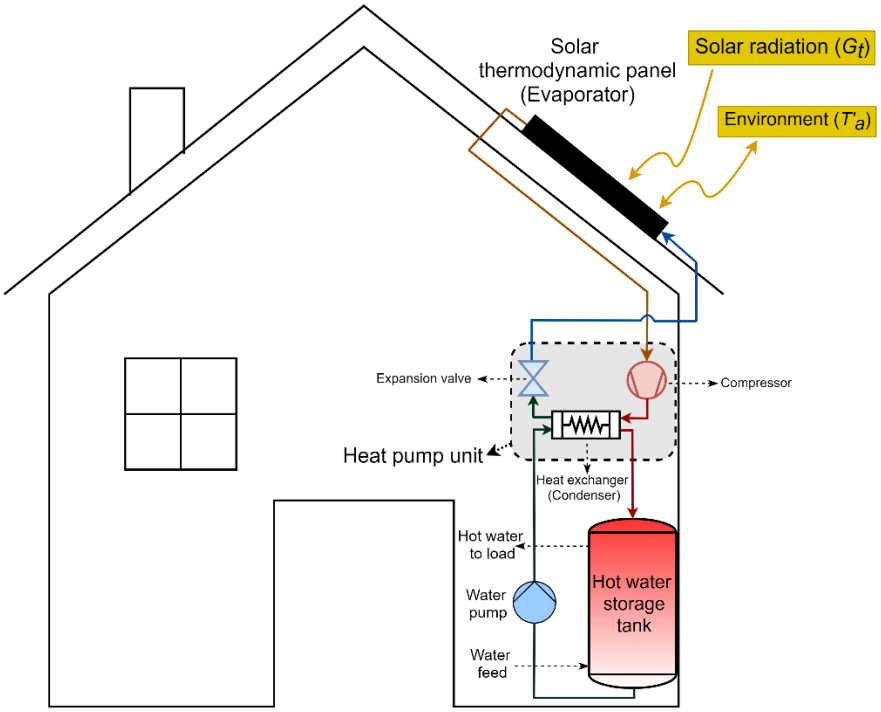


Figure 4-15 Solar assisted heat pump system integrated in residential building.

Solar assisted heat pump system can be divided in three mains components: (i) solar thermodynamic panel; (ii) heat pump unit, which contains the expansion valve, compressor, and heat exchanger/condenser; and (iii) heat storage unit (water tank).

4.3.2 Numerical modelling

Figure 4-16 presents the schematic diagram and the main components of the solar assisted heat pump (SAHP) considered in this work. A heat storage tank based in water is used to storage hot water aiming to mitigate the mismatch between availability of solar radiation and building heat demand. Based in the schematic of Figure 4-16, the ideal thermodynamic cycle of the heat pump consists in four processes:

- Between 1 or 1’ and 2 (condensation of the refrigerant): the refrigerant hot gas is converted to liquid by releasing heat to the heat storage tank through the heat exchanger. During this process the pressure is kept constant (isobaric process).
- Between 2 and 3 (expansion of the refrigerant): the liquid refrigerant expands in the expansion valve and its pressure and temperature decrease (isenthalpic process).
- Between 3 and 4 or 4’ (evaporation of the refrigerant): the refrigerant is heated in the solar thermodynamic panel due to the aborted solar radiation and heat from environment. During this process the refrigerant is transformed into vapour at constant pressure (isobaric process).
- Between 4 and 1 (or 4’ and 1’) (compression of the refrigerant): the refrigerant gas is compressed in the compressor, making its pressure and temperature to increase.

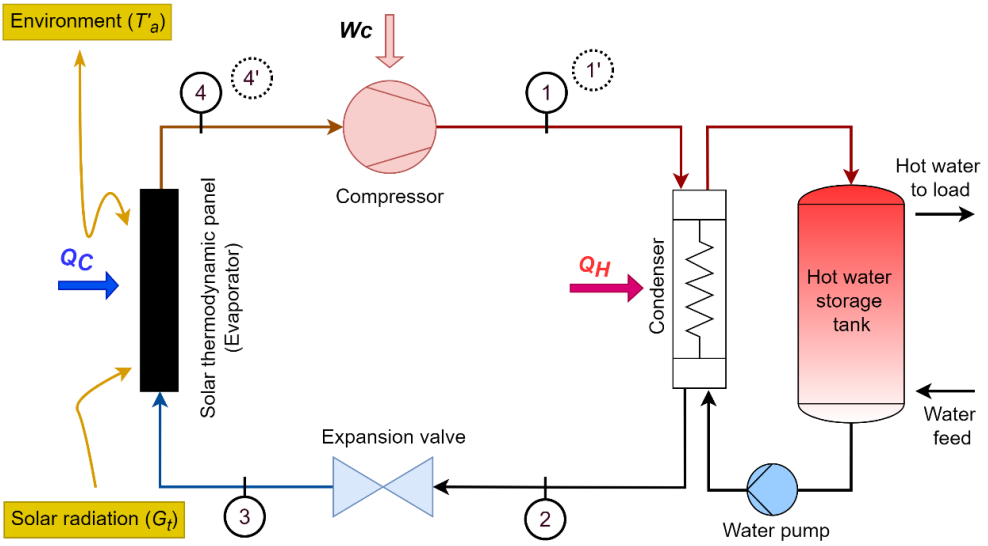


Figure 4-16: Schematic diagram of solar assisted heap pump.

For the circuit of the hot water storage tank, the heat transfer fluid is water and its modelling is described below:

For modelling of the heat pump thermal cycle, the following assumptions are considered:

1) There are no heat losses in the thermal cycle.
2) The heat extraction factor (F_R) of the solar collector is considered constant.
3) The mass flow rate of the system is automatically adjusted aiming to allow the refrigerant to be entirely evaporated in the solar panel (saturated vapour) or to be at least at super-heated condition with temperature equal to environment temperature near the solar panel (T'_a).
4) The environment temperature near the solar panel (T'_a, used in the modelling of heat transfer between environment and solar panel) is considered to be 3ºC above the real environment temperature ($T'_a = T_a + 3$ºC), once the solar collector is fixed in the building roof where the

tiles also absorb solar radiation, making the surrounding temperature to be higher.

5) The pressure before the thermodynamic panel can be adjusted according to the intensity of solar radiation, as described in Section 3.2.1.
6) The refrigerant is always saturated liquid after condenser (point 2).

The heat transfer fluid is the R134a refrigerant and its thermodynamic properties are obtained from (Urieli). Figure 4-17 presents the Pressure–Enthalpy (P-H) and Temperature–Entropy (T-S) diagrams for the thermal cycle.

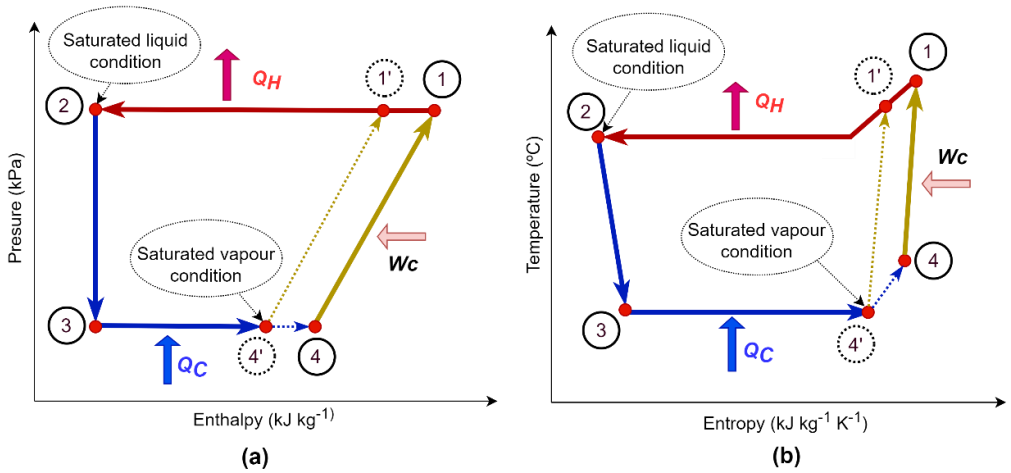


Figure 4-17: (a) Pressure - Enthalpy (P-h) and (b) Temperature – Entropy (T-s) diagrams of the therml cyle.

According to the described approaches, the enthalpy/energy balance in each process/component are:

- Condenser

$$Q_H = \dot{m}(h_1 - h_2) \qquad \text{Eq. (4-38)}$$

- Expansion valve

$$h_3 = h_2 \qquad \text{Eq. (4-39)}$$

- Evaporator

$$Q_C = \dot{m}(h_4 - h_3) \qquad \text{Eq. (4-40)}$$

- Compressor

$$W_C = \dot{m}(h_1 - h_4) \qquad \text{Eq. (1-41)}$$

where h_1, h_2, h_3 and h_4 are enthalpies at points 1, 2, 3 and 4, respectively (in case of saturated vapour condition (point 4'), h_4 and h_1 are h'_4 and h'_1, respectively), $\dot{m}$ is the mass flow rate of the refrigerant, and Q_H is the heat released in the condenser (storage tank), Q_C is the heat absorbed in the solar thermodynamic panel and W_C is the power consumed in the compressor.

The heat absorbed in the flat plate solar panel is also be calculated using:

$$Q_C = F_R A \left[\eta_0 G_t - U(T_3 - T'_a)\right] \qquad \text{Eq. (4-42)}$$

in which F_R is the ratio between actual power output and power output when $T_p = T_3$; T_p is the temperature of the plate of the solar thermodynamic panel; A is the heat transfer area of the solar panel; η_0 is the optical efficiency of the panel; G_t is solar radiation; U is heat transfer coefficient on the surface of the panel; T_3 is the refrigerant temperature at inlet of the solar panel and T'_a is the environment temperature near the panel.

The heat transfer coefficient U is calculated using (Kalogirou, 2014):

$$U = 5.7 + 3.8V \qquad \text{Eq. (4-43)}$$

where V (m/s) is the wind velocity. There can occurs cases of super-heated conditions of the refrigerant in the solar panel. This can occur in cases of high solar radiation intensity and/or high environment temperature. In these

situations, the relation between the super-heated temperature and the absorbed heat in the solar panel is:

$$Q_C = \dot{m}[Q_{cL} + c'_p(T'_4 - T_4)] \qquad \text{Eq. (4-44)}$$

in which Q_{cL} is the heat of evaporation of the refrigerant at the given pressure, c'_p is the heat capacity of the vapour at that pressure and T'_4 is the super-heated temperature at outlet of the solar panel (imposed to be at least equal to T'_a trough adjustments on the mass flow).

The power consumed in the compressor is also be calculated using:

$$W_C = \dot{m}\left(\frac{P_4 v_4}{\eta_c}\left(\frac{k}{k+1}\right)\left[\left(\frac{P_1}{P_4}\right)^{\frac{k-1}{k}} - 1\right]\right) \qquad \text{Eq. (4-45)}$$

where P_4 is the pressure at point 4 (same pressure if point 4' occurs), P_1 is the pressure at point 1 (same pressure if point 1' occurs), v_4 is the specific volume of the refrigerant at point 4 (or v'_4 if condition of point 4' occurs), η_c is the efficiency of the compressor and k is the ratio of specific heat of the refrigerant.

The heating coefficient of performance (COP_H) of the SAHP is calculated using:

$$COP_H = \frac{Q_H}{W_C} \qquad \text{Eq. (4-46)}$$

3.2.1. Parameters and conditions used in the simulations:

The following conditional between pressure before the solar thermodynamic panel and the solar radiation are assumed:

- If $0 \leq G_t < 200$ W m^{-2}, $P_3 = 320$ kPa ($T'_4 = 2.5$ ºC), $c'_p = 0.94$ kJ kg^{-1} K^{-1}
- If $200 \leq G_t < 400$ W m^{-2}, $P_3 = 400$ kPa ($T'_4 = 8.9$ ºC), $c'_p = 0.95$ kJ kg^{-1} K^{-1}
- If $400 \leq G_t < 600$ W m^{-2}, $P_3 = 500$ kPa ($T'_4 = 15.7$ ºC), $c'_p = 0.98$ kJ kg^{-1} K^{-1}
- If $G_t \geq 600$ W m^{-2}, $P_3 = 600$ kPa- ($T'_4 = 21.5$ ºC), $c'_p = 1$ kJ kg^{-1} K^{-1}

Table 4-7 presents the system geometric and thermal parameters and relevant thermodynamic properties of the R134a refrigerant.

Table 4-7: System geometric and thermal parameters and relevant thermodynamic properties (Leonforte et al., 2022) of the R134a refrigerant.

Parameter	Value
η_0	0.9
η_c	0.8
F_R	0.85
A (m^2)	1.6
k	1.2

All the other thermodynamics properties of the refrigerant (h, P, T, υ, c_p) not presented below are obtained through interpolated data from (Urieli). The solar panel is south oriented with 30º of vertical inclination.

4.3.2 Test rig setup

The experiments are carried out in University of Nottingham, with the dynamic panels installed vertical. The overall SAHP system is connecting with an existed hot water storage tank, to provide both hot water and space heating for the occupants. The test rig is shown in Figure 4-18. Inlet, outlet and tank-central water temperatures of hot water tanks are tested with K type thermocouples. Inlet and outlet air temperatures from the ventilation machine are tested with K type thermocouples. Besides, the air supply velocity is measured with Testo thermo-anemometer. Finally, a DT500 data logger collected all the data from the above sensors. Detailed information about the measure sensors, including the measurement accuracy and measurement range are shown in Table 4-8.

Table 4-8 Measurement devices and their accuracy

Instrumentation	Measured parameter	Measurement range	Accuracy
Testo thermo-anemometer	Air velocity	0–10 m/s	±5%
K-type thermocouple	Water and air temperature	0-1100 °C	±0.75%
Datalogger DT500	Data Acquisition	N/A	±0.15%
KIPP & ZONEN Pyranometer CMP3	Solar radiation	0-2000W/m^2	±5%
NEVSETPO Power meters	Electricity consumption	0-2900W	±4%

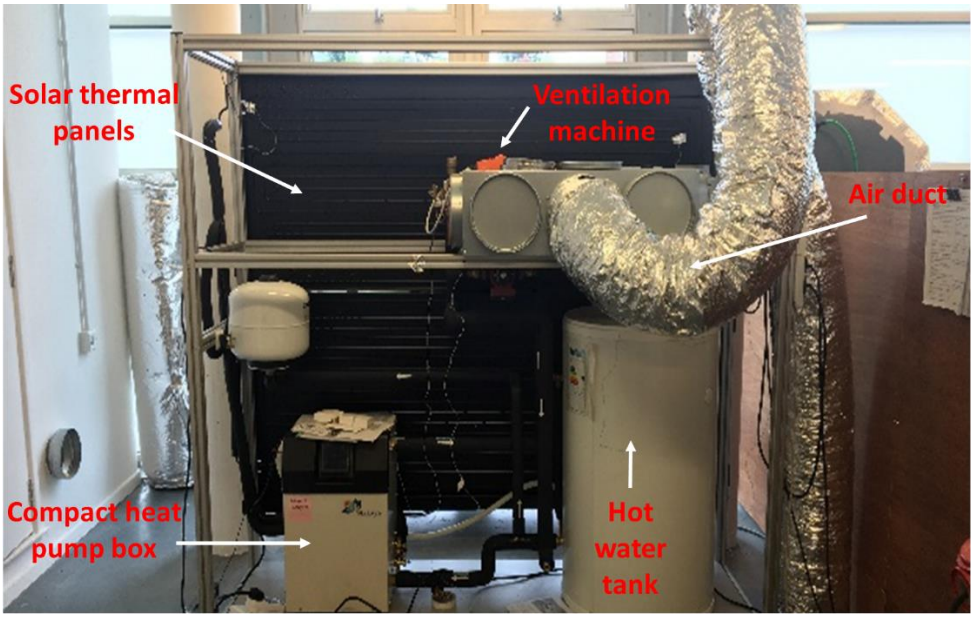


Figure 4-18 Test rig of the SAHP

The jacket containing the pure water is used to store and release the heat produced from the condenser of the SAHP system. The jacket is based on the single tank (HWT) configuration, which is shown in Figure 4-19. Figure 4-19 illustrates the existing SAHP retains its immersion heater for energy input connected to the hot water supply which is based on a heat pump coupled to ternary evaporator panels located in the loft space and exterior roof.



Figure 4-19 Hot water storage tank

To simulate solar radiation under laboratory conditions, an artificial portable light source combining metal-halide and thirty tungsten halogen floodlights source is assembled. The main reason of the solar simulator is to deliver a controllable indoor sun light for the heat pump system. This adjustable illuminate with wavelength ranges between 360-2500 nm and regulator switch, solar irradiance in the range 0 to 800 W/m^2 covering an area of 3.2m^2 as shown in *Figure 4-20*. The switch acts as a regulator in order to maintain solar irradiance variations evenly. The collector is placed indoor up-right in the lab, 200 cm distance in the front of the solar simulator to achieve the required operational conditions. In this case unevenness values at most points obtained is found less than 9%, which is in a good agreement with the British Standards values for indoor solar simulator. The working sample of thermodynamic panels is shown in Figure 4-21.

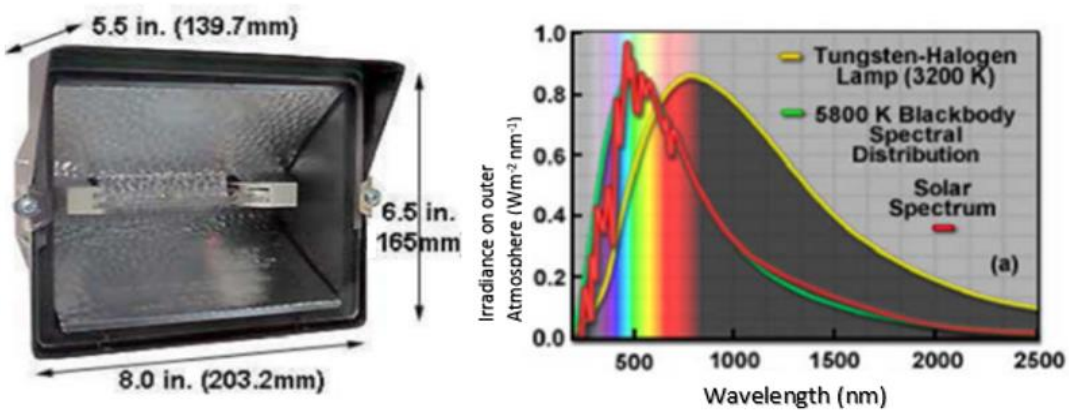




Figure 4-20 Solar radiation simulator and light regulator



Figure 4-21 Working sample of the thermodynamic panels

4.3.3 COP correlation

Solar radiation (G_t), environment temperature near the solar panel (T'_a) and wind speed (V) are combined in a single parameter and then used to describe the COP_H. This parameter is the plate temperature of the solar thermodynamic panel

(T_p), which is presented in Eq. (4-48), and it is obtained by combining Eqs. (4-42), (4-43) and (4-47).

$$Q_C = A\left[\eta_0 G_t - U(T_p - T'_a)\right] \quad \text{Eq. (4-47)}$$

$$T_p = (1 - F_R)\left[T'_a + \frac{\eta_0 G_t}{5.7+3.8V}\right] + F_R T_3 \quad \text{Eq. (4-48)}$$

Figure 4-22 presents the COP_H as function of T_p and the respective linear correlated equations for the four pilots. The mean squared error (R^2) of the linear regressions are 0.946.

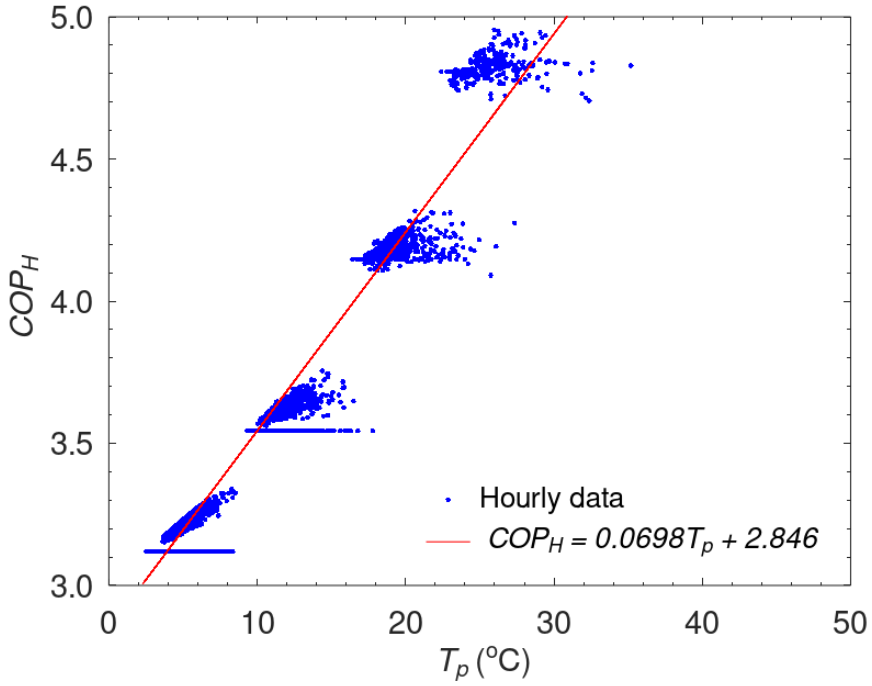


Figure 4-22 The relation between heating COP and plate surface temperature T_p

The general COP_H correlation is:

$$COP_H = 0.0698T_p + 2.825 \quad \text{Eq. (4-49)}$$

This correlation can be used to obtain the performance of the solar assisted heat pump for different climate conditions (solar radiation, environment temperature

and wind speed).

4.4 Summary

This chapter describes two advanced supply retrofit technologies, which are used to supply the space heating, cooling and dehumidification demand, including 1) Liquid desiccant based air cooling and dehumidification ; 2)Solar assisted heat pump (SAHP); Each technology is modelled and validated by measurement in laboratory or field test, with results data to clearly identify and calibrate the performance under real conditions.

Liquid desiccant based air cooling and dehumidification is used to supply space cooling load and dehumidification load. The hybrid system COP formulation is correlated as the relation with both inlet air temperature and relative humidity as shown below:

$$COP = (0.0034 \times T_{a,in} - 0.0331) \times RH_{a,in} + (0.0929 \times T_{a,in} - 3.6587)$$

Solar assisted heat pump integrates two commercial technologies, the heat pump and solar thermal collector. The extracted heat in the evaporator side varied by air source to the integrations of solar source and the external air source. The novel proposed system incorporates into a household using the existing hot water tank and hot water central heating pipe system, providing additional heat directly through the radiators valves to control the temperature to suit preferred comfort levels. This offers a distinct advantage for retrofitting with minimal disruption during installation. According to the application of the solar assisted heat pump, two modes results are discussed separately with 1) mode 1: SAHP will only be used in domestic hot water (DHW) in section 4.3.3.1; 2) mode 2: SAHP will be used in both DHW and ventilation space heating in section 4.3.3.2. The general

heating COP_H correlation is shown below:

$$COP_H = 0.0698T_p + 2.825$$

This correlation can be used to obtain the performance of the solar assisted heat pump for different climate conditions (solar radiation, environment temperature and wind speed).

The test results on-site of the technologies can be furtherly used in the modelling of the building energy consumption. Due to the calibration of the system performance, the final results of the building energy consumption can be more accurate compared with theory technical data.

5. An innovative Energy-Flow based Ensemble Calibration (EF-EC) model for retrofit building energy-economic performance prediction

5.1 Introduction

This section presents an innovative concept via a novel Energy-Flow based Ensemble Calibration (EF-EC) model, intending to predict the deep energy retrofit energy-economic performance rapidly and accurately in single-family houses, with the concept shown in Figure 5-1.

The proposed transient EF-EC model calculation process have three layers:

1) Input neurons (Stage 1);

2) Complex heat and electrical transfer models (Stage 2);

3) Output neurons (Stage 3).

The input neurons have four parameters in which the baseline heat and electrical demands and heat and electrical coefficients of individual retrofit measures are obtained and calculated from the dynamic simulation in IES VE (Stage 0). By replacing the layer of hidden neurons with complex heat and electricity transfer models in conventional Black-box models (Thrampoulidis et al., 2021), the coupling effects in deep energy retrofit combinations and complex heat transfer phenomena can significantly improve the accuracy of energy performance prediction in deep energy retrofitted single-family houses (Wang et al., 2022). Furthermore, in comparison with the high computational costs that are required in any white-box model for BPS, the required computational costs/efforts in the proposed EF-EC model for performing retrofit energy modelling (which is a key technical hurdle for promoting bespoke designed building retrofit (Chen et al., 2020)) can be substantially reduced. This is due to the fact that, as shown in

Stage 1, the Input neurons of the proposed EF-EC model consist of IES VE simulation output and each retrofit combination. In this way, instead of establishing and running countless potential retrofit combinations in IES VE dynamic simulation, which are extremely time-consuming, a rapid and transient numerical calculation could be achieved by Stage 2. Finally, the post-retrofit energy output results of comprehensive retrofit measure combinations are performed in Stage 3.

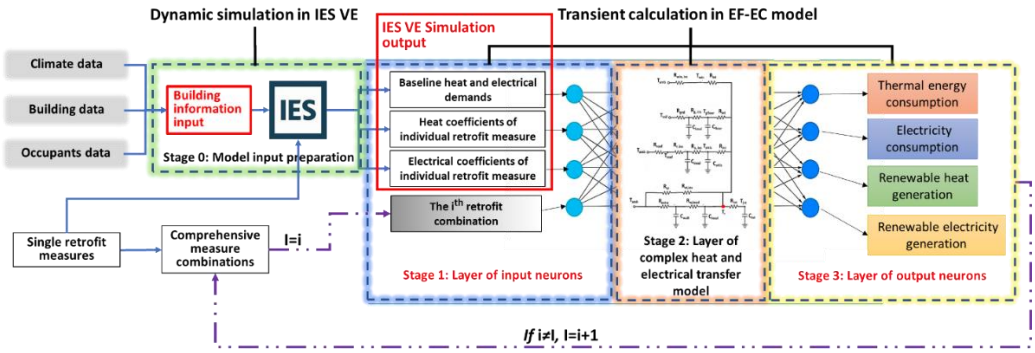


Figure 5-1 Concept of the EF-EC model

In the EF-EC model, the thermal and electrical hybrid energy flow framework is established to depict the network from the energy inputs ($E_{I\times 1}^{f,po}$) to the demand outputs ($D_{I\times J}^{po}$) via a new parameter- coupling matrix ($C_{I\times J}^{po,\text{int}}$) in section 5.2.1. And then, lifetime energy-economic performance is evaluated in three aspects, including initial retrofit investment (θ_i^{ii}), pre and post-retrofit annual bills ($\theta^{ab,pr}$, $\theta^{ab,po}$) in section 5.2.2. Afterwards, model uncertainty and sensitivity analysing approaches are defined in section 5.2.3. Finally, a case study analysis is conducted to demonstrate and validate the proposed EF-EC model in section 5.2.4. Model validation, uncertainty and results comparisons and calibration via sensitivity analysis are discussed in sections 5.4.

5.2 Post-retrofit energy model

The proposed EF-EC model and network connections from the demand outputs to energy inputs via the coupling matrices and factors are shown in the breakdown and calculation process in Figure 5-2. The post-retrofit final energy input calculation terminologies are listed in the following four steps, with details in sections 5.2.1 – 5.2.4. The post-retrofit final energy inputs of COMB are defined via the iteration processes from Combination number i=1 to i=I, which consist of the on- and off-grid energy inputs. The on-grid energy inputs comprise grid electricity, natural gas and other heat sources (i.e., coal, oil, biomass heat), whereas off-grid energy inputs incorporate renewable electricity generated by PV panels, wind turbines and renewable heat generated by solar collectors.

Step 1: The pre-retrofit building simulation model is constructed in the IES VE simulation engine, capable of generating the baseline demand/energy calculation results as outputs. In addition, the available individual retrofit measures are listed, and the improved energy performance after imposing each retrofit measure on the baseline model are calculated respectively in IES VE. Finally, all the selected individual retrofit measures will be further combined into a wide range of comprehensive combinations via a developed algorithm in MATLAB, with details described in section 5.2.1;

Step 2: The post-retrofit demand outputs are calculated by the multiplication between the pre-retrofit demand $D_{I\times J}^{pr}$ and the post-retrofit demand efficiency $D_{I\times J}^{e,pr}$ with details described in section 5.2.2;

Step 3: The integrated post-retrofit coupling factors $C_{I\times J}^{po,\mathrm{int}}$ are calculated as minimum values of the integrated post-retrofit coupling factors

$\min\left(\left(M_{1,n}C_{N\times J}^{po,ind}\right)\Big|_{n=1}^{N}\right)$ of all the retrofit measures in each combination with details described in section 5.2.3;

Step 4: The post-retrofit final energy inputs $E_i^{f,po}$ are calculated by the difference of the post-retrofit on- and off-grid energy inputs ($E_i^{on,po}$ and $E_i^{off,po}$), in section 5.2.4.

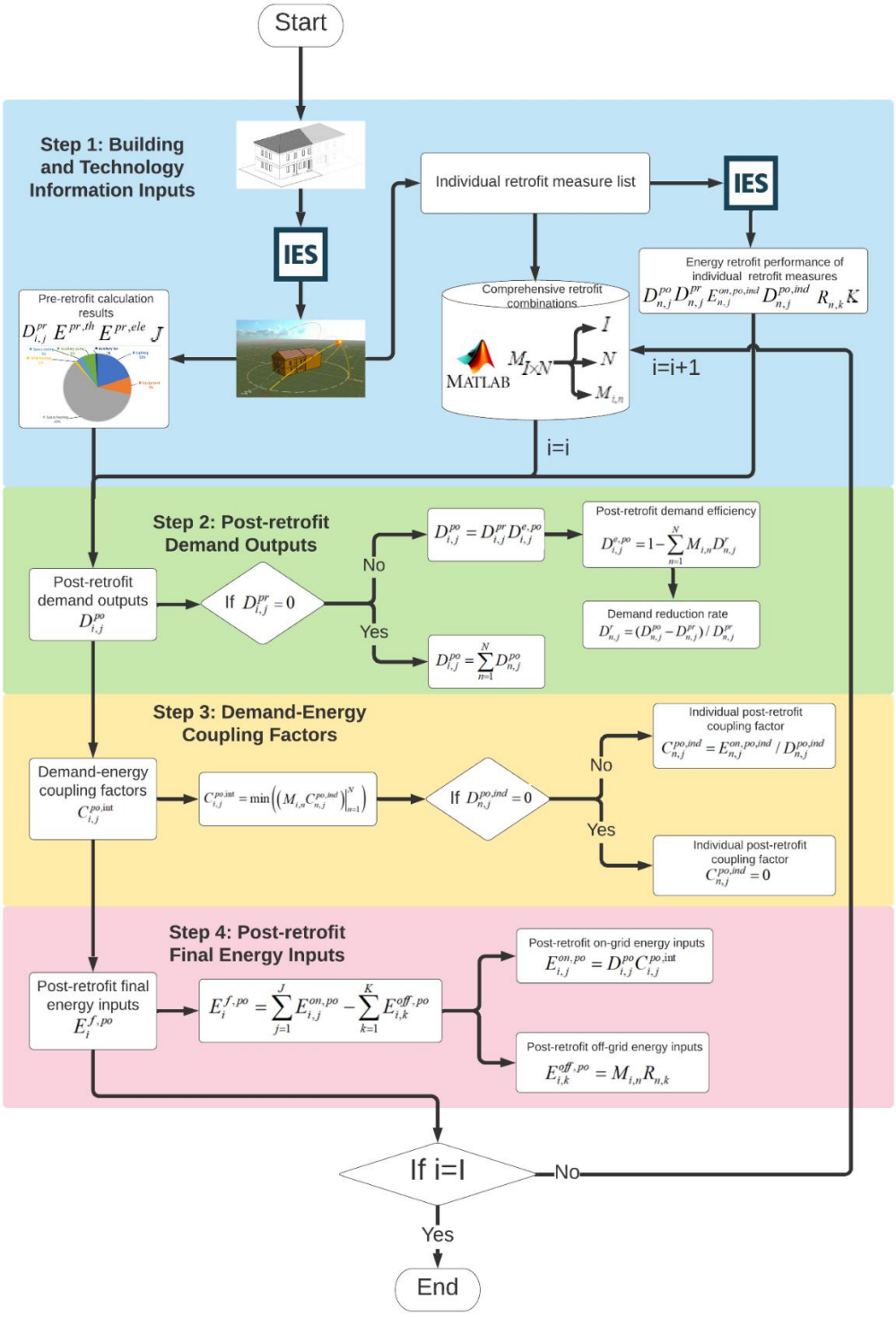


Figure 5-2 Breakdown and calculation process of EF-EC model

Moreover, the aim is to explicitly interconnect the couplings among the various energy sources with demand outputs and on/off-grid energy inputs and derive a model with energy flows from inputs to outputs. As shown in Figure 5-3, the

general concept to cover typical energy flows illustrates the hybrid thermal, and electrical energy flows considering a diversified range of thermal and electric energy sources from renewables.

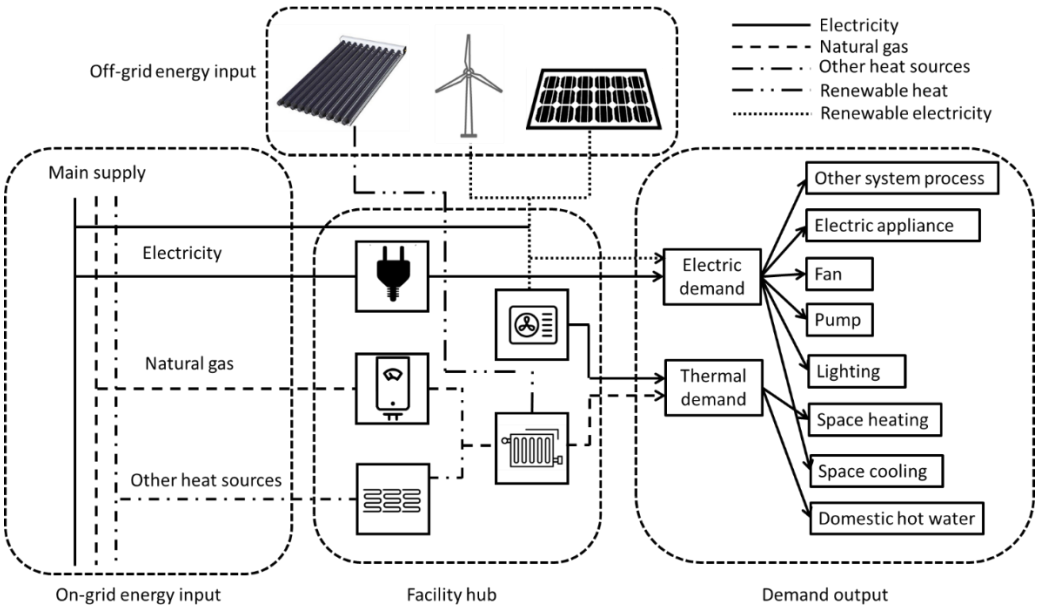


Figure 5-3 Sketch of the hybrid thermal and electrical energy flows in a single building scenario

5.2.1 Input-output energy flow framework

The final post-retrofit energy input is calculated by the difference between the on-grid and off-grid post-retrofit energy input, as shown in Eq. (5-1). The matrix $E_{I\times1}^{f,po}$ represents the calculated net energy consumption of comprehensive energy combinations from COMB1 to COMB i, the combination number. Furthermore, $E_i^{f,po}$ indicates the final post-retrofit energy input of COMB i. The on-grid post-retrofit energy input of COMB i ($E_i^{on,po}$) is the sum of the total energy consumption due to different occupancy's demand requirements, divided into J sections determined by the actual building types and functions as space heating/cooling DHW, etc. The off-grid post-retrofit energy input of COMB i (

$E_i^{off,po}$) is the sum of the total renewable energy generation from different sources, divided into K sections, such as PV electricity, solar thermal energy, etc.

$$E_{I\times1}^{f,po} = E_{I\times1}^{on,po} - E_{I\times1}^{off,po}$$

$$= \overbrace{\begin{bmatrix} E_1^{f,po} \\ E_2^{f,po} \\ \vdots \\ E_i^{f,po} \\ \vdots \\ E_I^{f,po} \end{bmatrix}_{I\times1}}^{E_{I\times1}^{f,po}} = \begin{bmatrix} \overbrace{\sum_{j=1}^{J} E_{I\times J}^{on,po}\big|_{i=1,j}}^{E_{I\times1}^{on,po}} - \overbrace{\sum_{k=1}^{K} E_{I\times K}^{off,po}\big|_{i=1,k}}^{E_{I\times1}^{off,po}} \\ \sum_{j=1}^{J} E_{I\times J}^{on,po}\big|_{i=2,j} - \sum_{k=1}^{K} E_{I\times K}^{off,po}\big|_{i=2,k} \\ \vdots \\ \sum_{j=1}^{J} E_{I\times J}^{on,po}\big|_{i,j} - \sum_{k=1}^{K} E_{I\times K}^{off,po}\big|_{i,k} \\ \vdots \\ \sum_{j=1}^{J} E_{I\times J}^{on,po}\big|_{i=I,j} - \sum_{k=1}^{K} E_{I\times K}^{off,po}\big|_{i=I,k} \end{bmatrix} \quad \text{Eq. (5-1)}$$

Where: The matrices of $E_{I\times1}^{f,po}$, $E_{I\times1}^{on,po}$, $E_{I\times1}^{off,po}$ have the exact dimensions of $I\times1$; $\sum_{j=1}^{J} E_{I\times J}^{on,po}\big|_{i,j}$ represents the sum of the total energy consumption due to different occupancy's demand requirements, with the demand of j ranging from 1 to J ; $\sum_{k=1}^{K} E_{I\times K}^{off,po}\big|_{i,k}$ represents for the sum of the total renewable energy generation with different sources k ranging from 1 to K . The calculation method of matrices $E_{I\times J}^{on,po}$ and $E_{I\times K}^{off,po}$ will be further introduced in Eq. (5-2) and Eq. (5-3).

To model the transformations from the post-retrofit on-grid energy input $E_{I\times J}^{on,po}$ to the post-retrofit demand output $D_{I\times J}^{po}$ via the facility hub, the Hadamard matrix multiplication (Salata et al., 2017) is employed. The on-grid energy input

is modelled through the coupling matrix $C_{I\times J}^{po,\text{int}}$, representing the post-retrofit conversion factor between energy input and demand output, as shown in Eq. (5-2). The Hadamard matrix multiplication (Salata et al., 2017) (element-wise multiplication $\odot$) is a binary operation that takes two matrices of the same dimensions and produces another matrix of the same dimension as the operands, with elements given by $(A \odot B)_{ij} = (A)_{ij}(B)_{ij}$.

$$
\begin{aligned}
E_{I\times J}^{on,po} &= D_{I\times J}^{po} \odot C_{I\times J}^{po,\text{int}} \\
&= \overbrace{\begin{bmatrix} E_{1,1}^{on,po} & E_{1,2}^{on,po} & \cdots & E_{1,J}^{on,po} \\ E_{2,1}^{on,po} & E_{2,2}^{on,po} & \cdots & E_{2,J}^{on,po} \\ \vdots & \vdots & E_{i,j}^{on,po} & \vdots \\ E_{I,1}^{on,po} & \cdots & \cdots & E_{I,J}^{on,po} \end{bmatrix}}^{E_{I\times J}^{on,po}}_{I\times J} \\
&= \overbrace{\begin{bmatrix} D_{1,1}^{po} & D_{1,2}^{po} & \cdots & D_{1,J}^{po} \\ D_{2,1}^{po} & D_{2,2}^{po} & \cdots & D_{2,J}^{po} \\ \vdots & \vdots & D_{i,j}^{po} & \vdots \\ D_{I,1}^{po} & \cdots & \cdots & D_{I,J}^{po} \end{bmatrix}}^{D_{I\times J}^{po}}_{I\times J} \odot \overbrace{\begin{bmatrix} C_{1,1}^{po,\text{int}} & C_{1,2}^{po,\text{int}} & \cdots & C_{1,J}^{po,\text{int}} \\ C_{2,1}^{po,\text{int}} & C_{2,2}^{po,\text{int}} & \cdots & C_{2,J}^{po,\text{int}} \\ \vdots & \vdots & C_{i,j}^{po,\text{int}} & \vdots \\ C_{I,1}^{po,\text{int}} & \cdots & \cdots & C_{I,J}^{po,\text{int}} \end{bmatrix}}^{C_{I\times J}^{po,\text{int}}}_{I\times J} \\
&= \begin{bmatrix} D_{1,1}^{po}C_{1,1}^{po,\text{int}} & D_{1,2}^{po}C_{1,2}^{po,\text{int}} & \cdots & D_{1,J}^{po}C_{1,J}^{po,\text{int}} \\ D_{2,1}^{po}C_{2,1}^{po,\text{int}} & D_{2,2}^{po}C_{2,2}^{po,\text{int}} & \cdots & D_{2,J}^{po}C_{2,J}^{po,\text{int}} \\ \vdots & \vdots & D_{i,j}^{po}C_{i,j}^{po,\text{int}} & \vdots \\ D_{I,1}^{po}C_{I,1}^{po,\text{int}} & \cdots & \cdots & D_{I,J}^{po}C_{I,J}^{po,\text{int}} \end{bmatrix}_{I\times J}
\end{aligned}
$$

Eq. (5-2)

Where: The three matrices $E_{I\times J}^{on,po}$, $D_{I\times J}^{po}$, $C_{I\times J}^{po,\text{int}}$ keep the same dimension of $I \times J$; $E_{i,j}^{on,po}$ represents the post-retrofit on-grid energy input of COMB i due to the jth occupancy's demand requirement; $D_{i,j}^{po}$ defines the post-retrofit demand of COMB i with the jth occupancy's demand requirement, $C_{i,j}^{po}$ denotes the

coupling conversion factor in COMB i between the jth $E_{i\times j}^{on,po}$ and its $D_{i\times j}^{po}$. The calculation methods of matrices $D_{I\times J}^{po}$ and $C_{I\times J}^{po,\text{int}}$ are introduced in Eq. (5-4) and Eq. (5-8).

The off-grid post-retrofit energy input $E_{I\times K}^{off,po}$ is calculated by the matrix multiplication between the renewable energy generation $R_{N\times K}$ and the matrix $M_{I\times N}$ of measures selection in COMB, as shown in Eq. (5-3). $M_{I\times N}$ corresponds to the measure selection from COMB01 to COMB I, with maximum numbers N of retrofit measures in each retrofit combination. In the matrix $M_{I\times N}$, operators 0 and 1 represent different retrofit measures' absence and presence in each combination. To explore all the possible ERM combinations, n mixed variables are deducted in a continuous or discrete range. $R_{N\times K}$ corresponds to the matrix of renewable energy generation with the dimension of $N\times K$; K represents for different renewable energy generation sources, such as renewable electricity, renewable domestic hot water, etc.

$$E_{I\times K}^{off,po} = M_{I\times N} \square R_{N\times K}$$

$$= \overbrace{\begin{bmatrix} E_{1,1}^{off,po} & E_{1,2}^{off,po} & \cdots & E_{1,K}^{off,po} \\ E_{2,1}^{off,po} & E_{2,2}^{off,po} & \cdots & E_{2,K}^{off,po} \\ \vdots & \vdots & E_{i,k}^{off,po} & \vdots \\ E_{I,1}^{off,po} & \cdots & \cdots & E_{I,K}^{off,po} \end{bmatrix}}^{E_{I\times K}^{off,po}}_{I\times K}$$

$$= \overbrace{\begin{bmatrix} M_{1,1} & M_{1,2} & \cdots & M_{1,N} \\ M_{2,1} & M_{2,2} & \cdots & M_{2,N} \\ \vdots & \vdots & M_{i,n} & \vdots \\ M_{I,1} & \cdots & \cdots & M_{I,N} \end{bmatrix}}^{M_{I\times N}}_{I\times N} \square \overbrace{\begin{bmatrix} R_{1,1} & R_{1,2} & \cdots & R_{1,K} \\ R_{2,1} & R_{2,2} & \cdots & R_{2,K} \\ \vdots & \vdots & R_{n,k} & \vdots \\ R_{N,1} & \cdots & \cdots & R_{N,K} \end{bmatrix}}^{R_{N\times K}}_{N\times K}$$

$$= \begin{bmatrix} M_{1,1}R_{1,1} & M_{1,2}R_{1,2} & \cdots & M_{1,N}R_{1,K} \\ M_{2,1}R_{2,1} & M_{2,2}R_{2,2} & \cdots & M_{2,N}R_{2,K} \\ \vdots & \vdots & M_{i,n}R_{n,k} & \vdots \\ M_{I,1}R_{N,1} & \cdots & \cdots & M_{I,N}R_{N,K} \end{bmatrix}_{I\times K}$$

Eq. (5-3)

Where: $E_{i,k}^{off,po}$ represents the post-retrofit off-grid energy input of COMBi in the kth renewable energy source; $M_{i,n}$ illustrates the nth measure selection in COMBi; $R_{n,k}$ denotes the renewable energy generation of nth measure in kth energy source. The calculation method of the matrix $M_{I\times N}$ is generated in MATLAB, which can cover comprehensive combinations for all available retrofit measures in actual buildings. The matrix $R_{N\times K}$ is obtained from the individual simulation results in building energy dynamic simulation engines.

5.2.2 Post-retrofit demand outputs

As described in Eq. (5-2), the post-retrofit on-grid energy input $E_{I\times J}^{on,po}$ is connected to networks between the post-retrofit demand $D_{I\times J}^{po}$ with its coupling

matrix $C_{I\times J}^{po}$. In the network, the post-retrofit demand $D_{I\times J}^{po}$ is first modelled as the energy flow balance with the introduction of retrofit measures, which is calculated by the Hadamard multiplication between the pre-retrofit demand $D_{I\times J}^{pr}$ and the post-retrofit demand efficiency $D_{I\times J}^{e,po}$, as shown in Eq. (5-4). The three matrices $D_{I\times J}^{po}$, $D_{I\times J}^{pr}$, $D_{I\times J}^{e,po}$ have the same dimension $I\times J$.

The post-retrofit demand efficiency $D_{I\times J}^{e,po}$ is calculated by the difference of the pre-retrofit demand efficiency $D_{I\times J}^{e,pr}=1_{I\times J}$ (each pre-retrofit demand efficiency equals 1 due to no retrofit interventions involved) and the actual demand reduction rate $M_{I\times N}\square D_{N\times J}^{r}$ shown in Eq. (5-5).

The matrix of demand reduction rate $D_{N\times J}^{r}$ has the dimension of $N\times J$, with elements individually calculated by the Hadamard division between the post and pre-retrofit demand differences ($D_{N\times J}^{po}-D_{N\times J}^{pr}$) and the pre-retrofit demand of each retrofit measure in every occupancy's required demand $D_{N\times J}^{pr}$, as shown in Eq. (5-6). The post and pre-retrofit demand of occupancy's requirements can be obtained from any building energy simulation engine.

$$
\begin{aligned}
D^{po}_{I\times J} &= D^{pr}_{I\times J} \odot D^{e,po}_{I\times J} \\
&= \overbrace{\begin{bmatrix} D^{po}_{1,1} & D^{po}_{1,2} & \cdots & D^{po}_{1,J} \\ D^{po}_{2,1} & D^{po}_{2,2} & \cdots & D^{po}_{2,J} \\ \vdots & \vdots & D^{po}_{i,j} & \vdots \\ D^{po}_{I,1} & \cdots & \cdots & D^{po}_{I,J} \end{bmatrix}}^{D^{po}_{I\times J}}_{I\times J} \\
&= \overbrace{\begin{bmatrix} D^{pr}_{1,1} & D^{pr}_{1,2} & \cdots & D^{pr}_{1,J} \\ D^{pr}_{2,1} & D^{pr}_{2,2} & \cdots & D^{pr}_{2,J} \\ \vdots & \vdots & D^{pr}_{i,j} & \vdots \\ D^{pr}_{I,1} & \cdots & \cdots & D^{pr}_{I,J} \end{bmatrix}}^{D^{pr}_{I\times J}}_{I\times J} \odot \overbrace{\begin{bmatrix} D^{e,po}_{1,1} & D^{e,po}_{1,2} & \cdots & D^{e,po}_{1,J} \\ D^{e,po}_{2,1} & D^{e,po}_{2,2} & \cdots & D^{e,po}_{2,J} \\ \vdots & \vdots & D^{e,po}_{i,j} & \vdots \\ D^{e,po}_{I,1} & \cdots & \cdots & D^{e,po}_{I,J} \end{bmatrix}}^{D^{e,po}_{I\times J}}_{I\times J} \\
&= \begin{bmatrix} D^{pr}_{1,1}D^{e,po}_{1,1} & D^{pr}_{1,2}D^{e,po}_{1,2} & \cdots & D^{pr}_{1,J}D^{e,po}_{1,J} \\ D^{pr}_{2,1}D^{e,po}_{2,1} & D^{pr}_{2,2}D^{e,po}_{2,2} & \cdots & D^{pr}_{2,J}D^{e,po}_{2,J} \\ \vdots & \vdots & D^{pr}_{i,j}D^{e,po}_{i,j} & \vdots \\ D^{pr}_{I,1}D^{e,po}_{I,1} & \cdots & \cdots & D^{pr}_{I,J}D^{e,po}_{I,J} \end{bmatrix}_{I\times J}
\end{aligned}
$$

Eq. (5-4)

Where: $D^{po}_{i,j}$ represents the post-retrofit jth demand in COMB i, $D^{pr}_{i,j}$ defines the pre-retrofit jth demand in COMB i, $D^{e,po}_{i,j}$ denotes the post-retrofit jth demand efficiency in COMB i; Meanwhile, the pre-retrofit jth demand for each retrofit combination keeps the same in the baseline, which does not change with ith combination, therefore $D^{pr}_{1,j} = D^{pr}_{2,j} = \cdots = D^{pr}_{i,j} = d^{pr}_{j}$ (constant).

$$D^{s,po}_{I\times J} = 1_{I\times J} - M_{I\times N} \bullet D^{r}_{N\times J}$$

$$= \overbrace{\begin{bmatrix} D^{s,po}_{1,1} & D^{s,po}_{1,2} & \cdots & D^{s,po}_{1,J} \\ D^{s,po}_{2,1} & D^{s,po}_{2,2} & \cdots & D^{s,po}_{2,J} \\ \vdots & \vdots & D^{s,po}_{i,j} & \vdots \\ D^{s,po}_{I,1} & \cdots & \cdots & D^{s,po}_{I,J} \end{bmatrix}}^{D^{s,po}_{I\times J}}_{I\times J}$$

$$= \overbrace{\begin{bmatrix} 1 & 1 & \cdots & 1 \\ 1 & 1 & \cdots & 1 \\ \vdots & \vdots & 1 & \vdots \\ 1 & \cdots & \cdots & 1 \end{bmatrix}}^{1_{I\times J}}_{I\times J} - \overbrace{\begin{bmatrix} M_{1,1} & M_{1,2} & \cdots & M_{1,N} \\ M_{2,1} & M_{2,2} & \cdots & M_{2,N} \\ \vdots & \vdots & M_{i,n} & \vdots \\ M_{I,1} & \cdots & \cdots & M_{I,N} \end{bmatrix}}^{M_{I\times N}}_{I\times N} \bullet \overbrace{\begin{bmatrix} D^{r}_{1,1} & D^{r}_{1,2} & \cdots & D^{r}_{1,J} \\ D^{r}_{2,1} & D^{r}_{2,2} & \cdots & D^{r}_{2,J} \\ \vdots & \vdots & D^{r}_{n,j} & \vdots \\ D^{r}_{N,1} & \cdots & \cdots & D^{r}_{N,J} \end{bmatrix}}^{D^{r}_{N\times J}}_{N\times J}$$

Eq. (5-5)

Where: $M_{i,n}$ illustrates the nth measure selection in COMB i; $D^{r}_{n,j}$ denotes the nth measure's post-retrofit jth demand reduction rate.

$$D^{r}_{N\times J} = (D^{po}_{N\times J} - D^{pr}_{N\times J}) \oslash D^{pr}_{N\times J}$$

$$= \overbrace{\begin{bmatrix} D^{r}_{1,1} & D^{r}_{1,2} & \cdots & D^{r}_{1,J} \\ D^{r}_{2,1} & D^{r}_{2,2} & \cdots & D^{r}_{2,J} \\ \vdots & \vdots & D^{r}_{n,j} & \vdots \\ D^{r}_{N,1} & \cdots & \cdots & D^{r}_{N,J} \end{bmatrix}}^{D^{r}_{N\times J}}_{N\times J}$$

$$= \left(\overbrace{\begin{bmatrix} D^{po}_{1,1} & D^{po}_{1,2} & \cdots & D^{po}_{1,J} \\ D^{po}_{2,1} & D^{po}_{2,2} & \cdots & D^{po}_{2,J} \\ \vdots & \vdots & D^{po}_{n,j} & \vdots \\ D^{po}_{N,1} & \cdots & \cdots & D^{po}_{N,J} \end{bmatrix}}^{D^{po}_{N\times J}}_{N\times J} - \overbrace{\begin{bmatrix} D^{pr}_{1,1} & D^{pr}_{1,2} & \cdots & D^{pr}_{1,J} \\ D^{pr}_{2,1} & D^{pr}_{2,2} & \cdots & D^{pr}_{2,J} \\ \vdots & \vdots & D^{pr}_{n,j} & \vdots \\ D^{pr}_{N,1} & \cdots & \cdots & D^{pr}_{N,J} \end{bmatrix}}^{D^{pr}_{N\times J}}_{N\times J} \right) \oslash \overbrace{\begin{bmatrix} D^{pr}_{1,1} & D^{pr}_{1,2} & \cdots & D^{pr}_{1,J} \\ D^{pr}_{2,1} & D^{pr}_{2,2} & \cdots & D^{pr}_{2,J} \\ \vdots & \vdots & D^{pr}_{n,j} & \vdots \\ D^{pr}_{N,1} & \cdots & \cdots & D^{pr}_{N,J} \end{bmatrix}}^{D^{pr}_{N\times J}}_{N\times J}$$

$$= \begin{bmatrix} (D^{po}_{1,1} - D^{pr}_{1,1})/D^{pr}_{1,1} & (D^{po}_{1,2} - D^{pr}_{1,2})/D^{pr}_{1,2} & \cdots & (D^{po}_{1,J} - D^{pr}_{1,J})/D^{pr}_{1,J} \\ (D^{po}_{2,1} - D^{pr}_{2,1})/D^{pr}_{2,1} & (D^{po}_{2,2} - D^{pr}_{2,2})/D^{pr}_{2,2} & \cdots & (D^{po}_{2,J} - D^{pr}_{2,J})/D^{pr}_{2,J} \\ \vdots & \vdots & (D^{po}_{n,j} - D^{pr}_{n,j})/D^{pr}_{n,j} & \vdots \\ (D^{po}_{N,1} - D^{pr}_{N,1})/D^{pr}_{N,1} & \cdots & \cdots & (D^{po}_{N,J} - D^{pr}_{N,J})/D^{pr}_{N,J} \end{bmatrix}_{N\times J}$$

Eq. (5-6)

Where: $D_{n,j}^{po}$ illustrates the post-retrofit jth demand with the installation of only the nth retrofit measure; $D_{n,j}^{pr}$ denotes the pre-retrofit jth demand. However, the pre-retrofit jth demand for each retrofit combination keeps the same in the baseline, which does not change with nth retrofit intervention $D_{1,j}^{pr} = D_{2,j}^{pr} = \cdots = D_{n,j}^{pr} = d_j^{pr}$ (constant).

Eq. (5-4) to Eq. (5-6) only applies when the jth pre-retrofit demand $D_{1,j}^{pr}$ is not equal to 0. However, the jth post-retrofit demand in COMB *i* is calculated by the sum of the selected n technologies' post-retrofit demand values if $D_{1,j}^{pr}$ is equal to 0, as shown in Eq. (5-7).

$$\begin{cases} if \quad D_{i,j}^{pr} \neq 0, \quad D_{i,j}^{po} = D_{i,j}^{pr} D_{i,j}^{e,po} \\ if \quad D_{i,j}^{pr} = 0, \quad D_{i,j}^{po} = \sum_{n=1}^{N} D_{n,j}^{po} \end{cases} \qquad \text{Eq. (5-7)}$$

5.2.3 Coupling matrices for input-output energy flow

As depicted in Eq. (5-2), the post-retrofit coupling matrix $C_{I\times J}^{po,\text{int}}$ is described as the energy flow from the on-grid energy input $E_{I\times J}^{on,po}$ to the demand output $D_{I\times J}^{po}$. The entries of the coupling matrix are called coupling factors, which can be derived from the energy system efficiencies, the energy flow typology and energy input dispatch. Usually, the energy system efficiencies are independent which are calculated according to the individual demand and energy simulation results of a single-retrofit measure.

Generally, the post-retrofit coupling matrix $C_{I\times J}^{po,\text{int}}$ equals the minimum values of the integrated post-retrofit coupling factors $\min\left(\left(M_{1,n} C_{N\times J}^{po,ind}\right)\Big|_{n=1}^{N}\right)$ of all the

retrofit measures in each combination, as shown in Eq. (5-8). $C_{N\times J}^{po,\mathrm{in}d}$ is calculated by the Hadamard division ⊘ between the post-retrofit individual on-grid energy input $E_{N\times J}^{on,po,ind}$ and demand output $D_{N\times J}^{po,ind}$, with the dimension of $N\times J$. The Hadamard matrix division (Wetzstein) (element-wise division ⊘) is a binary operation that takes two matrices of the same dimensions and produces another matrix of the same dimension as the operands, with elements given by $(A \oslash B)_{ij} = (A)_{ij}/(B)_{ij}$.

The entries of the post-retrofit individual coupling matrix $C_{N\times J}^{po,\mathrm{in}d}$ represents the coupling factors with installations of only the nth retrofit measure calculated by the division of the post-retrofit individual on-grid energy input and the post-retrofit individual demand output of the jth demand, as shown in Eq. (5-9).

$$C_{I\times J}^{po,\mathrm{int}} = \begin{bmatrix} C_{1\times J}^{po,\mathrm{int}} \\ C_{2\times J}^{po,\mathrm{int}} \\ \vdots \\ C_{i\times J}^{po,\mathrm{int}} \\ \vdots \\ C_{I\times J}^{po,\mathrm{int}} \end{bmatrix} = \begin{bmatrix} \min\left(\left(M_{1,n}C_{N\times J}^{po,ind}\right)\Big|_{n=1}^{N}\right) \\ \min\left(\left(M_{2,n}C_{N\times J}^{po,ind}\right)\Big|_{n=1}^{N}\right) \\ \vdots \\ \min\left(\left(M_{i,n}C_{N\times J}^{po,ind}\right)\Big|_{n=1}^{N}\right) \\ \vdots \\ \min\left(\left(M_{I,n}C_{N\times J}^{po,ind}\right)\Big|_{n=1}^{N}\right) \end{bmatrix}$$

$$= \begin{bmatrix} \min\left(\left(M_{i=1,n}C_{n,j=1}^{po,ind}\right)\Big|_{n=1}^{N}\right) & \min\left(\left(M_{i=1,n}C_{n,j=2}^{po,ind}\right)\Big|_{n=1}^{N}\right) & \cdots & \min\left(\left(M_{i=1,n}C_{n,j}^{po,ind}\right)\Big|_{n=1}^{N}\right) & \cdots & \min\left(\left(M_{i=1,n}C_{n,j=J}^{po,ind}\right)\Big|_{n=1}^{N}\right) \\ \min\left(\left(M_{i=2,n}C_{n,j=1}^{po,ind}\right)\Big|_{n=1}^{N}\right) & \min\left(\left(M_{i=2,n}C_{n,j=2}^{po,ind}\right)\Big|_{n=1}^{N}\right) & \cdots & \min\left(\left(M_{i=2,n}C_{n,j}^{po,ind}\right)\Big|_{n=1}^{N}\right) & \cdots & \min\left(\left(M_{i=2,n}C_{n,j=J}^{po,ind}\right)\Big|_{n=1}^{N}\right) \\ \vdots & \vdots & & \vdots & & \vdots \\ \vdots & \vdots & & \min\left(\left(M_{i,n}C_{n,j}^{po,ind}\right)\Big|_{n=1}^{N}\right) & & \vdots \\ \vdots & \vdots & & \vdots & & \vdots \\ \min\left(\left(M_{i=I,n}C_{n,j=1}^{po,ind}\right)\Big|_{n=1}^{N}\right) & \min\left(\left(M_{i=I,n}C_{n,j=2}^{po,ind}\right)\Big|_{n=1}^{N}\right) & \cdots & \min\left(\left(M_{i=I,n}C_{n,j}^{po,ind}\right)\Big|_{n=1}^{N}\right) & \cdots & \min\left(\left(M_{i=I,n}C_{n,j=J}^{po,ind}\right)\Big|_{n=1}^{N}\right) \end{bmatrix}$$

Eq. (5-8)

Where: $C_{i\times J}^{po,\mathrm{int}}$ represents the integrated post-retrofit coupling matrix of J

demand sections in COMB i ; $\min\left(\left(M_{i,n}C_{n,j}^{po,ind}\right)\Big|_{n=1}^{N}\right)$ denotes the minimum value of the integrated coupling factor for the jth demand considering all the selected retrofit technologies in COMB i .

$$C_{N\times J}^{po,ind} = E_{N\times J}^{on,po,ind} \oslash D_{N\times J}^{po,ind}$$
$$= \begin{bmatrix} E_{1,1}^{on,po,ind}/D_{1,1}^{po,ind} & E_{1,2}^{on,po,ind}/D_{1,2}^{po,ind} & \cdots & E_{1,j}^{on,po,ind}/D_{1,j}^{po,ind} & \cdots & E_{1,J}^{on,po,ind}/D_{1,J}^{po,ind} \\ E_{2,1}^{on,po,ind}/D_{2,1}^{po,ind} & E_{2,2}^{on,po,ind}/D_{2,2}^{po,ind} & \cdots & E_{2,j}^{on,po,ind}/D_{2,j}^{po,ind} & \cdots & E_{2,J}^{on,po,ind}/D_{2,J}^{po,ind} \\ \vdots & \vdots & & \vdots & & \vdots \\ & \vdots & & E_{n,j}^{on,po,ind}/D_{n,j}^{po,ind} & & \vdots \\ \vdots & \vdots & & \vdots & & \vdots \\ E_{N,1}^{on,po,ind}/D_{N,1}^{po,ind} & E_{N,2}^{on,po,ind}/D_{N,2}^{po,ind} & \cdots & E_{N,j}^{on,po,ind}/D_{N,j}^{po,ind} & \cdots & E_{N,J}^{on,po,ind}/D_{N,J}^{po,ind} \end{bmatrix}$$

Eq. (5-9)

Eq. (5-9) is only applied when the jth pre-retrofit demand $D_{n,j}^{po,ind}$ is not equal to 0.

However, when $D_{n,j}^{po,ind}$ equals 0, $C_{n,j}^{po,ind}$ is regarded as 0, as shown in Eq. (5-10).

$$\begin{cases} if \quad D_{n,j}^{po,ind} \neq 0, \quad C_{n,j}^{po,ind} = E_{n,j}^{on,po,ind} / D_{n,j}^{po,ind} \\ \quad if \quad D_{n,j}^{po,ind} = 0, \quad C_{n,j}^{po,ind} = 0 \end{cases}$$

Eq. (5-10)

5.2.4 Post-retrofit energy inputs

To calculate the post-retrofit final energy input for COMB i , Eq. (5-1) to Eq. (5-10) are integrated with elements described as one equation set in Eq. (5-11), illustrated with thermal and electrical energy flow in the entire building energy systems. The equation set contains the energy input and demand output and their coupling factors. The initial inputs of this model include twelve parameters $D_{i,j}^{pr}$, $D_{n,j}^{po}$, $D_{n,j}^{pr}$, $E_{n,j}^{on,po,ind}$, $D_{n,j}^{po,ind}$, $R_{n,k}$, $E^{pr,the}$, $E^{pr,ele}$ $M_{i,n}$, I , J and K with

detailed described before. To apply the proposed EF-EC, the pre-retrofit building energy baseline results are obtained from building simulation software such as EnergyPlus, IES VE, ICE IDA, TRNSYS, etc. According to the simulation results, $D_{i,j}^{pr}$, $D_{n,j}^{po}$, $D_{n,j}^{pr}$, $E_{n,j}^{on,po,ind}$, $D_{n,j}^{po,ind}$, $R_{n,k}$, $E^{pr,the}$ and $E^{pr,ele}$ are calculated and served as the foundation of the pre-retrofit building energy condition. Based on the occupancy's demand requirements in the baseline, the individual demand is categorised into different sections with total numbers represented by J . Generally, the occupancy's demands comprise space heating, space cooling, DHW, lighting and other household-related electricity. By analysing the energy demands in the baseline, alternative retrofit measures are proposed and categorised into passive, active and renewable measures (Qu et al., 2020, Chen et al., 2020), with total numbers represented by I . The comprehensive combinations $M_{i,n}$ of retrofit measures are generated automatically by MATLAB with a '0,1' pattern. Meanwhile, renewable energy sources are classified into several sections with total numbers represented by K solar thermal energy, solar electricity, wind electricity, etc.

$$
\begin{cases}
E_i^{f,po} = \sum_{j=1}^{J} E_{i,j}^{on,po} - \sum_{k=1}^{K} E_{i,k}^{off,po} \\
E_{i,k}^{off,po} = M_{i,n} R_{n,k} \\
E_{i,j}^{on,po} = D_{i,j}^{po} C_{i,j}^{po,\text{int}} \\
\begin{cases}
if \quad D_{i,j}^{pr} \neq 0, \quad D_{i,j}^{po} = D_{i,j}^{pr} D_{i,j}^{e,po} \\
if \quad D_{i,j}^{pr} = 0, \quad D_{i,j}^{po} = \sum_{n=1}^{N} D_{n,j}^{po}
\end{cases} \\
D_{i,j}^{e,po} = 1 - \sum_{n=1}^{N} M_{i,n} D_{n,j}^{r} \\
D_{1,j}^{pr} = D_{2,j}^{pr} = \cdots = D_{i,j}^{pr} = d_j^{pr} \text{ (constant)} \\
D_{n,j}^{r} = (D_{n,j}^{po} - D_{n,j}^{pr}) / D_{n,j}^{pr} \\
D_{1,j}^{pr} = D_{2,j}^{pr} = \cdots = D_{n,j}^{pr} = d_j^{pr} \text{ (constant)} \\
C_{i,j}^{po,\text{int}} = \min\left(\left(M_{i,n} C_{n,j}^{po,ind} \right) \Big|_{n=1}^{N} \right) \\
\begin{cases}
if \quad D_{n,j}^{po,ind} \neq 0, \quad C_{n,j}^{po,ind} = E_{n,j}^{on,po,ind} / D_{n,j}^{po,ind} \\
if \quad D_{n,j}^{po,ind} = 0, \quad C_{n,j}^{po,ind} = 0
\end{cases}
\end{cases}
\qquad \text{Eq. (5-11)}
$$

By solving the integrated equation set Eq. (5-11), the final post-retrofit energy input $E_i^{f,po}$ is derived in Eq. (5-12). The on- and off-grid post-retrofit energy input ($E_i^{on,po}$ and $E_i^{off,po}$) are derived in Eq. (5-13) and Eq. (5-14). The pre-retrofit final energy input $E^{f,pr}$ is calculated by the sum of pre-retrofit thermal $E^{pr,the}$ and electrical energy input $E^{pr,ele}$, as shown in Eq. (5-15). Thus, as shown in Eq. (5-16), the energy reduction rate $\eta_i^{f,e}$ is calculated by dividing the differences between post and pre-retrofit energy input $(E^{f,pr} - E_i^{f,po})$ and the pre-retrofit energy input $E^{f,pr}$.

$$
E_i^{f,po} = \sum_{j=1}^{J} \left(D_{i,j}^{pr} \left(1 - \sum_{n=1}^{N} M_{i,n} \left(D_{n,j}^{po} - D_{n,j}^{pr} \right) / D_{n,j}^{pr} \right) \right) \times \min\left(\left(M_{i,n} (E_{n,j}^{on,po,ind} / D_{n,j}^{po,ind}) \right) \Big|_{n=1}^{N} \right) - \sum_{k=1}^{K} M_{i,n} R_{n,k}
$$

$$
\text{Where,} \quad \begin{matrix} if \quad D_{n,j}^{po,ind} = 0, & E_{n,j}^{on,po,ind} / D_{n,j}^{po,ind} = 0 \\ if \quad D_{i,j}^{pr} = 0, & D_{i,j}^{pr} \left(1 - \sum_{n=1}^{N} M_{i,n} \left(D_{n,j}^{po} - D_{n,j}^{pr} \right) / D_{n,j}^{pr} \right) = \sum_{n=1}^{N} D_{n,j}^{po} \end{matrix}
$$

Eq. (5-12)

$$E_i^{on,po} = \sum_{j=1}^{J}\left(D_{i,j}^{pr}\left(1-\sum_{n=1}^{N} M_{i,n}\left(D_{n,j}^{po}-D_{n,j}^{pr}\right)/D_{n,j}^{pr}\right)\right)\times \min\left(\left(M_{i,n}(E_{n,j}^{on,po,ind}/D_{n,j}^{po,ind})\right)\Big|_{n=1}^{N}\right)$$

Eq. (5-13)

$$E_i^{off,po} = \sum_{k=1}^{K} M_{i,n} R_{n,k}$$ Eq. (5-14)

$$E^{f,pr} = E^{pr,the} + E^{pr,ele}$$ Eq. (5-15)

$$\eta_i^{f,e} = (E^{f,pr} - E_i^{f,po})/E^{f,pr} = \frac{(E^{pr,the}+E^{pr,ele}) - \left(\sum_{j=1}^{J}\left(D_{i,j}^{pr}\left(1-\sum_{n=1}^{N} M_{i,n}\left(D_{n,j}^{po}-D_{n,j}^{pr}\right)/D_{n,j}^{pr}\right)\right)\times \min\left(\left(M_{i,n}(E_{n,j}^{on,po,ind}/D_{n,j}^{po,ind})\right)\Big|_{n=1}^{N}\right) - \sum_{k=1}^{K} M_{i,n}R_{n,k}\right)}{(E^{pr,the}+E^{pr,ele})}$$

Eq. (5-16)

5.3 Case study

The selected case study building is a single-family house of social housing typology (owned by a local Italian municipality), with a total floor area of 158 m², as shown in Figure 5-4. It is located in the inland town of Martellago Municipality (Community of Venice, Italy), under the Mediterranean climate. As agreed with the local municipality, the RezBuild project (REZBUILD, October 2017) will conduct retrofit interventions on only the left part of the building, as shown in Figure 5-5. The details of the building site, surroundings and climate conditions are shown in Appendix 5-1.



(a) South view (b) North view

Figure 5-4 Southern and Northern facade views for the case study building

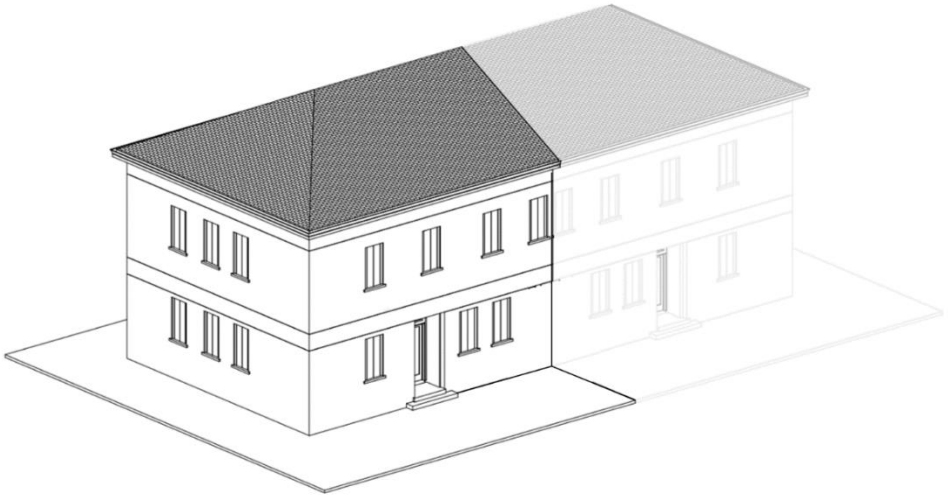


Figure 5-5 Study section and the part for retrofit intervention (the left half of the building)

The single-family house was constructed in the 1960s, with deficient insulation levels. The building fabrics and construction details could be referred to Italian residential building taxonomy (Carnieletto et al., 2021). The specific building fabric layers are listed below, with thermal conductivities and the overall heat transfer coefficients (U-values) of the building elements listed in Appendix 5-2.

- Envelope: load-bearing masonry in solid non-insulated brick plastered on both sides with an average perimeter thickness of 30 cm.

- Interior walls: the internal partitions are made with horizontally perforated brick blocks of 15 cm.
- Windows: The windows have wooden frames with both single glass and double glazing, so the performance is very different between the two systems.
- Doors: the interior doors are predominantly of wood while the entrance door has glazed fields.
- Intermediate floor: lightened floor with joints and hollow brick not insulated.
- Attic floor: lightened floor with joists and hollow brick not insulated.
- Roof: lightened roof with joists and planks, waterproofed and covered with tiles.

The temperature distributions are displayed in the thermal imaging photos taken during the site inspections with the aim to identify the localised problem of dampness, airtightness and thermal bridging, with details included in Appendix 5-2. Results indicate dampness on the ground floor due to the absence of a ventilated crawl space. The thermal bridges occur in the junctions between the horizontal and vertical structures and in the main nodes of the construction details. The sign of mould accumulations could be recognised mainly inside the bathrooms and other rooms, potentially due to condensation and poor ventilation.

The heating system is composed of a 24.8 kW (ground floor) and 25.1 kW (first floor) condensing boiler placed in the utility room that relies upon natural gas.

The primary cooling device on the ground floor is a portable air conditioner connected with an air-to-air heat pump system, with a maximum cooling capacity of 2.4kW and an Energy Efficient Rate (EER) of 2.5. On the first floor, the cooling device is a fixed air conditioner in the corridor, a split air-to-air heat pump system with a maximum cooling capacity of 3.5kW and an EER of 2.5.

The baseline building model (established in the IES VE simulation engine, as shown in Figure 5-6) comprises the following indoor spaces: corridor, kitchen, dining room, living room, toilet, bathroom and bedroom, as shown in Figure 5-7.

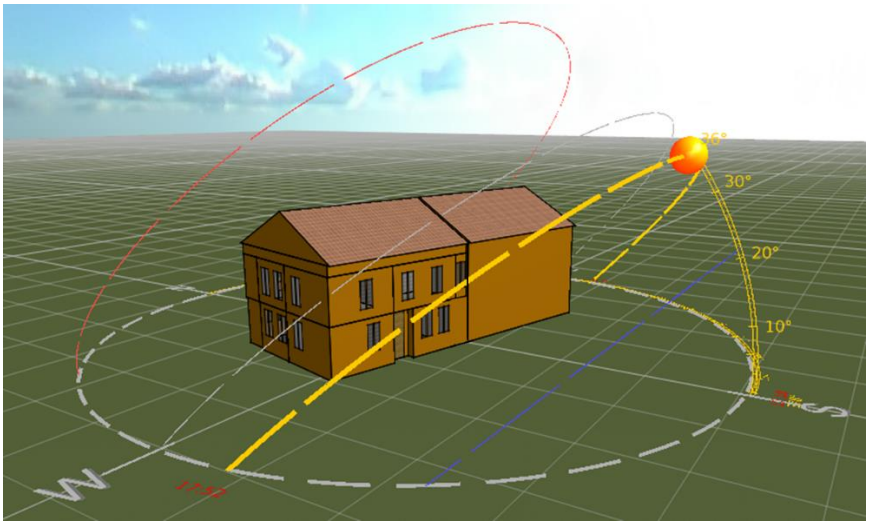
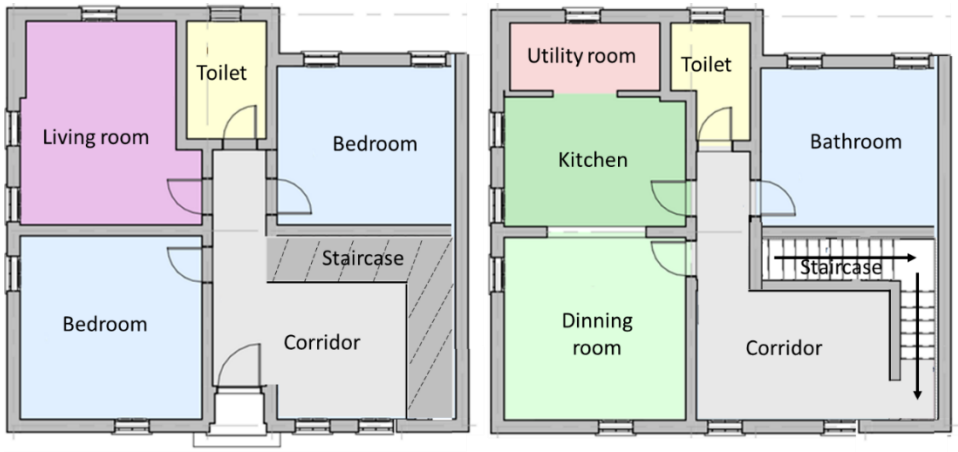


Figure 5-6 Baseline model in IES VE



(a) Ground floor (b) First floor

Figure 5-7 Floor plans for the case study building

The detailed input parameters are summarised in Table 5-1, including the labour cost, installation cost, energy bills, carbon emissions, feed-in tariffs, market interest rate, and inflation rate.

Table 5-1 Main parameters for the cost-optimal analysis of the proposed research

Estimated hourly labour costs, 2019 (Eurostat, 2019)	€28.8/hour	
Installation cost (other construction materials) (Atanasiu, 2013)	€34/m^2 floor area	
Energy price (Atanasiu, 2013)	Electricity €/kWh (incl VAT)	0.24
	Increasing rate	1.71%
	Natural gas €/kWh (incl VAT)	0.08
	Increasing rate	1.55%
VAT rate (MAROSA)	22%	
Carbon emission factors (Mayors)	Electricity (kg/kWh)	0.483
	Natural gas (kg/kWh)	0.202
Feed-In Tariffs (FITs) (Scerrato)	0.171 €/kWh	

Market interest rate (YCHARTS, May 2021)	1.79%
Inflation rate (Economics, 2021)	3.80%

5.3.1 Baseline building energy simulation (Pre-retrofit energy inputs)

The baseline building model simulation reveals that the case study building consumes final energy of 62.97MWh (equal to the specific energy consumption of 398.56 kWh/m^2), consisting of 156.11 kWh/m^2 of electricity and 242.45 kWh/m^2 of natural gas. The specific monthly energy and carbon consumption are summarised in Table 5-2. The maximum energy consumption occurred between November to March, with monthly electricity consumption varying between 46.28 and 66.15 kWh/m^2, which converted to equivalent carbon emissions between 12.91 and 17.01 kgCO_2/m^2. Besides, due to the cooling requirements, electricity demands increase in July and August to 16.91 and 14.08 kWh/m^2, equivalent to carbon emissions of 8.24 and 6.87 kgCO_2/m^2. Moreover, during the whole year, energy consumption in May, June and September is the three lowest compared with the other months.

Table 5-2 Baseline monthly building energy consumptions based on the simulation results

	Total energy (kWh/m^2)	Total electricity (kWh/m^2)	Total natural gas (kWh/m^2)	Total carbon emission ($kgCO_2/m^2$)

Jan	66.15	12.98	53.17	17.01
Feb	52.41	11.76	40.65	13.89
Mar	47.00	13.06	33.94	13.16
Apr	28.23	10.41	17.82	8.63
May	13.01	11.16	1.85	5.76
Jun	13.01	12.43	0.58	6.12
Jul	17.26	16.91	0.35	8.24
Aug	14.44	14.08	0.35	6.87
Sep	12.50	11.58	0.92	5.78
Oct	23.88	11.11	12.77	7.95
Nov	46.28	12.67	33.61	12.91
Dec	59.51	13.07	46.44	15.69
Annual Total	398.56	156.11	242.45	124.37

Furthermore, the case study building energy input is converted into seven demand outputs with space heating of 238.29 kWh/m^2 (60%), DHW of 4.88 kWh/m^2 (1%), space cooling of 12.54 kWh/m^2 (3%). In addition, about 4.39 kWh/m^2 (1%) of energy input is consumed by the auxiliary fan, 25.36 kWh/m^2 (6%) for the auxiliary pump, 79.49 kWh/m^2 (20%) for lighting and 33.61 kWh/m^2 (9%) consumed by household equipment, as shown in Figure 5-8. This information will serve as crucial input data for the post-retrofit demand

calculation process, as outlined in section 5.2.2 for the proposed EF-EC model

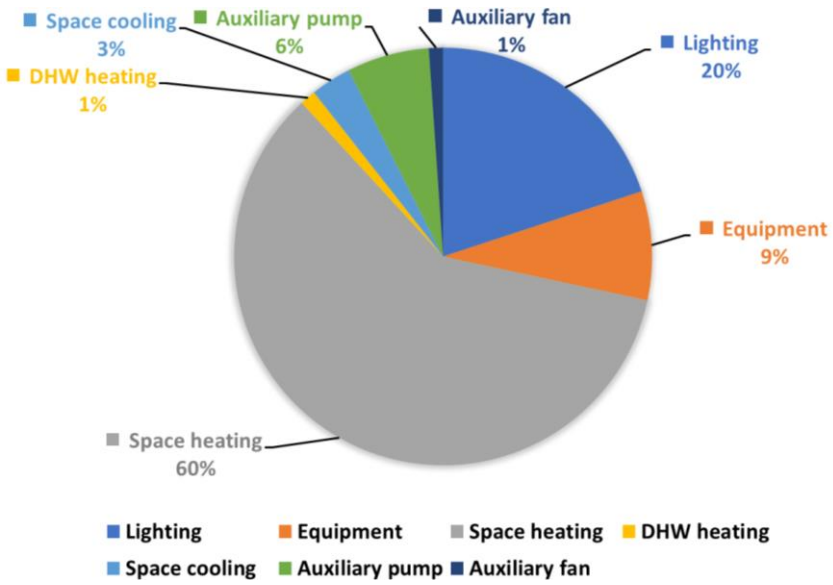


Figure 5-8 Demand output loads by types

5.3.2 Comprehensive retrofit combinations

According to the baseline model energy output results, the RezBuild project (REZBUILD, October 2017) proposed 17 high-efficient energy retrofit measures to achieve deep energy retrofit with more than 60% of primary energy reduction compared with the baseline, which has been classified into 11 categories as passive, active and renewable measures, as shown in the schematic 3D diagram in Figure 5-9 and in Table 5-3, where the definitions of three measures can be found in (Qu et al., 2020). The energy reduction results of individual retrofit measures are simulated and obtained from the IES VE simulation engine model. The 17 alternative retrofit measures are comprehensively combined into a total of 20735 combination numbers. The detailed energy performances of individual technology are summarised in Appendix 5-3.

Table 5-3 Summary of the selected energy retrofit measures

		Retrofit measures	Retrofit number	Unit cost (€/m2)	Life span (years)
Passive measures	Glazing renovation	Vacuum glazing window insulation (VG)	ERM01-1	563 €/m^2 (Glass)	20 (Koebel et al., 2010)
		Triple glazing window insulation (TG)	ERM01-2	336 €/m^2 (Best)	25 (Menzies and Wherrett, 2005)
	Wall external insulation	Si-VIP external wall insulation (EWI-VIP)	ERM02-1	92 €/m^2 (Kingspan)	25 (Kim et al., 2017)
		PIR external wall insulation (EWI-PIR)	ERM02-2	103 €/m^2 (EcoTherm)	30 (Choi et al., 2021)
	Wall internal insulation	Si-VIP party wall insulation (PWI-VIP)	ERM03-1	46 €/m^2 (Kingspan)	30 (Kim et al., 2017)
	Attic insulation	Starch aerogel attic floor	ERM04-1	131 €/m^2 (Alliance	30 (Kumar

		insulation (AFI-SA)		)	and Saxena, 2020)
	Ground floor insulation	Si-VIP ground floor insulation (GFI-VIP)	ERM05-1	92 €/m^2 (Kingspan)	30 (Kim et al., 2017)
	Airtightness improvement	Gypsum airtightness insulation (GAI)	ERM06-1	122 €/m^2 (technologies)	15 (technologies)
		Sealings of windows and joint places (SW-JP)	ERM06-2	15 €/m^2 (SOUDAL)	5 (SOUDAL)
Active measures	MVHR technology	Mechanical ventilation with heat recovery (MVHR)	ERM07-1	60 €/m^2 floor area (Solution)	15 (Asdrubali et al., 2015)
	Efficient lighting device	LED lighting + Daylighting pipes (ELD)	ERM08-1	247 €/unit (PHILIPS)	10 (Nardelli et al., 2017)
Renewable measures	Building-integrated PV	Multi-crystalline silicon PV	ERM09-1	353 €/m^2 (Power)	20 (Hong et al.,

	panels	glazing panels (PV-Si)			2016)
		Thin-film PV glazing with high insulation (PV-VG)	ERM09-2	1072 €/m^2 (Solar)	15 (Kato et al., 2001)
	HVAC technology	Solar assisted heat pump (SAHP)	ERM10-1	612 €/kW (Energy)	20 (Thygesen and Karlsson, 2013)
		Air-water heat pump (AWHP)	ERM10-2	640 €/kW (DAIKIN)	15 (DAIKIN)
		Desiccant based air cooling and dehumidification system (ACD)	ERM10-3	97 €/kW (SARTORIUS)	15 (SARTORIUS)
	Solar thermal	Solar collector (SC)	ERM11-1	1122 €/unit (Energy)	10 (Fan et al., 2009)

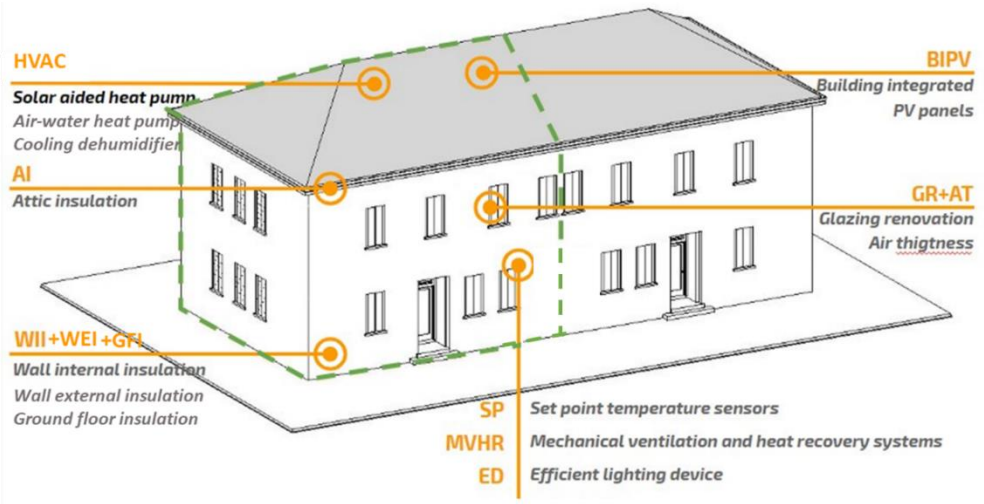


Figure 5-9 Schematic illustration for the selected individual retrofit measures

5.4 Model validation and uncertainty analysis

Firstly, uncertainty analysis is obtained by comparing the EF-EC model energy calculation and the IES VE simulation results, as discussed in section 5.4.2.1. Uncertainty variation rate (UVR) is defined as the differences between the post-retrofit final energy inputs with the two calculation methods, divided by the energy inputs of IES VE, as shown in Eq. (5-17), with the absolute value of the average UVR of x combination numbers ($\overline{UVR}$) shown in Eq. (5-18). Secondly, the selections of different retrofit measures as input parameters (including passive, active and renewable retrofit measures) are essential factors for the model sensitivity analysis. The impact of mild, moderate and deep energy combination stages on the final energy inputs are discussed in section 5.4.2.2.

$$UVR(x) = \frac{Energy\ inputs\ from\ "EF-EC"\ \ model - Energy\ inputs\ from\ "IES\ VE"}{Energy\ inputs\ from\ "IES\ VE"} \quad \text{Eq. (5-17)}$$

$$\overline{UVR} = \frac{1}{X}\sum_{x=1}^{X}|UVR(x)| \quad \text{Eq. (5-18)}$$

Guidelines regarding the model validation and accuracy are provided by the International Performance Measurement and Verification Protocol (IPMVP) (ORGANIZATION) with recommendations that the predicted energy savings should not exceed 10% of actual energy savings.

The case study building is applied to validate the proposed EF-EC energy model to verify robustness and reliability for performing comprehensive energy-economic assessments. All input parameters of the pre- and post-retrofit model are displayed in Appendix 5-4. By applying the proposed EF-EC model for 17 selected retrofit measures, a domain of 20,735 possible combinations are conducted, with the calculation time of 4.14 hours (0.72s per combination), which is significantly reduced in comparison with the total time required if performing the simulations over 20,735 times in IES VE simulation engine, with the calculation time of 1728 hours (300s per combination). Albeit the Black-box model computation is time-saving compared with the White-box model varying between 7.12s and 66s, this research using the EF-EC model could save up to 90% of calculation time, as shown in Table 5-4.

This enables the evolution of a novel and effective energy-economic assessment with great accuracy that is also highly replicable not only for individual building retrofit cases but also for urban scale building renovations and therefore well aligns with the goal of EPBD Recast (i.e., to reduce the computational burden for conventional energy simulation) (Parliament, January 2012).

Table 5-4 Computing time on a single combination

Ref.	Method	computing time on a single

		combination (s)
This research	IES VE	300
(Bui et al., 2020)	ANN	66
(Seyedzadeh et al., 2020)	ANN-GBRNT	31.22
(Shen et al., 2019)	ANN-NSGA-II	55.2
(Sharif and Hammad, 2019)	ANN-SBMO	7.12
This research	EF-EC	0.72

5.4.1 Model validation

In order to identify the natural gas and electricity consumption in baseline and the EF-EC model, the electric and natural gas meters are connected to the main supply switch. All the metering devices are connected with the gateway, installed in the general panel that sends data directly to the cloud. The energy monitoring of the pre-retrofit baseline was conducted from 1st of Jan 2019 to 31st of Dec 2019, and the post-retrofit monitoring period was from 1st of Jan 2021 to 31st of Dec 2021. The detailed retrofit measures in the real building are summarised in Appendix 5-5. Table 5-5 indicates the model validation results among real building energy consumption, IES VE simulation and EF-EC model before and

after renovation. Comparing the real building energy consumption and IES VE simulation of baseline, the discrepancy of -0.66% demonstrates that the baseline is accurate at an acceptable level with a maximum of 10% (Mutani and Todeschi, 2020) for buildings constructed before the 1970s. Besides, the discrepancy of 1.03% between the EF-EC modelling and real building energy consumption also indicates the EF-EC modelling results are in the range of acceptable level.

Table 5-5 Model validation among real building energy consumption, IES VE simulation and EF-EC model

	Real building energy consumption (MWh)	IES-VE (MWh)	Discrepancy between IES-VE and real building energy consumption	EF-EC (MWh)	Discrepancy between EF-EC and real building energy consumption
Baseline	63.39	62.97	-0.66%	62.97	-0.66%
Post-retrofit scenario	8.78	8.41	-4.21%	8.87	1.03%

5.4.2 Uncertainty and sensitivity analysis

The proposed EF-EC energy model is validated by the case study building with 30 representative combinations selected from a domain of 20735 combinations. The selected thirty combinations are classified into mild, moderate and deep combination stages according to the following criteria:

1) Mild combination stages: in which individual category of either passive, active, or renewable retrofit measures;
2) Moderate combination stages: from combinations with passive retrofit measures and only one measure selected from the active and renewable retrofit categories;
3) Deep combination stages: from combinations of more than one retrofit measure in each of three retrofit categories.

The uncertainty of the proposed EF-EC model is analysed through the comparisons among two calculation methods, including the EF-EC model calculation and IES VE simulation, with results summarized in section 5.4.2.1.

The sensitivity of the proposed EF-EC model is analysed via the different calculated post-retrofit final energy inputs affected by independent combination stages as the input variables. Furthermore, the overall uncertainty of the mathematical model is statistically summarised, with results stated in section 5.4.2.2.

5.4.2.1 Uncertainty analysis

This section discusses the uncertainty variation rate (UVR) and the absolute value of the average ($\overline{UVR}$) to investigate to what extent the retrofit measures and combinations have substantial impacts on the final energy inputs by comparing the EF-EC model and IES VE simulation. Results indicate that the absolute value of the average ($\overline{UVR}$) is 2.58% with the UVR of a single combination ranging from -4.97% to 6.03%, as shown in Figure 5-10. In terms of the three combination stages, $\overline{UVR}$s are varied with 1.90%, 1.33% and 4.17% in mild, moderate and deep combination stages, respectively. It is concluded that

substantial impact occurs when combination integrated with efficient lighting devices, heat pumps and solar collectors.

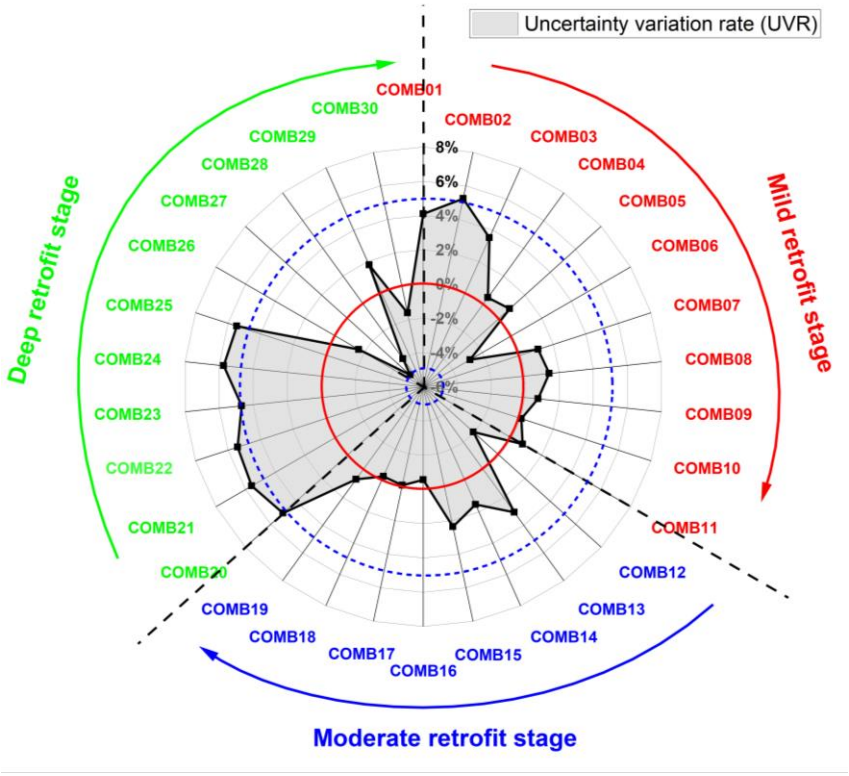


Figure 5-10 Uncertainty variation rates (UVRs) for the selected 30 retrofit combinations

The mild retrofit stage includes the combinations from COMB01 to COMB11, with COMB01-COMB05 representing only passive retrofit measures, where the relatively high $UVRs$ appear in COMB01-COMB03. Comparing COMB04-COMB05 with COMB01-COMB03, the $UVRs$ increase from 0.43%-0.80% to 3.52%-5.23%, due to the introduction of 'Sealings of windows and joint places ' (SW-JP) measure. This may be ascribed to the mismatch between fixed convection coefficients used in IES VE's convection heat transfer model and actual air thermodynamic behaviour in air-tightened buildings. COMB06 is the combination of only active retrofit measures, with the UVR of -2.84%.

COMB07-COMB11 demonstrate the combinations of only renewable energy retrofit measures with relatively low UVR values, which is varied from 0.03% to 1.41%.

In the moderate retrofit stage, the $UVRs$ vary from -2.06% to 3.06% for eight selected retrofit combinations (COMB12-COMB19), representing the passive retrofit measures with an individual measure in either the active or renewable energy retrofit category. COMB13 has the maximum UVR value due to introducing the 'Efficient lighting device ' (ELD) measure. It may result from a lack of an accurate solar and heat balance model through the daylighting pipe module in IES VE. It also indicates that the UVR maintains to be relatively low when integrating single renewable energy measures with passive retrofit combinations.

COMB20-COMB30 illustrate the deep energy retrofit stage with integrations of any passive retrofit and renewable energy retrofit measures, which results in higher $UVRs$ ranging from -4.97% to 6.03%. In comparison with COMB18, COMB21 and COMB22, it could be noted that the integrations of ' Mechanical ventilation with heat recovery ' (MVHR), ' Efficient lighting device ' (ELD) and ' Solar assisted heat pump ' (SAHP) with passive retrofit combinations do not lead to large UVR. The introduction of external wall insulation measure does not obviously affect the UVR values when analysing COMB20-COMB22. Furthermore, heat pump technology substantially impacts the UVR value in all combinations due to the COP mismatch between the EF-EC model (annual average COP) and IES VE simulation (real-time COP). Comparing COMB20 with COMB28, the ' Solar collector ' (SC) measure considerably affects the

UVR value since IES VE simulation may lack an accurate control strategy to negotiate the integration of the solar collector and heat pump.

5.4.2.2 Results comparisons and calibration via sensitivity analysis

This section analyses the impacts of various retrofit measures on the final energy input by performing sensitivity analysis where the impacts are also compared to two different calculation methods via the proposed EF-EC model and IES VE simulation. Results indicate that to ensure the reliability of the proposed model, it is recommended to select a group of combinations within the energy discrepancy intervals rather than the minimum single optimised combination calculated by the EF-EC model, serving as the calibration approach to the calculation results, depending on different retrofit stages below.

Final energy input results of two different calculation methods for mild, moderate and deep combination stages have been denoted in Appendix 5-6, where the minimum final energy inputs of mild, moderate and deep energy inputs are different from the two methods of IES VE simulation and the EF-EC model. To have a deep understanding of the discrepancies, final energy inputs from the EF-EC model are analysed by comparing that of the IES VE simulation, where discrepancies range from -10.1 kWh/m^2 to 9.1 kWh/m^2, as shown in Figure 5-11. Due to the discrepancies, the combinations with minimum final energy inputs are varied when the combinations have similar energy inputs ranges. However, the final energy inputs in different calculation methods have minor differences of a maximum of 9.1 kWh/m^2, 4.1 kWh/m^2 and 2.9 kWh/m^2 in mild, moderate, and deep energy retrofit stages. Moreover, the absolute

discrepancy ranges between – 10.1 kWh/m^2 and 9.1 kWh/m^2 in mild and moderate combination stages, which shrinks to – 3.6 kWh/m^2 and 4.1 kWh/m^2 in deep combination stage with final energy inputs varying between 45.5 kWh/m^2 and 94.5 kWh/m^2.

The discrepancy of the mild combination stage (- 2.8% to 5.2%) is slightly higher than that of the moderate stage (- 2.1% to 3.1%) since the final energy consumption of the mild combination stage is relatively high. Although the discrepancy of the deep combination stage ranges from -5.0% to 6.0%, the lower absolute discrepancy occurs with only – 3.6 kWh/m^2 and 4.1 kWh/m^2.

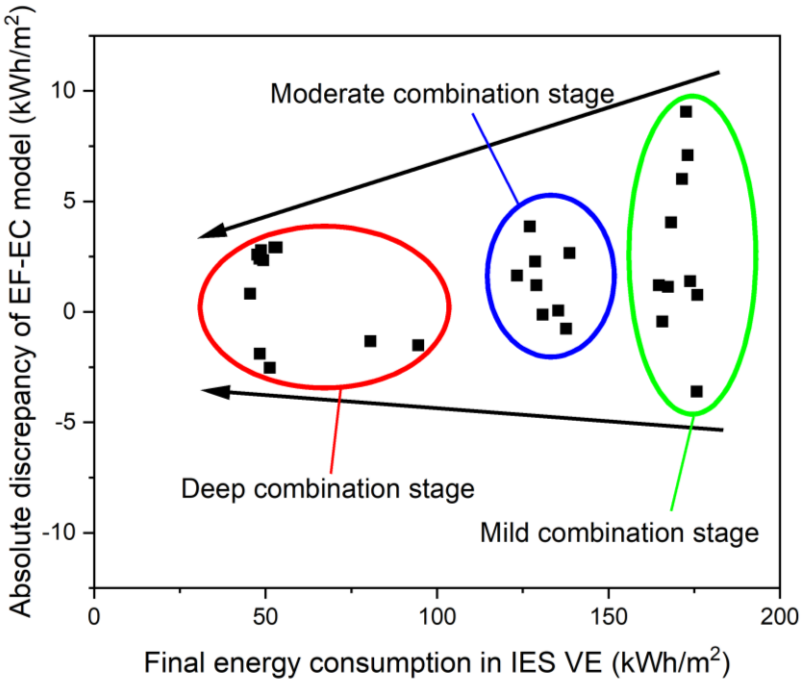


Figure 5-11 Final energy inputs discrepancies compared with the IES VE simulation

Among 30 selected retrofit combinations, 19 deep energy retrofit combinations are found featuring a final energy reduction rate between 65% - 89%. Table 5-6 presents the previous literatures on average calculation and absolute

discrepancies using the Black-box model in deep energy retrofit prediction of single-family houses. Results indicate that those Black-box models have large uncertainty with a maximum calculation (16% - 24%) and an absolute discrepancy (16.0 - 23.1 kWh/m^2) to predict the deep energy retrofit performance in single-family houses. However, this proposed EF-EC model reduces the calculation discrepancy to a maximum of 6% with an absolute discrepancy of only 3.9 kWh/m^2 within reasonable ranges.

Table 5-6 Average calculation and absolute discrepancies using the Black-box model in deep energy retrofit prediction of single-family houses

Ref.	Prediction method	Comparison method	Energy reduction rate	Maximum calculation discrepancy	Maximum absolute discrepancy (kWh/m^2)
(Wang et al., 2019a)	ANN	measurement	80%	21%	20.9
(Khayatian et al., 2016)	ANN	CENED software	60%	16%	16.0
(Finck et al., 2019)	ANN	measurement	76%	18%	18.7
(Ascione et al., 2017a)	ANN	EnergyPlus	71%	22%	22.6
(Ascione et al., 2017b)	ANN	EnergyPlus	64%	24%	23.1

This research	EF-EC	IES VE	76% - 89%	6%	2.9

5.5 Conclusion

This chapter proposes a novel Energy-Flow based Ensemble Calibration (EF-EC) model to tackle the issue of **'Rapid and accurate energy-economic performance prediction of deep energy retrofit in single-family houses'**. In the EF-EC model, only a few simulations of baseline heat and electrical demands and heat and electrical coefficients of individual retrofit measures conducted by IES VE building dynamic simulation rather than numerous simulations in the conventional White-box model. Thus, time-consuming and numerous dynamic simulations are replaced by rapid and transient numerical calculations in the EF-EC model. This research using the EF-EC model could save up to 90% of calculation time, with 0.72s computing time on a single combination.

The EF-EC model is applied in a case study building representing a single-family house constructed in the 1960s in northern Italy with poor insulation and high energy consumption under the typical Mediterranean climatical context. Furthermore, 17 retrofit measures are proposed by the RezBuild Project Consortium, and classified into passive, active and renewable categories, with a domain of 20,735 comprehensive energy retrofit combinations generated. The baseline model is developed in IES VE with final energy consumption of 398.56 kWh/m^2. Comparing real energy consumption and EF-EC calculation results in baseline and post-retrofit scenario, the discrepancies are -0.66% and 1.03%, presenting that the EF-EC model is accurate at an acceptable level.

Among them, 30 representative combinations are selected and categorised into mild, moderate and deep combination stages to investigate the uncertainty and sensitivity of the proposed model. Compared with the IES VE simulation results, the maximum discrepancy of the EF-EC model is 6% with an absolute discrepancy of 2.9 kWh/m^2, where the energy reduction rate is in the range of 76% - 89%. Therefore, the calculation discrepancy has been improved by 63% - 75%. To ensure the model reliability in deep energy retrofit, it is recommended to select a group of combinations within the maximum discrepancy range rather than the single optimised combination calculated by the EF-EC model.

For similar deep energy retrofit of single-family houses in the Mediterranean area, there are four essential retrofit measures combined to shorten the DPP**,** including external wall insulation, efficient lighting devices, solar-assisted heat pump and solar collector. Moreover, four suggested measures could be combined to improve the AROI with attic wall insulation, party-wall insulation, airtightness insulation and solar-assisted heat pump.

Thus, the proposed EF-EC model provides rapid and accurate post-retrofit energy prediction with comprehensive retrofit combinations for deep energy retrofit in single-family houses. Nonetheless, several limitations of this study could be ameliorated such as: 1) Limited retrofit measures have been discussed; 2) The impact of climate conditions on model sensitivity is not considered; 3) The economic results of this case study only represent similar building retrofit in the Mediterranean climate region; 4) The method of cost-optimal retrofit decision-makings is not emphasized since this research focuses on energy-economic performance prediction of deep energy retrofit in single-family houses. A more detailed Pareto analysis using the NSGA-II (Son and Kim, 2018)

to find out the cost-optimal retrofit could be considered in the future study. Besides, the integration of life-cycle assessment and the EF-EC model would be substantial for the embodied carbon emission of the building upgrade.

The case study investigated in this research could also be served as a guideline for similar building retrofits in the Mediterranean climate region. The decision makers could select the cost-optimal energy retrofit measures based on different priorities (e.g. DPP or AROI) that aligns with investment profitability and future energy consumption profile, thereby ensuring significant environmental benefits toward carbon neutrality in the EU building stocks.

6. An innovative Motivation-Objective-Criteria (MOC) retrofit optimisation approach integrating homeowners' engagement

6.1 Introduction

In general, the decision-making criteria and objects are optimised individually or combined, and homeowners' motivations are ignored or not carefully undefined in most research, which may conflict with householder values and preferences. Based on the barriers underneath the low retrofit rate of residential building markets and motivations for building energy-efficient upgrades, this chapter established an inclusive human-based optimisation approach to support the decision-making process for selecting building retrofit measures, which adapts to different homeowners' retrofit motivations, objectives and criteria. Hence, adopting an inclusive human-based approach to pre-retrofit design and management has substantial energy, economic, environmental, and social benefits for different stakeholders (users, employers, and suppliers), facilitating acceleration and succession technically and commercially.

6.2 Methods

This section establishes a method to solve the conflicts between householder preferences and the selection of maximised retrofitted energy-saving measures in which the decision-making strategies are multi-objective and are affected by both human weights (subjective factors and requirements) and criteria (objective conditions, such as regulations and legislation, limited funds). The weighted sum method (WSM) is adopted to evaluate the comprehensive energy-retrofit combinations for analysing and discussing the impacts of different motivations weights on selecting retrofit technologies and combinations. Apart from homeowners' motivations, the impacts of building locations on the decision-

making of retrofit measures are also considered.

The structure of this section is presented in the flowchart shown in Figure 6-1:

1) Definitions of three motivations including self-living, rental or sale and investment, and their relevant objectives, weights and selection hypotheses (section 6.2.1);
2) Definitions of Weighted Sum Method (WSM) and assessments using a multi-motivation performance factor (MPF) to optimise the energy-retrofit combinations (section 6.2.2);
3) Calculation methods for the lifecycle energy and cost performance, and its post-retrofit assessment factors (section 6.2.3);
4) Reference building analyses in the UK context including baseline descriptions and complex technological combinations (section 6.3);
5) Results and discussions covering: i) Baseline model validation (section 6.4) ii) Analyses of cost-optimal decision-making optimisations without considering homeowners' engagement (section 6.4.1); iii) Analyses of the impact of homeowners' motivations on optimised retrofit combinations and their characteristics considering homeowners' engagement (section 6.4.2); iv) Sensitivity analysis (section 6.4.3).

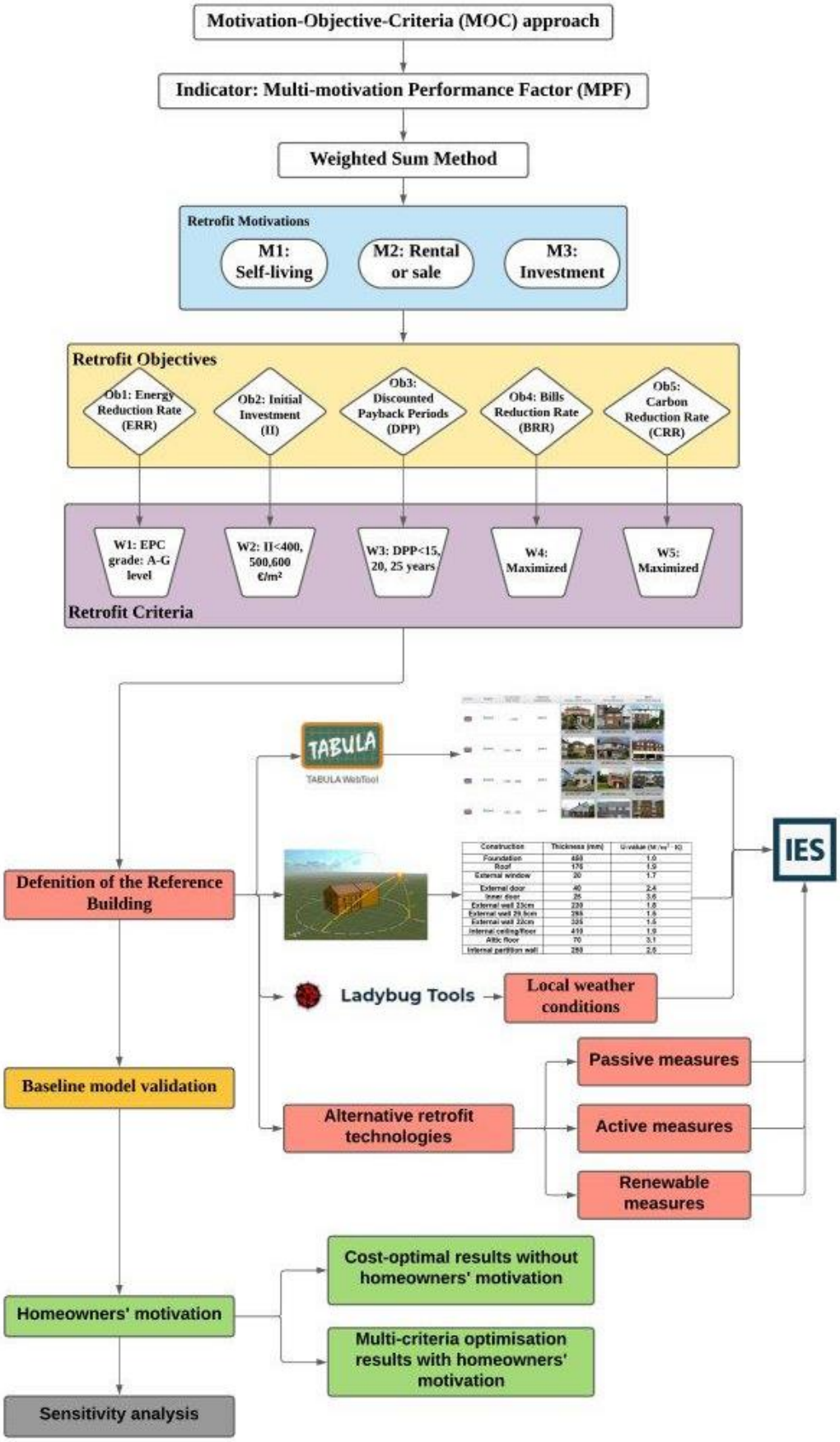


Figure 6-1 Flowchart of the research structure

6.2.1 Multi-objective assessment approach

The proposed MOC approach is established upon a number of possible motivations or purposes for undertaking residential building retrofit, including 1) Self-living; 2) Rental or Sale; 3) Investment.

To make decisions on comprehensive energy-retrofit combinations considering the retrofit motivations from the decision-makers' perspectives, a multi-motivation performance factor (MPF) is proposed to evaluate the overall performance with the comprehensive energy retrofit combinations. The homeowners or investors are considered the critical stakeholders for the decision-making stage of most residential buildings. The actual weights of each motivation objective defined by the proposed Multi-motivation Performance Factor (MPF) can be adjusted according to the homeowners' preferences and financial conditions. The global optimum with maximum MPF is decided according to homeowners' different weights of motivations. Thus, the optimal energy retrofit combinations can be obtained from those combinations that can achieve the maximum value of the MPF.

$$MPF\ (i)= \sum_{i=1}^{n} W_k Ob_k(i)\ \ (i=1, 2, \ldots, n;\ k=1, 2, 3, 4,5) \qquad \text{Eq. (6-1)}$$

Where,

Ob_1 – To achieve expected/required or higher Energy Reduction Rate (ERR);

W_1 - The weighted score for Ob_1;

Ob_2 – To reduce the Initial Investment (II) to an affordable level;

W_2 - The weighted score for Ob_2;

Ob_3 – To reduce the Discounted Payback Period (DPP) to a profitable performance;

W_3 - The weighted score for Ob_3;

Ob_4 – To achieve expected/required or higher Bills Reduction Rate (BRR);

W_4 - The weighted score for Ob_4;

Ob_5 – To achieve expected/required or higher Carbon Reduction Rate (CRR);

W_5 - The weighted score for Ob_5;

According to the key stakeholders' various retrofit motivations, the following five objectives are considered, including Energy Reduction Rate (ERR), Initial Investment (II), Discounted Payback Period (DPP), Bills Reduction Rate (BRR) and Carbon Reduction Rate (CRR). Therefore, the Weighted Sum Method (WSM) is defined to evaluate the overall performance of comprehensive energy retrofit combinations, with the individual function defined for each objective shown in Eqs. (6-2 to 6-8):

$$Ob_1\ (i)= ERR\ (i),\ \eta_{ERR,\ lo} \leq ERR\ (i) \leq \eta_{ERR,\ up} \quad \text{Eq. (6-2)}$$

Ob_2

$$(i)= min\left(II(i)\right)/II(i)\ ,\ II\ (i) \leq C_{set,up} \quad \text{Eq. (6-3)}$$

$$Ob_3\ (i)= min\left(DPP(i)\right)/DPP(i)\ ,\ DPP\ (i) \leq T_{set,up} \quad \text{Eq. (6-4)}$$

$$Ob_4(i)=BRR\ ,\ BRR\ (i\ ) \geq \varphi_{set,lo} \quad \text{Eq. (6-5)}$$

$$Ob_5\ (i)= CRR\ (i),\ \eta_{CRR,\ lo} \leq CRR\ (i) \leq \eta_{CRR,\ up} \quad \text{Eq. (6-6)}$$

subject to:

$W_k \in (0,1)$, k=1, 2, 3, 4, 5 Eq. (6-7)

$\sum_{k=1}^{5} W_k = 1$, k=1, 2, 3, 4, 5 Eq. (6-8)

The stakeholders looking to sell or rent their properties will value ERR significantly, which is directly related to the EPC level. $\eta_{ERR,\,lo}$ and $\eta_{ERR,\,up}$ are the lower and upper bound of the energy reduction rate; $\eta_{CRR,\,lo}$ and $\eta_{CRR,\,up}$ are the lower and upper bound of the carbon reduction rate; $C_{set,up}$ is the upper bound of the investment cost, subject to the availability of funding or financial incentives; $T_{set,up}$ is the upper bound of the discounted payback periods, due to an acceptable/affordable upper bound of the investment cash return, especially for the stakeholders who view the benefits of energy savings and immediate property market value increase after retrofit; $\varphi_{set,lo}$ is the lower bound of the annual energy bills reduction rate for homeowners; the subscript "i" indicates the various retrofit combination numbers while the subscript "min" indicates the minimum outputs of the objective functions.

Energy Performance Certificates (EPC) provide information on the building energy efficiency and how it could be improved. Buildings are rated on a scale from A - G, with A being the most efficient. There are seven of these bands on an EPC which are run on a sliding scale from 'A' (the most energy-efficient) to 'G' (the least efficient). They are also colour coded for ease of reference from dark green (an 'A' rating) to red (a 'G' rating). Most homes in the UK fall into a 'D' band.

The EPC assessment records specific information such as the size and layout of the building, how it has been constructed, and how it is insulated, heated,

ventilated, and lighted (Watson, 2010). The EPC is produced using a UK Government calculation methodology (Dodoo et al., 2017, Niemelä et al., 2017). In addition, the EPC calculation methodology was also mentioned by Qu et al. (Qu et al., 2020). More detailed technical information on the calculation methodologies can be found in Appendix 6-1.

Obviously, the optimised multi-objective results are influenced by the subjective evaluation of weights scores in different cases. The final decision is selected under the negotiated weights values between the key stakeholders and the government requirements. Sensitivity analysis can be used by adjusting the values of the weights of each item from W_1 to W_5 to investigate the influence of each criterion on the final decision-making optimised results.

6.2.2 Retrofit motivations, objectives and weights

This research is built upon an EU Horizon 2020 funded project SureFit , aiming to achieve fast-track and affordable building retrofits for five selected demo site buildings in Norway, Greece, Portugal, the UK, and Spain. Using the SureFit project as an example, the five demo site project leaders (University of Nottingham-UK, Aalto University-Norway, ISQ-Portugal, FMS-Spain, AMS-Greece) work closely with the occupants to collect pre-retrofit survey results, with the aim to understand the occupants' motivations and preferences for the retrofit process. Moreover, the demo site leaders act as project coordinators who liaise with homeowners to emphasise retrofit motivations and preferences through surveys and questionnaires. In order to capture various homeowners' retrofit preferences and motivations, the "lessons learned" online survey covered a wide range of questions from multi-objective perspectives (1. reducing energy bills; 2. reducing energy consumption to achieve certain EPC level; 3. Reducing

carbon emission; 4. Initial investment; 5. Discounted payback periods) was designed and distributed within Surefit project partners and their clients, who represent a wide range of stakeholders. Meanwhile, to make the weighting factor more reliable to reflect the homeowners' motivations and perspectives, 42 surveys were collected with the weighting factors (in the range of 0–1) to represent various homeowners' preferences as summarised in Appendix 6-2. A higher weighting factor value means that the stakeholders expressed special attention in this respect. In Table 1, Appendix 6-2, the numerical weighting score "1" stands for the most attractive and beneficial objectives while "0" indicates lack of interest. Finally, the average weighting scores of the abovementioned five multi-objective perspectives are calculated in Table 6-1, referring to the survey data in Appendix 6-2. In Table 6-1, the weighting of each objective is described as Mx, with x varied from 1 to 3 representing the three types of motivations for undertaking building renovation.

Table 6-1 Weight assumption of five motivations

Type of Motivations	*Code*	*ERR* (W_1)	*II* (W_2)	*DPP* (W_3)	*BRR* (W_4)	*CRR* (W_5)
Self-living	M1	0	0.3	0.1	0.6	0
Rent or Sale	M2	0.6	0.2	0.2	0	0
Investment	M3	0	0.4	0.6	0	0

Regarding the survey results, although a few homeowners also considered the environmental impact in the pre-retrofit design, the average weighting scores of CRR (W_5) are zero in the three motivations, as shown in Appendix 6-2. This is due to the fact that there are no transparent links between the economic benefits

reflected in CRR. All other four weighting scores impact the household carbon emission reduction directly or indirectly.

For self-living-oriented motivation (M1), homeowners seek to reduce their energy bills compared with pre-retrofit scenarios. Occupants face ever-increasing financial burdens due to the rise of energy prices, especially those whose dwellings are at low energy-efficient levels. In addition, the degradation of existing buildings, poor insulation and inefficient energy systems will cause unnecessary energy consumption, leading to poor indoor comfortable conditions. However, due to financial issues, in most cases, the retrofit investment capacity is limited and affected by the affordability of the homeowners. During the retrofit process, homeowners prefer to seek energy-economic measures with shorter payback periods, reinforcing usability and building efficiency rather than some less cost-effective components. Therefore, in the M1 scenario, the bills reduction rate (BRR) is the homeowners' first-order consideration, with initial investment (II) as the second-order consideration and the last of discounted payback periods (DPP). Thus, in the weighted sum method, the weights of first-order motivation (W_4) are assumed higher than the weights of the second and last order motivations (W_2 and W_3).

In rental or sale-oriented motivation (M2), homeowners tend to achieve a higher building energy efficiency represented by Energy Reduction Rate (ERR). Due to regulations and legislation in most EU countries, the rental and sale of residential properties must satisfy a minimum energy performance certification (EPC), linking with the ERR ranges. In addition, homeowners will consider the initial investment and payback periods to pursue a balance between them

(Institute, May 2020, Arikan et al., 2005). Thus, in the weighted sum method, the weights of first-order motivations (W_1) are assumed higher than the other two motivations (W_2 and W_3) with the same weights.

In investment-oriented motivation (M3), homeowners wish to make profits by adopting renovations, which can be achieved with shorter payback periods, lower initial investment costs and associated risks. However, selecting the initial investment as an individual objective and criteria is a crucial subject to funding availability and affordability of the homeowners. Secondly, the initial investment, annual maintenance, operation, and replacement costs defined in lifecycle cost, allow net present values to be conducted, which could be valuable for comprehensive economic calculation of discounted payback periods. Therefore, global cost and net present value are represented by the lifecycle cost considered in the DPP calculation as the most significant factor, with the second-order initial investment cost (II). Thus, in the weighted sum method, the weights of first-order motivations (W_3) are assumed higher than the second-order weights (W_2).

The Energy Reduction Rate and Bills Reduction Rate are non-linear depending on energy-specific prices. However, it is still essential to keep both indicators due to the following reasons:

1) The potential energy reduction rate (ERR) will be at a fixed value when the retrofit combination is well-defined, however, energy bills reduction rate (BRR - calculated by the sum of electricity and natural gas bills reduction) will be influenced by the changing energy prices under the same BRR, since BRR is derived from the multiplication of energy

reduction (ERR) and its price (according to the different energy sources). Besides, energy prices are subjected to different increasing rates from a long term perspective, which will affect the lifetime net present values of the energy bill savings. Therefore, defining bills reduction rate (BRR), on top of energy reduction rate(ERR), will allow the homeowners to evaluate the potential economic benefits of undertaking building renovation by jointly taking into the joint of both changing energy prices and their impacts on ERR;

2) Different retrofit combinations may have similar energy reduction rates (ERR), however, the proportions of thermal energy and electricity can be diversified, which may result in different energy bill savings;

According to the survey results, the retrofit motivations can be different, as defined in the section above (e.g. retrofit for rent or sale, retrofit for self-living). The willingness to invest in deep energy retrofit is relatively low because the potential of BRR as a result of undertaking renovation is not quantified and well communicated to the homeowners and investors.

6.2.3 Calculation method

This section introduces the calculation methods for pre/post-building energy performance and five objectives with the following 8 steps:

Step 1: Energy performance of building baseline and individual ERM calculated using IES VE software

Step 2: Comprehensive energy retrofit combinations generated in MATLAB

Step 3: Post-retrofit final energy consumption calculated in MATLAB

Step 4: Energy Reduction Rate (ERR) calculation for comprehensive retrofit combinations

Step 5: Carbon Reduction Rate (CRR) calculation for comprehensive retrofit combinations

Step 6: Initial Investment (II) calculation for comprehensive retrofit combinations

Step 7: Discounted Payback Period (DPP) calculation for comprehensive retrofit combinations

Step 8: Bills Reduction Rate (BRR) calculation for comprehensive retrofit combinations

The building's baseline energy performance is assessed in IES VE software evaluating thermal energy demand for space cooling, space heating and DHW, and electricity demand for fans, lighting, pumps, and equipment. The IES VE model needs to be set initially using:

- The thermal-physics features of building envelopes such as U-value of different facades and glazing types;
- Hourly schedules for different thermal zones including occupancy, DHW demand, people activity, ventilation need, lighting and household equipment power density;
- HVAC system and its operation schedules based on set-point temperatures;
- Different HVAC types for heating and cooling needs;

- Climatic boundary conditions include solar radiation, wind velocity and external temperature.

After the simulation of the baseline model in IES VE software, thermal and electricity demand are decoupled during the process in which the post-retrofit final energy consumption is assessed in MATLAB. In the meantime, thermal energy demand for space heating, space cooling, and DHW and direct electricity usage are simulated as input values to the next stage of the retrofit calculation process. In addition, random combinations of alternative retrofit measures are considered comprehensive retrofit combinations (COMB), where a set of energy retrofit measures (ERMs) are determined based on energy performance.

Operators 0 and 1 represent different technologies' absence and presence during the process. To explore all possible ERM combinations, n mixed variables are deducted in a continuous or discrete range. For instance, if thermal insulation is used as one of the ERMs in COMB1, the post-retrofit heating/cooling energy consumption is calculated by multiplying its corresponding heating/cooling demand efficiency with baseline heating/cooling demand values.

The heat pump system is also engaged in COMB1 with thermal insulation to replace the existing boiler. In that case, the post-retrofit heating/cooling energy consumption is calculated by multiplying its system energy efficiency due to different energy carriers with demand to energy conversion rates. Then, the final energy consumption is the coupled results of both thermal and electrical consumption.

Energy reduction rate (ERR) is proposed to determine the energy-saving potential for each retrofit combination, whose final energy consumption will be

compared with that of the baseline reference building with the unit of percentage (%). As shown in Eq. (6-9), ERR can be calculated as the ratio between the post-retrofit scenario's primary energy consumption and the primary energy reduction between the post-retrofit and baseline model.

$$\mathrm{ERR} = \sigma(\mathrm{i})/(\sigma(\mathrm{i}) - \sigma(0)) \qquad \text{Eq. (6-9)}$$

Where, $\sigma(\mathrm{i})$ is the final energy consumption (kWh/m^2) with the selected retrofit combination COMBi; $\sigma(0)$ is the baseline final energy consumption.

One of the purposes for ERR is to examine and compare the final energy consumption reduction between baseline and retrofit sceneries ($\sigma(\mathrm{i}) - \sigma(0)$) and economic benefits for post-renovation scenarios under different climatic conditions.

Carbon reduction rate CRR is proposed to determine the energy-saving potential for each retrofit combination, whose final carbon emission will be compared with that of the baseline reference building with the unit of percentage (%). As shown in Eq. (6-10), CRR can be calculated as the ratio between the post-retrofit scenario's carbon emission and the carbon reduction between the post-retrofit and baseline model.

$$\mathrm{CRR} = \lambda(\mathrm{i})/(\lambda(\mathrm{i}) - \lambda(0)) \qquad \text{Eq. (6-10)}$$

Where, $\lambda(\mathrm{i})$ is the final carbon emission (kWh/m^2) with the selected retrofit combination COMBi; $\lambda(0)$ is the baseline carbon emission.

According to Statista, the average hourly labour cost is estimated as 28.5 €/h (Clark, May 4, 2021) and the installation cost as 34 €/m^2 (Kouloumpi, 2013). The initial investment (II) is calculated by the sum of the capital cost of

components and the labour cost for installation, as shown in Eq. (6-11):

$$\phi_{II} = \phi_{capital} + \phi_{labour} \quad \text{Eq. (6-11)}$$

DPP is defined as variation and modification of payback period that accounts for the time value and uses discounted cash flows when calculating the payback period with the unit of years (Ergonomics of the physical environment, 2005). DPP represents the economic performance of a specific combination to assess the rapidity of the investment payback period. To assess DPP, the cumulative discounted net present values (CNPV) are calculated first through the difference of initial investment and the cumulative annual net cash flows in Eq. (6-12):

$$\mathrm{CNPV}\ (t = n) = \phi_{II} - \sum_{t=1}^{n} \mathrm{NPV}(t = n) \quad \text{Eq. (6-12)}$$

Therefore, DPP equals to 't = n' year when the CNPV (t=0) =0, with details in Eq. (6-13):

$$\mathrm{DPP}\ (i) = n, \text{when } \mathrm{CNPV}(t = n) = 0 \quad \text{Eq. (6-13)}$$

The Net Present Value Method (NPV) is the difference between the present value of cash inflows and the present value of cash outflows over a period used in capital budgeting and investment planning to analyse a combination retrofit's profitability. The following Eq. (6-14) is used to calculate NPV of annual energy bill savings:

$$\mathrm{NPV}\ (t) = R_d(t) \times (\phi_b(t = 0) - \phi_b(t) - \phi_{operation}(t)) \quad \text{Eq. (6-14)}$$

The discount rate $R_d(t)$ depends on the real discount rate R_r and the years (t) of the considered costs. The discount rate can be expressed as Eq. (6-15):

$$R_d\ (t) = (1/(1 + R_r))^t \quad \text{Eq. (6-15)}$$

Where t is the number of years and R_r is the real discount rate, which is closely related to market interest R and inflation rate R_i. It can be calculated using Eq. (6-16):

$$R_r = (R - R_i)/(1 + R_i) \quad \text{Eq. (6-16)}$$

The market values of interest & inflation rate and energy price & their increasing rate for Nottingham are shown in Table 6-2.

Table 6-2 Economic indicators and energy prices

	Market interest rate R (%)	Inflation rate R_i (%)	Real discount rate R_r (%)	Electricity price increase rate (%)	Natural gas increase rate (%)	Natural gas price (€/kWh)	Electricity price (€/kWh)
UK-Nottingham	0.57 (Ma et al., 2012)	0.7 (Ma et al., 2012)	0.689 (Ma et al., 2012)	5.89 (ASHRAE, 2013)	12.99 (ASHRAE, 2013)	0.0476 (ASHRAE, 2013)	0.2203 (ASHRAE, 2013)

6.3 Case study

Between 1945 and 1964, the UK experienced a severe housing shortage after the Second World War. This led to the construction of a vast majority of semi-detached single-family houses featuring masonry walls with poor insulation, which occupies around 23% of the total UK building stocks (D'Agostino et al., 2017). Moreover, the semi-detached house accounts for approximately 59% of the total building stocks (D'Agostino et al., 2017), which is the most popular type compared with the other types, including detached houses (22%), terraced houses (18%) and apartment blocks (1%). According to Ref. (D'Agostino et al.,

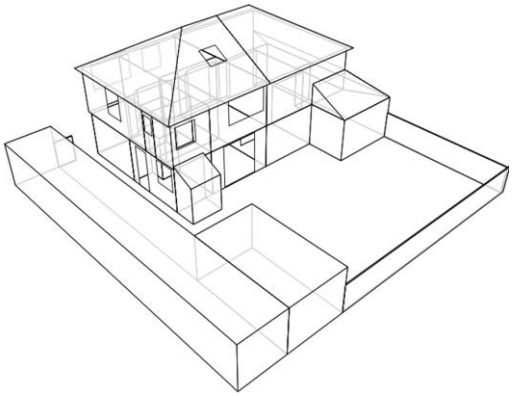
2017), the semi-detached houses (in the form of 2 bedrooms) constructed between 1945 and 1964 usually are dedicated to two occupants with an average floor area of 88 m^2 (range: 85m^2-90m^2). The building construction materials and U-value specifications are summarized in Appendix 6-3, with pitched roof (U-value=2.3 W/m^2.K), concrete floor (U-value=0.8 W/m^2.K), masonry wall (U-value=2.0 W/m^2.K) and double glazing windows (U-value=2.2 W/m^2.K).

In this research, a semi-detached 2-bedroom single-family house with a total floor area of 85 m^2 is selected according to the building typology, with case study model depicted in Figure 6-2. The building is a solid masonry wall constructed in 1948 with U-value of 2.1 W/m^2.K, which belongs to the typical post-war masonry housing style. All windows applied double glazing with U-value of 2.5 W/m^2.K and pitched roofs with U-value of 2.3 W/m^2.K. Besides, the ground floor is a concrete constructed with U-value of 0.85 W/m^2, and the attic floor is insulated with rock wool with a total U-value of 0.90 W/m^2.K. The airtightness for the main building and the loft are tested with 2.69 ACH and 4.18 ACH under a pressure difference of 50Pa. The 30-years average ambient weather conditions with solar radiation, ambient temperature and wind velocity are obtained from the WeatherOnline website (WeatherOnline), as shown in Figure 6-3. It is figured out that the high-intensity solar radiation periods are between May and August, while low-intensity periods are for the rest of months (Burnett et al., 2014). The highest and lowest ambient temperatures are 33.6 ℃ and -2.0 ℃. The high-intensity wind energy periods are between January and February, with the highest wind speed of 17.7 m/s.

The dwelling was conjectured to be occupied by two adults with predominantly space heating, DHW and cooking systems. Therefore, the primary energy source

of the baseline building is considered as electricity and natural gas. Specifically, the space heating and DHW were powered only by natural gas, and the cooking system consists of both gas cooker and electric oven, along with other appliances (lighting, electric heater, kettle, food processor, integrated washing machine and dryer, as well as coffee machine) powered by electricity. In addition, the space heating and DHW systems were driven by combi-boilers with seasonal space and water heating energy efficiency of 94% and 85%, respectively. Furthermore, 80 % of lights were activated during 15:00-22:00 h and 19:00-22:00 h for winter and summertime, with an average illuminance of 4.8 W/m^2. For the bathroom DHW system, it is marked from the schedule that the average water consumption periods occurred during 12:00-12:30 h (Mon, Tue, Wed and Sun), 07:00-07:30 h (Fri) and 15:00-15:30 h (Thu and Sat) due to different consumption behaviours. Moreover, the initial set temperature for corridor and kitchen, living room and bedroom were 19 ℃ (08:00-17:00 h) and 22 ℃ (00:00-08:00 h, 17:00-24:00 h), 19 ℃ (08:00-17:00 h) and 24 ℃ (00:00-08:00 h, 17:00-24:00 h) with the central heating loop in space heating sector, respectively. However, to maintain the indoor air quality and avoid summer overheating, natural ventilation is applied by opening the windows. 25% of windows are open from 8 am to 9 am and from 5 pm to 6 pm in the winter, while half of the windows are open from 8 am to 11 am, and all windows are open from 11 am to 5 pm, and 30% of windows open from 5 pm to 8 pm in the summer. No cooling system was installed according to the local weather data. In terms of the cooking system, the profiles were distinctive for Mon-Thu, Fri and Sat-Sun with installed 4-burner gas hob and single oven. Furthermore, several profiles were used with the modulate values, including lighting, secondary electric heater, cooking and other household

appliances in which the schedule scale was varied in the range of 0-1: ‘1’ indicating the maximum load for relevant sectors, and ‘0’ for schedule off. Three peak intervals occurred each day in the cooking profile. The secondary electric heater was only used in December, January and February. Finally, the unit rates for natural gas and electricity used in this research are 2.872 p/kWh and 19.22 p/kWh (day), 10.15 p/kWh (night).



(a)

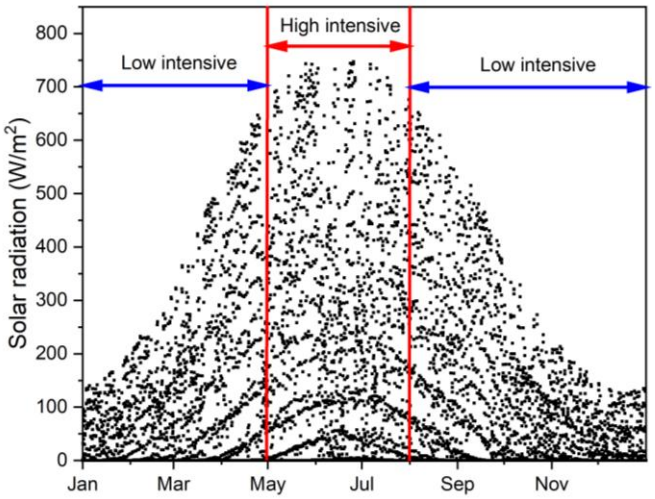


(b)

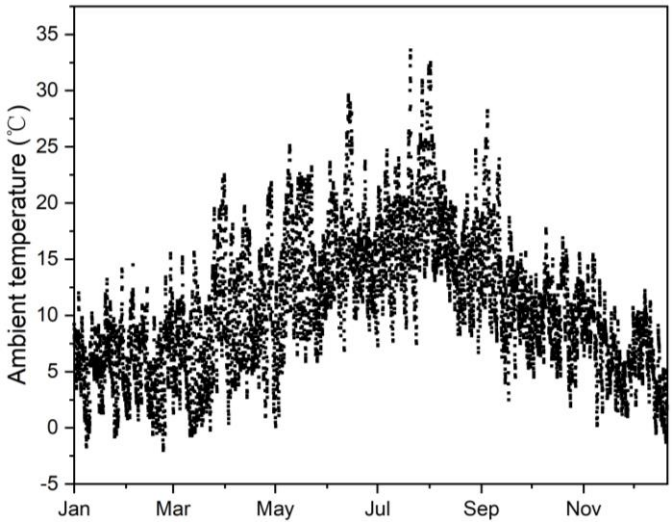


(c)

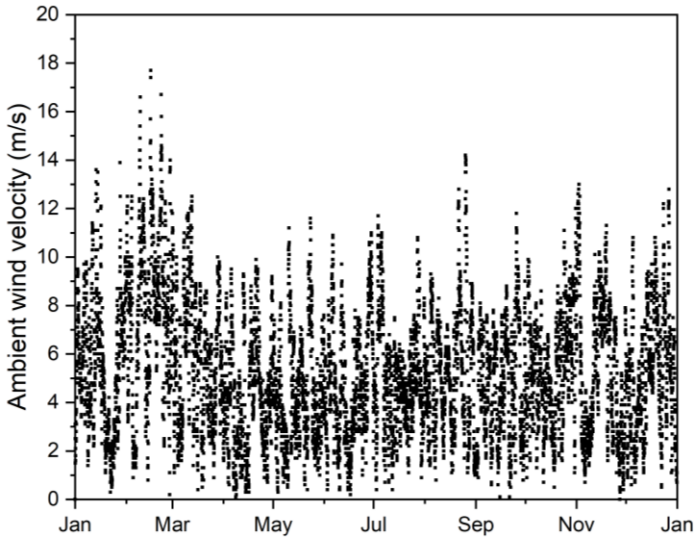
Figure 6-2 Case study building models (a) established in IES in combination with its adjacent building (left half is the research object) (b) 3D geometric wireframe view (c) On-site image



(a) 30-years average solar radiation



(b) 30-years average ambient temperature



(c) 30-years average ambient wind velocity

Figure 6-3 30-years average ambient weather conditions (a-solar radiation, b-temperature, c-wind velocity)

17 retrofit technologies were selected as alternative energy retrofit measures (ERM), categorised as passive, active, and renewable (Qu et al., 2020). The information on the life cycle and costs of 17 ERMs have been described the same as shown in section 5.3.2, also shown in Appendix 6-4.

Passive measures: ERM01-1 (Vacuum glazing insulation windows); **ERM01-2** (Triple glazing windows); **ERM02-1** (Silicon-based vacuum insulation panels for external wall); **ERM02-2** (Polyisocyanurate insulation panels); **ERM03-1** (Silicon-based vacuum insulation panels for party wall); **ERM04-1** (Starch aerogel insulation panels); **ERM05-1** (Silicon-based vacuum insulation panels for ground floor); **ERM06-1** (Gypsum insulation); **ERM06-2** (Sealings of the windows and joint places).

Active measures: ERM07-1 (Mechanical ventilation with heat recovery); **ERM08-1** (LED lighting + Daylighting pipes).

Renewable measures: ERM09-1 (Multi-crystalline silicon PV glazing panels); **ERM09-2** (Thin-film PV glazing with high insulation); **ERM10-1** (Solar assisted heat pump); **ERM10-2** (Air-water heat pump); **ERM10-3** (Desiccant based air cooling dehumidifier); **ERM11-1** (Solar collector).

6.4 Results and discussions

The baseline energy consumption and bills were calculated in IES VE building simulation software using Nottingham weather values and compared with on-site measurement results, as listed in Table 6-3. The discrepancies between simulation and on-site measurement results were calculated by the ratio of their energy differences and the on-site measurement results, as shown in Eq. (6-17).

$$Energy\ performance\ discrepancy = \frac{Simulation\ results - measurement\ results}{Measurement\ results}$$

Eq. (6-17)

In general, the final energy consumption had a discrepancy of -0.5%, with simulated results slightly lower than the on-site measurements. From the perspective of different energy sources, the simulated natural gas consumption and bills yield a -1.7% discrepancy compared with the measurement results. On the contrary, the simulated electricity consumption and bills had 2.3% and 1.9% discrepancies compared with the measurement results. As concluded in Ref. (Michael et al., 2017), the estimation of energy simulation with $\pm$ 5% uncertainty is usually reasonable. The model results in terms of this uncertainty range rarely affected the energy-saving performance, validating the effectiveness of the baseline model.

Table 6-3 The baseline energy performance and validation

	Simulation results by IES VE	On-site measurement results	Discrepancies
Final energy consumption (kWh/m^2)	419	421	-0.5%
Natural gas consumption (kWh/m^2)	284	289	-1.7%
Electricity consumption (kWh/m^2)	135	132	2.3%
Annual energy bills (€)	3410	3385	0.8%
Annual natural gas bill (€)	1069	1087	-1.7%
Annual electricity bill (€)	2341	2298	1.9%

6.4.1 Cost-optimal results neglecting homeowners' motivation

Homeowners' engagement is rarely addressed in pre-retrofit building design, leading to the fact that homeowners may be dissatisfied with the final retrofit choices of the design teams. According to the Energy Performance and Building Directive (EPBD) guidance (Union, 19 May 2010), the cost optimum methodology is proposed and applied in most research to assure the trade-off between associated costs and energy consumption reductions. The optimal retrofit combinations will be those with minimum energy performance requirements with the lowest investment cost, which is technologically neutral and does not favour one technological solution over another. In this section, the cost-optimal results of comprehensive retrofit combinations are calculated in Figure 6-4 with the minimum II region and Figure 6-5 with the minimum DPP region under UK climate conditions. Table 1 and Table 2 in Appendix 6-5 show

the assessment values and cost-optimal combinations.

As shown in the initial investment performance curves, the initial investment has an increasing rate under three stages, which includes 1) a slow increase with the enhancement of ERR without heat pump technologies, and 2) a dramatic drop outside specific ranges of ERR due to the lack of renewable technologies, such as PV panels and solar, with 3) rapid increase due to whole-house insulation and adoption of renewable technologies. Therefore, the cost-optimised II (minimum II region) is derived with 374-378 €/m^2 with energy reduction rates between 72%-79%, respectively. It is significant to note that the rapid increase of initial investment may cause financial burdens when the energy reduction rates are beyond the cost-optimal level with a 35.1 €/m^2 increase in the initial investment for every 1% ERR increment.

However, the discounted payback periods are relatively high in the minimum II region with 18 years from the perspective of energy-economic purposes. DPP of comprehensive retrofit combinations is illustrated in Table 6-5, with the ERR ranging from 82%-93% in the minimum DPP region, which results in a minimum DPP of 13 years. However, the initial investment has a surge increment to 449-835 €/m^2. Therefore, it is evident that the mismatch of optimal retrofit combinations occurs between the minimum II and DPP regions.

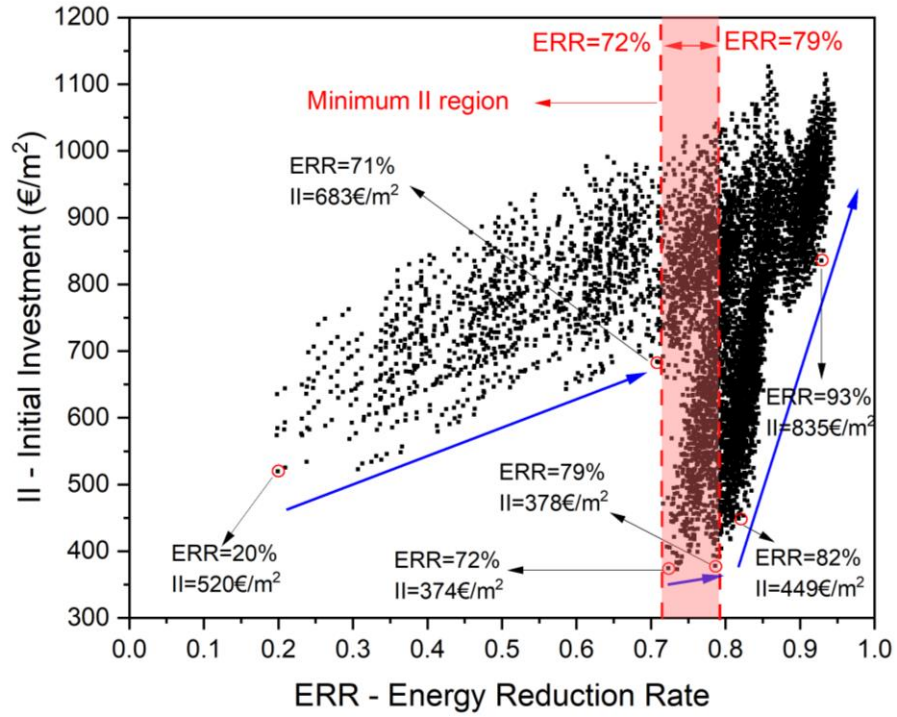


Figure 6-4 Initial Investment (II) under full-scale energy reduction rate (ERR)

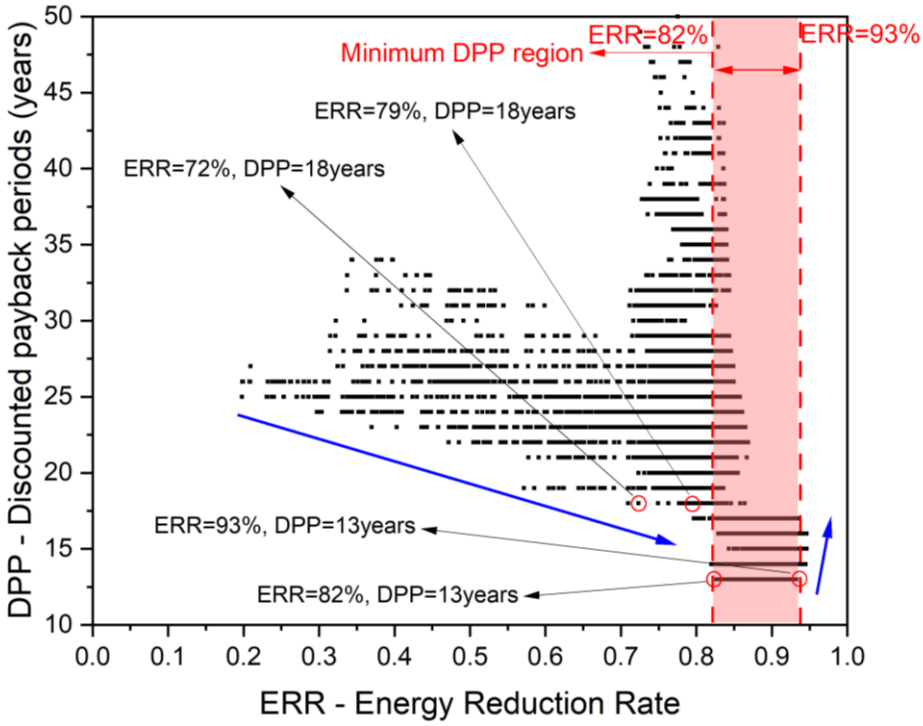


Figure 6-5 Discounted payback periods (DPP) under full-scale energy reduction rate (ERR)

6.4.2 Multi-criteria optimisation results and discussion

In section 6.4.1, the optimisations of different combinations are analysed based on the cost-optimal assessment method. Nonetheless, the multi-objective method should be addressed and specified to provide a more comprehensive perspective by considering the impacts of retrofit motivations on decision-making retrofit measures. This section discusses three homeowners' motivations and priorities for building retrofit to achieve a multi-motivation optimisation process. It is noted that all the combinations and results are demonstrated with DPP lower than 50 years. Thus, the relationships of the priorities of each motivation and maximum MPF in different motivations are illustrated in Figure 6-6 to Figure 6-8 The results, including specific criteria, optimal combinations and other assessment values, are listed in Appendix 6-6. The optimal technology selections from M1 to M3 are also discussed, as shown in Figure 6-9.

Insufficient initial investment (II) is a significant limitation for those who retrofit their own house for self-living. Figure 6-6 illustrates the maximum MPF trends with II increase in self-living type (M1), with assessment values and optimal combinations illustrated in Table 1 and Table 2 (Appendix 6-6). It is evident that the optimised points of maximum MPF are more concentrated when II is greater than 600 €/m^2 with a maximum MPF of 0.408 and ERR of 93%. However, a high initial investment of 917 €/m^2 is required due to high-performance whole-house insulation materials and PV panels. Considering the limited funding, four criteria for initial investment are classified 1) II < 400€/m^2; 2) 400€/m^2≤II<500€/m^2; 3) 500€/m^2≤II<600€/m^2;4) II>600€/m^2. It is noticeable that the optimised initial investment increases from 383 €/m^2 to 917 €/m^2, which is selected according to the maximum MPF in each criterion. It is also found that

the DPP has a shorter period (from 19 years to 13 years) with the II increment. Meanwhile, there are four fundamental technologies for self-living motivated retrofit in the four criteria, including party wall insulation, ground floor insulation, efficient lighting improvement and solar-assisted heat pump. For II < 400€/m^2, only the three fundamental technologies are applied; For 400€/m^2 ≤ II < 500€/m^2, external wall insulation is also involved; For 500€/m^2≤II<600€/m^2, attic floor insulation is applied; For II>600€/m^2, window glazing insulation and PV panels are applied. Airtightness insulation, heat recovery ventilation and solar collector are not suitable for self-living retrofit in the four criteria.

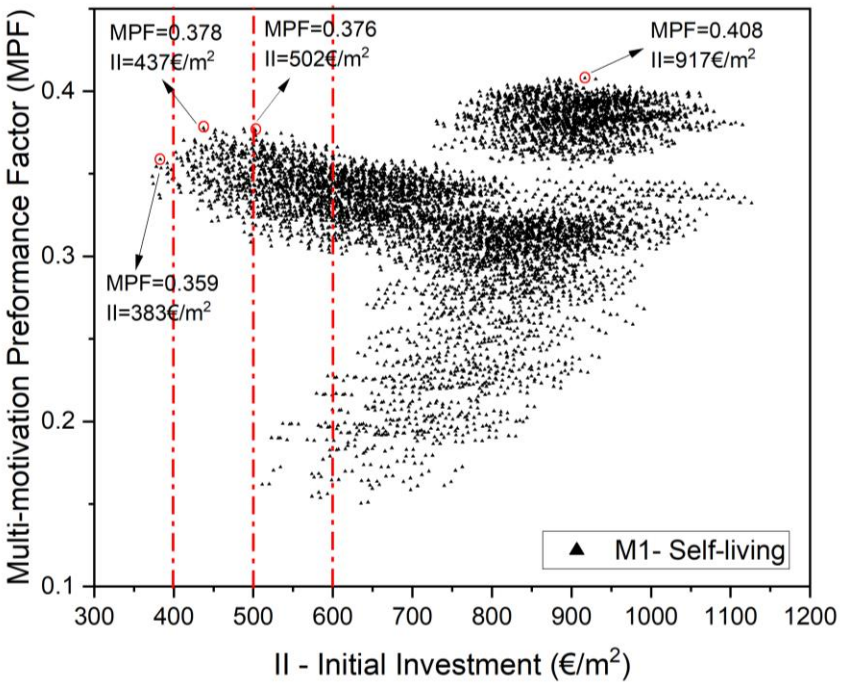


Figure 6-6 The relation between II and MPF under M1 type

Achievement of the required Energy Performance Certification (EPC) level is essential for homeowners who retrofit to sell or rent. Hence, a minimum ERR for each EPC level is required for retrofit rather than higher ERR and EPC level

achievement. According to the EPC calculation method described in Appendix 6-1, seven EPC levels from A to G has been converted to the indicator of energy reduction rate (ERR) for the reference building in the UK context. The relations between EPC and ERR are listed in Table 6-4:

Table 6-4 The relations between EPC and ERR for the reference building

EPC level	G	F	E	D	C	B	A
ERR range	≤50%	50%-74%	74%-81%	81%-87%	87%-92%	92%-97%	>97%

Figure 6-7 demonstrates the maximum MPF trends with ERR increase in the rental or sale type (M2), with assessment values and optimal combinations illustrated in Table 1 and Table 3 (Appendix 6-6). The maximised MPF is selected at the lower bound of ERR ranges to obtain the optimised retrofit combinations in each EPC level. It is found that the maximised MPF increases from 0.409 to 0.920 when EPC is improved from level F to level A, with the ERR rising from 51% to 93%. It is also found that the II is relatively high; however, the DPP is reduced from 24 years to 13 years. There are four fundamental technologies for rental or sale motivated retrofit, including attic floor and ground floor insulation, efficient lighting improvement and PV panels. Specifically, glazing insulation is required to achieve level B, E and F; external wall insulation is required to achieve level B, D and E; party wall insulation is required to achieve level C, D and F; heat recovery ventilation and solar collector are only used in level F. It should be noted that the air-water heat pump is applied when level D and higher EPC is required due to significant energy reduction

achievement. Airtightness insulation is unsuitable for rental or sale retrofit in all EPC levels. It is concluded that more insulation measures are applied when the EPC is higher than level C due to deep energy saving requirements or lower than level C as passive insulation retrofit measures could result in a relatively lower energy reduction.

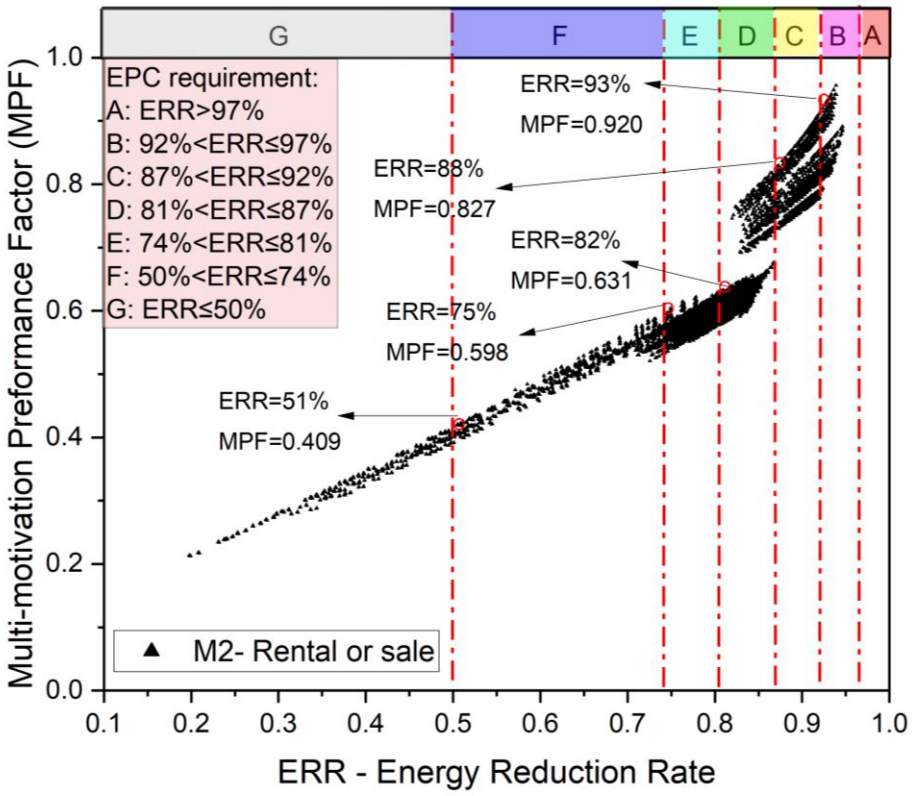


Figure 6-7 The relation between the ERR and MPF under M2 type

A rapid return on investment with the discounted payback period (DPP) indicator is a significant limitation for those who retrofit for investment. Figure 6-8 depicts the maximum MPF trends with DPP increasing in investment type (M3), with assessment values and optimal combinations illustrated in Table 1 and Table 4 (Appendix 6-6). It is evident that the optimised points of maximum

MPF are more concentrated when DPP is lower than 15 years with a maximum MPF of 0.707, DPP of 13 years, ERR of 61% and II of 870 €/m^2. It is found that the II is reduced from 870 €/m^2 to 392 €/m^2 with DPP increasing from 13 years to 25 years. Moreover, ERR increases from 61% to 93%. Therefore, four criteria are classified, including 1) DPP<15 years; 2) 15 years ≤DPP<20 years; 3) 20 years ≤ DPP<25 years; 4) DPP ≥ 25 years. There are three fundamental technologies for investment motivated retrofit for the four criteria: external wall insulation, efficient lighting improvement, and PV panels. For DPP<15 years, no heat pump technology and whole-house insulation are applied, with ERR of 61%. However, the whole-house insulation enhancement measures are adopted in other criteria, with ERR increasing to 84%-93% and II declining to 392 €/m^2 when DPP is 25 years.

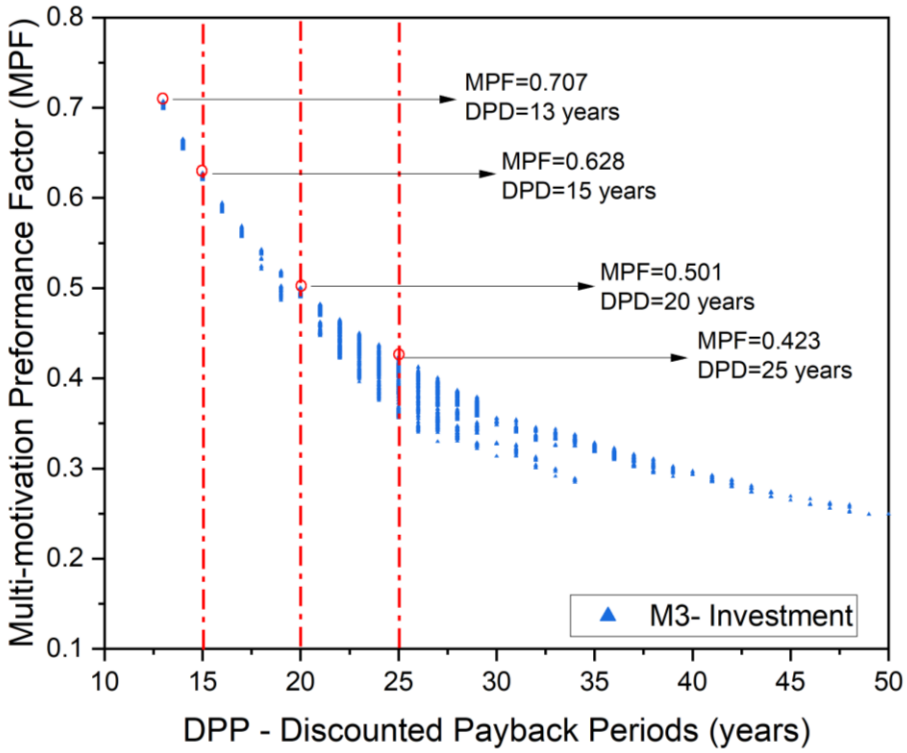


Figure 6-8 The relation between DPP and MPF under M3 type

The optimal technology selections from M1 to M3 are summarised in Figure 6-9 with two necessary technologies of ground floor insulation and efficient lighting improvement, which must be adopted regardless of the motivation preferences. Party wall insulation is the common fundamental technology for both self-living and rental or sale motivated types. Installing PV panels is fundamental for rental, sale, and investment motivations. From the perspective of applying heat pump technologies, solar-assisted and air-water heat pumps are selected by self-living and rental or sale types, respectively, not selected by investment type. The attic floor and external wall insulation are selected by rental or sale and investment types.

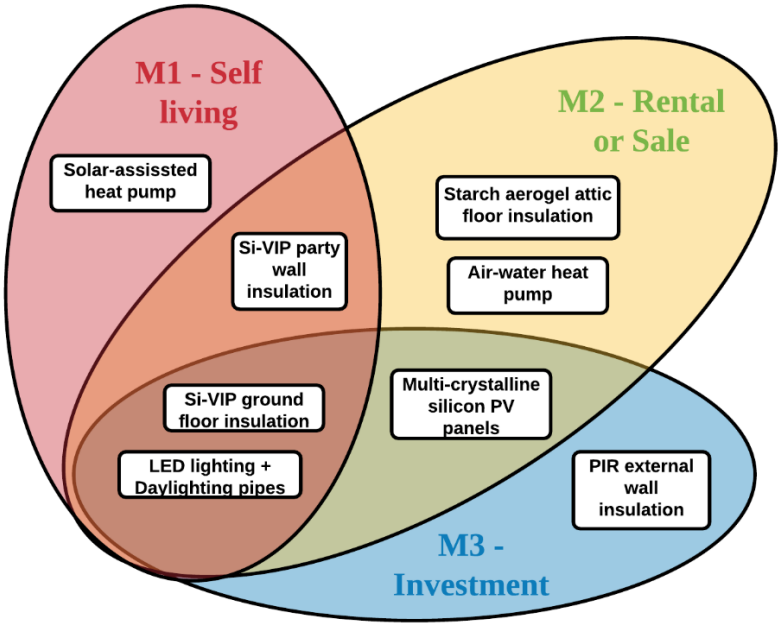


Figure 6-9 Optimal technologies from M1 to M3

6.4.3 Sensitivity analysis with respect to input data

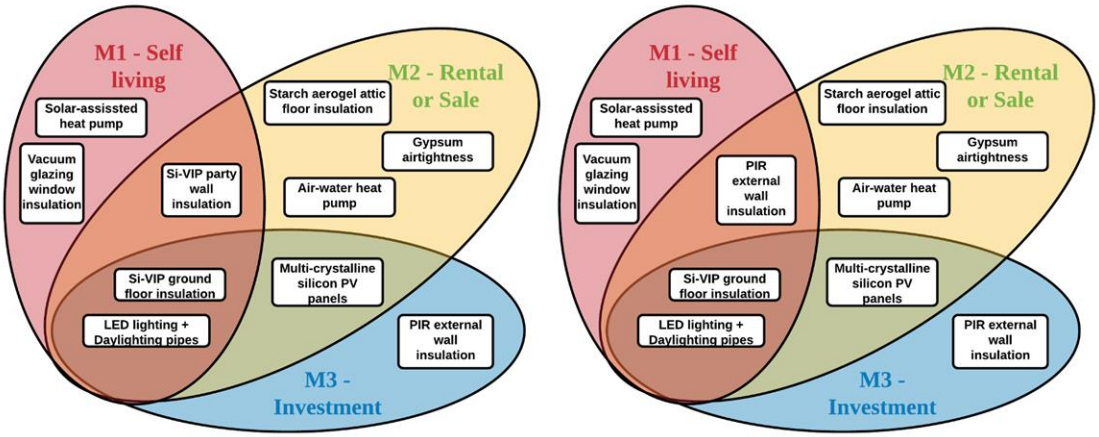
As shown in Figure 6-9, most of the optimal technologies are summarised from the calculation in the perspective of motivation M1 to M3. The baseline energy consumption accuracy could bring uncertainties to the optimal retrofit measures

in terms of the energy savings obtained by the model. In order to validate that the optimal retrofit measures selection in each motivation type will not be severely affected by the accuracy of energy savings figures obtained from the building energy simulation model, a sensitivity analysis is performed. The calculated baseline energy consumption input data was adjusted in uniform increments, with 10% (−5% to 5%). 20% (-10% to 10%) and 30% (-15% to 15%), which induces the adjustments of the energy savings in each retrofit combination.

It was observed from the model output that the optimal output selections of retrofit measures in each motivation type remained the same for 10% (−5% to 5%) adjustment of baseline energy consumption input data. With the adjustment of 20% (-10% to 10%), it is found that the vacuum glazing window insulation has also been adopted in self-living-oriented type (M1); Moreover, the gypsum airtightness insulation has been selected for rental or sale-oriented type (M2). In addition, for a 30% baseline energy consumption increment, the Si-VIP party wall insulation technology has been replaced by the PIR external wall insulation in common fundamental technologies of M1 and M2 types based on the optimal technologies with 20% adjustment of baseline energy. The optimal technologies from M1 to M3 with 20% and 30% of baseline energy consumption as the input data is shown in Figure 6-10.

The final energy consumption discrepancy is -0.5%, validated with the on-site measurement results as mentioned before, where the range is within 10% (-5% to 5%) baseline energy consumption increment. It is concluded that the model result in terms of selected measures is robust against the baseline energy consumption input data. Meanwhile, compared with the average energy

consumption ranging from 402 kWh/m^2 to 425 kWh/m^2 defined for the reference building with similar age and type, the baseline energy consumption has the discrepancy of -4.1% to 1.4%, locating in 10% baseline energy consumption differences, which indicates the result concerning the optimised retrofit measures by using the method proposed in this section is not significantly affected by the baseline energy consumption estimation with an uncertainty range of ±5%.



(a) 20% adjustment of baseline energy (b) 30% adjustment of baseline energy

Figure 6-10 Optimal technologies from M1 to M3 with 20% and 30% of baseline energy consumption as the input data

6.5 Conclusions

This section establishes an innovative retrofit Motivation-Objective-Criteria (MOC) approach to support the decision-making process for selecting building retrofit measures, which adapts to different homeowners' retrofit motivations, objectives and criteria. With a clear understanding of purposes for homeowners to take retrofit measures for their properties, three retrofit motivations are

proposed: M1-Self-living (homeowners will occupy the post-retrofit houses), M2-Rental or sale (the post-retrofit houses will be used for rental or sale) and M3-Investment (homeowners would like to profit from investment). Five main objectives are considered as the retrofit motivations, including energy consumption reduction (ERR), initial investment (II), discounted payback periods (DPP), bills reduction rate (BRR) and carbon reduction rate (CRR), where the corresponding weights are from W_1 to W_5, respectively. The assessment criteria for the three motivations vary: M1 type focuses on the initial investment limitations; the Energy Performance Certification (EPC) is the prior consideration for the M2 type; M3 type focuses on the discounted payback periods.

To make the weighting factor more reliable to reflect the homeowners' motivations and perspectives, 42 surveys were collected from the five demo site leaders of the SureFit project as an example with the weighting factors (in the range of 0–1) to understand the occupants' motivations and preferences for the retrofit work.

A semi-detached multi-family house is applied as the reference building to demonstrate the proposed MOC decision-making approach to select comprehensive energy-retrofit combinations with and without the homeowners' engagement. The house was built in the 1960s with a total floor area of 158 m^2, which has poor insulation and inefficient heating and cooling energy systems. According to the IES VE software simulation, the building baseline has a specific energy consumption of 419 kWh/m^2 in the UK context. By comparing the simulation results with on-site measurements, the final energy consumption has a discrepancy of -0.5%, with simulated results slightly lower than the on-site

measurement. As concluded in Ref. (Michael et al., 2017), the estimation of energy simulation with ± 5% uncertainty is usually reasonable accuracy. The model results in terms of this uncertainty range will rarely affect the energy-saving performance, validating the effectiveness of the baseline model.

Alternative retrofit measures are selected and categorised as passive, active, and renewable. Without homeowners' engagement, cost-optimal retrofit combinations are discussed according to single-objective optimisation in DPP and II with the comprehensive range of energy reduction rates.

According to the cost-optimal results neglecting homeowners' motivation, it is evident that the mismatch of optimal retrofit combinations occurs between the minimum II and DPP regions, with optimal ERR of 72%-79% and 82%-93%, respectively. The optimisation results are compared to the cost-optimal (models without homeowners' engagement) and multi-objective (models with homeowners' engagement). It is concluded that homeowners' retrofit priorities have an apparent influence on the selection of retrofit measures as listed below:

1) Two necessary technologies of ground floor insulation and efficient lighting improvement must be adopted regardless of the motivation preferences;
2) Party wall insulation is the common fundamental technology for both self-living and rental or sale motivated types;
3) PV panels installation is the common fundamental technology for rental or sale and investment motivated types;
4) Solar-assisted heat pumps are suitable for the self-living motivated retrofit type, while the air-water heat pumps are selected for the rental or sale type. Neither are necessary for the investment type;

5) Attic floor and external wall insulation are essential for rental or sale and investment types, respectively.

Meanwhile, compared with the average energy consumption ranging from 402 kWh/m^2 to 425 kWh/m^2 defined for the reference building with similar age and type, the baseline energy consumption has the discrepancy of -4.1% to 1.4%, locating in 10% baseline energy consumption differences, which indicates the result concerning the optimised retrofit measures by using the method proposed in this section is not significantly affected by the baseline energy consumption estimation with an uncertainty range of ±5%

Therefore, the proposed inclusive decision-making approach can support the process of selecting building retrofit measures with substantial energy and economic benefits for different retrofit motivations (self-living, rental or sale, and investment), which will facilitate acceleration and success both technically and commercially.

7. Conclusions and future works

7.1 Discussion and conclusions

This PhD research mainly contains three sections: laboratory/field tests, modelling work, and case study demonstration, which has the financial support and contributions from the European Commission Horizon 2020 project RezBuild (project contract number: 768623). Therefore, this chapter will discuss and conclude the research work from the three sections mentioned above.

7.1.1 Modelling and experimental results of innovative retrofit technologies

Innovative envelope and system retrofit technologies are analysed with modelling and experimental tests. Envelope retrofit technologies are classified into three categories: 1) façade insulation, 2) glazing insulation, 3) efficient daylighting pipes, which can reduce the electricity demand and thermal demand for both heating and cooling requirements.

Innovative energy system retrofit technologies are classified into two categories, including 1) liquid desiccant based air cooling and dehumidification and 2) solar assisted heat pumps.

7.1.2 EF-EC energy prediction model

This research proposes a novel Energy-Flow based Ensemble Calibration (EF-EC) model to tackle the issue of 'Rapid and accurate energy-economic performance prediction of deep energy retrofit in single-family houses'. In the EF-EC model, only a few simulations of baseline heat and electrical demands and heat and electrical coefficients of individual retrofit measures conducted by IES VE building dynamic simulation rather than numerous simulations in the conventional White-box model. Thus, time-consuming and numerous dynamic

simulations are replaced by rapid and transient numerical calculations in the EF-EC model. Comparing real energy consumption and EF-EC calculation results in baseline and post-retrofit scenarios, the discrepancies are -0.66% and 1.03%, presenting that the EF-EC model is accurate at an acceptable level. Besides, this proposed EF-EC model reduces the calculation discrepancy to a maximum of only 6%, with an absolute discrepancy of only 3.9 kWh/m^2 within reasonable ranges.

7.1.3 MOC retrofit optimisation approach

This section establishes an innovative retrofit Motivation-Objective-Criteria (MOC) approach to support the decision-making process for selecting building retrofit measures, which adapts to different homeowners' retrofit motivations, objectives and criteria. With a clear understanding of the purposes for homeowners to take retrofit measures for their properties, three retrofit motivations are proposed: M1-Self-living (homeowners will occupy the post-retrofit houses), M2-Rental or sale (the post-retrofit houses will be used for rental or sale) and M3-Investment (homeowners would like to profit from investment). According to the cost-optimal results neglecting homeowners' motivation, it is evident that the mismatch of optimal retrofit combinations occurs between the minimum II and DPP regions, with optimal ERR of 72%-79% and 82%-93%, respectively.

Therefore, the proposed inclusive decision-making approach can support the process of selecting building retrofit measures with substantial energy and economic benefits for different retrofit motivations (self-living, rental or sale,

and investment), which will facilitate acceleration and success both technically and commercially.

7.2 Recommendations and future work

Residential building retrofit has a significant promising advantage in carbon reduction and indoor comfort improvement through improving the building energy efficiency, which could encourage a high-technologized sector and sustainable business. Despite the encouraging decision-making optimisation algorithm establishment and results obtained within this study, future works are recommended in the following four aspects.

7.2.1 Algorithm improvement, interaction and visualisation

Although this study has proposed an innovative and time-saving algorithm for energy consumption calculation and decision-making optimisation, this algorithm can not allow an automatic run with direct input and output pattern; manually operation in some steps are still required between calculation tools of MATLAB, EXCEL, and simulation software (Energy Plus/IESVE). Future work needs to improve the algorithms for more effortless operation for better engineering use, such as full embedded systems, user-friendly operation interface and developed visualisation software. Besides, due to the limited retrofit technologies in the research, future work needs to extend more available technologies with energy performance and cost information. Moreover, in the cost calculation section, the presented study only works in a constant interest rate based calculation of discounted payback periods. Future work needs to insert more variants or functions to demonstrate the sensitivity of changing the interest rate and other economic impact factors.

7.2.2 multi-scale retrofit strategy

According to the present research, this algorithm can be developed to investigate the retrofit strategy on different scales, such as street scale, community scale, town scale, urban scale, which could help policy designers design more friendly and adaptable retrofit strategies for residential buildings.

7.2.3 Fast retrofit strategy and operation analysis

From the perspective of innovative retrofit technologies, it is recommended to investigate a fast retrofit strategy by applying the concept of prefabricated facades with 3D technologies, multi-functional facades, and modular systems.

Nowadays, the production of walls, glazing, roof elements and other compact modular facilities with prefabrication and modules are state of the art in industrial construction. Assemble line with standard, precise and monitored production in the manufacturing process in the factory allows for a high standard of quality. The off-site production will be transported to the on-site assembly, making an easier and faster retrofit installation process, which leads to less disruption to the retrofit installation process and fewer disturbances to the residents and their living environment. Figure 7-1 is a UK residential building retrofit case study, which demonstrates the example of a combination of ‘future-fit’ retrofit technologies with on-site existing building fabric and construction. Figure 7-2 is the post-retrofit renderings demonstration.

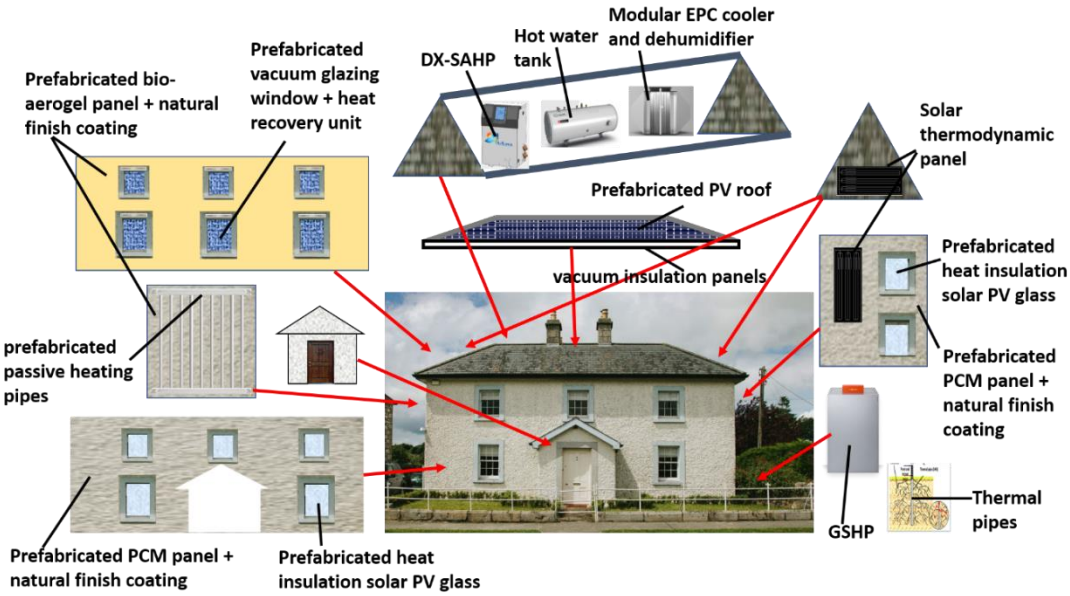


Figure 7-1 Retrofit example of a residential house with fast retrofit technologies

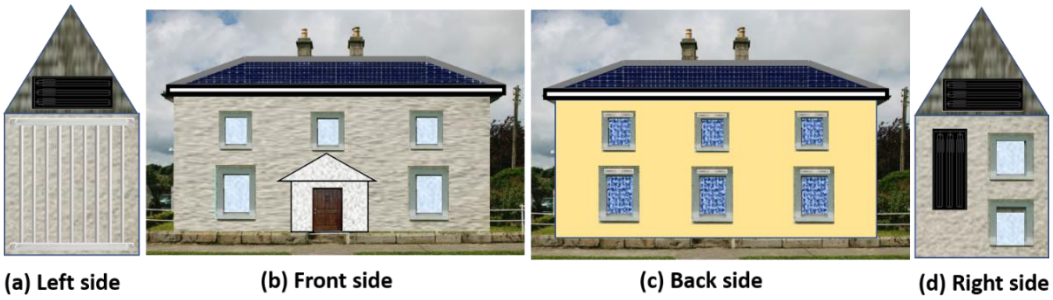


Figure 7-2 Post-retrofit renderings demonstration

The prefabrication and modules are manufactured in the factory with a standard assembly line, allowing for a high-quality standard. The off-site production will be transported to the on-site assembly, making an easier and faster retrofit installation process, which leads to less disruption to the retrofit installation process and fewer disturbances to the residents and their living environment. The basic idea of the 'off-site manufacture & on-site assembly' cycle is shown in Figure 7-3.

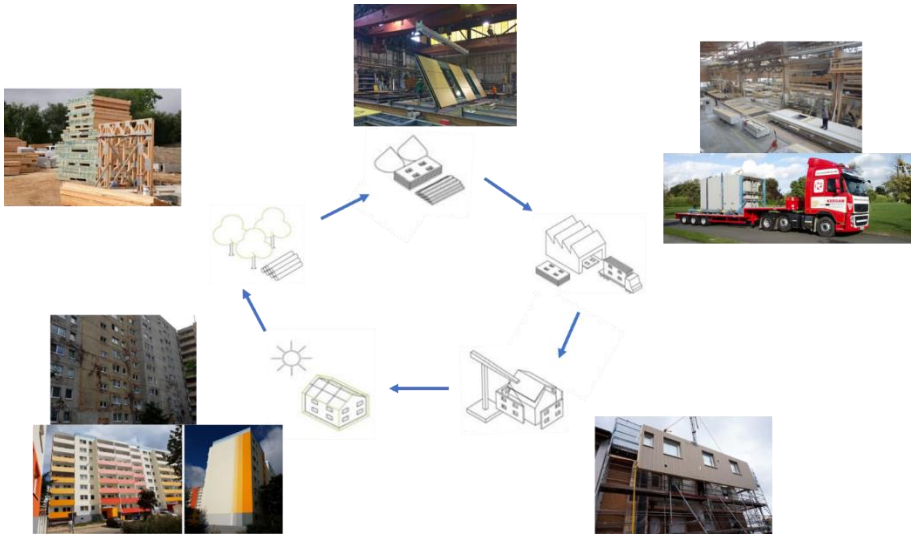


Figure 7-3 Cycle of 'off-site manufacture & on-site assembly' retrofit implementation

7.2.4 Cost-effective dwelling electrification retrofit

Despite the aim of energy retrofit strategy with 100% energy reduction rate (zero energy building), carbon retrofit strategy with 100% carbon reduction rate (zero carbon building) has promising advantages in the economic section, which indicates the aim of retrofit focusing on how to reduce the final carbon account in residential buildings to zero. In other words, carbon retrofit pays attention to energy sources' carbon reduction rather than concentrating on the maximum energy reduction rate with ultra-high efficient technologies, which will usually cause unacceptable high payback periods. Therefore, future work on carbon retrofit is recommended with the concept of building electrification retrofit, which transfers the primary energy used technologies to low-carbon energy supplied technologies, such as renewable electricity, renewable thermal energy. And in this way, the cost-effective optimisation can be better integrated with electrification retrofit to reduce the payback periods in an acceptable scale.

Reference

Illuminance - Recommended Light Level [Online]. Available: https://www.engineeringtoolbox.com/light-level-rooms-d_708.html [Accessed].

RezBuild project [Online]. Available: https://rezbuildproject.eu/ [Accessed].

November 2002. Light and lighting - Lighting of work places - Part 1: Indoor work places.

(BPIE), B. P. I. E. October 2011. Europe's buildings under the microscope.

(EU), D. 30 May 2018. The energy performance of buildings and Directive *In:* COUNCIL, E. P. A. O. T. (ed.).

ADITYA, L., MAHLIA, T. M. I., RISMANCHI, B., NG, H. M., HASAN, M. H., METSELAAR, H. S. C., MURAZA, O. & ADITIYA, H. B. 2017. A review on insulation materials for energy conservation in buildings. *Renewable and Sustainable Energy Reviews,* 73**,** 1352-1365.

AGENCY, I. E. *Cost-Effective Energy and Carbon Emissions Optimization in Building Renovation (Annex 56)* [Online]. Available: http://www.iea-annex56.org/ [Accessed October 2017].

AL-SAADI, S. N. J., AL-HAJRI, J. & SAYARI, M. A. 2017. Energy-Efficient Retrofitting Strategies for Residential Buildings in hot climate of Oman. *Energy Procedia,* 142**,** 2009-2014.

ALAM, M., SINGH, H., SURESH, S. & REDPATH, D. A. G. 2017. Energy and economic analysis of Vacuum Insulation Panels (VIPs) used in non-domestic buildings. *Applied Energy,* 188**,** 1-8.

ALLIANCE, T. M. O. B. R. T. Available: https://www.tecnalia.com/en/technological-assets/inacell-cellulose-aerogels-for-thermal-insulation-in-buildings [Accessed 13/11/2021].

ALVES, T., MACHADO, L., DE SOUZA, R. G. & DE WILDE, P. 2018. Assessing the energy saving potential of an existing high-rise office building stock. *Energy and Buildings,* 173**,** 547-561.

ANDRADE-CABRERA, C., BURKE, D., TURNER, W. J. N. & FINN, D. P. 2017. Ensemble Calibration of lumped parameter retrofit building models using Particle Swarm Optimization. *Energy and Buildings,* 155**,** 513-532.

ANDRADE-CABRERA, C., O'DWYER, C. & FINN, D. P. 2020. Integrated cost-optimal residential envelope retrofit decision-making and power systems optimisation using Ensemble models. *Energy and Buildings,* 214**,** 109833.

ANDRADE-CABRERA, C., TURNER, W. J. N. & FINN, D. P. 2019. Augmented Ensemble Calibration of lumped-parameter building models. *Building Simulation,* 12**,** 207-230.

ARAÚJO, C., ALMEIDA, M., BRAGANÇA, L. & BARBOSA, J. A. 2016. Cost–benefit analysis method for building solutions. *Applied Energy,* 173**,** 124-133.

ARAVENA, C., RIQUELME, A. & DENNY, E. 2016. Money, Comfort or Environment? Priorities and Determinants of Energy Efficiency Investments in Irish Households. *Journal of Consumer Policy,* 39**,** 159-186.

ARIKAN, M., SUCUOGLU, H. & MACIT, G. 2005. ECONOMIC ASSESSMENT OF THE SEISMIC RETROFITTING OF LOW-COST APARTMENT BUILDINGS. *Journal of Earthquake Engineering,* 9**,** 577-584.

ARIOSTO, T., MEMARI, A. M. & SOLNOSKY, R. L. 2019. Development of designer aids for energy efficient residential window retrofit solutions. *Sustainable Energy Technologies and Assessments,* 33**,** 1-13.

ASADI, E., SILVA, M. G. D., ANTUNES, C. H., DIAS, L. & GLICKSMAN, L. 2014. Multi-

objective optimization for building retrofit: A model using genetic algorithm and artificial neural network and an application. *Energy and Buildings,* 81**,** 444-456.

ASCIONE, F., BIANCO, N., DE MASI, R. F., MASTELLONE, M., MAURO, G. M. & VANOLI, G. P. 2020. The role of the occupant behavior in affecting the feasibility of energy refurbishment of residential buildings: Typical effective retrofits compromised by typical wrong habits. *Energy and Buildings,* 223**,** 110217.

ASCIONE, F., BIANCO, N., DE STASIO, C., MAURO, G. M. & VANOLI, G. P. 2017a. Artificial neural networks to predict energy performance and retrofit scenarios for any member of a building category: A novel approach. *Energy,* 118**,** 999-1017.

ASCIONE, F., BIANCO, N., DE STASIO, C., MAURO, G. M. & VANOLI, G. P. 2017b. CASA, cost-optimal analysis by multi-objective optimisation and artificial neural networks: A new framework for the robust assessment of cost-optimal energy retrofit, feasible for any building. *Energy and Buildings,* 146**,** 200-219.

ASCIONE, F., BIANCO, N., MAURO, G. M. & NAPOLITANO, D. F. 2019. Retrofit of villas on Mediterranean coastlines: Pareto optimization with a view to energy-efficiency and cost-effectiveness. *Applied Energy,* 254**,** 113705.

ASDRUBALI, F., BALDINELLI, G., BIANCHI, F. & CORNICCHIA, M. 2015. Experimental Performance Analyses of a Heat Recovery System for Mechanical Ventilation in Buildings. *Energy Procedia,* 82**,** 465-471.

ASHRAE 2013. Standard 55-2013 -- Thermal Environmental Conditions for Human Occupancy. ANSI/ASHRAE.

ASHRAFIAN, T., YILMAZ, A. Z., CORGNATI, S. P. & MOAZZEN, N. 2016. Methodology to define cost-optimal level of architectural measures for energy efficient retrofits of existing detached residential buildings in Turkey. *Energy and Buildings,* 120**,** 58-77.

ATANASIU, I. K. B. 2013. Implementing the cost-optimal methodology in eu countries-Lessons learned from case studies. Build. Perform. Insit. Eur. BPIE

AZAR, E., NIKOLOPOULOU, C. & PAPADOPOULOS, S. 2016. Integrating and optimizing metrics of sustainable building performance using human-focused agent-based modeling. *Applied Energy,* 183**,** 926-937.

BAELI, M. Oct 2013. *Residential Retrofit: Twenty Case Studies*, RIBA Publishing.

BAETENS, R., JELLE, B. P., GUSTAVSEN, A. & GRYNNING, S. 2010. Gas-filled panels for building applications: A state-of-the-art review. *Energy and Buildings,* 42**,** 1969-1975.

BAO, M., LIU, X., YANG, J. & BAO, Y. 2014. Novel hybrid vacuum/triple glazing units with pressure equalisation design. *Construction and Building Materials,* 73**,** 645-651.

BARBOSA, J. D. & AZAR, E. 2018. Modeling and implementing human-based energy retrofits in a green building in desert climate. *Energy and Buildings,* 173**,** 71-80.

BAUMHOF, R., DECKER, T., RÖDER, H. & MENRAD, K. 2018. Which factors determine the extent of house owners' energy-related refurbishment projects? A Motivation-Opportunity-Ability Approach. *Sustainable Cities and Society,* 36**,** 33-41.

BEN, H. & STEEMERS, K. 2014. Energy retrofit and occupant behaviour in protected housing: A case study of the Brunswick Centre in London. *Energy and Buildings,* 80**,** 120-130.

BENZAR, B.-E., PARK, M., LEE, H.-S., YOON, I. & CHO, J. 2020. Determining retrofit technologies for building energy performance. *Journal of Asian Architecture and Building Engineering,* 19**,** 367-383.

BERARDI, U. & MANCA, M. 2017. The Energy Saving and Indoor Comfort Improvements with Latent Thermal Energy Storage in Building Retrofits in Canada. *Energy Procedia,* 111**,** 462-471.

BERTHOU, T., STABAT, P., SALVAZET, R. & MARCHIO, D. 2014. Development and validation of a gray box model to predict thermal behavior of occupied office buildings. *Energy and Buildings,* 74**,** 91-100.

BEST, E. F. T. Available: https://www.everest.co.uk/double-glazing-windows/?gclid=Cj0KCQiA4b2MBhD2ARIsAIrcB-Tf7sPPf6Dh8zUebIxRtL-DQSxzm85DCuS3GvZatUdMgB2MVhKA4NcaApEbEALw_wcB&gclsrc=aw.ds [Accessed 13/11/2021].

BIRKHA MOHD ALI, S., HASANUZZAMAN, M., RAHIM, N. A., MAMUN, M. A. A. & OBAIDELLAH, U. H. 2021. Analysis of energy consumption and potential energy savings of an institutional building in Malaysia. *Alexandria Engineering Journal,* 60**,** 805-820.

BISWAS, K., PATEL, T., SHRESTHA, S., SMITH, D. & DESJARLAIS, A. 2019. Whole building retrofit using vacuum insulation panels and energy performance analysis. *Energy and Buildings,* 203**,** 109430.

BROWN, P., SWAN, W. & CHAHAL, S. 2014. Retrofitting social housing: reflections by tenants on adopting and living with retrofit technology. *Energy Efficiency,* 7**,** 641-653.

BUI, D.-K., NGUYEN, T. N., NGO, T. D. & NGUYEN-XUAN, H. 2020. An artificial neural network (ANN) expert system enhanced with the electromagnetism-based firefly algorithm (EFA) for predicting the energy consumption in buildings. *Energy,* 190**,** 116370.

BURNETT, D., BARBOUR, E. & HARRISON, G. 2014. The UK solar energy resource and the impact of climate change. *Renewable Energy,* 71**,** 333–343.

BUSINESS, E. A. I. S. C. U. 2017. Energy efficiency: building towards net zero.

CARNIELETTO, L., FERRANDO, M., TESO, L., SUN, K., ZHANG, W., CAUSONE, F., ROMAGNONI, P., ZARRELLA, A. & HONG, T. 2021. Italian prototype building models for urban scale building performance simulation. *Building and Environment,* 192**,** 107590.

CASCIO, E. L., MA, Z., BORELLI, D. & SCHENONE, C. 2017. Residential Building Retrofit through Numerical Simulation: A Case Study. *Energy Procedia,* 111**,** 91-100.

CASKEY, S. L. & GROLL, E. A. 2018. Hybrid air-hydronic HVAC performance in a residential net-zero energy retrofit. *Energy and Buildings,* 158**,** 342-355.

CATALINA, T., IORDACHE, V. & CARACALEANU, B. 2013. Multiple regression model for fast prediction of the heating energy demand. *Energy and Buildings,* 57**,** 302-312.

CATRINI, P., PANNO, D., CARDONA, F. & PIACENTINO, A. 2020. Characterization of cooling loads in the wine industry and novel seasonal indicator for reliable assessment of energy saving through retrofit of chillers. *Applied Energy,* 266**,** 114856.

CHANGE, D. O. E. C. 2015. UK progress towards GHG emissions reduction targets.

CHARLES, A., MAREF, W. & OUELLET-PLAMONDON, C. M. 2019. Case study of the upgrade of an existing office building for low energy consumption and low carbon emissions. *Energy and Buildings,* 183**,** 151-160.

CHEN, S., GUAN, J., LEVINE, M. D., HAIYING, L. & YOWARGANA, P. 2015a. Evaluation on Retrofit of One Existing Residential Building in North China: Energy Saving, Environmental and Economic Benefits. *Procedia Engineering,* 121**,** 3-10.

CHEN, X., QU, K., CALAUTIT, J., EKAMBARAM, A., LU, W., FOX, C., GAN, G. & RIFFAT, S. 2019a. Multi-Criteria Assessment Approach for a Residential Building Retrofit

in Norway. *Energy and Buildings*, 109668.
CHEN, X., QU, K., CALAUTIT, J., EKAMBARAM, A., LU, W., FOX, C., GAN, G. & RIFFAT, S. 2020. Multi-criteria assessment approach for a residential building retrofit in Norway. *Energy and Buildings,* 215, 109668.
CHEN, X., SU, Y., AYDIN, D., DING, Y., ZHANG, S., REAY, D. & RIFFAT, S. 2018. A novel evaporative cooling system with a polymer hollow fibre spindle. *Applied Thermal Engineering,* 132, 665-675.
CHEN, X., SU, Y., AYDIN, D., REAY, D., LAW, R. & RIFFAT, S. 2016a. Experimental investigations of polymer hollow fibre heat exchangers for building heat recovery application. *Energy and Buildings,* 125, 99-108.
CHEN, X., SU, Y., REAY, D. & RIFFAT, S. 2016b. Recent research developments in polymer heat exchangers – A review. *Renewable and Sustainable Energy Reviews,* 60, 1367-1386.
CHEN, X., ZHANG, N., SU, Y., AYDIN, D., ZHENG, H., BAI, H., GEORGAKIS, A., JARIMI, H. & RIFFAT, S. 2019b. Performance analysis and design implementation of a novel polymer hollow fiber liquid desiccant dehumidifier with aqueous potassium formate. *Thermal Science and Engineering Progress,* 13, 100366.
CHEN, Z., CHEN, Z., YANG, Z., HU, J., YANG, Y., CHANG, L., LEE, L. J. & XU, T. 2015b. Preparation and characterization of vacuum insulation panels with super-stratified glass fiber core material. *Energy,* 93, 945-954.
CHO, H. M., YANG, S., WI, S., CHANG, S. J. & KIM, S. 2020a. Hygrothermal and energy retrofit planning of masonry façade historic building used as museum and office: A cultural properties case study. *Energy,* 201, 117607.
CHO, H. M., YUN, B. Y., YANG, S., WI, S., CHANG, S. J. & KIM, S. 2020b. Optimal energy retrofit plan for conservation and sustainable use of historic campus building: Case of cultural property building. *Applied Energy,* 275, 115313.
CHOI, H.-J., AHN, H., CHOI, G.-S., KANG, J.-S. & HUH, J.-H. 2021. Analysis of Long-Term Change in the Thermal Resistance of Extruded Insulation Materials through Accelerated Tests. *Applied Sciences,* 11.
CHOW, T. T., PEI, G., FONG, K. F., LIN, Z., CHAN, A. L. S. & HE, M. 2010. Modeling and application of direct-expansion solar-assisted heat pump for water heating in subtropical Hong Kong. *Applied Energy,* 87, 643-649.
CHRISTERSSON, M., VIMPARI, J. & JUNNILA, S. 2015. Assessment of financial potential of real estate energy efficiency investments–A discounted cash flow approach. *Sustainable Cities and Society,* 18, 66-73.
CISTERNAS, L. A. & LAM, E. J. 1991. An analytic correlation for the vapour pressure of aqueous and non-aqueous solutions of single and mixed electrolytes. Part II. Application and extension. *Fluid Phase Equilibria,* 62, 11-27.
CLARK, D. May 4, 2021. *Average hourly labor cost in selected European countries in 2020* [Online]. Available: https://www.statista.com/statistics/1211601/hourly-labor-cost-in-europe/ [Accessed].
COMMISION, E. 2016. Policy Departmernt Economic and Scientific policy. *In:* INDUSTRY, R. A. E. (ed.).
COMMISSION, E. Renovation Wave: CoR and EU Commission launch cooperation to boost building overhaul. *In:* REPRESENTATIVES, T. E. S. A. O. R. A. L. (ed.).
COMMISSION, E. Summary of the Impact Assessment accompanying the proposal for a recast of the EPBD.
COMMISSION, E. 2002. Directive 2002/91/EC of the European Parliament on the Energy Performance of Buildings.
CRAWLEY, D. B., LAWRIE, L. K., WINKELMANN, F. C., BUHL, W. F., HUANG, Y. J.,

PEDERSEN, C. O., STRAND, R. K., LIESEN, R. J., FISHER, D. E., WITTE, M. J. & GLAZER, J. 2001. EnergyPlus: creating a new-generation building energy simulation program. *Energy and Buildings,* 33**,** 319-331.

CRISTOFARI, C., NORVAIŠIENĖ, R., CANALETTI, J. L. & NOTTON, G. 2015. Innovative alternative solar thermal solutions for housing in conservation-area sites listed as national heritage assets. *Energy and Buildings,* 89**,** 123-131.

D'AGOSTINO, D., ZANGHERI, P. & CASTELLAZZI, L. 2017. Towards Nearly Zero Energy Buildings in Europe: A Focus on Retrofit in Non-Residential Buildings. *Energies,* 10**,** 117.

DAIKIN. Available: https://www.daikin.co.uk/en_gb/product-group/air-to-water-heat-pump-high-temperature.html [Accessed 13/11/2021].

DAVIDSON, R. 23rd March 2018. *CHANGES TO EPC REGULATIONS – 1ST APRIL 2018* [Online]. Available: https://www.burnetts.co.uk/publications/blogs/changes-to-epc-regulations-1-april-2018 [Accessed].

DEB, C., DAI, Z. & SCHLUETER, A. 2021. A machine learning-based framework for cost-optimal building retrofit. *Applied Energy,* 294**,** 116990.

DEB, C. & SCHLUETER, A. 2021. Review of data-driven energy modelling techniques for building retrofit. *Renewable and Sustainable Energy Reviews,* 144**,** 110990.

DELMASTRO, C., MUTANI, G. & CORGNATI, S. P. 2016. A supporting method for selecting cost-optimal energy retrofit policies for residential buildings at the urban scale. *Energy Policy,* 99**,** 42-56.

DESIDERI, U., ARCIONI, L., LEONARDI, D., CESARETTI, L., PERUGINI, P., AGABITINI, E. & EVANGELISTI, N. 2013. Design of a multipurpose "zero energy consumption" building according to European Directive 2010/31/EU: Architectural and technical plants solutions. *Energy,* 58**,** 157-167.

DODOO, A., GUSTAVSSON, L. & TETTEY, U. Y. A. 2017. Final energy savings and cost-effectiveness of deep energy renovation of a multi-storey residential building. *Energy,* 135**,** 563-576.

DROUTSA, K. G., KONTOYIANNIDIS, S., DASCALAKI, E. G. & BALARAS, C. A. 2016. Mapping the energy performance of hellenic residential buildings from EPC (energy performance certificate) data. *Energy,* 98**,** 284-295.

EBRAHIMPOUR, A. & MAEREFAT, M. 2011. Application of advanced glazing and overhangs in residential buildings. *Energy Conversion and Management,* 52**,** 212-219.

ECONOMICS, T. 2021. *Italy Inflation Rate* [Online]. Available: https://tradingeconomics.com/italy/inflation-cpi [Accessed].

ECONOMIDOU, M., ATANASIU, B., STANIASZEK, D., MAIO, J., NOLTE, I., RAPF, O., LAUSTSEN, J., RUYSSEVELT, P., STRONG, D. & ZINETTI, S. 2011. *Europe's buildings under the microscope. A country-by-country review of the energy performance of buildings*.

ECOTHERM. Available: https://www.ecotherm.co.uk/products [Accessed 13/11/2021].

ELMER, T. 2017. Appendix A Potassium Formate Property Calculations.

ELNOZAHY, A., RAHMAN, A. K. A., ALI, A. H. H., ABDEL-SALAM, M. & OOKAWARA, S. 2015. Performance of a PV module integrated with standalone building in hot arid areas as enhanced by surface cooling and cleaning. *Energy and Buildings,* 88**,** 100-109.

ELSHARKAWY, H. & RUTHERFORD, P. 2015. Retrofitting social housing in the UK: Home energy use and performance in a pre-Community Energy Saving Programme (CESP). *Energy and Buildings,* 88**,** 25-33.

ELSHARKAWY, H. & RUTHERFORD, P. 2018. Energy-efficient retrofit of social housing

in the UK: Lessons learned from a Community Energy Saving Programme (CESP) in Nottingham. *Energy and Buildings,* 172**,** 295-306.
ENERGY, A. Available: http://arkaya.co.uk/ [Accessed 13/11/2021].
ENERGY SAVING TRUST. 2007. *Energy saving trust* [Online]. Available: http://www.icax.co.uk/pdf/Domestic_Ground_Source_Heat_Pumps_Design_Installation.pdf [Accessed].
ERDMANN, C. 2002. Indoor carbon dioxide concentrations and sick building syndrome symptoms in the BASE study revisited: Analyses of the 100 building dataset. *Proceedings of Indoor Air 2002,* 3.
ERGONOMICS OF THE PHYSICAL ENVIRONMENT 2005. Ergonomics of the thermal environment. *Analytical determination and interpretation of thermal comfort using calculation of the PMV and PPD indices and local thermal comfort criteria.* ISO.
EUR-LEX 2018. DIRECTIVE (EU) 2018/844 OF THE EUROPEAN PARLIAMENT AND OF THE COUNCIL of 30 May 2018 amending Directive 2010/31/EU on the energy performance of buildings and Directive 2012/27/EU on energy efficiency. *In:* DIRECTIVE, B. P. O. B. A. (ed.). Ofiicial journal of the European Union.
EUR-LEX 2019. Commission Recommendation (EU) 2019/786 of 8 May 2019 on building renovation. Official Journal of the European Union: European Commission.
EUREOPEAN COMMISSION 2018. Energy performance of buildings. *In:* COMMISSION, E. (ed.). Energy.
EUROPEAN COMMISSION 2007a. 2020 climate & energy package.
EUROPEAN COMMISSION 2007b. 2050 climate & energy package.
EUROPEAN COMMISSION 2011. A Roadmap for moving to a competitive low carbon economy in 2050 EUROPEAN COMMISSION
EUROSTAT 2016. Greenhouse gas emissions per capita. Eurostat: European Commission.
EUROSTAT. 2019. *Hourly labour costs* [Online]. Eurostat. Available: https://ec.europa.eu/eurostat/statistics-explained/index.php/Hourly_labour_costs [Accessed 31 March 2020].
FAN, J., CHEN, Z., FURBO, S., PERERS, B. & KARLSSON, B. 2009. Efficiency and lifetime of solar collectors for solar heating plants. *29th ISES Biennial Solar World Congress 2009, ISES 2009,* 1**,** 331-340.
FAN, Y. & XIA, X. 2018. Building retrofit optimization models using notch test data considering energy performance certificate compliance. *Applied Energy,* 228**,** 2140-2152.
FANG, Y., HYDE, T., HEWITT, N., EAMES, P. C. & NORTON, B. 2010. Thermal performance analysis of an electrochromic vacuum glazing with low emittance coatings. *Solar Energy,* 84**,** 516-525.
FANG, Y., HYDE, T. J., ARYA, F., HEWITT, N., WANG, R. & DAI, Y. 2015. Enhancing the thermal performance of triple vacuum glazing with low-emittance coatings. *Energy and Buildings,* 97**,** 186-195.
FANTUCCI, S., FENOGLIO, E., GROSSO, G., SERRA, V., PERINO, M., MARINO, V. & DUTTO, M. 2019. Development of an aerogel-based thermal coating for the energy retrofit and the prevention of condensation risk in existing buildings. *Science and Technology for the Built Environment,* 25**,** 1178-1186.
FINCK, C., LI, R. & ZEILER, W. 2019. Economic model predictive control for demand flexibility of a residential building. *Energy,* 176**,** 365-379.
FLECKINGER, P., GLACHANT, M. & TAMOKOUÉ KAMGA, P.-H. 2019. Energy Performance Certificates and investments in building energy efficiency: A

theoretical analysis. *Energy Economics,* 84**,** 104604.
FONTAN, J. Feb 6, 2021. *Single Family House Definition* [Online]. Available: https://fontanarchitecture.com/single-family-house-definition/ [Accessed Feb 13 2022].
FRANCISCO PINTO, J. & CARRILHO DA GRAÇA, G. 2018. Comparison between geothermal district heating and deep energy refurbishment of residential building districts. *Sustainable Cities and Society,* 38**,** 309-324.
FRANCO, G., MAGRINI, A., CARTESEGNA, M. & GUERRINI, M. 2015. Towards a systematic approach for energy refurbishment of historical buildings. The case study of Albergo dei Poveri in Genoa, Italy. *Energy and Buildings,* 95**,** 153-159.
GANGOLELLS, M., CASALS, M., FERRÉ-BIGORRA, J., FORCADA, N., MACARULLA, M., GASPAR, K. & TEJEDOR, B. 2020. Office representatives for cost-optimal energy retrofitting analysis: A novel approach using cluster analysis of energy performance certificate databases. *Energy and Buildings,* 206**,** 109557.
GARCÍA KERDAN, I., RASLAN, R. & RUYSSEVELT, P. 2016. An exergy-based multi-objective optimisation model for energy retrofit strategies in non-domestic buildings. *Energy,* 117**,** 506-522.
GHAZI WAKILI, K., BINDER, B., ZIMMERMANN, M. & TANNER, C. 2014. Efficiency verification of a combination of high performance and conventional insulation layers in retrofitting a 130-year old building. *Energy and Buildings,* 82**,** 237-242.
GHOSH, A. & NORTON, B. 2018. Advances in switchable and highly insulating autonomous (self-powered) glazing systems for adaptive low energy buildings. *Renewable Energy,* 126**,** 1003-1031.
GHOSH, A., NORTON, B. & DUFFY, A. 2017. Effect of atmospheric transmittance on performance of adaptive SPD-vacuum switchable glazing. *Solar Energy Materials and Solar Cells,* 161**,** 424-431.
GHOSH, A., SUNDARAM, S. & MALLICK, T. K. 2018. Investigation of thermal and electrical performances of a combined semi-transparent PV-vacuum glazing. *Applied Energy,* 228**,** 1591-1600.
GLASS, L. T. V. I. Available: https://www.landvac.net/vacuumglass/glasslist_one.html?gclid=Cj0KCQiA4b2MBhD2ARIsAIrcB-Tla84gE6czH70t8-WZdVDuQEma2mHr9qV0000oPrCdUYkLI-bXgeUaAjamEALw_wcB [Accessed 13/11/2021].
GODWIN, P. J. 2011. Building Conservation and Sustainability in the United Kingdom. *Procedia Engineering,* 20**,** 12-21.
GOUDA, M. M., DANAHER, S. & UNDERWOOD, C. P. 2000. Low-order model for the simulation of a building and its heating system. *Building Services Engineering Research and Technology,* 21**,** 199-208.
GOYAL, S. & BAROOAH, P. 2012. A method for model-reduction of non-linear thermal dynamics of multi-zone buildings. *Energy and Buildings,* 47**,** 332-340.
GUO, Y., WANG, J., CHEN, H., LI, G., LIU, J., XU, C., HUANG, R. & HUANG, Y. 2018. Machine learning-based thermal response time ahead energy demand prediction for building heating systems. *Applied Energy,* 221**,** 16-27.
GUSTAFSSON, S.-I. 1998. Mixed integer linear programming and building retrofits. *Energy and Buildings,* 28**,** 191-196.
HABIBI, S. 2017. Micro-climatization and real-time digitalization effects on energy efficiency based on user behavior. *Building and Environment,* 114**,** 410-428.
HADDAD, S., BARKER, A., YANG, J., KUMAR, D. I. M., GARSHASBI, S., PAOLINI, R. & SANTAMOURIS, M. 2020. On the potential of building adaptation measures to

counterbalance the impact of climatic change in the tropics. *Energy and Buildings,* 229**,** 110494.

HAFFNER, K. D. A. M. September 2010. Housing Statistics in the European Union 2010. Delft University of Technology: OTB Research Institute for the Built Environment.

HAMDAOUI, M.-A., BENZAAMA, M.-H., EL MENDILI, Y. & CHATEIGNER, D. 2021. A review on physical and data-driven modeling of buildings hygrothermal behavior: Models, approaches and simulation tools. *Energy and Buildings,* 251**,** 111343.

HARRISON, S. 2017. The Potential and Challenges of Solar Boosted Heat Pumps for Domestic Hot Water Heating. *12th IEA heat pump conference.*

HASILA JARIMI , K. Q., SHIHAO ZHANG, QINGHUA LV, JUN LIAO, BENYUAN CHEN, HUI LV, CHUNFU CHENG, JIN LI, YUEHONG SU, SHIJIE DONG, SAFFA RIFFAT 2020. Performance Analysis of a Hybrid Thin Film Photovoltaic (PV) Vacuum Glazing. *Future Cities and Environment*.

HE, Y., LIAO, N., BI, J. & GUO, L. 2019. Investment decision-making optimization of energy efficiency retrofit measures in multiple buildings under financing budgetary restraint. *Journal of Cleaner Production,* 215**,** 1078-1094.

HIRST, E., WHITE, D. & GOELTZ, R. 1985. Indoor temperature changes in retrofit homes. *Energy,* 10**,** 861-870.

HONG, J., CHEN, W., QI, C., YE, L. & XU, C. 2016. Life cycle assessment of multicrystalline silicon photovoltaic cell production in China. *Solar Energy,* 133**,** 283-293.

HROVATIN, N. & ZORIĆ, J. 2018. Determinants of energy-efficient home retrofits in Slovenia: The role of information sources. *Energy and Buildings,* 180.

HU, X., XIANG, Y., ZHANG, H., LIN, Q., WANG, W. & WANG, H. 2021. Active–passive combined energy-efficient retrofit of rural residence with non-benchmarked construction: A case study in Shandong province, China. *Energy Reports,* 7**,** 1360-1373.

HUANG, S.-M., ZHANG, L.-Z., TANG, K. & PEI, L.-X. 2012. Fluid flow and heat mass transfer in membrane parallel-plates channels used for liquid desiccant air dehumidification. *International Journal of Heat and Mass Transfer,* 55**,** 2571-2580.

HUANG, S.-M., ZHONG, Z. & YANG, M. 2016. Conjugate heat and mass transfer in an internally-cooled membrane-based liquid desiccant dehumidifier (IMLDD). *Journal of Membrane Science,* 508**,** 73-83.

HULME, M. 2016. 1.5 °C and climate research after the Paris Agreement. *Nature Clim Change* 6**,** 222-224.

HWANG, B.-G., SHAN, M., XIE, S. & CHI, S. 2017. Investigating residents' perceptions of green retrofit program in mature residential estates: The case of Singapore. *Habitat International,* 63**,** 103-112.

IBN-MOHAMMED, T., GREENOUGH, R., TAYLOR, S., OZAWA-MEIDA, L. & ACQUAYE, A. 2014. Integrating economic considerations with operational and embodied emissions into a decision support system for the optimal ranking of building retrofit options. *Building and Environment,* 72**,** 82-101.

IBROAD June 2020. Beyond the single-family house. *Potential extension of iBRoad to other building types.* ifeu – Institute for Energy and Environmental Research.

INSTITUTE, G. F. May 2020. Financing energy efficient buildings: the path to retrofit at scale.

INTERGOVERNMENTAL PANEL ON CLIMATE CHANGE 2018. Special report on the impacts of global warming of 1.5°C. IPCC.

ITO, S., MIURA, N. & TAKANO, Y. 2005. Studies of Heat Pumps Using Direct Expansion Type Solar Collectors. *Journal of Solar Energy Engineering,* 127**,** 60-64.

ITO, S., MIURA, N. & WANG, K. 1999. PERFORMANCE OF A HEAT PUMP USING DIRECT EXPANSION SOLAR COLLECTORS1Paper presented at the ISES Solar World Congress, Taejon, South Korea, 24–29 August 1997.1. *Solar Energy,* 65**,** 189-196.

JAFARI, A. & VALENTIN, V. 2017. An optimization framework for building energy retrofits decision-making. *Building and Environment,* 115**,** 118-129.

JAMES WELTY, G. L. R., DAVID G. FOSTER 2006. *Fundamentals of Momentum, Heat and Mass Transfer, 6th Edition,* New York, Wiley.

JANKOVIC, L. 2019. Lessons learnt from design, off-site construction and performance analysis of deep energy retrofit of residential buildings. *Energy and Buildings,* 186**,** 319-338.

JELLE, B. P. 2011. Traditional, state-of-the-art and future thermal building insulation materials and solutions – Properties, requirements and possibilities. *Energy and Buildings,* 43**,** 2549-2563.

JERMYN, D. & RICHMAN, R. 2016. A process for developing deep energy retrofit strategies for single-family housing typologies: Three Toronto case studies. *Energy and Buildings,* 116**,** 522-534.

JI, Y., XU, P., DUAN, P. & LU, X. 2016. Estimating hourly cooling load in commercial buildings using a thermal network model and electricity submetering data. *Applied Energy,* 169**,** 309-323.

JONES, R. 1st April, 2018. *Are some landlords bending energy efficiency rules?* [Online]. Available: https://www.theguardian.com/money/2018/jun/23/rent-property-energy-efficiency-rating-score-fraud [Accessed].

KALOGIROU, S. A. 2014. Chapter 4 - Performance of Solar Collectors. *In:* KALOGIROU, S. A. (ed.) *Solar Energy Engineering (Second Edition).* Boston: Academic Press.

KATO, K., HIBINO, T., KOMOTO, K., IHARA, S., YAMAMOTO, S. & FUJIHARA, H. 2001. A life-cycle analysis on thin-film CdS/CdTe PV modules. *Solar Energy Materials and Solar Cells,* 67**,** 279-287.

KATSURA, T., MEMON, S., RADWAN, A., NAKAMURA, M. & NAGANO, K. 2020. Thermal performance analysis of a new structured-core translucent vacuum insulation panel in comparison to vacuum glazing: Experimental and theoretically validated analyses. *Solar Energy,* 199**,** 326-346.

KHADRA, A., HUGOSSON, M., AKANDER, J. & MYHREN, J. A. 2020. Development of a Weight Factor Method for Sustainability Decisions in Building Renovation. Case Study Using Renobuild. *Sustainability,* 12.

KHATIB, H. 2012. IEA world energy outlook 2011: a comment. *Energy Policy,* 48**,** 737-743.

KHAYATIAN, F., SARTO, L. & DALL'O, G. 2017. Building energy retrofit index for policy making and decision support at regional and national scales. *Applied Energy,* 206**,** 1062-1075.

KHAYATIAN, F., SARTO, L. & DALL'O', G. 2016. Application of neural networks for evaluating energy performance certificates of residential buildings. *Energy and Buildings,* 125**,** 45-54.

KIM, J.-H., BOAFO, F. E., KIM, S.-M. & KIM, J.-T. 2017. Aging performance evaluation of vacuum insulation panel (VIP). *Case Studies in Construction Materials,* 7**,** 329-335.

KINGSPAN. Available: https://www.kingspan.com/gb/en-gb/products/insulation-boards/insulation-boards/optim-r [Accessed 13/11/2021].

KOEBEL, M. M., MANZ, H., EMANUEL MAYERHOFER, K. & KELLER, B. 2010. Service-life

limitations in vacuum glazing: A transient pressure balance model. *Solar Energy Materials and Solar Cells,* 94**,** 1015-1024.
KOULOUMPI, B. A. I. 2013. Implementing the cost-optimal methodology in EU countries. *Lessons learned from three case studies.* The Buildings Performance Institute Europe (BPIE).
KUANG, Y. H. & WANG, R. Z. 2006. Performance of a multi-functional direct-expansion solar assisted heat pump system. *Solar Energy,* 80**,** 795-803.
KUMAR, Y. & SAXENA, D. 2020. *A Review on Starch Aerogel: Application and Future Trends*.
KUUSK, K., KALAMEES, T. & MAIVEL, M. 2014. Cost effectiveness of energy performance improvements in Estonian brick apartment buildings. *Energy and Buildings,* 77**,** 313-322.
KYLILI, A. & FOKAIDES, P. A. 2015. European smart cities: The role of zero energy buildings. *Sustainable Cities and Society,* 15**,** 86-95.
LAW, H. 2018. *NEW EPC REGULATIONS COMING INTO FORCE FROM 1 APRIL 2018 – WHAT DO LANDLORDS NEED TO DO?* [Online]. Available: https://helix-law.co.uk/property-law-blogs/new-epc-regulations-coming-into-force-from-1-april-2018-what-do-landlords-need-to-do/ [Accessed].
LEONFORTE, F., MIGLIOLI, A., DEL PERO, C., ASTE, N., CRISTIANI, N., CROCI, L. & BESAGNI, G. 2022. Design and performance monitoring of a novel photovoltaic-thermal solar-assisted heat pump system for residential applications. *Applied Thermal Engineering,* 210**,** 118304.
LI, Y., KUBICKI, S., GUERRIERO, A. & REZGUI, Y. 2019. Review of building energy performance certification schemes towards future improvement. *Renewable and Sustainable Energy Reviews,* 113**,** 109244.
LI, Y., O'NEILL, Z., ZHANG, L., CHEN, J., IM, P. & DEGRAW, J. 2021. Grey-box modeling and application for building energy simulations - A critical review. *Renewable and Sustainable Energy Reviews,* 146**,** 111174.
LIOR, N. 2012. Sustainable energy development (May 2011) with some game-changers. *Energy,* 40**,** 3-18.
LOHSE, R., STALLER, H. & RIEL, M. 2016. The economic challenges of deep energy renovation--differences, similarities, and possible solutions in Central Europe: Austria and Germany. *ASHRAE Transactions,* 122**,** 69+.
LORENZATI, A., FANTUCCI, S., CAPOZZOLI, A. & PERINO, M. 2017. The Effect of Temperature on Thermal Performance of Fumed Silica Based Vacuum Insulation Panels for Buildings. *Energy Procedia,* 111**,** 490-499.
LOWE, R. & CHIU, L. F. 2020. Innovation in deep housing retrofit in the United Kingdom: The role of situated creativity in transforming practice. *Energy Research & Social Science,* 63**,** 101391.
LRG., W. 2006. *La consommation énergétique de nos bâtiments, un enjeu crucial pour l'avenir* [Online]. Available: http://energiewalloniebe [Accessed].
LUO, J., ROHN, J., XIANG, W., BERTERMANN, D. & BLUM, P. 2016. A review of ground investigations for ground source heat pump (GSHP) systems. *Energy and Buildings,* 117**,** 160-175.
MA, Z., COOPER, P., DALY, D. & LEDO, L. 2012. Existing building retrofits: Methodology and state-of-the-art. *Energy and Buildings,* 55**,** 889-902.
MAROSA. *VAT in Italy* [Online]. Available: https://marosavat.com/manual/vat/italy/ [Accessed].
MARSHALL, J. W., IAN 1986. *The Victorian House,* London: Sidgwick and Jackson Limited.
MARTEK, I., HOSSEINI, M. R., SHRESTHA, A., EDWARDS, D. J., SEATON, S. & COSTIN, G.

2019. End-user engagement: The missing link of sustainability transition for Australian residential buildings. *Journal of Cleaner Production,* 224**,** 697-708.
MATOSOVIĆ, M. & TOMŠIĆ, Ž. 2018. Evaluating homeowners' retrofit choices – Croatian case study. *Energy and Buildings,* 171**,** 40-49.
MAYER, Z., VOLK, R. & SCHULTMANN, F. 2022. Analysis of financial benefits for energy retrofits of owner-occupied single-family houses in Germany. *Building and Environment,* 211**,** 108722.
MAYORS, C. O. Technical annex to the SEAP template instructions document: THE EMISSION FACTORS.
MAZZARELLA, L. 2015. Energy retrofit of historic and existing buildings. The legislative and regulatory point of view. *Energy and Buildings,* 95**,** 23-31.
MCARTHUR, J. J. & JOFEH, C. G. H. 2016. Portfolio retrofit evaluation: A methodology for optimizing a large number of building retrofits to achieve triple-bottom-line objectives. *Sustainable Cities and Society,* 27**,** 263-274.
MCKINLEY, T. L., & ALLEYNE, A. G 2008. Identification of building model parameters and loads using on-site data logs. *Proceedings of SimBuild.*
MEMON, S. 2017. Experimental measurement of hermetic edge seal's thermal conductivity for the thermal transmittance prediction of triple vacuum glazing. *Case Studies in Thermal Engineering,* 10**,** 169-178.
MEMON, S. & EAMES, P. C. 2017. Predicting the solar energy and space-heating energy performance for solid-wall detached house retrofitted with the composite edge-sealed triple vacuum glazing. *Energy Procedia,* 122**,** 565-570.
MEMON, S., FANG, Y. & EAMES, P. C. 2019. The influence of low-temperature surface induction on evacuation, pump-out hole sealing and thermal performance of composite edge-sealed vacuum insulated glazing. *Renewable Energy,* 135**,** 450-464.
MENZIES, G. & WHERRETT, J. R. 2005. Multiglazed windows: Potential for savings in energy, emissions and cost. *Building Services Engineering Research & Technology - BUILD SERV ENG RES TECHNOL,* 26**,** 249-258.
MICHAEL, M., ZHANG, L. & XIA, X. 2017. An optimal model for a building retrofit with LEED standard as reference protocol. *Energy and Buildings,* 139**,** 22-30.
MICHAŁ PIASECKI , E. Z. R.-Z., PIOTR CZERSKI , MAŁGORZATA FEDORCZAK-CISAK , MICHAŁ ZIELINA , PAWEŁ KRZY´SCIAK , & GRZE´SKOWIAK, P. K. S.-S. A. W. 19 November 2020. Implementation of the Indoor Environmental Quality (IEQ) Model for the Assessment of a Retrofitted Historical Masonry Building. *Energies*.
MIKULIĆ, D., BAKARIĆ, I. R. & SLIJEPČEVIĆ, S. 2016. The economic impact of energy saving retrofits of residential and public buildings in Croatia. *Energy Policy,* 96**,** 630-644.
MILLS, E. & ROSENFELD, A. 1996. Consumer non-energy benefits as a motivation for making energy-efficiency improvements. *Energy,* 21**,** 707-720.
MILSOM, E. 2016. Solid wall heat losses and the potential for energy saving. *In situ U-value measurement method review.* Building Research Establishment Ltd. (BRE)
MINISTRY OF HOUSING, C. L. G. 2019. English Housing Survey 2018 to 2019: headline report. *In:* STATISTICS, N. (ed.).
MIU, L. & HAWKES, A. D. 2020. Private landlords and energy efficiency: Evidence for policymakers from a large-scale study in the United Kingdom. *Energy Policy,* 142**,** 111446.
MONTANA, F., KANAFANI, K., WITTCHEN, K. B., BIRGISDOTTIR, H., LONGO, S., CELLURA, M. & RIVA SANSEVERINO, E. 2020. Multi-Objective Optimization of Building

Life Cycle Performance. A Housing Renovation Case Study in Northern Europe. *Sustainability,* 12.

MORELLI, M., RØNBY, L., MIKKELSEN, S. E., MINZARI, M. G., KILDEMOES, T. & TOMMERUP, H. M. 2012. Energy retrofitting of a typical old Danish multi-family building to a "nearly-zero" energy building based on experiences from a test apartment. *Energy and Buildings,* 54**,** 395-406.

MURPHY, M. D., O'SULLIVAN, P. D., CARRILHO DA GRAÇA, G. & O'DONOVAN, A. 2021. Development, Calibration and Validation of an Internal Air Temperature Model for a Naturally Ventilated Nearly Zero Energy Building: Comparison of Model Types and Calibration Methods. *Energies,* 14.

MURRAY, F. W. 1966. *On the Computation of Saturation Vapor Pressure,* Santa Monica, CA, RAND Corporation.

MURRAY, S. N., ROCHER, B. & O'SULLIVAN, D. T. J. 2012. Static Simulation: A sufficient modelling technique for retrofit analysis. *Energy and Buildings,* 47**,** 113-121.

MURTAGH, N., GATERSLEBEN, B. & FIFE-SCHAW, C. 2019. Occupants' motivation to protect residential building stock from climate-related overheating: A study in southern England. *Journal of Cleaner Production,* 226**,** 186-194.

MURTAGH, N., GATERSLEBEN, B. & FIFE-SCHAW, C 2019. Occupants' motivation to protect residential building stock from climate-related overheating: A study in southern England. *Journal of Cleaner Production, 226, 186-194.*

MUTANI, G. & TODESCHI, V. 2020. Building energy modeling at neighborhood scale. *Energy Efficiency,* 13**,** 1353-1386.

NARDELLI, A., DEUSCHLE, E., DE AZEVEDO, L. D., PESSOA, J. L. N. & GHISI, E. 2017. Assessment of Light Emitting Diodes technology for general lighting: A critical review. *Renewable and Sustainable Energy Reviews,* 75**,** 368-379.

NATIONS;, U. 2015. PARIS AGREEMENT. *In:* NATIONS, U. (ed.).

NIEMELÄ, T., KOSONEN, R. & JOKISALO, J. 2017. Energy performance and environmental impact analysis of cost-optimal renovation solutions of large panel apartment buildings in Finland. *Sustainable Cities and Society,* 32**,** 9-30.

NIŽETIĆ, S., ČOKO, D., YADAV, A. & GRUBIŠIĆ-ČABO, F. 2016. Water spray cooling technique applied on a photovoltaic panel: The performance response. *Energy Conversion and Management,* 108**,** 287-296.

Ó BROIN, E., MATA, É., GÖRANSSON, A. & JOHNSSON, F. 2013. The effect of improved efficiency on energy savings in EU-27 buildings. *Energy,* 57**,** 134-148.

O'DELL, M. P., MITCHELL, J. W. & BECKMAN, W. A. 1984. Design Method and Performance of Heat Pumps With Refrigerant-Filled Solar Collectors. *Journal of Solar Energy Engineering,* 106**,** 159-164.

OPHER, T., DUHAMEL, M., POSEN, I. D., PANESAR, D. K., BRUGMANN, R., ROY, A., ZIZZO, R., SEQUEIRA, L., ANVARI, A. & MACLEAN, H. L. 2021. Life cycle GHG assessment of a building restoration: Case study of a heritage industrial building in Toronto, Canada. *Journal of Cleaner Production,* 279**,** 123819.

ORGANIZATION, E. V. *International Performance Measurement and Verification Protocol (IPMVP)* [Online]. Available: https://evo-world.org/en/products-services-mainmenu-en/protocols/ipmvp [Accessed].

ORTIZ, J., FONSECA I CASAS, A., SALOM, J., GARRIDO SORIANO, N. & FONSECA I CASAS, P. 2016. Cost-effective analysis for selecting energy efficiency measures for refurbishment of residential buildings in Catalonia. *Energy and Buildings,* 128**,** 442-457.

PAPADOPOULOS, A. M. 2005. State of the art in thermal insulation materials and aims for future developments. *Energy and Buildings,* 37**,** 77-86.

PAPADOPOULOS, S. & AZAR, E. 2016. Integrating building performance simulation in

agent-based modeling using regression surrogate models: A novel human-in-the-loop energy modeling approach. *Energy and Buildings,* 128**,** 214-223.

PAPADOPOULOS, S., AZAR, E., WOON, W. & KONTOKOSTA, C. 2017. Evaluation of tree-based ensemble learning algorithms for building energy performance estimation. *Journal of Building Performance Simulation***,** 1-11.

PARLIAMENT, E. 2010. Directive 2010/31/EU of 19 May 2010 on the energy performance of buildings. *In:* (EPBD), E. C. E. (ed.).

PARLIAMENT, E. C. A. January 2012 supplementing Directive 2010/31/EU of the European Parliament and of the Council on the energy performance of buildings.

PÉREZ-LOMBARD, L., ORTIZ, J., CORONEL, J. & MAESTRE, I. 2011. A review of HVAC systems requirements in building energy regulations. *Energy and Buildings,* 43**,** 255-268.

PÉREZ-LOMBARD, L., ORTIZ, J. & POUT, C. 2008. A review on buildings energy consumption information. *Energy and Buildings,* 40**,** 394-398.

PHILIPS. Available: https://www.lighting.philips.co.uk/prof/led-lamps-and-tubes/led-tubes [Accessed 13/11/2021].

PISELLO, A. L. & ASDRUBALI, F. 2014. Human-based energy retrofits in residential buildings: A cost-effective alternative to traditional physical strategies. *Applied Energy,* 133**,** 224-235.

POKHREL, S. R., HEWAGE, K., CHHIPI-SHRESTHA, G., KARUNATHILAKE, H., LI, E. & SADIQ, R. 2021. Carbon capturing for emissions reduction at building level: A market assessment from a building management perspective. *Journal of Cleaner Production,* 294**,** 126323.

POWER, G. G. Available: https://www.geogreenpower.com/solar-panels/types/ [Accessed 13/11/2021].

PRABATHA, T., HEWAGE, K., KARUNATHILAKE, H. & SADIQ, R. 2020. To retrofit or not? Making energy retrofit decisions through life cycle thinking for Canadian residences. *Energy and Buildings,* 226**,** 110393.

PRECIADO-PÉREZ, O. A. & FOTIOS, S. 2017. Comprehensive cost-benefit analysis of energy efficiency in social housing. Case study: Northwest Mexico. *Energy and Buildings,* 152**,** 279-289.

PROJECT, O.-M. 2013 January. Energy Efficiency Trends in the EU. *Available at http://www.odyssee-mure.eu/publications/*.

PSOMAS, T., HEISELBERG, P., DUER, K. & BJØRN, E. 2016. Overheating risk barriers to energy renovations of single family houses: Multicriteria analysis and assessment. *Energy and Buildings,* 117**,** 138-148.

QIONG, L., PENG, R. & QINGLIN, M. Prediction model of annual energy consumption of residential buildings. 2010 International Conference on Advances in Energy Engineering, 19-20 June 2010 2010. 223-226.

QU, K., CHEN, X., EKAMBARAM, A., CUI, Y., GAN, G., ØKLAND, A. & RIFFAT, S. 2020. A novel holistic EPC related retrofit approach for residential apartment building renovation in Norway. *Sustainable Cities and Society,* 54**,** 101975.

QU, K., CHEN, X., WANG, Y., CALAUTIT, J., RIFFAT, S. & CUI, X. 2021. Comprehensive energy, economic and thermal comfort assessments for the passive energy retrofit of historical buildings - A case study of a late nineteenth-century Victorian house renovation in the UK. *Energy,* 220**,** 119646.

RABANI, M., MADESSA, H. B. & NORD, N. 2017. A state-of-art review of retrofit interventions in buildings towards nearly zero energy level. *Energy Procedia,* 134**,** 317-326.

REZBUILD. October 2017. *REZBUILD* [Online]. Available: https://rezbuildproject.eu/

[Accessed].
ROBERTSON, J. J., POLLY, B. J. & COLLIS, J. M. 2015. Reduced-order modeling and simulated annealing optimization for efficient residential building utility bill calibration. *Applied Energy,* 148**,** 169-177.
ROBIN BRYLEWSKI, A. M. September 2016. *Sustainability: The housing 'trilemma'* [Online]. Building. Available: https://www.building.co.uk/focus/sustainability-the-housing-trilemma/5084109.article [Accessed 30th August 2021].
ROSSO, F., CIANCIO, V., DELL'OLMO, J. & SALATA, F. 2020. Multi-objective optimization of building retrofit in the Mediterranean climate by means of genetic algorithm application. *Energy and Buildings,* 216**,** 109945.
SALATA, F., GOLASI, I., DOMESTICO, U., BANDITELLI, M., LO BASSO, G., NASTASI, B. & DE LIETO VOLLARO, A. 2017. Heading towards the nZEB through CHP+HP systems. A comparison between retrofit solutions able to increase the energy performance for the heating and domestic hot water production in residential buildings. *Energy Conversion and Management,* 138**,** 61-76.
SALVAĎO, L. L., VILLENEUVE, E. & MASSON, D. 2019. Decision Making in Near Zero Energy Building Refurbishment: A Technology Alternatives Ranking Tool. *IFAC-PapersOnLine,* 52**,** 313-318.
SANDBERG, N. H., SARTORI, I., HEIDRICH, O., DAWSON, R., DASCALAKI, E., DIMITRIOU, S., VIMM-R, T., FILIPPIDOU, F., STEGNAR, G., ŠIJANEC ZAVRL, M. & BRATTEBØ, H. 2016. Dynamic building stock modelling: Application to 11 European countries to support the energy efficiency and retrofit ambitions of the EU. *Energy and Buildings,* 132**,** 26-38.
SARTORIUS. Available: https://www.sartorius.com/en/products/process-filtration/tangential-flow-filtration/hollow-fiber-tff?gclid=Cj0KCQiA4b2MBhD2ARIsAIrcB-RUd0yVPeB8W8WPitSQdJg0SXSjmkJhW_0-MR-GoUvgkEEkze69YHoaAt2JEALw_wcB [Accessed 13/11/2021].
SCERRATO, G. Solar PV feed-in Tariff: the distortion of Italian power market. *In:* ENGINEERING, X. S. S. F. T.-I. S. (ed.).
SCHIAVONI, S., D'ALESSANDRO, F., BIANCHI, F. & ASDRUBALI, F. 2016. Insulation materials for the building sector: A review and comparative analysis. *Renewable and Sustainable Energy Reviews,* 62**,** 988-1011.
SCHIBUOLA, L., SCARPA, M. & TAMBANI, C. 2018. Innovative technologies for energy retrofit of historic buildings: An experimental validation. *Journal of Cultural Heritage,* 30**,** 147-154.
SEDDIKI, M., ANOUCHE, K., BENNADJI, A. & BOATENG, P. 2016. A multi-criteria group decision-making method for the thermal renovation of masonry buildings: The case of Algeria. *Energy and Buildings,* 129**,** 471-483.
SERRANO-JIMENEZ, A., BARRIOS-PADURA, A. & MOLINA-HUELVA, M. 2017. Towards a feasible strategy in Mediterranean building renovation through a multidisciplinary approach. *Sustainable Cities and Society,* 32**,** 532-546.
SERRANO-JIMÉNEZ, A., LIZANA, J., MOLINA-HUELVA, M. & BARRIOS-PADURA, Á. 2020. Indoor environmental quality in social housing with elderly occupants in Spain: Measurement results and retrofit opportunities. *Journal of Building Engineering,* 30**,** 101264.
SEYEDZADEH, S., POUR RAHIMIAN, F., OLIVER, S., RODRIGUEZ, S. & GLESK, I. 2020. Machine learning modelling for predicting non-domestic buildings energy performance: A model to support deep energy retrofit decision-making. *Applied Energy,* 279**,** 115908.
SHAIKH, P. H., SHAIKH, F., SAHITO, A. A., UQAILI, M. A. & UMRANI, Z. 2017. Chapter 9

- An Overview of the Challenges for Cost-Effective and Energy-Efficient Retrofits of the Existing Building Stock. *In:* PACHECO-TORGAL, F., GRANQVIST, C.-G., JELLE, B. P., VANOLI, G. P., BIANCO, N. & KURNITSKI, J. (eds.) *Cost-Effective Energy Efficient Building Retrofitting.* Woodhead Publishing.

SHAO, Y., GEYER, P. & LANG, W. 2014. Integrating requirement analysis and multi-objective optimization for office building energy retrofit strategies. *Energy and Buildings,* 82**,** 356-368.

SHARIF, S. A. & HAMMAD, A. 2019. Developing surrogate ANN for selecting near-optimal building energy renovation methods considering energy consumption, LCC and LCA. *Journal of Building Engineering,* 25**,** 100790.

SHEN, P., BRAHAM, W., YI, Y. & EATON, E. 2019. Rapid multi-objective optimization with multi-year future weather condition and decision-making support for building retrofit. *Energy,* 172**,** 892-912.

SHEN, P., WANG, Z. & JI, Y. 2021. Exploring potential for residential energy saving in New York using developed lightweight prototypical building models based on survey data in the past decades. *Sustainable Cities and Society,* 66**,** 102659.

SIMSON, K. 18/03/2021. *Renovation Wave: CoR and EU Commission launch cooperation to boost building overhaul* [Online]. The EU's Assembly of Regional and Local Representatives. Available: https://cor.europa.eu/en/news/Pages/renovation-wave-CoR-and-Commission-launch-cooperation-to-boost-building-overhaul.aspx#:~:text=The%20Renovation%20Wave%20was%20launched%20on%2014%20October,aims%20to%20remove%20barriers%20for%20%20building%20renovations. [Accessed 19/02 2021].

SKARAN, A. M. 2013. *Typologies and energy demand modelling of the Norwegian building stock – Part 2 Apartment blocks built after 1980.* Project thesis, Norwegian University of Science and Technology (NTNU).

SMARRA, F., JAIN, A., DE RUBEIS, T., AMBROSINI, D., D'INNOCENZO, A. & MANGHARAM, R. 2018. Data-driven model predictive control using random forests for building energy optimization and climate control. *Applied Energy,* 226**,** 1252-1272.

SOLAR, O. Available: https://www.onyxsolar.com/ [Accessed 13/11/2021].

SOLUTION, A. I. A. Available: https://www.airwoods.com/compact-hrv-high-efficiency-top-port-vertical-heat-recovery-ventilator-product/?gclid=Cj0KCQiA4b2MBhD2ARIsAIrcB-QM5cU-ej35B_XNNmRrdHPEmUc1s8LEo4aRjecYWx0_LJmfm3Mh6ZgaAutVEALw_wcB [Accessed 13/11/2021].

SOMASUNDARAM, S., CHONG, A., WEI, Z. & THANGAVELU, S. R. 2020. Energy saving potential of low-e coating based retrofit double glazing for tropical climate. *Energy and Buildings,* 206**,** 109570.

SON, H. & KIM, C. 2018. Evolutionary many-objective optimization for retrofit planning in public buildings: A comparative study. *Journal of Cleaner Production,* 190**,** 403-410.

SOUDAL. Available: https://www.soudal.co.uk/diy/applications/sealing-windows [Accessed 13/11/2021].

STREICHER, K. N., MENNEL, S., CHAMBERS, J., PARRA, D. & PATEL, M. K. 2020. Cost-effectiveness of large-scale deep energy retrofit packages for residential buildings under different economic assessment approaches. *Energy and Buildings,* 215**,** 109870.

STURZENEGGER, D., GYALISTRAS, D., MORARI, M. & SMITH, R. S. 2016. Model Predictive Climate Control of a Swiss Office Building: Implementation, Results,

and Cost–Benefit Analysis. *IEEE Transactions on Control Systems Technology,* 24**,** 1-12.

SUGÁR, V., TALAMON, A., HORKAI, A. & KITA, M. 2020. Energy saving retrofit in a heritage district: The case of the Budapest. *Journal of Building Engineering,* 27**,** 100982.

SUNPOWER October 2015. SunPower TM X-Series Data Sheet. *In:* SUNPOWER (ed.).

SYNNEFA, A., VASILAKOPOULOU, K., MASI, R. F. D., KYRIAKODIS, G.-E., LONDORFOS, V., MASTRAPOSTOLI, E., KARLESSI, T. & SANTAMOURIS, M. 2017. Transformation through Renovation: An Energy Efficient Retrofit of an Apartment Building in Athens. *Procedia Engineering,* 180**,** 1003-1014.

TADEU, S., RODRIGUES, C., TADEU, A., FREIRE, F. & SIMÕES, N. 2015. Energy retrofit of historic buildings: Environmental assessment of cost-optimal solutions. *Journal of Building Engineering,* 4**,** 167-176.

TANG, F., CHEN, J., LI, J. & RODRIGUEZ, D. 2020. Energy saving actions toward NZEBs with multiple-criteria optimization in current residential buildings. *Energy Reports,* 6**,** 3008-3022.

TANG, R. & WANG, S. 2019. Model predictive control for thermal energy storage and thermal comfort optimization of building demand response in smart grids. *Applied Energy,* 242**,** 873-882.

TECHNOLOGIES, W. Available: https://www.winco-tech.com/en/produit/insulation-skytech-pro-xl/ [Accessed 13/11/2021].

TETLOW, D., DE SIMON, L., LIEW, S. Y., HEWAKANDAMBY, B., MACK, D., THIELEMANS, W. & RIFFAT, S. 2017. Cellulosic-crystals as a fumed-silica substitute in vacuum insulated panel technology used in building construction and retrofit applications. *Energy and Buildings,* 156**,** 187-196.

THALFELDT, M., KURNITSKI, J. & LATÕŠOV, E. 2018. Exhaust air heat pump connection schemes and balanced heat recovery ventilation effect on district heat energy use and return temperature. *Applied Thermal Engineering,* 128**,** 402-414.

THILAKARATHNE, D. J. & TREUR, J. 2016. Cognitive Simulation Driven Domestic Heating Energy Management. *Procedia Environmental Sciences,* 34**,** 80-93.

THOMSEN, K. E., ROSE, J., MORCK, O., JENSEN, S. Ø. & ØSTERGAARD, I. 2015. Energy Consumption in an Old Residential Building Before and After Deep Energy Renovation. *Energy Procedia,* 78**,** 2358-2365.

THRAMPOULIDIS, E., MAVROMATIDIS, G., LUCCHI, A. & OREHOUNIG, K. 2021. A machine learning-based surrogate model to approximate optimal building retrofit solutions. *Applied Energy,* 281**,** 116024.

THYGESEN, R. & KARLSSON, B. 2013. Economic and energy analysis of three solar assisted heat pump systems in near zero energy buildings. *Energy and Buildings,* 66**,** 77-87.

TONELLATO, G., HEIDARI, A., PEREIRA, J., CARNIELETTO, L., FLOURENTZOU, F., DE CARLI, M. & KHOVALYG, D. 2021. Optimal design and operation of a building energy hub: A comparison of exergy-based and energy-based optimization in Swiss and Italian case studies. *Energy Conversion and Management,* 242**,** 114316.

TRONCHIN, L. & FABBRI, K. 2012. Energy Performance Certificate of building and confidence interval in assessment: An Italian case study. *Energy Policy,* 48**,** 176-184.

TUOMINEN, P., KLOBUT, K., TOLMAN, A., ADJEI, A. & DE BEST-WALDHOBER, M. 2012. Energy savings potential in buildings and overcoming market barriers in member states of the European Union. *Energy and Buildings,* 51**,** 48-55.

TWINN, R. 2019. *Scaling Up Retrofit 2050* [Online]. The Institute of Engineering and

Technology and Nottingham Trent University. Available: http://miller-klein.com/wp-content/uploads/2019/03/Scaling-Up-Retrofit-2050.pdf [Accessed accessed on 20/04/2020].

UDOVICHENKO, A., FLECK, B. A., WEIS, T. & ZHONG, L. 2021. Framework for design and optimization of a retrofitted light industrial space with a renewable energy-assisted hydroponics facility in a rural northern canadian community. *Journal of Building Engineering,* 37**,** 102160.

UK-GBC. 2019. *Net Zero Carbon Buildings: A Framework Definition* [Online]. UK GBC. Available: https://www.ukgbc.org/wp-content/uploads/2019/04/Net-Zero-Carbon-Buildings-A-framework-definition.pdf [Accessed].

UNION, E. 19 May 2010. DIRECTIVE 2010/31/EU OF THE EUROPEAN PARLIAMENT AND OF THE COUNCIL on the energy performance of buildings. *153/13*

URIELI, I. *Thermodynamic Properties of R134a TetraFlouroEthane - CF3CH2F* [Online]. Available: https://www.ohio.edu/mechanical/thermo/property_tables/R134a/ [Accessed].

VILCHES, A., BARRIOS PADURA, Á. & MOLINA HUELVA, M. 2017. Retrofitting of homes for people in fuel poverty: Approach based on household thermal comfort. *Energy Policy,* 100**,** 283-291.

WALKER, S., KHAN, W., KATIC, K., MAASSEN, W. & ZEILER, W. 2020. Accuracy of different machine learning algorithms and added-value of predicting aggregated-level energy performance of commercial buildings. *Energy and Buildings,* 209**,** 109705.

WANG, Q., LAURENTI, R. & HOLMBERG, S. 2015a. A novel hybrid methodology to evaluate sustainable retrofitting in existing Swedish residential buildings. *Sustainable Cities and Society,* 16**,** 24-38.

WANG, Q., PLOSKIĆ, A., SONG, X. & HOLMBERG, S. 2016. Ventilation heat recovery jointed low-temperature heating in retrofitting—An investigation of energy conservation, environmental impacts and indoor air quality in Swedish multifamily houses. *Energy and Buildings,* 121**,** 250-264.

WANG, R., LU, S. & LI, Q. 2019a. Multi-criteria comprehensive study on predictive algorithm of hourly heating energy consumption for residential buildings. *Sustainable Cities and Society,* 49**,** 101623.

WANG, X., LU, M., MAO, W., OUYANG, J., ZHOU, B. & YANG, Y. 2015b. Improving benefit-cost analysis to overcome financing difficulties in promoting energy-efficient renovation of existing residential buildings in China. *Applied Energy,* 141**,** 119-130.

WANG, Y., QU, K., CHEN, X., ZHANG, X. & RIFFAT, S. 2022. Holistic electrification vs deep energy retrofits for optimal decarbonisation pathways of UK dwellings: A case study of the 1940s' British post-war masonry house. *Energy,* 241**,** 122935.

WANG, Y., SU, Y., WANG, W., FANG, Y., RIFFAT, S. B. & JIANG, F. 2019b. The advances of polysaccharide-based aerogels: Preparation and potential application. *Carbohydrate Polymers,* 226**,** 115242.

WATSON, P. 2010. An introduction to UK Energy Performance Certificates (EPCs). *Journal of Building Appraisal,* 5**,** 241-250.

WEATHERONLINE. *Nottingham/Watnall (117m)* [Online]. Available: https://www.weatheronline.co.uk/weather/maps/city?LANG=en&CEL=C&SI=mph&MAPS=over&CONT=ukuk&LAND=MID&REGION=0003&WMO=03354&UP=0&R=0&LEVEL=150&NOREGION=0 [Accessed].

WEBB, A. L. 2017. Energy retrofits in historic and traditional buildings: A review of

problems and methods. *Renewable and Sustainable Energy Reviews,* 77**,** 748-759.

WETZSTEIN, G. L., DOUGLAS; HIRSCH, MATTHEW; RASKAR, RAMESH "Supplementary Material: Tensor Displays: Compressive Light Field Synthesis using Multilayer Displays with Directional Backlighting".

WHITMAN, C., PRIZEMAN, ORIEL ELIZABETH CLARE AND LACEY-BARNACLE, MAX 2016. *Correlating maintenance, energy efficiency and fuel poverty for traditional buildings in the UK*, Welsh School of Architecture, Cardiff University.

WIKIPEDIA. 2011. *Aerogel* [Online]. Wikipedia. Available: http://en.wikipedia.org/wiki/Aerogel [Accessed].

WIKIPEDIA. 2018. *Photovoltaics* [Online]. Wikipedia. Available: https://en.wikipedia.org/wiki/Photovoltaics#Efficiency [Accessed].

WILSON, C., PETTIFOR, H. & CHRYSSOCHOIDIS, G. 2018. Quantitative modelling of why and how homeowners decide to renovate energy efficiently. *Applied Energy,* 212**,** 1333-1344.

WONG, S. L., WAN, K. K. W. & LAM, T. N. T. 2010. Artificial neural networks for energy analysis of office buildings with daylighting. *Applied Energy,* 87**,** 551-557.

WU, S., DAI, Y., LI, X., OPPONG, F. & XU, C. 2018. A review of ground-source heat pump systems with heat pipes for energy efficiency in buildings. *Energy Procedia,* 152**,** 413-418.

WU, Z., WANG, B. & XIA, X. 2016. Large-scale building energy efficiency retrofit: Concept, model and control. *Energy,* 109**,** 456-465.

XIN, L., CHENCHEN, W., CHUANZHI, L., GUOHUI, F., ZEKAI, Y. & ZONGHAN, L. 2018. Effect of the energy-saving retrofit on the existing residential buildings in the typical city in northern China. *Energy and Buildings,* 177**,** 154-172.

Y.W. LI, R. Z. W., J.Y. WU, Y.X. XU December 2007. Experimental performance analysis on a direct-expansion solar-assisted heat pump water heater. *Applied Thermal Engineering,* 27.

YAO, J., HUANG, Y. & CHENG, K. 2021. Coupling effect of building design variables on building energy performance. *Case Studies in Thermal Engineering,* 27**,** 101323.

YCHARTS. May 2021. *Italy Long Term Interest Rate* [Online]. Available: https://ycharts.com/indicators/italy_long_term_interest_rates [Accessed].

YU, J. Z., Y.; HUANG, J. 2014. Towards High Performance Organic Photovoltaic Cells: A Review of Recent Development in Organic Photovoltaics. *Polymers,* 6**,** 2473-2509.

ŽÁČEKOVÁ, E., VÁŇA, Z. & CIGLER, J. 2014. Towards the real-life implementation of MPC for an office building: Identification issues. *Applied Energy,* 135**,** 53-62.

ZEBRA. 2015. *Energy efficiency trends in buildings- Equivalent major renovation* [Online]. Enerdata: ZEBRO2020. Available: https://zebra-monitoring.enerdata.net/overall-building-activities/share-of-new-dwellings-in-residential-stock.html#equivalent-major-renovation-rate.html [Accessed 16th Jan 2020].

ZHANG, L.-Z. 2011. Heat and mass transfer in a randomly packed hollow fiber membrane module: A fractal model approach. *International Journal of Heat and Mass Transfer,* 54**,** 2921-2931.

ZHANG, L.-Z., HUANG, S.-M., CHI, J.-H. & PEI, L.-X. 2012. Conjugate heat and mass transfer in a hollow fiber membrane module for liquid desiccant air dehumidification: A free surface model approach. *International Journal of Heat and Mass Transfer,* 55**,** 3789-3799.

ZHANG, L.-Z. & ZHANG, N. 2014. A heat pump driven and hollow fiber membrane-

based liquid desiccant air dehumidification system: Modeling and experimental validation. *Energy,* 65**,** 441-451.

ZHANG, L. Z., JIANG, Y. & ZHANG, Y. P. 2000. Membrane-based humidity pump: performance and limitations. *Journal of Membrane Science,* 171**,** 207-216.

ZHANG, N., YIN, S.-Y. & ZHANG, L.-Z. 2016. Performance study of a heat pump driven and hollow fiber membrane-based two-stage liquid desiccant air dehumidification system. *Applied Energy,* 179**,** 727-737.

ZHANG, W., LU, L. & CHEN, X. 2017. Performance Evaluation of Vacuum Photovoltaic Insulated Glass Unit. *Energy Procedia,* 105**,** 322-326.

ZHANG, X., ZHAO, X., SHEN, J., HU, X., LIU, X. & XU, J. 2013. Design, fabrication and experimental study of a solar photovoltaic/loop-heat-pipe based heat pump system. *Solar Energy,* 97**,** 551-568.

ZHANG, Y. & AUGENBROE, G. 2018. Optimal demand charge reduction for commercial buildings through a combination of efficiency and flexibility measures. *Applied Energy,* 221**,** 180-194.

ZHENG, D., YU, L., WANG, L. & TAO, J. 2019a. Integrating willingness analysis into investment prediction model for large scale building energy saving retrofit: Using fuzzy multiple attribute decision making method with Monte Carlo simulation. *Sustainable Cities and Society,* 44**,** 291-309.

ZHENG, D., YU, L., WANG, L. & TAO, J. 2019b. A screening methodology for building multiple energy retrofit measures package considering economic and risk aspects. *Journal of Cleaner Production,* 208**,** 1587-1602.

ZHIVOV, A. & LOHSE, R. 2021. Deep Energy Retrofit in Public Buildings—EBC Annex 61 Approach.

ZUHAIB, S., MANTON, R., GRIFFIN, C., HAJDUKIEWICZ, M., KEANE, M. M. & GOGGINS, J. 2018. An Indoor Environmental Quality (IEQ) assessment of a partially-retrofitted university building. *Building and Environment,* 139**,** 69-85.

Appendix 5-1 Building site, surroundings and climate conditions

The building chosen as a case study in Italy is a single-family house of social housing typology. It is located in the inland town of Martellago (Municipality of Venice), and benefits from a mild climate. The case house has no surrounding buildings and has a relevant amount of windows.



Figure 1 Surrounding buildings of the case site

Typology: Single-family house

Climate: Temperate Zone (Csa)

Number of floors: 2

Main orientation: EW/NS - latitude 45.54°N, longitude 12.15°E

Total building floor Area: 158 sqm

Structure: Load-bearing masonry in solid brick

Envelope: Solid bricks

Insulating layer: none

Types of flats:

- Type 1: Single unit Area: 80m^2;
- Type 2: Single unit Area: 78m^2

The climatic data uses standard simulation weather files which are sourced from various places and converted into the standard FWT. file format. These are individual weather years sourced from the MET office and most files are sourced directly from the energy plus website. On hourly basis, they provide:

- Outside dry-bulb temperature (°C)

  Annual average dry-bulb temperature: 13.2℃

  Extreme temperature range: -4.4℃ to 33.0 ℃

  Average temperature range: 1℃ to 24℃

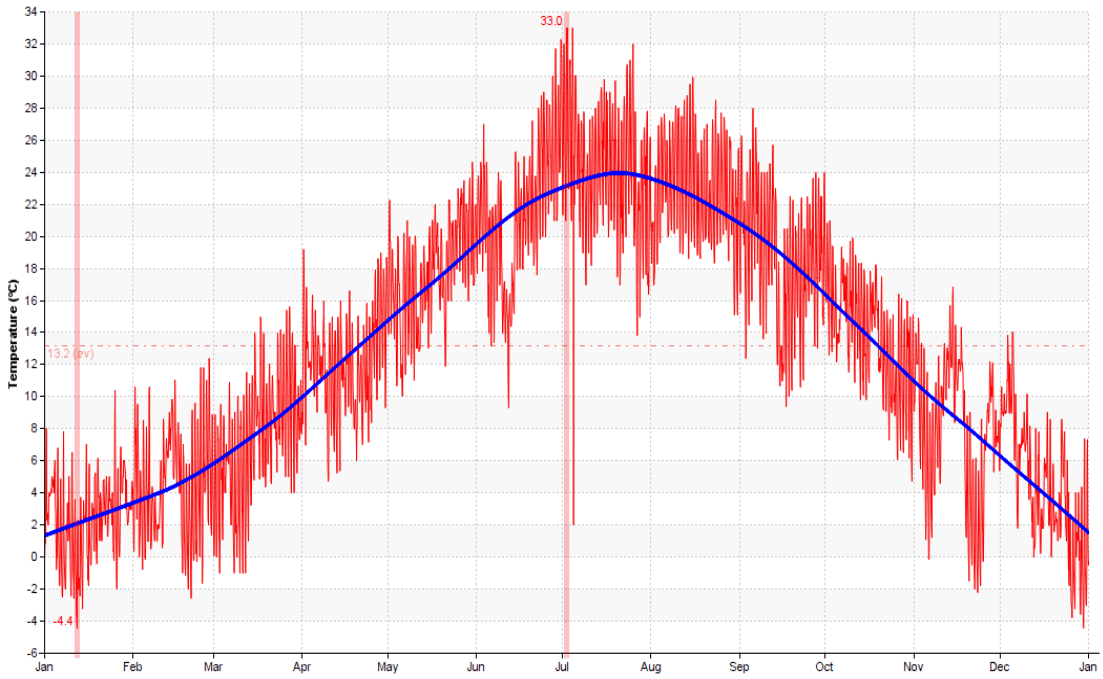


Figure 2 Martellago – Annual outside dry-bulb temperature (°C)

- Wind speed (m/s)

  Annual wind speed: 1.9m/s

  Extreme wind speed range: 0-15.5 m/s

Average wind speed range: 0.7-2.6 m/s

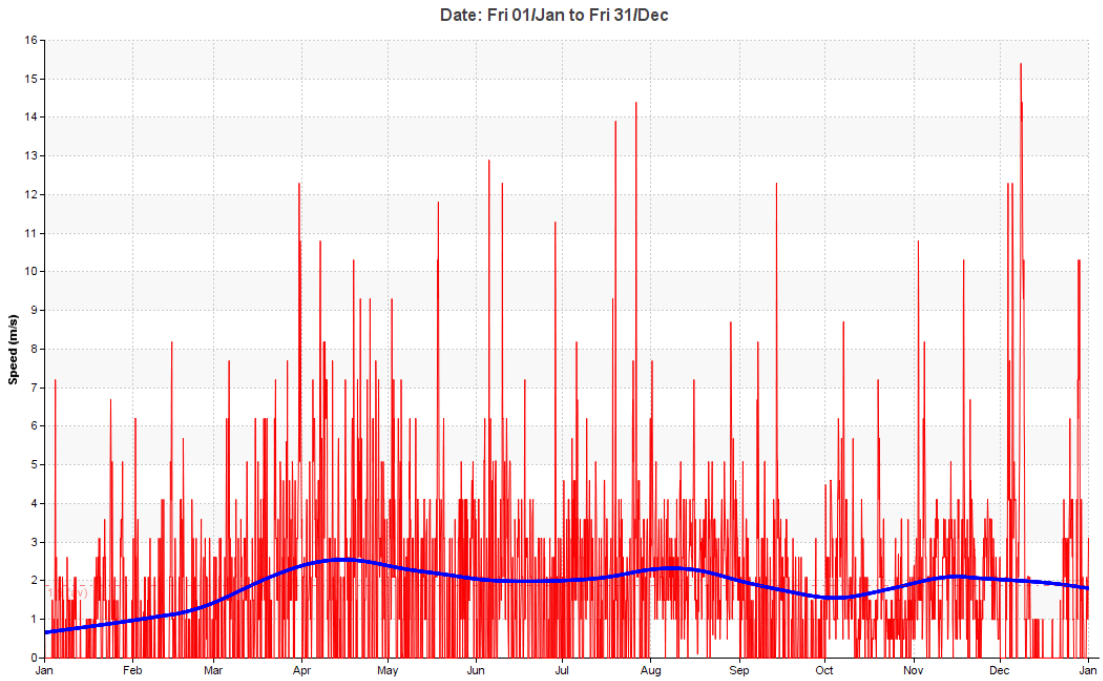


Figure 3 Martellago – Annual outside wind speed (m/s)

- Direct solar radiation (W/m2)

  Annual average direct solar radiation: 96 W/m^2

  Peak direct solar radiation variation rage: 0-875 W/m^2

  Average direct solar radiation variation rage: 35-190 W/m^2

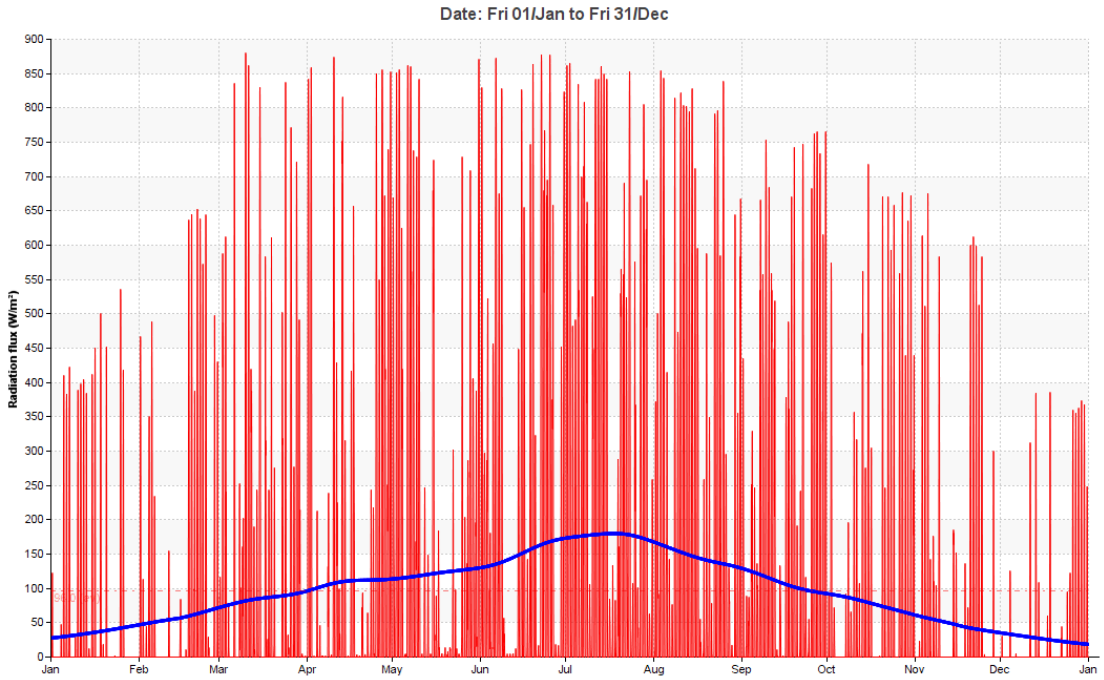


Figure 4 Martellago – Annual direct solar radiation (W/m2)

- Relative Humidity (%)

  Annual relative humidity: 75%

  Extreme relative humidity variation range: 10%-100%

  Average relative humidity variation range: 72%-87%

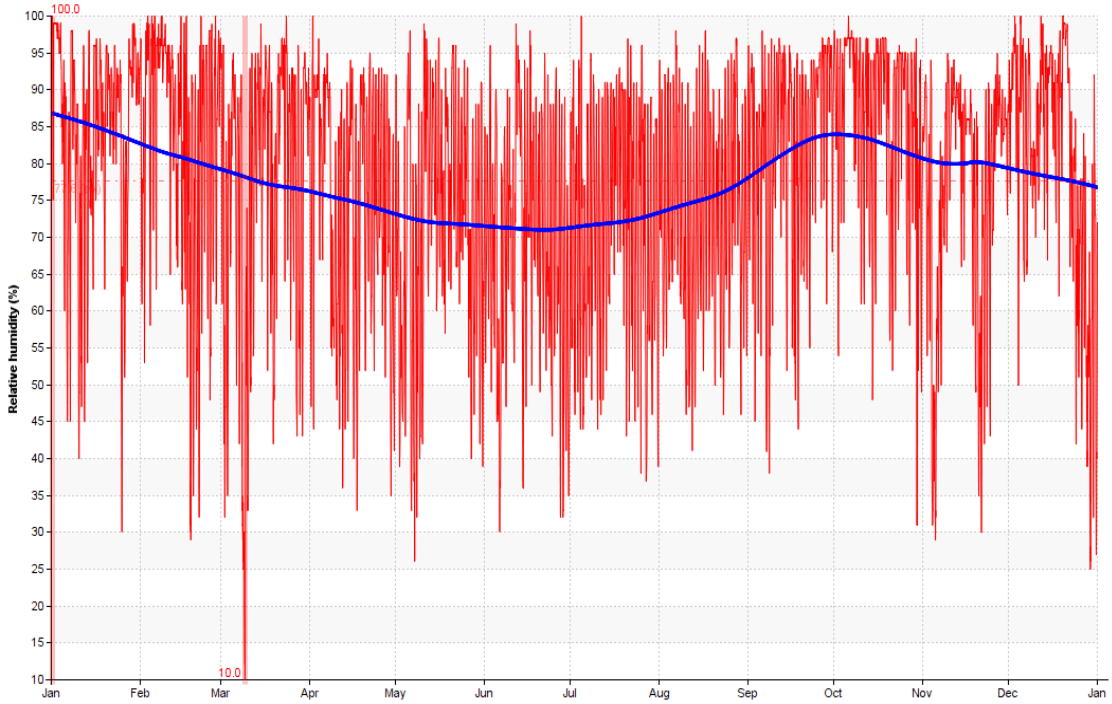


Figure 5 Martellago – Annual Outside relative humidity (%)

Appendix 5-2 Building fabric, airtightness, thermal bridging and energy systems

1. Building fabric

The semi-detached house was constructed between the 1960s and 1970s, with very low insulation levels. The thermal construction of the house is referenced by the Italy residential building taxonomy. Specific layers, thermal conductivities, and the overall heat transfer coefficients (U-value) of the building elements are listed in Table 1.

Table 1 Thermal construction specification of demo site buildings

Construction	Layers description (from outside to inside)	Total Thickness (mm)	Total U-value ($W/m^2 \cdot k$)	Total R-value ($m^2 \cdot k/W$)	Thermal bridge coefficient ($W/m^2 \cdot k$)	Thermal mass C_m ($Kj/m^3 \cdot K$)
Foundation	White marble Dense plaster	450	1.0064	0.7800	0.0990	177.1120
Roof	Clay brick pitched roof	176	1.881	0.3943	0.1870	64.3486
External window	Clear float Cavity Clear float Softwood frame External shading: wood louver	20 (only glazing)	3.1198 (only glazing) 1.7411 (including frame)	0.3205	0.1640	Visible light normal transmittance: 0.76

	Internal shading: curtain					
External door	chipboard	40	2.4018	0.2667	0.2290	33.4880
Inner door	oak	25	3.5553	0.1316	0.0299	20.9125
External wall 23cm	Gypsum plasterboard (10mm) Common brick HF – C4 (220mm) Gypsum plasterboard (10mm)	230	1.7745	0.4135	0.6000	152.7643
External wall 29.5cm	Gypsum plasterboard (10mm) Common brick HF – C4 (275mm) Gypsum plasterboard (10mm)	295	1.5315	0.7000	0.4000	85.8720
External wall 32cm	Gypsum plasterboard	325	1.4549	0.5377	0.4000	152.7643

	(10mm) Common brick HF – C4 (300mm) Gypsum plasterboard (10mm)					
Internal ceiling/floor	Cast concrete (dense) Clay tiles	410	1.9360	0.3017	0.1990	174.5208
Attic floor	Dense cast concrete Gypsum board – HF–E1	70	3.1229	0.1054	0.3270	50.8044
Internal partition wall	Aerated concrete slab Reinforced concrete Aerated concrete slab	250	2.4609	0.1668	0.2340	220.6000

2. Airtightness and thermal bridge through thermal imaging

The temperature distribution shown in the thermal photo taken during the inspections, testifies the localized problem of airthigtness, as shown in Figure 1-4. This problem is

mainly located in the ground floor, probably due to the absence of a ventilated crawl space that causes rising damp from the foundation plane.

Along the walls there are no particular problems due to the absence of a point-bearing structure that would have created discontinuity. In this case the thermal bridges occur in the junctions between the horizontal and vertical structure and in the main nodes of the construction details. The clear stains of humidity present inside the bathrooms (mainly) and inside the various rooms are due to the poor ventilation caused by the habits of the occupants.

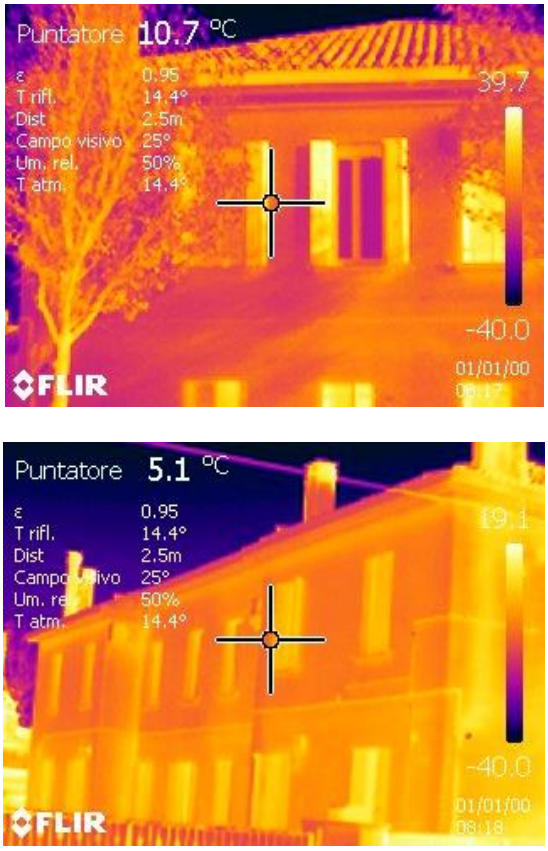


Figure 1 Staircase and balconies thermal distributions

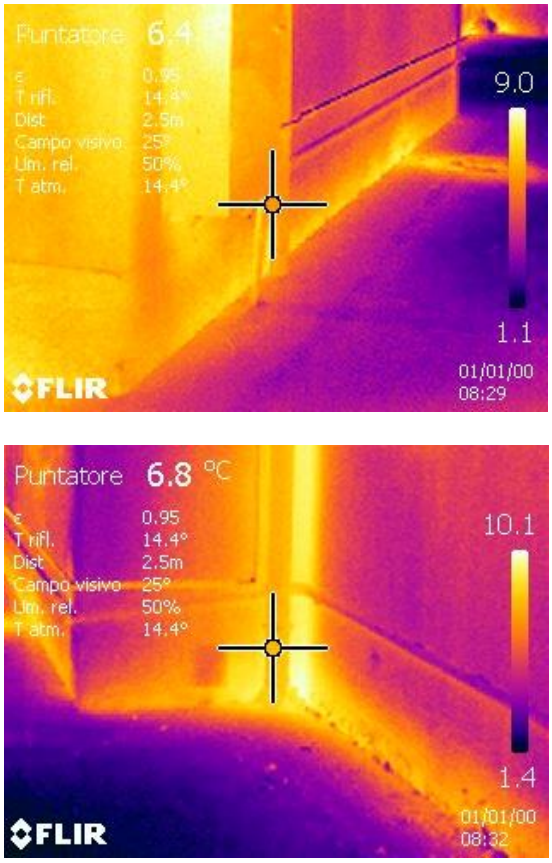


Figure 2 Ground floor facade and node between structure and ceiling in the garage

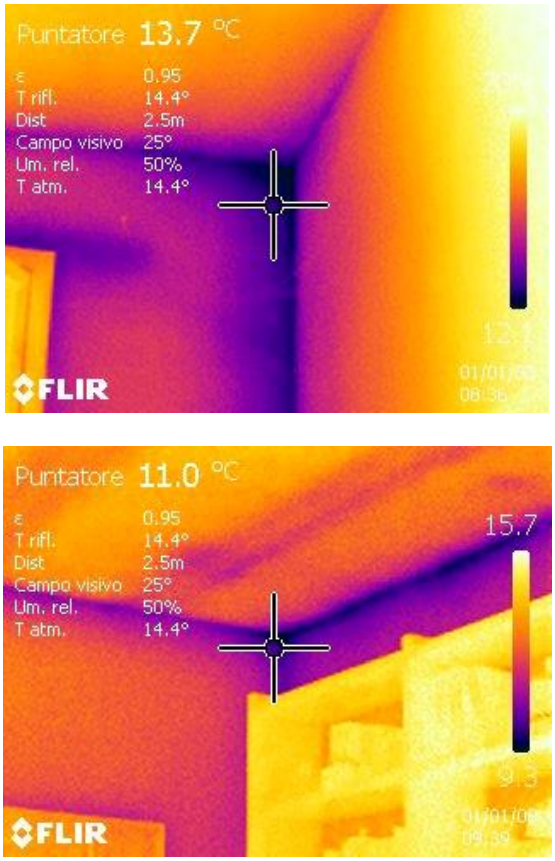


Figure 3 Internal thermal distributions

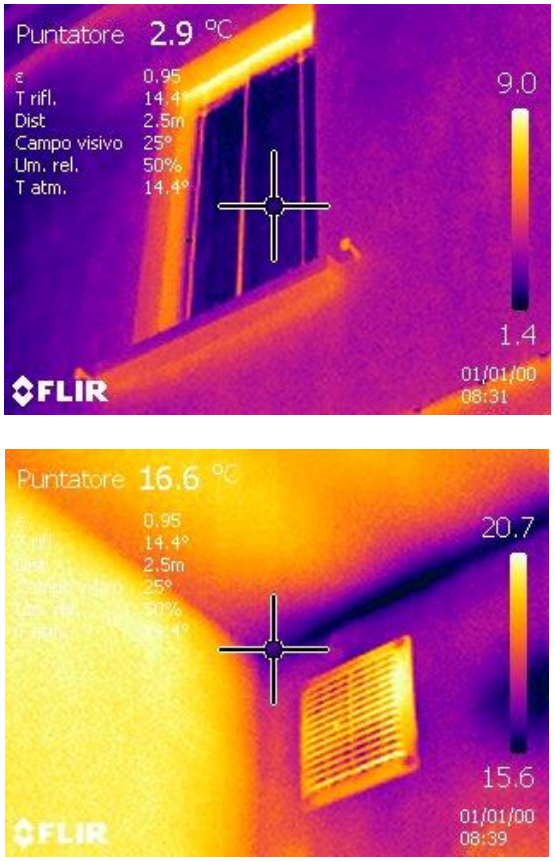


Figure 4 Internal thermal distributions

Appendix 5-3 The details energy performances of individual technology

Passive measures: ERM01-1 (Vacuum glazing insulation windows); ERM01-2 (Triple glazing windows); ERM02-1 (Silicon-based vacuum insulation panels); ERM02-2 (Polyisocyanurate insulation panels); ERM03-1 (Silicon-based vacuum insulation panels); ERM04-1 (Starch aerogel insulation panels); ERM05-1 (Silicon-based vacuum insulation panels); ERM06-1 (Gypsum insulation); ERM06-2 (Sealings of the windows and joint places).

Active measures: ERM07-1 (Mechanical ventilation with heat recovery); ERM08-1 (LED lighting + Daylighting pipes).

Renewable measures: ERM09-1 (Multi-crystalline silicon PV glazing panels); ERM09-2 (Thin-film PV glazing with high insulation); ERM10-1 (Solar assisted heat pump); ERM10-2 (Air-water heat pump); ERM10-3 (Potassium formate-water cascade air cooling dehumidifier); ERM11-1 (Solar collector).

Table 1 Technical specification of alternatives retrofit measures

Category	Retrofit number	Material and system	Technical specification
Windows glazing insulation	ERM01-1	Vacuum glazing insulation windows	Double glazing with vacuum inside the two panels; U-value of the glazing is 0.8 W/m^2.K; U-value of the whole system is 0.9 W/m^2.K
	ERM01-2	Triple glazing insulation windows	Triple glazing with air inside panels; U-value of the glazing is 1.24 W/m^2.K; U-value of the whole system is 1.12 W/m^2.K
External wall	ERM02-1	Silicon based vacuum	Thickness=20mm; Thermal conductivity

insulation		insulation panels	of 0.008 W/mK; Specific heat capacity=800J/kg.K; Density=288kg/m^3
	ERM02-2	Polyisocyanurate insulation panels	Thickness=70mm; Thermal conductivity of 0.022 W/mK; Specific heat capacity=1800J/kg.K; Density=45kg/m^3
Party wall insulation	ERM03-1	Silicon based vacuum insulation panels	Thickness=10mm; Thermal conductivity of 0.008 W/mK; Specific heat capacity=800J/kg.K; Density=288kg/m^3
Attic floor insulation	ERM04-1	Starch aerogel insulation panels	Thickness=40mm; Thermal conductivity of 0.024 W/mK; Specific heat capacity=2260J/kg.K; Density=1500kg/m^3
Ground floor insulation	ERM05-1	Silicon based vacuum insulation panels	Thickness=20mm; Thermal conductivity of 0.008 W/mK; Specific heat capacity=800J/kg.K; Density=288kg/m^3
Airtightness improvement	ERM06-1	Gypsum insulation	Infiltration rate improved to 0.6ACH under pressure difference of 50Pa
	ERM06-2	Sealings of the windows and joint places	Infiltration rate improved to 3.6ACH under pressure difference of 50Pa
Efficient ventilation	ERM07-1	Mechanical ventilation with heat recovery	Ventilation rate: drive of 0.58ACH, and extractions of 0.74ACH; Enthalpy heat recovery rate=93%; recovery temperature difference of 3℃; Specific energy consumption of maximum 3W/m^2 used in fan power
Efficient lighting device	ERM08-1	LED lighting + Daylighting pipes	Lighting retrofit from fluorescent lighting 2900Lux with power of 28W. (104Lux/W) to self-dimmable LED

			lighting of maximum luminance of 500Lux with power of 5W(100Lux/W), Lighting pipes could reduce 11.5% of the lighting energy based on the LED lighting energy
Building integrated PV electricity generation	ERM09-1	Multi-crystalline silicon PV glazing panels	Single panel size:700mm*700mm*7.8mm with front and back side each 3mm glass; Cell efficiency=16.4%, panel efficiency=13.06%; unit panel electricity capacity of 64Wp; Temperature Coefficient of Pmax=-0.43%/℃; U-value of the overall panel is 5.26W/m^2.K
	ERM09-2	Thin-film PV glazing with high insulation	U-value of the whole system including the frame is 0.65 W / m^2.K; panel efficiency=3.50%, which can be installed on the east and south windows
HVAC technology	ERM10-1	Solar assisted heat pump	DHW seasonal performance factor varied between 2.8-3.8, space heating seasonal performance factor varied between 3.7-4.9 with under 40℃ water temperature difference
	ERM10-2	Air-water heat pump	Heating COP=4.30 with air temperature difference of 23℃; Cooling EER=3.50 with air temperature difference of 15℃; DHW=1.87 with water temperature difference of 53℃
	ERM10-3	Liquid desiccant based air cooling	Cooling EER=4.36 under nominal operating conditions at 35 degrees

		dehumidifier	Celsius, temperature control set up with humidity varied between 40%-60%
Solar thermal heat generation	ERM11-1	Solar collector	275LTS Compact Solar Water Heater with evacuated Tube Panel, surface area of 4m^2; Thermal efficiency of 60%

Table 2 Cost and lifespan of retrofit measures

Retrofit number	Unit cost	Quantity	Annual maintenance cost	Life span (year)	Replacement cost
ERM01-1	€563/m^2	24.0	0.00%	30	64%
ERM01-2	€336/m^2	24.0	0.00%	30	64%
ERM02-1	€92/m^2	170.0	0.00%	30	64%
ERM02-2	€103/m^2	170.0	0.00%	30	64%
ERM03-1	€46/m^2	40.0	0.00%	30	64%
ERM04-1	€131/m^2	80.0	0.00%	30	64%
ERM05-1	€92/m^2	80.0	0.00%	30	64%
ERM06-1	€122/m^2	24.0	0.00%	5	64%
ERM06-2	€15/m	100.0	0.00%	5	64%
ERM07-1	€60/m^2 floor area	158.0	2.00%	15	64%
ERM08-1	€247/unit	50.0	0.00%	10	64%
ERM09-1	€353/m^2	70.0	2.00%	20	64%
ERM09-2	€1072/m^2	19.0	2.00%	15	64%
ERM10-1	€612/kW	Dependent on the maximum heating capacity	0.00%	15	64%

ERM10-2	€640/kW	Dependent on the maximum heating/cooling capacity	0.75%	15	64%
ERM10-3	€97/kW	Dependent on the maximum cooling capacity	0.50%	15	64%
ERM11-1	€1122/unit	1.0	3.00%	10	64%

Appendix 5-4 All input parameters of the pre- and post-retrofit model

Table 1 Input parameters for pre-retrofit baseline heat and electrical demand and coefficients

The pre-retrofit space heating load	30.11 MWh
The pre-retrofit humidify load	0.0064 MWh
The pre-retrofit space cooling load	2.9283MWh
The pre-retrofit dehumidify load	2.4203 MWh
The pre-retrofit DHW load	0.6862 MWh
The post-retrofit coupling factors of DHW from load to demand	1.00
The post-retrofit coupling factors of DHW from demand to energy	1.12
The post-retrofit coupling factors of space heating from load to demand	1.11
The post-retrofit coupling factors of space heating from demand to energy	1.12
The post-retrofit coupling factors of space cooling from load to demand	0.93
The post-retrofit coupling factors of space cooling from demand to energy	0.40
The pre-retrofit lighting electricity energy input	12.5597 MWh
The pre-retrofit equipment electricity energy input	5.3103 MWh
The pre-retrofit pump electricity energy input	4.0065 MWh

The pre-retrofit fan electricity energy input	1.9502 MWh

Table 2 Input parameters of heat and electrical coefficients for individual retrofit measure

	ERM01-1	ERM01-2	ERM02-1	ERM02-2	ERM03-1	ERM04-1	ERM05-1	ERM06-1	ERM06-2	ERM07-1	ERM08-1	ERM09-1	ERM09-2	ERM10-1	ERM10-2	ERM10-3	ERM11-1
The post-retrofit space heating load reduction rate	-8.83%	-6.99%	-39.31%	-41.20%	-7.05%	-17.47%	-16.50%	-30.74%	-24.97%	-2.45%	-0.78%	-3.71%	-9.34%	-1.31%	-1.31%	-2.45%	-2.44%
The post-retrofit space heating humidify load reduction rate	0.00%	0.00%	0.00%	0.00%	0.00%	0.00%	0.00%	-100.00%	-100.00%	0.00%	0.00%	0.00%	0.00%	0.00%	0.00%	2068.75%	-1.56%
The post-retrofit space cooling load reduction rate	20.55%	14.46%	4.89%	-5.50%	0.01%	-0.16%	-9.97%	-22.61%	-17.09%	-0.76%	3.62%	0.28%	-16.36%	1.69%	1.69%	-0.29%	-0.39%
The post-retrofit space cooling dehumidify load reduction rate	3.84%	2.64%	8.05%	-8.71%	-1.88%	-3.22%	-4.82%	143.02%	86.22%	-0.28%	0.85%	-0.07%	-3.28%	0.27%	0.27%	89.23%	-50.20%
The post-retrofit DHW load reduction rate	0.00%	0.00%	0.00%	0.00%	0.00%	0.00%	0.00%	0.00%	0.00%	0.00%	0.00%	0.00%	0.00%	400.00%	400.00%	0.00%	-100.00%
The post-retrofit lighting electricity energy reduction rate	0.00%	0.00%	0.00%	0.00%	0.00%	0.00%	0.00%	0.00%	0.00%	0.00%	-58.37%	0.00%	0.00%	0.00%	0.00%	0.00%	0.00%
The post-retrofit equipment electricity energy reduction rate	0.00%	0.00%	0.00%	0.00%	0.00%	0.00%	0.00%	0.00%	0.00%	8.12%	0.00%	0.00%	0.00%	-15.07%	-15.07%	0.00%	0.00%
The post-retrofit pump electricity energy increased rate	0.00%	0.00%	0.00%	0.00%	0.00%	0.00%	0.00%	0.00%	0.00%	0.00%	0.00%	0.00%	0.00%	-100.00%	-100.00%	0.00%	7.87%
The post-retrofit fan electricity energy reduction rate	0.00%	0.00%	0.00%	0.00%	0.00%	0.00%	0.00%	0.00%	0.00%	0.00%	0.00%	0.00%	0.00%	-100.00%	-100.00%	0.00%	0.00%
The post-retrofit DHW load to demand factor	100.00%	100.00%	100.00%	100.00%	100.00%	100.00%	100.00%	100.00%	100.00%	100.00%	100.00%	100.00%	100.00%	100.00%	100.00%	100.00%	100.00%
The post-retrofit DHW demand to energy	112.36%	112.36%	112.36%	112.36%	112.36%	112.36%	112.36%	112.36%	112.36%	112.36%	112.36%	112.36%	112.36%	20.41%	23.26%	112.36%	112.36%
The post-retrofit space heating load to demand factor	111.27%	111.27%	111.27%	111.27%	111.27%	111.27%	111.27%	111.27%	111.27%	111.27%	111.27%	111.27%	111.27%	104.26%	104.88%	111.25%	111.27%
The post-retrofit space heating demand to energy factor	112.36%	112.36%	112.36%	112.36%	112.36%	112.36%	112.36%	112.36%	112.36%	112.36%	112.36%	112.36%	112.36%	20.41%	23.26%	112.36%	112.36%
The post-retrofit space cooling load to demand factor	92.59%	92.59%	92.59%	92.59%	92.59%	92.59%	92.59%	92.59%	92.59%	92.59%	92.59%	92.59%	92.59%	102.88%	69.93%	66.59%	92.59%
The post-retrofit space cooling demand to energy factor	40.00%	40.00%	40.00%	40.00%	40.00%	40.00%	40.00%	40.00%	40.00%	40.00%	40.00%	40.00%	40.00%	40.00%	30.30%	22.22%	40.00%
The post-retrofit DHW load to energy factor	112.36%	112.36%	112.36%	112.36%	112.36%	112.36%	112.36%	112.36%	112.36%	112.36%	112.36%	112.36%	112.36%	20.41%	23.26%	112.36%	112.36%
PV generated electricity (MWh)	0.00	0.00	0.00	0.00	0.00	0.00	0.00	0.00	0.00	0.00	0.00	-5.44	-0.29	0.00	0.00	0.00	0.00

Appendix 5-5 Detailed retrofit measures in real building

		Retrofit measures	Retrofit number	Unit cost (€/m^2)	Life span (years)
Passive measures	Wall external insulation	Si-VIP external wall insulation (EWI-VIP)	**ERM02-1**	92 €/m^2	30
	Airtightness improvement	Sealings of windows and joint places (SW-JP)	**ERM06-2**	15 €/m^2	5
Active measures	MVHR technology	Mechanical ventilation with heat recovery (MVHR)	**ERM07-1**	60 €/m^2 floor area	15
	Efficient lighting device	LED lighting + Daylighting pipes (ELD)	**ERM08-1**	247 €/unit	10
Renewable measures	Building-integrated PV panels	Thin-film PV glazing with high insulation (PV-VG)	**ERM09-2**	1072 €/m^2	15
	HVAC technology	Solar assisted heat pump (SAHP)	**ERM10-1**	612 €/kW	15
	Solar thermal	Solar collector (SC)	**ERM11-1**	1122 €/unit	10

Appendix 5-6 Details of 30 retrofit combinations and calculation results

Table 1 Combinations results with different calculation methods

	COMB No.	Simulation results in IESVE (MWh)	calculation results with the EF-EC model (MWh)	Discrepancy between IESVE and EF-EC model
Baseline		**62.97**	**62.97**	
Mild retrofit stage	COMB01	27.35	28.47	4.09%
	COMB02	27.27	28.70	5.23%
	COMB03	27.09	28.04	3.52%
	COMB04	27.80	27.92	0.43%
	COMB05	27.46	27.68	0.80%
	COMB06	56.16	54.56	-2.84%
	COMB07	19.48	19.74	1.06%
	COMB08	20.32	20.68	1.41%
	COMB09	20.38	20.57	0.75%
	COMB10	21.38	21.39	0.03%
	COMB11	26.03	26.22	0.71%
Moderate retrofit stage	COMB12	27.77	27.20	-2.06%
	COMB13	20.07	20.68	3.06%
	COMB14	21.91	22.33	1.53%
	COMB15	26.59	27.23	2.36%

	COMB16	21.75	21.63	-0.56%
	COMB17	20.66	20.64	-0.11%
	COMB18	26.18	26.11	-0.27%
	COMB19	26.44	26.62	0.68%
Deep retrofit stage	COMB20	7.62	8.00	5.04%
	COMB21	8.31	8.77	5.58%
	COMB22	7.52	7.93	5.42%
	COMB23	7.80	8.17	4.68%
	COMB24	7.70	8.14	5.73%
	COMB25	8.41	8.87	5.46%
	COMB26	12.74	12.53	-1.64%
	COMB27	8.10	7.70	-4.97%
	COMB28	7.63	7.33	-3.98%
	COMB29	7.19	7.32	1.78%
	COMB30	14.93	14.69	-1.60%

Table 2 Combination measure details

	No	error	ERM01-1	ERM01-2	ERM02-1	ERM02-2	ERM03-1	ERM04-1	ERM05-1	ERM06-1	ERM06-2	ERM07-1	ERM08-1	ERM09-1	ERM09-2	ERM10-1	ERM10-2	ERM10-3	ERM11-1
Mild retrofit stage	COMB01	4.09%	1		1		1	1	1		1								
	COMB02	5.23%		1	1		1	1	1		1								
	COMB03	3.52%	1			1	1	1	1		1								
	COMB04	0.43%	1		1		1	1	1	1									
	COMB05	0.80%		1		1	1	1	1	1									
	COMB06	-2.84%										1	1						
	COMB07	1.06%												1	1	1		1	1
	COMB08	1.41%												1	1		1	1	1
	COMB09	0.75%												1	1		1		1
	COMB10	0.03%												1			1	1	1
	COMB11	0.71%													1		1	1	1
Moderate retrofit stage	COMB12	-2.06%	1		1		1	1	1		1	1							
	COMB13	3.06%	1		1		1	1	1		1		1						
	COMB14	1.53%	1		1		1	1	1		1			1					
	COMB15	2.36%			1		1	1	1		1				1				
	COMB16	-0.56%	1		1		1	1	1		1					1			
	COMB17	-0.11%	1		1		1	1	1		1						1		
	COMB18	-0.27%	1		1		1	1	1		1							1	
	COMB19	0.68%	1		1		1	1	1		1								1
Deep retrofit stage	COMB20	5.04%			1		1	1	1		1	1	1	1	1	1		1	1
	COMB21	5.58%					1	1	1		1	1	1	1	1	1		1	1
	COMB22	5.42%				1	1	1	1		1	1	1	1	1	1		1	1
	COMB23	4.68%			1		1	1	1	1		1	1	1	1	1		1	1
	COMB24	5.73%			1		1	1	1		1	1	1	1	1		1	1	1
	COMB25	5.46%			1		1	1	1		1	1	1	1	1	1			1
	COMB26	-1.64%			1		1	1	1		1	1	1	1	1			1	1
	COMB27	-4.97%	1		1		1	1	1		1	1	1	1		1		1	1
	COMB28	-3.98%			1		1	1	1		1	1	1	1	1	1		1	
	COMB29	1.78%			1		1	1	1		1		1	1	1	1		1	1
	COMB30	-1.60%			1		1	1	1		1	1		1	1	1		1	1

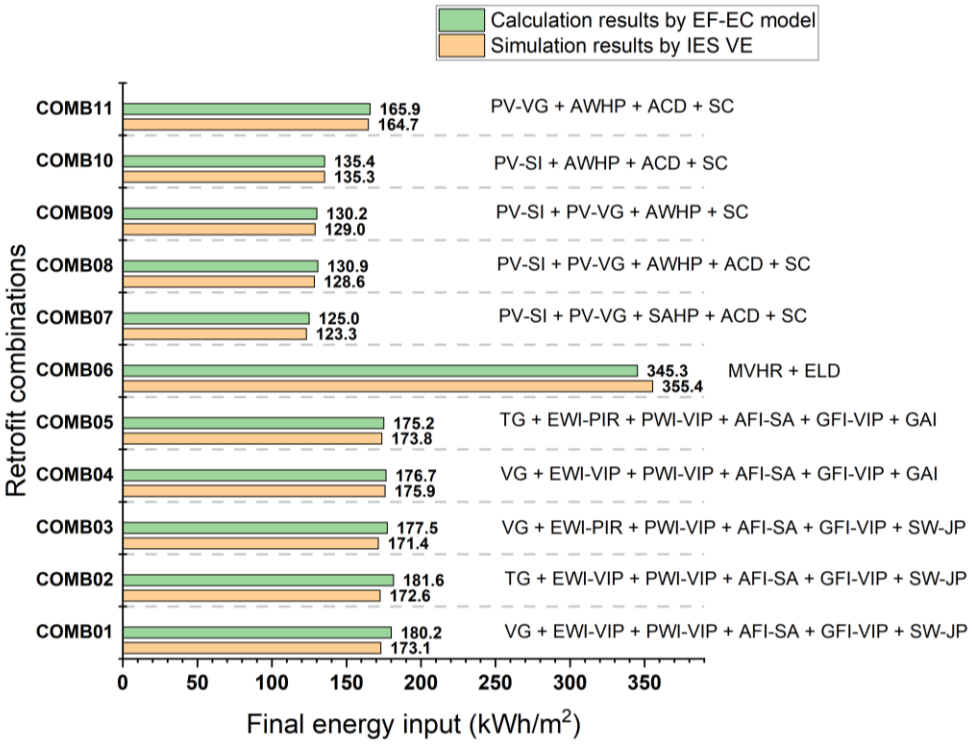


Figure 1 Calculation results of mild retrofit combinations between IES VE and EF-EC model

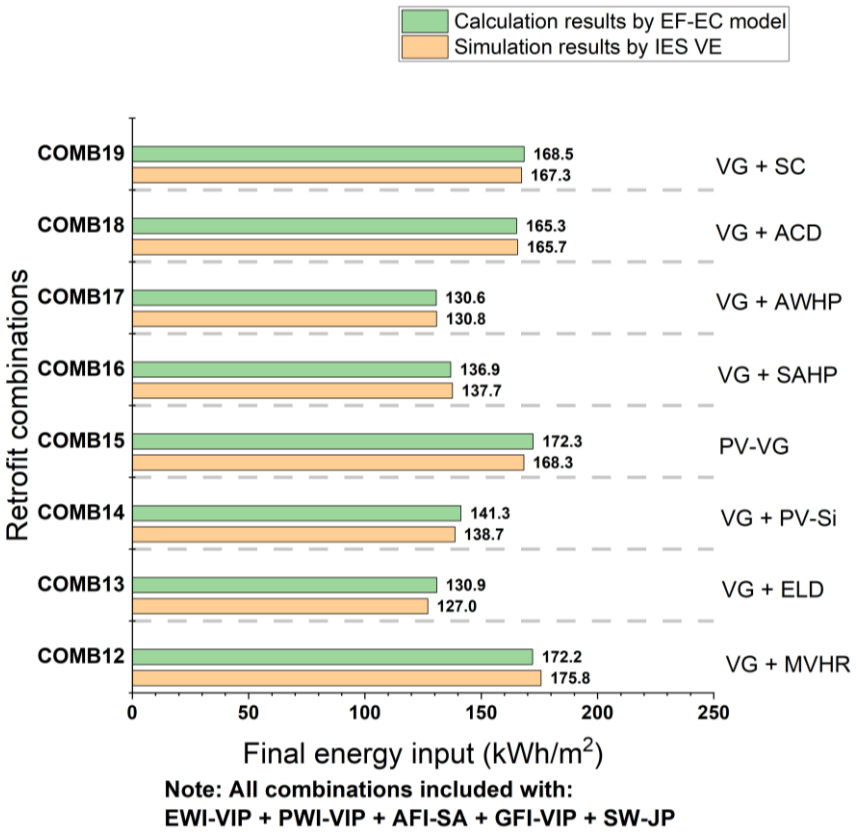


Figure 2 Calculation results of moderate retrofit combinations between IES VE and EF-EC model

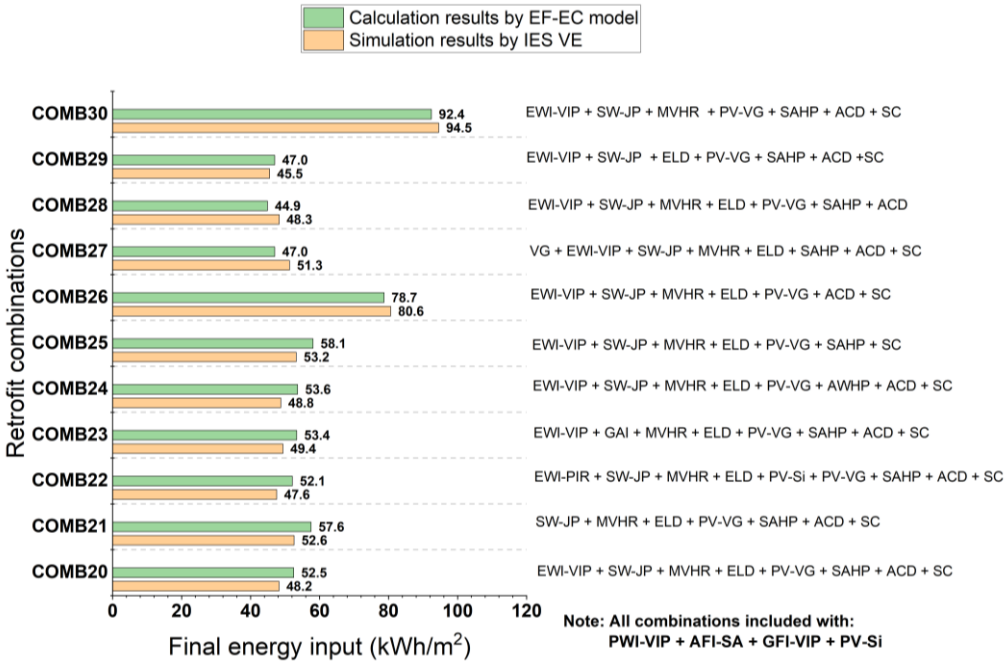


Figure 3 Calculation results of deep retrofit combinations between IES VE and EF-EC model

Appendix 6-1 Energy Performance Certification (EPC) calculation method

Energy Performance Certificates (EPC) provide information on the building energy efficiency and how it could be improved. Buildings are rated on a scale from A - G, with A being the most efficient. There are seven of these bands on an EPC which are run on a sliding scale from 'A' (the most energy-efficient) to 'G' (the least efficient). They are also colour coded for ease of reference from dark green (an 'A' rating) to red (a 'G' rating). Most homes in the UK fall into a 'D' band.

The EPC assessment will record specific information such as the size and layout of the building, how it has been constructed, and how it is insulated, heated, ventilated, and lighted.

The EPC is produced using a UK Government calculation methodology. More detailed technical information on the calculation methodologies can be found on the government website:

- Dwellings - http://www.bre.co.uk/sap2012.
- Other building types - http://www.ncm.bre.co.uk.

A brief calculation method is described as below:

Energy efficiency certification (EPC) bands are defined by the Standard Assessment Procedure (SAP) rating according to a points system which runs as follows:

- EPC rating A = 92-100 SAP points
- EPC rating B = 81-91 SAP points
- EPC rating C = 69-80 SAP points
- EPC rating D = 55-68 SAP points
- EPC rating E = 39-54 SAP points
- EPC rating F = 21-38 SAP points
- EPC rating G = 1-20 SAP points

The SAP rating is related to the total energy cost by the equations:

ECF = deflator × total cost / (TFA + 45)

if ECF > 3.5, SAP = 117 – 121 * log10(ECF)

if ECF < 3.5, SAP = 100 – 13.95 * ECF

Where,

- deflator is a constant value of 0.47;
- total cost is calculated as the total energy cost related to building space heating, space cooling, ventilation, domestic hot water heating and lighting usage, and also energy generated in the dwelling.

The SAP rating scale has been set so that SAP 100 is achieved at zero-ECF. It can rise above 100 if the dwelling is a net exporter of energy. The SAP rating is essentially independent of floor area.

Appendix 6-2 Multi-objective weighting scores for various homeowners' survey with three retrofit motivations

Motivation	Homeowner number	Required EPC level	Initial investment	Payback period	Bills reduction	Carbon emission reduction
Self-living (M1)	No.1	0	0.1	0.2	0.7	0
	No.2	0.1	0.3	0	0.5	0.1
	No.3	0	0.1	0.1	0.8	0
	No.4	0	0.3	0.3	0.4	0
	No.5	0	0.2	0.2	0.6	0
	No.6	0	0.1	0	0.9	0
	No.7	0.1	0.4	0	0.5	0
	No.8	0.1	0.3	0	0.6	0
	No.9	0	0.3	0.1	0.6	0
	No.10	0	0.1	0.2	0.7	0
	No.11	0	0.5	0	0.5	0
	No.12	0	0.2	0.3	0.5	0
	No.13	0	0.3	0	0.7	0
	No.14	0.1	0.4	0	0.4	0.1
Rent or sale (M2)	No.1	0.8	0.1	0	0	0.1
	No.2	0.5	0.3	0.1	0.1	0
	No.3	0.6	0.2	0.2	0	0
	No.4	0.6	0.1	0.1	0.1	0.1
	No.5	0.5	0.3	0.2	0	0

	No.6	0.4	0.3	0.3	0	0
	No.7	0.9	0	0.1	0	0
	No.8	0.5	0.3	0.1	0.1	0
	No.9	0.6	0.2	0.2	0	0
	No.10	0.6	0.2	0.2	0	0
	No.11	0.7	0.1	0.2	0	0
	No.12	0.8	0	0.1	0.1	0
	No.13	0.5	0.3	0.1	0	0.1
	No.14	0.7	0.1	0.2	0	0
Investment (M3)	No.1	0	0.5	0.4	0.1	0
	No.2	0.1	0.6	0.3	0	0
	No.3	0	0.4	0.6	0	0
	No.4	0	0.3	0.6	0.1	0
	No.5	0	0.2	0.7	0	0.1
	No.6	0	0.3	0.7	0	0
	No.7	0	0.4	0.6	0	0
	No.8	0	0.5	0.5	0	0
	No.9	0	0.6	0.4	0	0
	No.10	0	0.7	0.3	0	0
	No.11	0	0.4	0.6	0	0
	No.12	0	0.3	0.7	0	0
	No.13	0.1	0.2	0.6	0	0.1
	No.14	0	0.4	0.5	0.1	0

Appendix 6-3 Residential Building Typology

Table C.1 Number of buildings in each construction period

Construction periods	Estimated number of buildings	Living space in 1000 m²	
	thousands		
Pre 1919	2811	246106	28%
1919-1944	3026	248479	30%
1945-1960	2291	184076	23%
1961-1975	695	47710	7%
1976-1990	716	53674	7%
1991- 2003	293	2663	3%
post 2004	214	30,281	2%
total	10046	810326	

Table C.2 Number of buildings in each building construction types

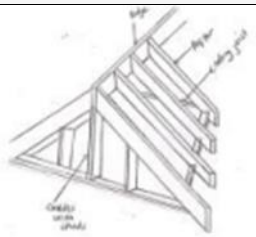
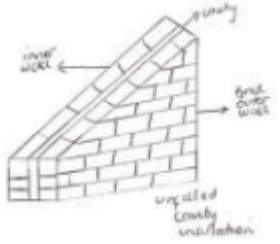
	Detached house	Semi-detached house	Terraced house	Apartment	Total
Building Numbers	4900	13091	3989	319	22299
Percentage (%)	22%	59%	18%	1%	

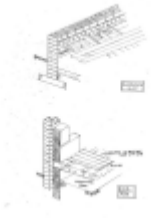
Table C.3 Average final energy consumption of semi-detached houses between 297

1961 and 1975

	Space heating (MWh)	Hot Water (MWh)	Cooking (MWh)	Lighting and Appliances	Total (MWh)
Gas	17.21	6.004	0.47	-	23.684
Electricity	-	-	0.38	6.611	6.991
Total	17.21	6.004	0.47	6.611	30.675

Table C.4 Building constructions and U-value of semi-detached houses between 1961 and 1975

		Existing state
Roof 1	**surface area**	**53.0m^2**
	type of construction	**Pitched with gables**
	picture	
	U-value	**1.5 W/(m^{2}K)**
Wall 1	**surface area**	**84.8m^2**
	type of construction	**masonry**
	picture	

	U-value	**1.8 W/(m^{2}K)**
Floor 1	**surface area**	**78m^2**
	type of construction	**Concrete floor**
	picture	
	U-value	**2.0 W/(m^{2}K)**
Window 1	**surface area**	**23.1m^2**
	type of construction	**UPVC double glazing**
	picture	
	U-value	**3.1 W/(m^{2}K) – only glazing** **1.7 W/(m^{2}K) – with frame**
Door 1	**surface area**	**3.8m^2**
	type of construction	**PVC door**
	picture	
	U-value	**2.4 W/(m^{2}K)**

Appendix 6-4 Retrofit measures and technical specifications

Retrofit number	Retrofit measures	Technical specification
ERM01-1	Vacuum glazing window insulation	Double glazing with a vacuum inside the two panels; U-value of the glazing is 0.8 W/m^2.K; U-value of the whole system is 0.9 W/m^2.K
ERM01-2	Triple glazing window insulation	Triple glazing with air inside panels; U-value of the glazing is 1.24 W/m^2.K; U-value of the whole system is 1.12 W/m^2.K
ERM02-1	Si-VIP external wall insulation	Thickness=20mm; Thermal conductivity of 0.008 W/mK; Specific heat capacity=800J/kg.K; Density=288kg/m^3
ERM02-2	PIR external wall insulation	Thickness=70mm; Thermal conductivity of 0.022 W/mK; Specific heat capacity=1800J/kg.K; Density=45kg/m^3
ERM03-1	Si-VIP party wall insulation	Thickness=10mm; Thermal conductivity of 0.008 W/mK; Specific heat capacity=800J/kg.K; Density=288kg/m^3
ERM04-1	Starch aerogel attic floor insulation	Thickness=40mm; Thermal conductivity of 0.024 W/mK; Specific heat capacity=2260J/kg.K; Density=1500kg/m^3
ERM05-1	Si-VIP ground floor insulation	Thickness=20mm; Thermal conductivity of 0.008 W/mK; Specific heat capacity=800J/kg.K; Density=288kg/m^3
ERM06-1	Gypsum airtightness insulation	Infiltration rate improved to 0.6ACH under pressure difference of 50Pa
ERM06-2	Sealings of windows and joint places	Infiltration rate improved to 3.6ACH under pressure difference of 50Pa
ERM07-1	Mechanical ventilation with heat recovery	Ventilation rate: drive of 0.58ACH, and extractions of 0.74ACH; Enthalpy heat recovery rate=93%; recovery temperature difference of 3℃; Specific energy consumption of maximum 3W/m^2 used in fan power
ERM08-1	LED lighting + Daylighting pipes	Lighting retrofit from fluorescent lighting 2900Lux with the power of 28W. (104Lux/W) to self-dimmable LED lighting of maximum luminance of 500Lux with the power of 5W(100Lux/W), Lighting pipes could reduce

		11.5% of the lighting energy based on the LED lighting energy
ERM09-1	Multi-crystalline silicon PV glazing panels	Single panel size:700mm*700mm*7.8mm with front and backside each 3mm glass; Cell efficiency=16.4%, panel efficiency=13.06%; unit panel electricity capacity of 64Wp; Temperature Coefficient of Pmax=-0.43%/°C; U-value of the overall panel is 5.26W/m^2.K
ERM09-2	Thin-film PV glazing with high insulation	U-value of the whole system, including the frame, is 0.65 W / m^2k; panel efficiency=3.50%, which can be installed on the east and south windows
ERM10-1	Solar assisted heat pump	DHW seasonal performance factor varied between 2.8-3.8, space heating seasonal performance factor varied between 3.7-4.9 with under 40°C water temperature difference
ERM10-2	Air-water heat pump	Heating COP=4.30 with an air temperature difference of 23°C; Cooling EER=3.50 with an air temperature difference of 15°C; DHW=1.87 with a water temperature difference of 53°C
ERM10-3	Liquid desiccant air cooling dehumidifier	Cooling EER=4.36 under nominal operating conditions at 35 degrees Celsius, temperature control set up with humidity varied between 40%-60%
ERM11-1	Solar collector	275LTS Compact Solar Water Heater with evacuated Tube Panel, the surface area of 4m^2; Thermal efficiency of 60%

Appendix 6-5 Criteria, optimal combinations and assessment values without considering motivations

Table 1 Assessment values of cost-optimal combinations

Energy consumption (kWh/m^2)	ERR	DPP (years)	Initial investment (€/m2)	Energy bills (€)	BRR
335	20%	26	520	3678	46%
122	71%	29	683	2531	63%
117	72%	18	374	2501	63%
88	79%	18	378	2569	62%
75	82%	13	449	2363	65%
29	93%	13	835	851	88%

Table 2 Cost-optimal combinations

Retrofit number	ERR=20%	ERR=71%	ERR=72%	ERR=79%	ERR=82%	ERR=93%
ERM01-1						
ERM01-2						
ERM02-1				√	√	√
ERM02-2						
ERM03-1					√	√
ERM04-1						√
ERM05-1					√	√
ERM06-1						
ERM06-2				√	√	√
ERM07-1						
ERM08-1	√		√	√	√	√
ERM09-1	√	√				√
ERM09-2						

ERM10-1				√		√
ERM10-2		√	√		√	
ERM10-3						
ERM11-1	√					

Appendix 6-6 Criteria, optimal combinations and assessment values for three motivation types

Table 1 Criteria and assessment values for three motivation types

Motivation type	Criteria	Energy consumption (kWh/m^2)	Energy bills (€)	BRR	ERR	DPP (years)	Initial investment (€/m2)	MPF
M_1	II<400€/m^2	109	2472	64%	74%	19	383	0.359
	400€/m^2≤II<500€/m^2	80	2257	67%	81%	17	437	0.378
	500€/m^2≤II<600€/m^2	71	2188	68%	83%	17	502	0.376
	II>600€/m^2	29	596	91%	93%	13	917	0.408
M_2	EPC: F level	210	2739	60%	51%	24	849	0.409
	EPC: E level	105	1926	72%	75%	19	889	0.598
	EPC: D level	80	2231	67%	82%	17	466	0.631
	EPC: C level	54	769	89%	88%	13	855	0.827
	EPC: B level	34	591	91%	93%	14	932	0.920
M_3	DPP<15 years	163	2500	63%	61%	13	870	0.703
	15 years≤DPP<20 years	34	890	87%	92%	15	821	0.628
	20 years≤DPP<25 years	67	2104	69%	84%	20	435	0.501
	DPP≥25 years	29	742	89%	93%	25	392	0.423

Table 2 Multi-objective optimal combinations for M1 type

Retrofit number	II<400€/m2	400€/m2≤II<500€/m2	500€/m2≤II<600€/m2	II>600€/m2
ERM01-1				
ERM01-2				√
ERM02-1		√		√
ERM02-2			√	
ERM03-1	√	√	√	√
ERM04-1			√	√
ERM05-1	√	√	√	√
ERM06-1				
ERM06-2				

ERM07-1				
ERM08-1	√	√	√	√
ERM09-1				√
ERM09-2				
ERM10-1	√	√	√	√
ERM10-2				
ERM10-3				
ERM11-1				

Table 3 Multi-objective optimal combinations for M2 type

Retrofit number	**EPC: F level**	**EPC: E level**	**EPC: D level**	**EPC: C level**	**EPC: B level**
ERM01-1	√	√			
ERM01-2					√
ERM02-1					√
ERM02-2		√	√		
ERM03-1	√		√	√	
ERM04-1	√	√	√	√	√
ERM05-1	√	√	√	√	√
ERM06-1					
ERM06-2					
ERM07-1	√				
ERM08-1	√	√	√	√	√
ERM09-1	√	√	√	√	√
ERM09-2					
ERM10-1					
ERM10-2			√	√	√
ERM10-3					
ERM11-1	√				

Table 4 Multi-objective optimal combinations for M3 type

Retrofit number	DPP<15 years	15 years≤DPP<20 years	20 years≤DPP<25 years	DPP≥25 years
ERM01-1				√
ERM01-2		√	√	
ERM02-1				
ERM02-2	√	√	√	√
ERM03-1		√		√
ERM04-1			√	
ERM05-1		√	√	√
ERM06-1		√		
ERM06-2	√			√
ERM07-1	√	√		
ERM08-1	√	√	√	√
ERM09-1	√	√	√	√
ERM09-2			√	
ERM10-1			√	
ERM10-2		√		√
ERM10-3	√			
ERM11-1	√		√	